

DYNAMIC SYNCHRONIZATION OF SYMPATHETIC OSCILLATORS

Hong-Shiu Chang

**Department of Physiology
University College London**

October 1999

A thesis for the award of a Doctor of Philosophy Degree
Submitted to the University of London



ProQuest Number: 10609356

All rights reserved

INFORMATION TO ALL USERS

The quality of this reproduction is dependent upon the quality of the copy submitted.

In the unlikely event that the author did not send a complete manuscript and there are missing pages, these will be noted. Also, if material had to be removed, a note will indicate the deletion.



ProQuest 10609356

Published by ProQuest LLC (2017). Copyright of the Dissertation is held by the Author.

All rights reserved.

This work is protected against unauthorized copying under Title 17, United States Code
Microform Edition © ProQuest LLC.

ProQuest LLC.
789 East Eisenhower Parkway
P.O. Box 1346
Ann Arbor, MI 48106 – 1346

ABSTRACT

Synchronous activity of single postganglionic sympathetic neurones (PGNs) underlies rhythmical or semi-rhythmical burst discharges recorded from peripheral sympathetic nerves. It is still controversial whether this rhythmicity is generated by an autonomous sympathetic oscillator. Previous studies have demonstrated that activity of single PGNs innervating the caudal ventral artery (CVA) of the rat's tail has a dominant rhythm (T-rhythm). The frequency of T-rhythm is different from the cardiac frequency and can be different from those of ventilatory and respiratory rhythms, suggesting that T-rhythm is generated by an oscillator independent of periodic drives originating from the arterial baroreceptors, the ventilation afferents and the respiratory network. Using the rat's tail circulation as a model, the purpose of the present study is: 1) to determine whether activity from different single PGNs is generated by multiple oscillators. 2) to establish whether synchronization of single PGNs is an obligatory feature and if not, how it is regulated. 3) to determine whether periodically driven single PGN oscillators exhibit dynamics as predicted by the theory of nonlinear coupled oscillators. 4) to explain the discharge behaviour of whole nerve activity based on the findings at single PGN level.

The experiments were conducted in anaesthetised Sprague-Dawley rats. Population PGN activity was recorded from the ventral collector nerve (VCN) of the tail. Single PGN activity was recorded focally from the surface of the CVA. The interaction between two single PGNs was studied by recording two units simultaneously. The discharge behaviours of PGNs in response to a periodic input were studied using the central respiratory drive (CRD) and lung-inflation cycle (LIC)-related activity as the driving forces.

The findings from the present study suggest that: 1) Activity of CVA PGNs is generated by multiple oscillators independent of CRD, LIC-related activity and cardiac activity. 2) The multiple PGN oscillators are capable of dynamic synchronization. 3) When subjected to frequency changes of LICs, single PGNs exhibit dynamics, such as 1:1 entrainment, relative coordination, high order rational frequency-lock, asynchrony, characterising nonlinear coupled oscillators. 4) Population PGN activity should be considered as output activity from a pool of dynamically interactive multiple oscillators rather than that from a single oscillator.

CONTENTS

ABSTRACT	2
ACKNOWLEDGEMENTS	10
LIST OF FIGURES	11
LIST OF PUBLICATIONS	14
CHAPTER1: GENERAL INTRODUCTION	15
1.1 Characteristic features of peripheral sympathetic nerve activity	16
1.2 Non-linear dynamics of periodically driven biologic oscillators	20
1.3 Synchronization: an important mechanism for information transmission and processing	22
1.4 Purpose of this study	28
CHAPTER TWO: MATERIALS AND METHODS	32
2.1 Experimental preparation	32
2.1.1 <i>General preparation and maintenance</i>	32
2.1.2 <i>Experiments where CRD was manipulated</i>	34
2.1.3 <i>Experiments where LIC-related activity was manipulated</i>	37
2.2 PGN activity recording	38
2.2.1 <i>Population PGN activity</i>	38
2.2.2 <i>Single PGN activity</i>	40
2.3 Drugs	42
2.4 Signal processing	43
2.5 Experiment conditions	44
2.5.1 <i>Experiments where CRD was manipulated</i>	44
2.5.2 <i>Experiments in which the frequency of LIC-related activity was manipulated</i>	45
2.6 Experimental Protocols	47

CHAPTER THREE: DATA ANALYSIS	48
3.1 Introduction	48
3.1.1 Determination of the dominant frequency of PGN activity	48
3.1.1A Population PGN activity	48
3.1.1B Single PGN activity	50
3.1.2 Synchrony of PGN activity	54
3.1.2A Population PGN activity	54
3.1.2B Single PGN activity	55
3.1.3 Stability of PGN activity	62
3.1.3A Population PGN activity	63
3.1.3B Single PGN activity	63
3.1.4 High order rational frequency-lock between single PGNs and LIC-related activity	65
3.2 Details of Analysis Methods	70
3.2.1 Spectral analysis: Autospectrum and coherence spectrum	70
3.2.2 Cross correlogram and Autocorrelogram	72
3.2.3 Envelope spectrum of cross correlogram	73
3.2.4 Joint peri-stimulus scatter plot (JPSP)	73
3.2.5 Ordinary correlation raster plot (OCRP) and reordered correlation raster plot (RCRP)	74
3.3 Statistics	74
CHAPTER FOUR: DYNAMIC SYNCHRONIZATION OF MULTIPLE SYMPATHETIC OSCILLATORS	76
4.1 Introduction	76
4.1.1 A single/common coupled PGN oscillator(s) vs. multiple autonomous PGN oscillators.	76
4.1.2 Dynamics of synchronization between PGNs under conditions of different CRD.	77
4.1.3 Modelling the discharge behavior of population PGN activity	78
4.2 Materials and Methods	79
4.2.1 Whole nerve experiments	79
4.2.2 Single PGN experiments	79
4.3 Data analysis	79
4.4 Results	81

4.4.1 Condition of animals	81
4.4.2 Whole nerve activity recorded from the VCN in artificially ventilated animals	81
4.4.2A Rhythmical and sympathetic nature of VCN activity	81
4.4.2B Synchronous components in VCN activity become more prominent with increased CRD	84
4.4.2C Stability of VCN rhythmical activity increases when the CRD is enhanced	87
4.4.2D Heart rate- and LIC-related discharge in the VCN activity	89
4.4.3 Whole nerve activity recorded from the VCN in spontaneously breathing animals	89
4.4.4 Paired recordings of PGNs innervating the CVA in artificially ventilated animals	92
4.4.4A In the absence of CRD the T-rhythms seen in PGNs recorded simultaneously show a low probability of synchronization	92
4.4.4B In control conditions some pairs show PGN→PGN synchronization through coupling to CRD	97
4.4.4C Enhanced CRD leads to PGN→PGN synchronization of T-rhythms	98
4.4.4D Summary of the data from paired recordings under various respiratory conditions	100
4.4.4E The stability of rhythmical synchronization of PGNs increases when CRD is enhanced	104
4.4.5 Paired recordings of PGNs innervating the CVA in spontaneously breathing animals	107
4.4.6 The mean discharge rate of PGNs does not significantly change with increases in CRD	109
4.5 Simulation: Explanation of the discharge behavior of CVA PGN population activity	110
4.6 Discussion	115
4.6.1 Multiple CVA PGN oscillators	115
4.6.2 Synchronization of CVA PGNs	116
4.6.3 Explanation of the population discharge behaviour	118
4.6.4 Conclusion	120

CHAPTER FIVE: DYNAMICS OF PERIODICALLY DRIVEN MULTIPLE	121
SYMPATHETIC OSCILLATORS	
5.1 Introduction	121
5.1.1 Dynamics of PGN activity in response to frequency changes	121
<i>of the LIC-related activity (f_{LIC})</i>	
5.1.2 Comparison of the discharge behaviours between single PGN	123
<i>and population PGN activity</i>	
5.2 Materials and Methods	124
5.2.1 Whole nerve experiments	124
5.2.2 Single PGN experiments	125
5.3 Data analysis	125
5.4 Results	127
5.4.1 Conditions of animals	127
5.4.2 Population PGN activity in response to f_{LIC} changes	130
5.4.2A The dominant frequency of population PGN activity is 1:1 locked	130
<i>to LIC-related activity across a broad f_{LIC} range</i>	
5.4.2B Moving f_{LIC} away from f_{INT} the temporal stability of population	135
<i>PGN rhythmical activity decreased</i>	
5.4.2C LIC-related rhythmical activity diminished without drop of total	137
<i>population PGN activity when f_{LIC} was moved away from f_{INT}</i>	
5.4.3 Single PGN activity in response to f_{LIC} changes	140
5.4.3A 1:1 frequency-lock of the dominant rhythm of single PGNs to	140
<i>LIC-related activity only occurs within a narrow range of f_{LIC}</i>	
5.4.3B Temporal stability of phase difference between PGNs decreased	146
<i>when f_{LIC} was moved away from f_{INT}</i>	
5.4.3C The change of PGN discharge patterns in response to change of	151
<i>f_{LIC} is not accompanied by a significant change of the mean</i>	
<i>discharge rate of single PGNs</i>	
5.4.4 Summary for difference of discharge behaviours of population	154
<i>and single PGN activity in response to f_{LIC} changes</i>	
5.4.5 PGN activity at cardiac frequency	156
5.4.6 Dynamic patterns of interaction between PGNs and LIC	156
5.5 Discussion	167
5.5.1 Afferent pathways involved in the interaction between LIC-	167

<i>related activity and CVA PGN activity</i>	
5.5.2 Comparison of discharge behaviours of single PGN and population PGN activity in response to f_{LIC} changes	168
5.5.3 Explanation of the population discharge behaviour in response to f_{LIC} changes	171
5.5.4 Conclusion	173
CHAPTER SIX: GENERAL DISCUSSION	174
6.1 The existence of independent sympathetic oscillators	174
6.2 Sympathetic oscillators in other vascular beds	177
6.3 Discharge behavior of PGNs in response to a periodic driving force	182
6.4 Physiological significance of synchronization	185
6.5 Conclusion	190
Appendix I: A stochastic model for simulated CVA PGN event series	193
Appendix II: Autospectrum of population activity	197
Appendix III: Empirical confidence interval for cross correlogram	202
Appendix IV: Detection of commensurate frequency-lock by reordered correlation raster plot (RCRP)	204
Appendix V: Matlab script file, SPECTRUM, for autospectrum and coherence spectrum	211
Appendix VI: Matlab script file, COEVENT, for the autocorrelogram and the cross correlogram	213
Appendix VII: Rhythmic sympathetic activity recorded from the ventral collector nerve (VCN) innervating the rat tail	214

Appendix VIII: Multiple “ oscillators” and the discharges of sympathetic neurons innervating the rat caudal ventral artery	216
Appendix IX: Synchronous and asynchronous rhythmical discharges of postganglionic sympathetic neurones innervating an identified blood vessel in the rat	217
Appendix X: Sympathetic neuronal oscillators are capable of dynamic synchronization	219
Appendix XI: List of Abbreviations	234
References	235

ACKNOWLEDGEMENTS

I would like to thank the staff in the department of physiology, Royal Free and University College Medical School, for their help during my study. I am particularly grateful to:

Dr. Michael P. Gilbey for his continuous support and inspiring supervision

Dr. Kevin Staras for his valuable discussions and help in some of my experiments

Mr. Bruce A. Cotsell for his excellent technical assistance

Miss Julia E. Smith for her assistance in some of my experiments

Chang Gung Memorial Hospital for funding my study

LIST OF FIGURES

1.1	Variation of amplitude and frequency of sympathetic nerve activity	18
1.2	Stimulus dependent synchronization of cortical neurones	26
2.1	The experimental preparations and signal processing procedures used for recording neural activities	35
2.2	Diagrammatic illustration of the origins of spinal segments for the somatic sensory-motor and sympathetic nerves to the rat's tail	39
3.1	Diagrammatic illustration of inadequacy of frequency determination based on inter-burst interval histograms	49
3.2	Quasi-periodic feature of single CVA PGN activity	52
3.3	Measurement of the coupling strength between two simulated single PGNs receiving a common input (trigger)	57
3.4	Diagrammatic illustration of the principle to generate a joint peri-stimulus scatter plot (JPSP)	61
3.5	Detection of higher order rational frequency-lock by using the reordered correlation raster plot (RCRP)	66
4.1	Physiological parameters of experiments under different respiratory conditions	82
4.2	The bursty and sympathetic nature of the VCN activity in an artificially ventilated animal under a control CRD condition	83
4.3	The autospectra and coherence spectra of the VCN and PN in an artificially ventilated animal under three conditions of CRD	85
4.4	Time evolving autospectra of VCN and PN activity under three conditions of CRD	88
4.5	Dynamic stability of rhythmical components evaluated by the variance of the relative power density of VCN activity across time in artificially ventilated animals under three conditions of CRD	90
4.6	Lung inflation cycle (LIC) related activity in VCN activity recorded from an artificially ventilated animal under a control CRD condition	91
4.7	Neurograms and frequency relationships of two PGNs and PN activity recorded simultaneously in an artificially ventilated animal under three conditions of CRD	93

4.8	Rhythmical PGN→PGN and PN→PGN synchronization revealed by cross correlograms under three conditions of CRD	95
4.9	Detection of weak coupling of PGNs through phase-lock to CRD	99
4.10	Summary scatter plots showing T-rhythm frequencies of pairs of postganglionic neurones (PGN1 and PGN2) in three conditions of CRD	102
4.11	Degree of rhythmical PGN→PGN synchronization in artificially ventilated animals under three conditions of CRD evaluated by the relative power density of the autospectrum of the cross correlogram envelope	103
4.12	Dynamic change of rhythmical PGN→PGN and PN→PGN synchronization evaluated by the ordinary correlation raster plot (OCRP) under three conditions of CRD	105
4.13	Dynamic stability of rhythmical synchronization between PGNs evaluated by the phase variation factor in artificially ventilated animals under three conditions of CRD	108
4.14	Simulation of population activity composed of multiple PGN oscillators	112
5.1	Scatter plots of physiological parameters of experiments under conditions of different f_{LIC}	128
5.2	f_{LIC} dependent LIC-related oscillations of BP	129
5.3	Neurograms and superimposed autospectra of VCN activity and LICs showing frequency dependent synchronization of VCN activity to LICs	131
5.4	The effect of chlorisondamine (3 mg kg^{-1} I.V.), a sympathetic ganglionic blocker, on LIC-related activity in VCN activity and BP	133
5.5	Change of strength of LIC-VCN activity linear correlation in response to f_{LIC} changes	134
5.6	Dynamic stability of synchronous rhythmical activity in VCN activity and TP evaluated by colour-coded time evolving autospectra	136
5.7	Summary scatter plot of the changes of temporal stability of rhythmical components in VCN activity in response to f_{LIC} changes	138
5.8	Relationship between the power density at f_{LIC} and the total power in VCN activity in response to f_{LIC} changes	139

5.9	Neurograms and superimposed autospectra of PGN activity, PGN1, PGN2 and LICs showing frequency dependent synchronization of single PGNs to LICs	141
5.10	Change of strength of LIC-single PGN and single PGN-single PGN linear correlation, evaluated by coherence spectrum, in response to f_{LIC} changes	144
5.11	Rhythmical synchronization between single PGNs in response to f_{LIC} changes	147
5.12	Detection of PGN-PGN weak coupling through LIC-related activity by the joint peri-stimulus scatter plot (JPSP)	150
5.13	Summary scatter plot for the temporal stability of rhythmical synchronization between two PGNs in response to f_{LIC} changes	152
5.14	Changes of the mean discharges rate (MDR) of single PGNs in response to f_{LIC} changes	153
5.15	Summary scatter plots showing frequency responses of single PGN activity and population PGN activity to changes of f_{LIC}	155
5.16	Interaction under 'free-run' conditions and 1:1 entrainment between LICs and single PGN activity	158
5.17	Asynchrony (or phase walk-through) and relative coordination between LICs and single PGN activity	160
5.18	High order rational frequency lock between LICs and single PGN activity	163
A1.1	Diagrammatic illustration of the calculation for the event dispersion ratio	195
A4.1	Diagrammatic illustration of the structure of the reordered correlation raster plot (RCRP) for a pair of periodic event series locked in a simple high rational frequency ratio	208

LIST OF PUBLICATIONS

- Appendix VII** Chang H-S., Gilbey M.P. (1998) Rhythmic sympathetic activity recorded from the ventral collector nerve (VCN) innervating the rat tail. *J. Physiol.* **506.P**, 134P
- Appendix VIII** Chang H-S., Smith J.E., Staras K., Cotsell B.A., Gilbey M.P. (1998) Multiple "oscillators" and the discharges of sympathetic neurons innervating the rat caudal ventral artery. *FASEB J.* **12**, A985
- Appendix IX** Chang H-S., Smith J.E., Staras K., Gilbey M.P. (1998) Synchronous and asynchronous rhythmical discharges of postganglionic sympathetic neurones innervating an identified blood vessel in the rat. *J. Physiol.* **509.P**, 123P-124P
- Appendix X** Chang H-S., Staras K., Smith J.E., Gilbey M.P. (1999) Sympathetic neuronal oscillators are capable of dynamic synchronization. *J. Neurosci.* **19**:3183-3197

CHAPTER ONE

GENERAL INTRODUCTION

Biorhythms are present in many physiological activities such as respiratory, heartbeat, peristalsis in the gastrointestinal tract, menstruation and wake-sleep circadian cycles. They are important in coordinating physiological functions. A disturbance of these rhythms may hamper normal physiology of the organisms and sometimes, for example some kinds of cardiac arrhythmia, may even result in a fatal outcome. On the other hand *de novo* rhythms may emerge in pathological conditions. For example, although slow brain wave oscillations in the delta frequency range (<4 Hz) were rarely observed in normal conscious people, they are frequently present in patients with diverse brain pathology. Recently, the concept of 'dynamical diseases' has been proposed to emphasise the importance of temporal derangement of biological activities in the pathogenesis of diseases and it was found that a drastic change of rhythmicity may arise from a minor change of the system parameters (for review see Mackey & Milton, 1987; Glass & Mackey, 1988). For example, it has been suggested that an increase of the circulation time from the lung to the brainstem chemo-sensitive areas can result in Cheyne-Stokes respiration, a pathological wax-and-wane breathing pattern (Mackey & Glass, 1977). In the sympathetic nervous system (SNS), rhythmical or semi-rhythmical burst activity arising from synchronous discharges of sympathetic neurones is frequently observed in the sympathetic output. However, little is known about what kind of discharge patterns should be considered as pathological. Part of the reason is that the underlying mechanisms for generating and regulating the rhythmicity of sympathetic activity are not clear. Some controversies regarding sympathetic

rhythmogenesis and synchrony and the purpose of this study are discussed in the following sections.

1.1 Characteristic features of peripheral sympathetic nerve activity

Since the first report by Adrian and Bronk (Adrian & Bronk, 1932), subsequent studies have established that peripheral sympathetic nerves of mammals are tonically active and individual action potentials are grouped into burst discharges (for review, see McAllen & Malpas, 1997). Burst activity arises from discharges of numerous postganglionic sympathetic neurones (PGNs) occurring at approximately the same time, i.e. synchrony in firing. This burst activity frequently displays some degree of rhythmicity and the rhythm may be 'locked' to other periodic activities such as baroreceptor afferent activity (Kezdi & Geller, 1968), central respiratory drive (CRD) (Gilbey & Spyer, 1997) or lung inflation cycle related activity (LICs) (Gerber & Polosa, 1978). The origin of these rhythms is controversial (Malpas, 1998). One possible explanation is that PGNs receive periodic inputs from, for example, the respiratory rhythm generating network (Connelly & Wurster, 1985; Bachoo & Polosa, 1987b; Richter & Spyer, 1990) or arterial baroreceptors (Green & Heffron, 1967; Cohen & Gootman, 1970; Ninomiya *et al.*, 1990; Hedman *et al.*, 1994). According to this hypothesis, tonic sympathetic nerve activity acquires its rhythms through 'phase editing' by these inputs, i.e., the sympathetic nervous activity simply follows or is gated by the periodic drives. If the interaction between SNS and the periodic inputs is stationary, this implies that the input-output relationship should be frequency invariant, i.e. it should behave like a linear system (Bendat & Piersol, 1986). However, when SNS was perturbed by periodic activities such as ventilation cycles (Porta *et al.*, 1996) or baroreceptor stimuli (Gebber *et al.*, 1997), it was

found that frequency-lock other than 1:1 entrainment could arise when the stimulation frequency was changed. These observations are difficult to reconcile by a model based on linear interaction.

Another theory for the genesis of sympathetic rhythms is based on a model of coupled oscillators. Previous studies have shown that rhythmicity of sympathetic activity could still exist in apneic and baroreflex deafferent animals, i.e. 'free-run' conditions (Taylor & Gebber, 1975; Barman & Gebber, 1976). In addition, when the periodic influences from CRD or baroreceptors were removed surgically or mathematically, significant correlation between sympathetic activities in different nerves were still observed (Gebber *et al.*, 1994a; Kocsis, 1995; Zhong *et al.*, 1997). These observations led Gebber and his colleagues to suggest that rhythmic sympathetic activities in different nerves are generated by coupled oscillators, which, though independent of, can be entrained to CRD or baroreceptor afferent activity (Gebber, 1980; Zhong *et al.*, 1997). Although the theory of periodically driven oscillators can explain some of the nonlinear phenomena observed in SNS, this hypothesis has nevertheless been criticised because of the 'aperiodic' behavior of the sympathetic activity (Bachoo & Polosa, 1987a): under 'free-run' conditions, the amplitude and frequency of integrated activity recorded from peripheral sympathetic nerves display great variability (Malpas, 1998). This is reflected in the autospectrum of sympathetic nerve activity where typically the power is not concentrated in a sharp frequency peak. Instead, the power is frequently spread across a broad range (For example, see Fig. 1.1, from Kocsis *et al.*, 1990) and it was argued that the dispersion of the power is not consistent with the existence of a well-defined sympathetic oscillator (Bachoo & Polosa, 1987a; McAllen & Malpas, 1997; Malpas, 1998). Furthermore, empirical and theoretical evidence indicates

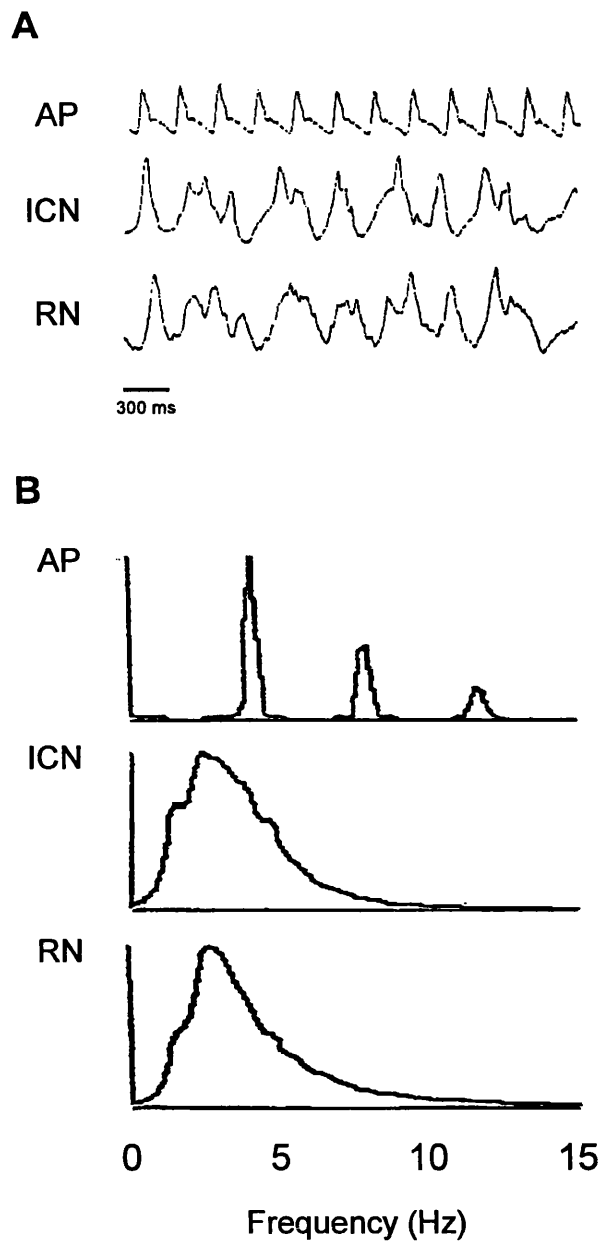


Fig. 1.1 Variation of amplitude and frequency of sympathetic nerve activity. *A*, Real time waveforms of arterial blood pressure (AP) and activity of the inferior cardiac nerve (ICN) and the renal nerve (RN). Unlike AP, amplitude and frequency of the sympathetic nerve activity recorded from the ICN and the RN displayed high variability. *B*, Autospectra of AP ICN activity and RN activity. In contrast to the sharp fundamental peak with its harmonics in the AP autospectrum, most power of ICN and RN activity concentrated in a broad spectral peak across a wide frequency range (2-6 Hz) in their autospectra. Activities were recorded from a cat. (Adapted from Fig. 1 in Kocsis *et al.*, 1990)

that for two coupled oscillators while maintaining stable 1:1 entrainment, if the frequency of the driving oscillator changes, the phase difference between the driving and driven oscillators will change accordingly (Pavlidis, 1973; Pinsker, 1977b; Ayers & Selverston, 1979). However, some studies have shown that in response to frequency changes of CRD (Bachoo & Polosa, 1987b) or baroreceptor afferent activity (Hedman *et al.*, 1994), there was no significant change of phase difference between sympathetic nerve activity and the periodic inputs. These findings question the hypothesis of entrained oscillators generating respiratory and cardiac related activity in the SNS.

It should be noted that in most of the previous studies multi-unit sympathetic activity was recorded. Even when nerve activity is recorded from one anatomical region, for example cervical sympathetic nerves, all the individual fibres in the nerve do not have similar discharge patterns. Indeed this would explain at least in part the variation of the amplitude and frequency of burst discharges. Thus, it is incorrect to interpret the discharge behavior of whole nerve activity as a coherent entity.

In studies where activity of single PGNs or oligo-PGNs was recorded using a teased fibre technique (Habler *et al.*, 1994) or using a microneurography technique (Macefield & Wallin, 1999), respiratory-modulated or cardiac-modulated discharges were observed in single PGNs with presumed but not well-identified target organs and functions (Jänig, 1988; Jänig & McLachlan, 1992). These findings, however, did not differentiate whether such discharges are phenomena of 'phase editing' effects of CRD and baroreceptor afferent activity, or arise from entrainment of periodically driven sympathetic oscillators. It is important to study the behavior of single PGN activity in response to the changes of strength and frequency of these periodic drives

because if single PGN activity is generated by an oscillator, then complex nonlinear dynamics are likely to occur (see below, section 1.2).

1.2 Non-linear dynamics of periodically driven biologic oscillators

Complex nonlinear coupling between biological rhythms have been observed in many experiments, e.g. axonal membrane oscillation to current injections (Guttman *et al.*, 1980), bursting neurones to synaptic inputs (Pinsker, 1977b), cardiac pacemaker to depolarising stimulation (Glass & Guevara, 1981), respiratory oscillator to mechanical ventilation (Petrillo *et al.*, 1983), respiration to locomotion (Bramble & Carrier, 1983), coupled inter-limb locomotion (Peper & Beek, 1998). Theoretical models based on nonlinear dynamics have been used to describe these phenomena (Glass *et al.*, 1984; Matsugu *et al.*, 1998). Although nonlinear dynamics of coupled oscillators are present in diverse biological systems, some basic patterns are observed repeatedly. These include asynchrony with constant phase shifting (or phase walk-through, Ermentrout & Rinzel, 1984), relative coordination where intermittency of phase locking occurs, high rational frequency-lock (e.g. 1:2, 1:3, 2:3, etc) and tight 1:1 entrainment (Glass & Mackey, 1988; Kelso, 1995). For a periodically driven oscillator, the transitions between these different state patterns depends on the input parameters such as frequency and amplitude (Glass & Mackey, 1988; Kelso, 1995) and background noise (Glass *et al.*, 1980). The transition between different states enables organisms to coordinate biological activities with different coupling strength. It has been proposed that unlike the rigid stimulus-response relationship in a linear system, nonlinear dynamics confer organisms with greater ability to adapt to physiological stresses (Lipsitz & Goldberger, 1992).

Previous studies from this laboratory have shown that discharges of single PGNs innervating the caudal ventral artery (CVA) of the rat's tail have a dominant rhythm (T-rhythm) with a frequency within a narrow range (0.4-1.2 Hz) (Johnson & Gilbey, 1994; Johnson & Gilbey, 1996). This T-rhythm is different from the cardiac or ventilatory rhythm. The dominant rhythm can be the same as the central respiratory rhythm but it is still present in the absence of CRD. These findings indicate that single CVA PGN activity is generated by autonomous oscillators, i.e. its existence is not dependent on CRD, LIC-related activity or baroreceptor afferent activity. These studies also demonstrated that it is possible for PGN activity and CRD to lock in high order rational frequency ratios such as 1:2, 1:3, etc (Johnson & Gilbey, 1996). This suggests that the interaction between CRD and CVA PGNs is not a linear relationship and a nonlinear model of coupled oscillators is more appropriate to describe their behaviour. As mentioned above, complex dynamics may arise from the interaction of coupled oscillators. Most importantly, for a constant input strength, stable 1:1 entrainment only exists in a limited frequency range of the driving oscillator and this frequency range is close to the intrinsic frequency of the driven oscillator (Pinsker, 1977b; Glass & Mackey, 1988; Hilborn, 1994). This implies that for a population of independent oscillators with different intrinsic frequencies, a common driving input activity may entrain some but not others. Therefore, as a 'phase coordinator', the driving oscillator may regulate the degree of synchronization of the population of driven oscillators through differential entrainment.

It is unknown whether the intrinsic rhythmic activity of separate CVA PGNs are generated by different oscillators or by a common/coupled oscillator because in previous studies only one unit was recorded at any one time

(Johnson & Gilbey, 1994; Johnson & Gilbey, 1996). If sympathetic activity controlling the rat's tail circulation arises from multiple oscillators, the nonlinear interaction of coupled oscillators poses a fundamental problem on the sympathetic regulation for the cardiovascular system: when a stress is imposed on the SNS, how does the nervous system regulate synchrony of individual PGNs to achieve optimal cardiovascular responses? Traditionally this problem was approached according to Sherrington's doctrine, simple reflex arcs acting as building blocks in the nervous system. The input-output relationships were considered simply as the result of combinatory effects from many elementary excitatory or inhibitory reflex arcs. However, it must be emphasised that in a system of coupled oscillators, afferent activity can induce complex efferent responses even through an elementary reflex loop consisting of two neurones, (Pinsker, 1977a; Pinsker, 1977b; Ayers & Selverston, 1979). When input parameters change, there are not only quantitative changes in output activity but it may also undergo qualitative transforms. For example, dependent on the frequency of the driving oscillator, inhibitory inputs may slow down or speed up the intrinsic rhythm of the driven oscillator (Reid, 1969; Pinsker, 1977a). Therefore, in view of growing evidence indicating the functional significance of coordinated neural activity (see section 1.3), the anatomical knowledge of networks in the SNS should be supplemented with the dynamic principles governing the neural interaction in order to understand how the complex autonomic responses are generated.

1.3 Synchronization: an important mechanism for information transmission and processing

Synchronization of neural activity is emerging as an important mechanism for

information processing and transmission and it may have an important function in the production of patterns of autonomic responses to environmental challenges (Gebber *et al.*, 1995b; McAllen & Malpas, 1997). Synchronous neuronal discharges can increase the synaptic strength (Zucker, 1989; Abeles, 1991) and enhance the reliability of information transmission across synapses (Lisman, 1997). This synchronization can arise either from temporal summation or spatial summation of the incoming action potentials and this will result in accumulation of intracellular Ca^{2+} to potentiate the effect of succeeding spikes on the terminal target cells (Wu & Saggau, 1994; Zucker, 1994). Temporal summation of sequential spikes with short inter-spike intervals, which appear as burst activity, is now considered an important information encoding mechanism for the central nervous system (Lisman, 1997). In fact, paired-pulse facilitation has long been used to study synaptic plasticity in the central nervous system (Andersen, 1960; Creager *et al.*, 1980; Usrey *et al.*, 1998) because in a pair of stimuli with short inter-pulse interval, even one stimulus is enough to enhance the effect of a second. Previous studies have shown most single CVA PGNs discharged in bursts of doublets or triplets (Johnson & Gilbey, 1996) and this suggests temporal summation may provide single PGNs with an efficient way to enhance prejunctional transmitter release and hence facilitate junctional transmission. However, it is unclear whether temporal summation of single PGN activity is the only major factor in the generation of bursts in the whole nerve because the amplitude of the burst activity is also greatly influenced by the degree of synchronization between different PGNs.

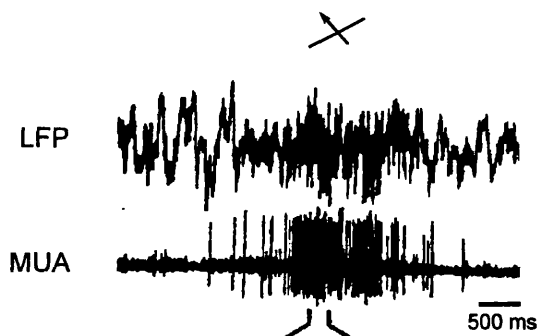
Studies based on stimulation of the peripheral sympathetic nerve have shown that in contrast to evenly spaced single stimuli, clustering the same number of stimuli into bursts produced a greater arterial smooth muscle

constriction (Andersson, 1983; Nilsson *et al.*, 1985). Furthermore, different stimulation paradigms could induce differential neurotransmitter release. High frequency burst stimulation is more likely to induce ATP release (Sneddon & Burnstock, 1985; Sjöblom-Widfeldt *et al.*, 1990) and increase amplitude of excitatory junctional potentials (Brock & Cunnane, 1988). However, simultaneous activation of sympathetic fibres in these studies is unlikely to represent the actual discharge behaviour in the *in vivo* situation. For the reason stated in section 1:1, it is questionable that individual PGNs fire in perfect synchrony, i.e. an exact spatial summation. Even 'bursting' is a characteristic of single PGNs, poor synchrony between different PGNs will result in phase dispersion and reduce the amplitude of population bursts. It remains to be established in *in vivo* situations if PGNs display any spatial summation, i.e. synchrony discharges from different PGNs, and if so, how the degree of synchronization is regulated.

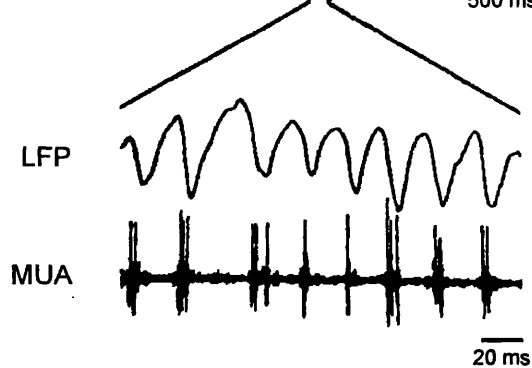
As well as representing an important mechanism to guarantee synaptic transmission, synchronization of neuronal discharges is also emerging as a fingerprint of information processing in the central nervous system. The doctrine that objects are perceived as a whole not just as a combination of its parts lays the foundation of Gestalt psychology but its underlying neural process is poorly understood. For example, when a face is looked at through a window with grids, how is it recognised as a face instead of many unfamiliar broken pieces (see Crick, 1994 for a general discussion)? The modern approach to this 'binding problem' was addressed by von der Malsburg who suggested perception is realised through correlated neural activity (see von der Malsburg, 1990). The basic idea is that perception arises from transient synchronization of different neural pools involving in the process of perception (von der Malsburg, 1995).

Studies in sensory perception (Galperin & Tank, 1990; Singer & Gray, 1995; DeCharms & Merzenich, 1996; Engel *et al.*, 1997), also extended to motor programming (Farmer, 1998; Fetz, 1997), support this hypothesis. For example, Gray and Singer showed that when cats were exposed to light bars, different neurones in the visual cortex could transiently synchronize their discharges in response to preferential stimuli (Gray & Singer, 1989). This dynamic synchronization is shown in Fig. 1.2A (adapted from Fig. 1 in Gray & Singer, 1989). In this case, when an optimally oriented light bar was moved across the receptive field of the tested area in the visual cortex (area 17), fast oscillations of local field potential (LFP) emerged and multiunit activity (MUA) became synchronous and phase-locked to LFP (Fig. 1.2Aii, expanded time scale from Fig. 1.2Ai). Likewise, Murthy and Fetz showed similar phenomenon in neurones of the motor cortex of monkeys during exploratory and manipulative movements requiring attention to sensorimotor integration. (Murthy & Fetz, 1992). This is shown in Fig. 1.2B (adapted from Fig. 1 in Murthy & Fetz, 1992). Local field potentials (LFP1, LFP2) with unit activity (UNIT1, UNIT2) were recorded from two adjacent areas in the motor cortex of a monkey. When the monkey received a raisin, there was a high incidence of fast oscillations in the LFP (arrow) and unit activity was phase locked to LFP during these periods and activity from the two adjacent areas became synchronized (Fig. 1.2 Bi). This was more clearly demonstrated in the LFP2 cycle triggered wave average for LFPs and the cross correlogram for unit activity (Fig. 1.2 Bii). These findings support the concept that different neural assemblies are capable of dynamic synchronization in response to a functional demand. Dynamic synchronization of neural activity has been observed also in the SNS. Coupling strength of sympathetic activity recorded peripherally from different nerves can vary across experiments

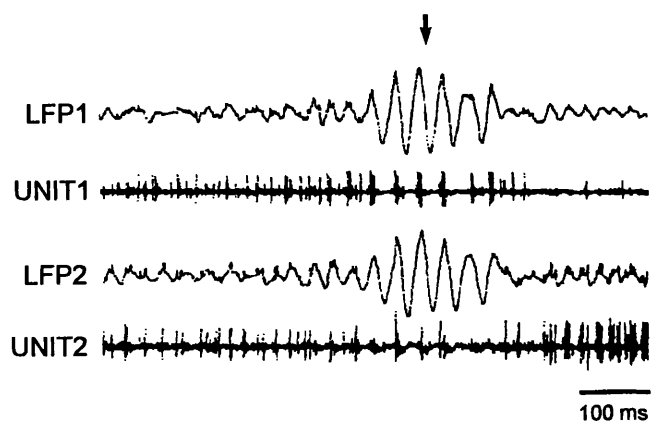
Ai



Aii



Bi



Bii

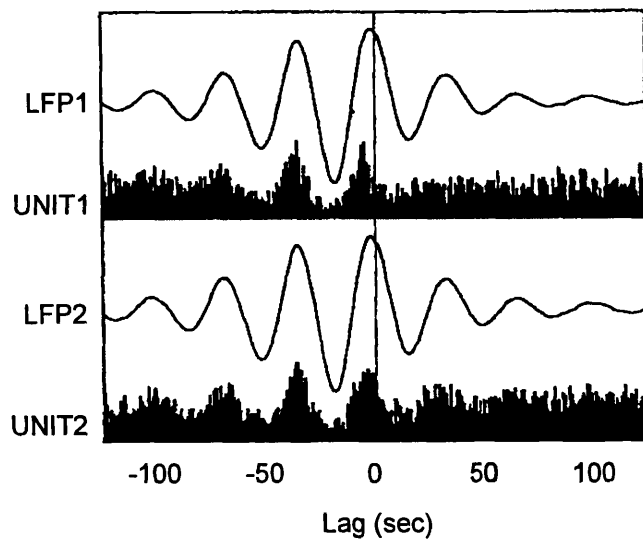


Fig. 1.2 Stimulus dependent synchronization of cortical neurones. *A*, Emergence of synchronous fast oscillations of neuronal activity in the visual cortex, area 17, of a cat in response to an optimally oriented light bar. *Ai*, Neurograms of local field potential (LFP) and multiunit activity (MUA) of cortical neurones recorded from the same area. The onset of the neuronal response was associated with emergence of high frequency oscillations (35-45 Hz) in LFP and MUA. *Aii*, Neurograms with an expanded time scale. During the periods of fast oscillations, MUA was phase-locked to LFP. (Adapted from Fig. 1 in Gray & Singer, 1989) *B*, Emergence of synchronous fast oscillations of neuronal activity in the motor cortex of a monkey receiving a raisin. *Bi*, Neurograms of two LFPs, LFP1 and LFP2, recorded from two nearby sites and two cortical unit activity, UNIT1 and UNIT2, recorded from the same areas, respectively. The behaviour was associated with occurrence of episodes of fast oscillations (25-35 Hz, arrow) in LFP1 and LFP2. UNIT1 and UNIT2 became synchronous to LFP1 and LFP2, respectively. *Bii*, Event (LFP2 cycles) triggered averages of LFPs and time histograms of unit activity. Peak activity was in phase for both LFPs and unit activity during the periods of fast oscillations. (Adapted from Fig. 1 in Murthy & Fetz, 1992)

(Gebber *et al.*, 1994b) and it was suggested that this dynamic coupling may be a mechanism by which complex cardiovascular patterns are generated (Gebber *et al.*, 1995b). This implies that the theory of synchronized neural activity as a solution to the binding problems in the cognitive process has its equivalent in autonomic processing. However, the dynamic features at single PGN level remain to be elucidated because whole nerve activity does not necessarily represent the discharge behaviour of a single PGN (as noted in section 1.1).

1.4 Purpose of this study

The main object of my study is to examine the dynamic aspect of interaction between single PGNs, and between PGNs and other periodic activities such as CRD and LIC-related activity. The subject of these experiments is the PGNs innervating the CVA. The CVA of the rat's tail is a good model to study sympathetic cardiovascular control based on functionally homogeneous PGNs because 1) its physiological function is well-defined as the major organ for thermoregulation of the rat (Grant, 1963). 2) it performs thermoregulatory function by regulating the vascular conductance which in turn is determined by the sympathetic tone (O'Leary *et al.*, 1985). 3) the anatomy of sympathetic nerve innervation along this artery is well understood (Sittiracha *et al.*, 1987) 4) the neurotransmitters released from its innervating sympathetic nerve endings are known and their postjunctional effect has been studied (Sneddon & Burnstock, 1985; Stjärne & Stjärne, 1995). 5) the location of CVA preganglionic neurones and the sympathetic ganglia where CVA PGNs come from are known (Sittiracha *et al.*, 1987; Smith & Gilbey, 1998b) and their central connection has been examined using a trans-synaptic viral tracing technique (Smith *et al.*, 1998). 6) single PGN activity can be recorded directly from the surface of the

CVA using a focal recording technique (Johnson & Gilbey, 1994). Using the rat's tail circulation as a model, I have investigated the following questions:

*1. Is sympathetic nerve activity generated by a single/common oscillator or by multiple autonomous oscillators? (see **Chapter Four**)*

In previous studies, activity of single CVA PGN was recorded one at a time. The dominant frequency of their discharges was in the range, 0.4-1.2 Hz (Johnson & Gilbey, 1994; Johnson & Gilbey, 1996). It is not clear whether the range of dominant frequencies arises from variation of conditions across experiments or whether it reflects the multiple oscillator origin of PGN activity. In this study these two possibilities were discriminated by comparing the discharge behaviours of activity of two single PGNs recorded simultaneously. The comparison is most important for the discharge patterns when the PGNs are free from a potential periodical driving force because identical frequencies may arise from coupling of both PGNs to a common drive. This was achieved by performing experiments under conditions of central apnea and minimising the effect arising from lung inflation (see **Chapter Two**). A difference in discharge behaviours of two PGNs in response to a common drive will further signify the inherent diversity of their intrinsic properties.

*2. Is behaviour of population activity of CVA PGNs the same as that of single PGN activity? (see **Chapters Four, Five**)*

As discussed in section 1.1, controversies regarding the behaviour of whole nerve activity may come from the difference of discharge patterns of single units. By examining both single unit and population PGN activity, I sought to explain the behaviour of population activity based on the findings from single units. This was achieved by studying the interaction between two PGNs using

both time domain and frequency domain analyses. This information was used to construct a stochastic model of population PGN activity (see **Chapter Four**) so that the population behavior observed in real experimental data could be described from a theoretical view point.

*3. Are CVA PGNs capable of dynamic synchronization? (see **Chapters Four, Five**)*

The functional implication of synchronization in autonomic control is discussed in section 1.3. The discharge behaviours of PGNs were studied when they were subjected to a common driving force, CRD or LIC-related activity. The dynamic aspect of synchronization was studied when either the strength of the drive (CRD) was changed or the driving frequency (LIC-related activity) was manipulated. Although it is important to understand how the single PGNs interact, a full understanding of sympathetic cardiovascular control cannot be obtained without understanding population activity which is likely to be more important than activity of an individual PGN for a target organ such as an artery. This is because the arterial smooth muscle cells are connected through gap junctions and can be considered as an integrator (Christ *et al.*, 1996). Local fluctuations of the discharge pattern of a single neurone may be smoothed out. Therefore, the findings in the single PGN experiments were correlated with those from whole nerve experiments in this study. In this way, it was possible to delineate how synchronization of single neurone discharges can influence the population outflow behaviour.

4. When subjected to frequency changes of a periodic input, does the interaction between single PGN activity and the input activity exhibit

phenomena indicative of nonlinear coupled oscillators? (see **Chapter Five**)

In the experiments where frequency of LICs (f_{LIC}) was manipulated, the possibility of non-linear coupling between LICs and single PGN activity was studied. In particular, the frequency response of single PGN activity was examined when f_{LIC} was changed. If there is effective linear coupling between LIC-related activity and CVA PGNs, f_{LIC} should be transmitted faithfully to single PGN activity across a very wide range of f_{LIC} . By contrast, in a system of nonlinear coupled oscillators, the input-output frequency invariance is not obligatory (Pavlidis, 1973; Bendat & Piersol, 1986). A new analysis method was developed to identify the non-linear coupling dynamics because of the limited resolution of spectral analysis, a tool most frequently used for frequency domain analysis (see **Chapter Three**). Again, population PGN activity in response to f_{LIC} changes was also examined to see if population behaves like a periodically driven oscillator as proposed by Gebber, et al. (Gebber *et al.*, 1997; Zhong *et al.*, 1997).

Part of this work has been published as abstracts (**Appendix VII-IX**) and a full article (**Appendix X**).

CHAPTER TWO

MATERIALS AND METHODS

All experiments were carried out in accordance with the Animal (Scientific Procedures) Act, UK, 1986.

2.1 Experimental preparation

2.1.1 General preparation and maintenance

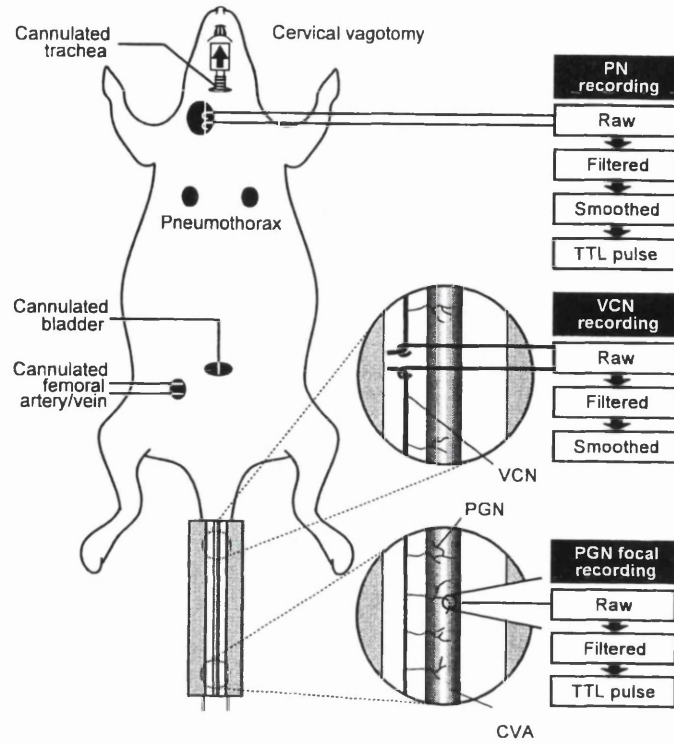
Male Sprague-Dawley rats (255-355 g) were anaesthetised initially with intraperitoneal injection of sodium pentobarbitone (60 mg kg⁻¹). Sometimes, if the anaesthesia induction was not adequate after pentobarbitone injection, judged by the absence or the presence of paw-pinch withdraw reflex, inhalation of a volatile anaesthetic, isoflurane, was given until the paw-pinch withdrawal reflex was absent. After exposure through a surgical opening in the inguinal area, the femoral artery and vein were cannulated (polyethylene tube, inner diameter, 0.4 mm, outer diameter, 0.8 mm; Portex, UK) for monitoring BP and infusing drugs, respectively. The arterial line was flushed occasionally with a heparinized normal saline to prevent obstruction by blood clots. The venous line was always flushed with normal saline every time after infusion of a drug. After cannulation of the femoral vein was established, supplemented α -chloralose (5-10 mg, intravenous) was given to maintain adequate anaesthetic level. Anaesthetic level was monitored and an appropriate depth was indicated by 1) stability of blood pressure (BP) with transient elevation in response to paw-pinch; 2) stability of respiratory activity monitored by phrenic nerve (PN) activity or diaphragm EMG (see below); 3) absence of both corneal and paw-pinch withdrawal reflexes. The trachea was exposed at lower cervical level and was

cannulated with a plastic tube with an appropriate length to ensure that the tip did not pass through the tracheal bifurcation to prevent unilateral lung ventilation. This cannula was tied around the trachea to prevent air leakage. In experiments where the rats were ventilated artificially, the tracheal cannula was connected to a ventilator (Model 55-3438, Harvard Apparatus, USA), otherwise it was left open to room air or O₂ enriched room air. Tracheal pressure (TP) waves were recorded and used as an indication of LICs. The urinary bladder was punctured and connected to a reservoir through a suprapubic cannula to ensure an unobstructed urine outflow to prevent reflex activation of sympathetic activity arising from bladder distension (Weaver, 1985). Oesophageal temperature was monitored using a homeothermic unit (Harvard Apparatus, USA) and normothermia, 36.5-37 °C, was maintained using a servo-heat blanket connected to the homeothermic unit and/or a lamp. When necessary, the animal was covered with a wool blanket to minimise heat loss during experiments. When the animals were ventilated artificially, peak expiratory CO₂ was monitored in every breath using a CO₂ meter (FM1, The Analytical Development Co., UK, or M455, Morgan Medical Ltd, UK). Arterial blood gas (pH, PaO₂, PaCO₂, HCO₃⁻¹, Base excess) sampled through the femoral arterial line was checked regularly (0.5-1 hr) during operation and data collection (M238, Ciba-Corning Ltd., UK). Metabolic acidosis was corrected by giving the animal sodium bicarbonate solution (1M, 0.1-0.4 ml, dependent on the severity of acidosis). When the animals were ventilated artificially, the presence of respiratory acidosis or respiratory alkalosis under control conditions was prevented by adjustment of the tidal volume or ventilation rate.

2.1.2 Experiments where CRD was manipulated (Chapter Four)

In experiments where the discharge patterns of PGN activity in response to changes of CRD were studied, PN activity was taken as an indication of CRD. The preparation for this type of experiments is shown in Fig. 2.1A. The PN was approached through a surgical opening at the level of the clavicle bone. The overlying muscles were stripped, cauterised and removed. The jugular and the subclavian veins were tied and cut. The remaining stump of brachiocephalic vein was tied. The clavicle was then removed. The PN was exposed from the region near the upper trunk of the brachial plexus. The distal end of the PN was cut or crushed to remove afferent nerve activity from the diaphragm (Balkowiec *et al.*, 1995) which may influence sympathetic nerve activity (Offner *et al.*, 1992). PN activity was recorded using bipolar silver wire electrodes covered with dental impression material (Coltène, Switzerland) to fix the nerve and insulate nerve activity from surrounding electrical activity. In cases where the rats were ventilated artificially, both cervical vagi were isolated at the mid-cervical level and cut to interrupt the Hering-Breuer reflex (Clark & von-Euler, 1972; Gaultier & Mortola, 1981). The rationale behind this was to dissociate the ventilation cycles and respiratory cycles so that changes of CRD were not complicated by the ventilation-related activity. The vagi were identified as the largest nerves containing myelinated fibres, which show characteristic striation, running parallel and adjacent to the carotid artery. Bilateral pneumothorax was given at the level of mid-sternum along the mid-axillary line and the chest cage was lifted to minimise the BP fluctuation arising from ventilation-induced changes of venous return. This procedure also diminished intercostal muscle spindle afferent activity (Critchlow & von Euler, 1963; Nakayama *et al.*, 1998), which may influence CRD (Shannon *et al.*, 1982). The disappearance of

A



B

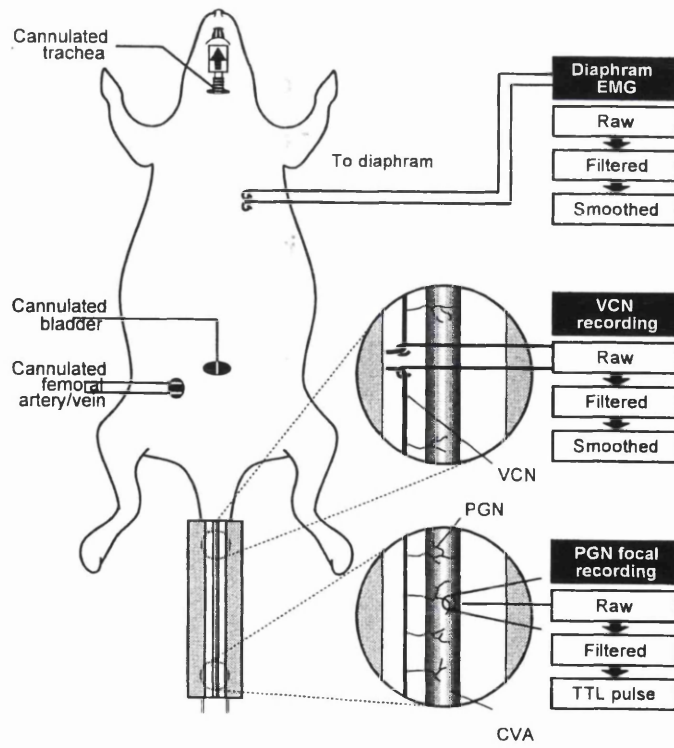


Fig 2.1 The experimental preparations and signal processing procedures used for recording neural activities. *A*, The preparation for experiments where the central respiratory drive was manipulated (**Chapter Four**). The femoral artery/vein, trachea and urinary bladder of the rats were cannulated. A pneumothoracotomy was performed and the vagi were cut (not shown) in the experiments where animals were ventilated artificially. Whole nerve activity of phrenic nerve (PN) was recorded from the neck. Activity was recorded from the ventral collector nerve (VCN) in the tail by cutting the nerve and placing the cut ends on bipolar electrodes (see top inset). The cauda equina was transected in the VCN whole nerve experiments (not shown). It should be noted there is one VCN on either side of the tail but only the right one is shown here for simplicity. Single postganglionic sympathetic neuron (PGN) activity was recorded from the surface of the CVA through a focal suction glass microelectrode (see bottom inset). When two PGNs were recorded, two focal electrodes were used simultaneously but only one is shown here for simplicity. For PN and VCN activity, the raw activity was filtered, rectified and smoothed and spectral analysis was performed on this smoothed data. Transistor to transistor logic (TTL) pulses representing the rising (inspiratory) phase of PN activity were generated from the smoothed data using a low frequency threshold trigger interface. For PGN activity, the raw signal was filtered and passed through a window preset in a spike processor to generate TTL pulses. *B*, The preparation for experiments where the ventilation frequency was manipulated (**Chapter Five**). The preparation and signal processing were similar to those for experiments where the central respiratory drive was manipulated (see above) except that the vagi were kept intact without pneumothoracotomy and the respiratory activity was monitored by recording diaphragm EMG instead of PN activity. Raw activity of diaphragm EMG was filtered rectified and smoothed. For further details see **Chapter Two**.

negative intra-pleural pressure due to pneumothoracotomy predisposed the lung to atelectasis. Under such situations, an end-expiratory positive pressure (2-3 cm H₂O) was applied through the expiratory tube to prevent lung collapse. During periods of data collection, animals were paralysed by injecting gallamine triethiodide (15 mg kg⁻¹ h⁻¹), a depolarising neuromuscular blocker, to prevent irregular cardiac output change due to TP fluctuations arising from uncoupled respiratory and ventilatory activity, and motion artifacts which might occur because of chloralose induced reflex myoclonus (Chadwick *et al.*, 1980). When the animals were paralysed, the depth of anaesthesia was assessed by monitoring the stability of the BP and phrenic discharges. In experiments where the rats breathed spontaneously, oxygen enriched room air was given. The vagi were left intact and no pneumothorax was given.

2.1.3 Experiments where LIC-related activity was manipulated (Chapter Five)

In experiments where the discharge behaviour of PGN activity in response to change of ventilation frequency was studied (for preparation see Fig. 2.1B), respiratory activity was monitored by recording diaphragm EMG activity using conventional bipolar hook electrodes. The electrodes were inserted transcutaneously along the lower border of the rib cage. Care was taken to avoid accidental puncture of the lung, which might result in tension pneumothorax. All the experiments of this kind were carried out under conditions of central apnea as indicated by the absence of diaphragm EMG activity. The animals were ventilated artificially and were not paralysed during experiments. The state of apnea was maintained by ventilating the animal with inspired gas of high oxygen concentration (~95%). The vagi were preserved

and the rats were not given a pneumothorax. No additional end expiratory positive pressure was added.

2.2 PGN activity recording

2.2.1 Population PGN activity

Population PGN activity for the CVA was recorded from the VCN. The VCNs are mixed nerves which contain both sympathetic and somatic sensory-motor axons. Around 80% of sympathetic nerve fibres innervating the CVA pass through these nerves to the tail (Sittiracha *et al.*, 1987). The preganglionic sympathetic neurones regulating the CVA are located in the lower thoracic and upper lumbar segments while the somatic motor neurones are located in the sacro-coccygeal segments (see Sittiracha *et al.*, 1987; Rathner & McAllen, 1998; Smith & Gilbey, 1998b; Smith *et al.*, 1998). It is thus possible by cutting the cauda equina at lumbar level to interrupt the somatic efferent and afferent nerve fibres innervating the tail while keep the sympathetic fibres intact (Fig. 2.2). This will avoid the contamination of sympathetic activity by somatic nerve activity.

In experiments where VCN activity was recorded, the cauda equina was routinely cut at L5 level. The cauda equina was approached dorsally at L5 level around the upper border of the gluteus maximus muscle. After an incision was made along the midline, the overlying muscles, paraspinous tendons and the vertebral arch were removed. The cauda equina was identified by its location in the spinal canal and its characteristic 'horse-tail' appearance. The cauda equina was subsequently cauterised.

To isolate the VCN, the skin of the ventral surface of the tail was cut along the midline and the tendon sheath of the tail was opened. Two or three layers of

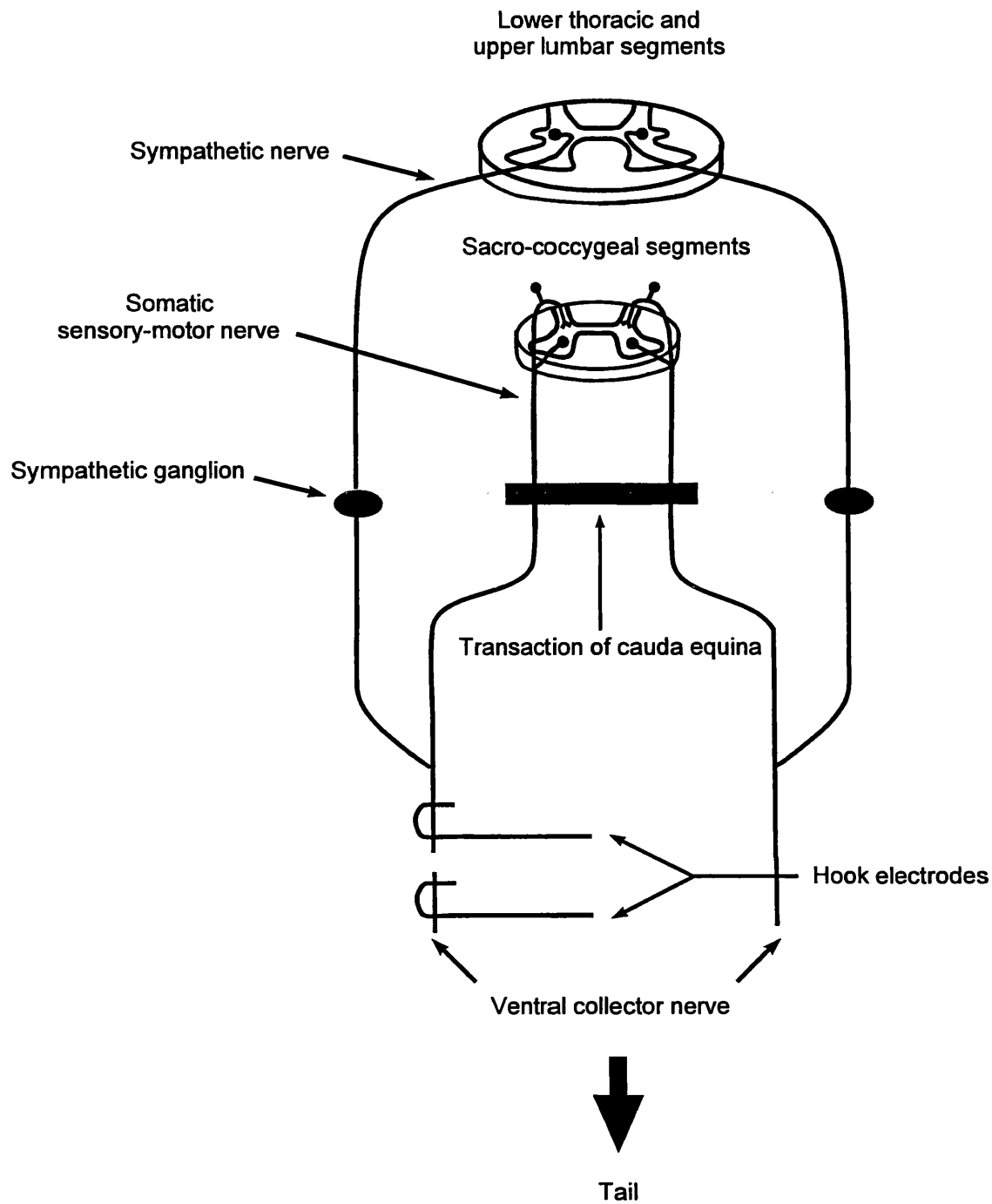


Fig. 2.2 Diagrammatic illustration of the origins of spinal segments for the somatic sensory-motor and sympathetic nerves to the rat's tail. While the somatic sensory and motor nerves originate from sacro-coccygeal segments, the sympathetic nerves come from lower thoracic and upper lumbar segments. By cutting the cauda equina at L5 vertebral level, sympathetic nerve activity could be recorded from the ventral collector nerve without contamination of somatic nerve activity.

tendons were removed and the VCN was exposed deep in the tendon groove. The VCN was identified by its relatively large calibre and the characteristic striation of its myelinated contents. The branches were cut and the VCN was freed. A 4-5 cm segment starting from the base of the tail was routinely isolated. The exposed VCN was bathed in paraffin oil, cut and desheathed. The distal end was crushed to remove afferent activity from periphery. The de-afferent state was confirmed by the absence of the afferent 'noise', monitored by spike processor speaker (D130, Digitimer, UK), when the surface of the tail was touched. The proximal and distal segments of the VCN were wrapped around conventional bipolar platinum electrodes to form a 'killed end' recording (Fig 2.1 upper inset). A platinum electrode inserted in the tail skin was used as the ground reference. The sympathetic activity of the VCN was characterised by its low pitch rumbling semi-regular noise monitored in the spike processor speaker. The sympathetic nature of VCN activity was confirmed by the abolition of ongoing nerve activity following intravenous injection of the ganglionic blocker chlorisondamine (3 mg kg^{-1} , see **Chapter Three**).

2.2.2 Single PGN activity

The CVA was exposed through cutting along the midline of ventral surface of the tail. The tough vascular sheath with overlying connective tissue was removed to expose the adventitia of this artery. Care was taken not to damage the adventitia because the sympathetic nerve endings form a 2-D web on the adventitial surface without deep penetration into the muscular layers (Stjärne & Stjärne, 1995) and damage to the adventitia may destroy the sympathetic nerve endings as well. The tail was positioned in a bath filled with glucose free Kreb's solution.

Glass microelectrodes made from non-filamented glass capillary tubes (GC150T-10, Clark Electromedical Instruments, UK) were used to record single PGN activity. The glass electrodes were made using an electrode puller and the tip was polished in a flame. To pick up single unit activity, glass electrodes with internal tip diameters, 20-50 μm , were used. Electrodes with larger diameter, 60-100 μm , were used to record multi-unit activity. The glass electrodes were fitted into an electrode holder which contained silver wire (port size 1.5mm, World Precision Instrument, USA). If the AgCl coating was dislodged, the silver wire was immersed in sodium hypochlorite solution (conc. < 5%) and 'recharged' by chloridization. The glass electrode, filled with Krebs's solution, was placed on the surface of the CVA (see Fig 2.1 lower inset) and to seal the tip gentle suction was applied using a syringe through the side hole of the electrode holder.

PGN activity was amplified differentially by comparing to an active platinum electrode which was placed in the Krebs's solution bath and its potential was also used as the ground reference. When two PGNs were recorded simultaneously through two separate glass electrodes (see below), this active platinum electrode was used as a common reference to both glass electrodes. Recorded activity was fed into a spike processor and monitored on a digital oscilloscope (VC-6023, Hitachi Denshi Ltd., Japan).

The glass electrode was moved around the surface of the CVA to search for PGN activity. Once active PGNs were within the opening of the glass electrode, a sound generated by action potentials could be heard through the spike processor speaker. Previous studies have confirmed that all units recorded from the surface of the CVA are sympathetic in nature with characteristic discharge patterns (Johnson & Gilbey, 1994; Johnson & Gilbey,

1996). The digital oscilloscope was triggered by transistor to transistor logic (TTL) pulses generated from the PGN spikes by the spike processor to display the action potentials. Activity from single PGNs was subsequently confirmed by its consistent spike waveform and amplitude as monitored on digital oscilloscopes. When activity of two single PGNs were simultaneously recorded, their discharges were either recorded at the same time through two independent electrodes (physical separation, 2.5-5.5 cm) or discriminated from multiunit activity recorded through one electrode. In each experiment where paired recordings were made, care was taken to establish that the latency between the firing of the two PGNs was not constant, since this would be evidence that both recordings arose from the same PGN (either its axon or branches). While constant latency firing was occasionally seen in single patch recordings between pairs of 'PGNs' (and these were therefore discarded), the latency between PGNs recorded from separate electrodes was always variable. During recording, the operation table was stabilised by an air cushion to secure the stability of recording electrodes.

2.3 Drugs

Pentobarbitone sodium (SAGATAL): Rhône Mérieux, UK

Isoflurane: Rhône-Poulenc Chemicals, Ltd. UK

α -chloralose (50mg/ml): SIGMA, UK or Vickers Laboratories Ltd. UK

Preparation: 1 gm of α -chloralose was dissolved in warm (~50 °C) Borax solution (1 gram sodium tetraborate [SIGMA, UK] in 20 ml distilled water).

Gallamine triethiodide BP (Flaxedil) (40mg/ml): May & Baker Ltd. UK

Chlorisondamine chloride(10 mg/ml): a gift from CIBA-Geigy Corporation, USA.

Prepared by dissolving in normal saline.

Sodium bicarbonate aqueous solution (1M): Fisons Scientific Equipment, UK

Normal saline: 0.9% sodium chloride aqueous solution

Heparinized saline (10 IU/ml): CP Pharmaceuticals Ltd. UK. Mixed with normal saline.

Glucose free Kreb's solution: NaCl 118.4mM, NaHCO₃ 25.0 mM, NaH₂PO₄ 1.13 mM, KCl 4.7 mM, MgCl₂.6H₂O 1.3mM, CaCl₂ 2.5 mM. Prepared by dissolving in distilled water.

2.4 Signal processing

BP and TP wave signals were recorded through pressure transducers (NL108T2, Digitimer, UK) and amplified (NL108, Digitimer, UK). The set-up for BP and TP recording were calibrated using a mercury manometer. All neuronal activity was recorded using high impedance headstages (NL100, Neurolog, Digitimer Ltd, UK), amplified (NL104, Neurolog) and filtered (bandpass 300-1kHz; NL125, Neurolog). PN activity, VCN activity and diaphragm EMG activity were rectified and smoothed with a 'leaky integrator' (time constant, PN or diaphragm EMG: 0.1 or 0.2 sec, VCN: 0.1 sec; NL703, Neurolog). Such narrow-band filtering followed by rectification and smoothing (or integration) is a well-established procedure for generating an envelope of the activity (for examples see Haselton & Guyenet, 1989; Czyzyk-Krzeska & Trzebski, 1990). One of the main advantages is that it removes movement-related artifacts which frequently appear as slow wave activity (Kenney & Fedde, 1994). However, the filtering causes little attenuation of individual action potentials since the instantaneous frequency of single fibre activity is higher than the high-pass cut-off value. All

data, digitized at 11.8 kHz (VR-100B, Digitimer, UK), were stored on a frequency modulation (FM) tape using a standard video recorder (V-404B, Toshiba, UK) for off-line analysis. In addition, BP, TP, smoothed PN, VCN activity, diaphragm EMG and single PGN activity were converted into digital signals via an analogue to digital conversion (ADC) interface (1401, Cambridge Electronic Design, UK) and sent to a computer for analysis. The ADC conversion rate or sampling frequency was: 13.3 kHz for single PGN activity; 100 Hz for VCN activity, PN activity, diaphragm EMG activity, BP and TP waves. Spike processors (D130, Digitimer, UK) were used to generate TTL pulses for single PGN action potentials when the amplitude exceeded a pre-set window. TTL pulses indicating the rising phase of inspiratory PN activity or the inflation phase of TP waves were generated using an interface (NL515, Neurolog). These TTL pulses were also sent to the computer to generate event series and used to create autocorrelograms, cross correlograms, correlation raster plots or joint peri-stimulus scatter plots of single PGN activity, PN activity and LIC-related activity (see **Chapter Three**). The flow chart of signal processing for different activities is summarised in Fig 2.1. During experiments, real-time data of BP, TP, diaphragm EMG activity and integrated VCN and PN activity were displayed on the computer monitor (SPIKE2, Cambridge Electronic Design, UK). The single PGN activity was monitored on the digital oscilloscopes. On-line analysis including autospectra, autocorrelograms and cross correlograms was also displayed on the computer screen (SPIKE2).

2.5 Experiment conditions

2.5.1 Experiments where CRD was manipulated (see Chapter Four)

Activity of the PGNs innervating the CVA was recorded under three respiratory

conditions, absence of CRD, control and enhanced CRD. The control condition was achieved by maintaining the blood gas parameters within a normal physiological range (see **Chapter Four**). The absence of CRD (apnea) was induced either by raising the oxygen concentration (60-90%) of the inflow and/or by hyperventilation hypocapnia. CRD was enhanced by raising inspired CO₂ to 5% (a gas mixture with O₂ and N₂) and inducing a hypercapnic state (St-John & Bianchi, 1985). After switching to a new condition, a minimum of 5 minutes was allowed for the condition of the rat to become stable before starting recording. Arterial blood gas samples were checked immediately before data was collected.

2.5.2 Experiments in which the frequency of LIC-related activity was manipulated (see Chapter Five)

All these experiments were carried out during central apnoea. In the first part of the experiment, the intrinsic frequency of PGN activity (f_{INT}) in single and population PGN activity was determined under 'free-run' conditions using high f_{INT} (1.9-2.5 Hz) and low tidal volume (V_T , 1-1.2 ml) in order to 'unlock' LIC and PGN activity. Although it is hardly possible in *in vivo* experiments to isolate the SNS from all the external inputs, i.e. a real 'free-run' condition, the conditions under the above ventilation parameters (i.e. low V_T and high f_{LIC}) could be realistically described as 'free-run' relative to the LIC-related activity. This is because when V_T is low afferent activities, which may influence sympathetic activity, such as pulmonary stretch receptor activity, proprioceptive activity from intercostal muscle spindles, cardiopulmonary receptor activity or large vessel baroreceptor activity diminished (see **Chapter Four**). At low driving strength, experimental and theoretical studies involving biological oscillators have

demonstrated that the driven oscillators could not maintain stable coupling to the driving oscillator and would revert to its 'free-run' state. This is especially true when the driving frequency is much higher than the f_{INT} of the driven oscillator (Winfree, 1980; Glass & Mackey, 1988). Under 'free-run' conditions, like single CVA PGN activity, VCN activity exhibited a dominant rhythm (see **Chapter Five**). However, the dominant rhythmicity always appeared as a broad spectral peak centred in the frequency range of the T-rhythm in the VCN autospectrum. The f_{INT} of population PGN activity was defined as this peak frequency. Although f_{INT} defined in this way for the population activity could not be a ubiquitous feature of all its constituent single PGNs, it nevertheless represents an 'average' of their individual outputs. This can be easily understood by considering the autospectrum of a group of weakly coupled oscillators. The autospectrum of such a population will have a broad spectral peak centred at the frequency range of its constituents with the peak frequency representing the frequency where most power density concentrates (see **Chapter Four** and **Appendix II**). Therefore, f_{INT} defined as the peak frequency of the modal spectral peak could represent the most likely central frequency at which the individual oscillators contributed to the dominant population rhythmical activity. Consequently, in the way a mean to a normal distribution, it could be considered as a measure of the average of the PGN f_{INT} distribution.

In the second part of these experiments, the frequency dependent nature of synchronization was examined by varying LIC frequency (f_{LIC}) while maintaining a constant high V_T (2-2.5 ml). Initially, f_{LIC} was adjusted to near f_{INT} of PGN activity and stable 1:1 entrainment was established. To demonstrate that 1:1 entrainment was not a chance phenomenon, this was repeated for two or three separate f_{LIC} steps (0.1 Hz in a step) away from f_{INT} to see if stable 1:1

entrainment still could be maintained. Following this, f_{LIC} was increased in 0.2 or 0.3 Hz steps up to ~1.5-1.8 Hz.

2.6 Experimental Protocols

The protocols for experiments where the strength of CRD or the frequency of LIC-related activity was manipulated are described in detail in **Chapter Four** and **Chapter Five**, respectively.

CHAPTER THREE

DATA ANALYSIS

3.1 Introduction

3.1.1 Determination of the dominant frequency of PGN activity

3.1.1A Population PGN activity

Different methods have been applied to detect the rhythmical activity of the sympathetic nerve. For example, techniques based on time domain information obtained from burst detection and inter-burst interval histograms have been used to study the sympathetic frequency (Ninomiya *et al.*, 1990; Malpas & Ninomiya, 1992; Kubota *et al.*, 1995). Aside from the subjectivity inherent in setting the criteria for burst detection (Malpas & Ninomiya, 1992), methods based on inter-burst histogram are subjected to erroneous attribution of different frequencies to different peaks because a favoured inter-burst interval does not necessarily indicate the existence of a stable rhythm. It simply reflects a high probability that sequential bursts are coupled with a fixed interval but this coupling may not cycle with a period equivalent to that inter-burst interval. In fact, it has been suggested that only when the inter-burst interval distributes normally does the frequency estimation based on the inter-burst histogram equal that determined by the autospectrum (Zhong *et al.*, 1996). This can be easily understood by considering time structures of inter-burst intervals. Fig. 3.1 illustrates this point. Series A and B represent two idealised burst event series generated by a burst detection procedure. The inter-burst interval histograms of both series consist of two peaks corresponding to the short (I_1) and long inter-burst intervals (I_2). However, it is inaccurate to ascribe two rhythmical components in these idealised burst trains. Series A is not stationary and

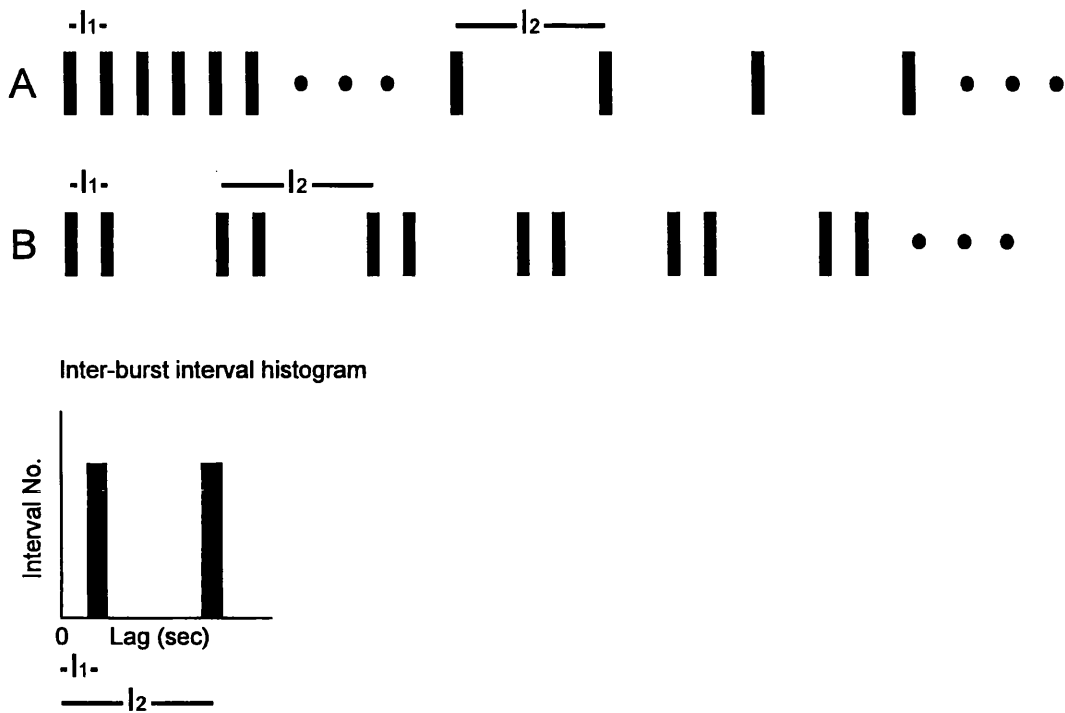


Fig. 3.1 Diagrammatic illustration of inadequacy of frequency determination based on inter-burst interval histograms. Two idealised burst event series, A and B, have different discharge patterns. Series A is not stationary with fast burst discharges followed by slower bursts. Series B is stationary with rhythmical activity composed of doublet bursts. However, their inter-burst interval histograms are similar and exhibit two peaks: one corresponds to the short inter-burst interval (I_1) and the other, to the long inter-burst interval (I_2).



although different frequencies are observed across time, they do not exist at the same time. Series B has only one rhythmical component with a period equal to I_2 .

Alternatively a more direct and powerful technique to extract frequency domain information from a neural signal is spectral analysis, which factorizes the activity into distinct rhythmical components (sinusoid waveforms) and estimates their associated power density (Bendat & Piersol, 1986). In this way, the contribution of each rhythmical component to the neural activity can be read out directly from its autospectrum. Spectral analysis has been extensively used by different research groups to study the rhythm of sympathetic nerve activity (e.g. Gebber *et al.*, 1990; Trzebski & Baradziej, 1992; Allen *et al.*, 1993; Suzuki *et al.*, 1993; Kenney, 1994; Kocsis, 1994). It was the method used in this study to determine the dominant frequency, defined by the frequency with maximal power density, of waveform signals such as VCN, PN, cardiac activity and TP waves.

3.1.1B Single PGN activity

Problems similar to those encountered in whole nerve activity analysis occur in the analysis of single PGN rhythm as well. Confusion frequently arises when the dominant frequency and the mean discharge rate (total number of spikes/time) are both used to describe the discharge behavior of single PGNs. The dominant frequency describes the periodic change of firing probability of PGN activity and on the other hand, the mean discharge rate directly reflects the mean of interspike intervals, a parameter more related to neuronal excitability. The two concepts are not necessarily the same. For example, a single PGN firing randomly with a mean discharge rate 2 Hz does not have a dominant

rhythmicity with a frequency equal to 2 Hz in its firing probability. The following consideration further elaborates this point. Although activity of single PGNs innervating the CVA exhibits a robust rhythm (T-rhythm), a previous study has shown that this rhythm was not perfectly regular and frequently the periodicity might be disrupted transiently (Johnson & Gilbey, 1996). It must be emphasised that the PGN rhythmicity is an emergent property across time because the periodicity may not be apparent during a short interval of observation. Fig. 3.2 shows a typical example of event series of TTL pulses generated from activity of a single PGN, PN activity, BP and TP under control conditions. Activity of the single PGN did not attain the same regularity inherent in the central respiratory, cardiac and artificial ventilatory cycles. More importantly, single PGNs frequently discharge in doublet (arrows) or even triplet bursts (see also Johnson & Gilbey, 1996). This results in a wide dispersion of inter-spike intervals and its distribution was frequently not normal (Johnson & Gilbey, 1996). For the same reason as that for the inadequacy of inter-burst interval histogram to detect the dominant frequency of whole nerve activity, mean discharge rate, as frequently used to measure respiratory or cardiac frequency, is not a good estimator for the frequency of dominant PGN rhythm. This is because for a spike train with a large number of events, the mean discharge rate is around the inverse of the mean of inter-spike intervals. Therefore, as mentioned above, the mean discharge rate is similar to the dominant frequency of single PGNs only when the inter-spike interval approaches a normal distribution.

Calculation of the time course of firing probability following a PGN action potential provides a more suitable way to evaluate the PGN rhythmicity. If activity of single PGNs has a dominant rhythm, it follows that the firing probability after a single PGN spike will undergo cyclic change. An estimator for

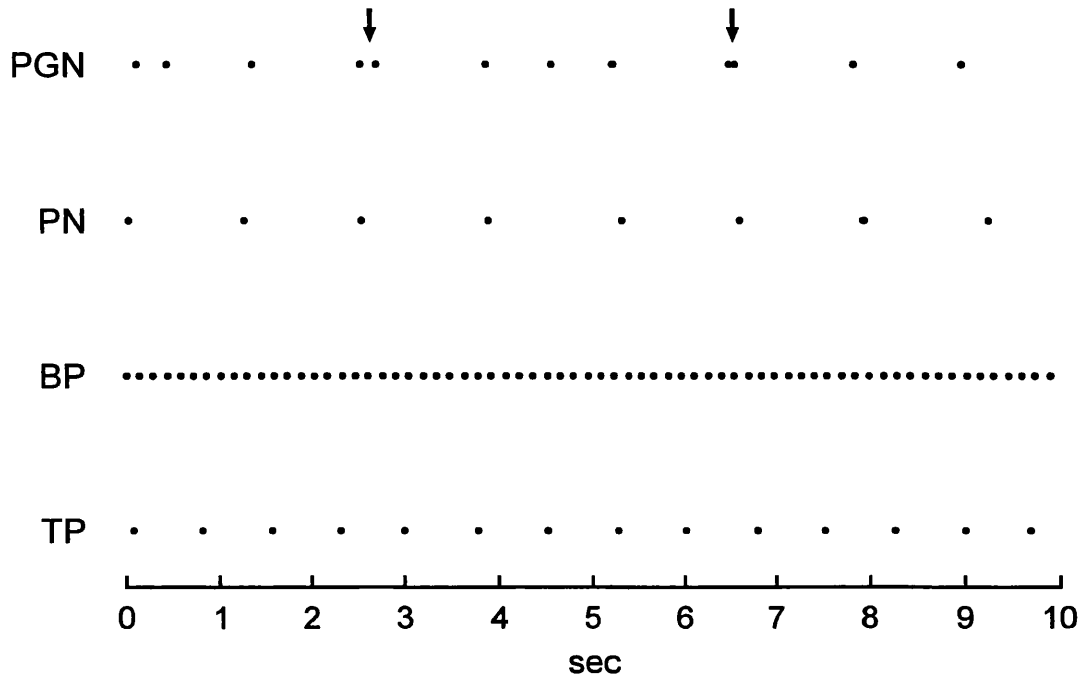


Fig. 3.2 Quasi-periodic feature of single CVA PGN activity. The event series of TTL pulses were generated from activity of a single CVA PGN, PN activity, BP and TP from an experiment under control CRD condition. Unlike PN activity, BP and lung-inflation cycles, activity of the single PGN was not very rhythmical and frequently doublet (arrows) or triplet discharges could be observed.

this conditional probability density function (i.e. renewal density or autocorrelation function, Perkel *et al.*, 1967a) is the autocorrelation histogram or autocorrelogram (Gerstein & Kiang, 1960; Perkel *et al.*, 1967a). In previous studies, the dominant frequency of single PGN activity was estimated by calculating the inverse of the period of the rhythmicity shown on its autocorrelogram. The peaks of the rhythm were determined subjectively by visual inspection (Johnson & Gilbey, 1996; Johnson & Gilbey, 1994). Although this gave a robust measure of the dominant frequency, a more accurate and objective method is needed to determine whether the dominant frequencies of two single PGNs were the same or different.

Same as the method for population PGN activity, spectral analysis on the event count series (see below 3.2.1 *Spectral analysis*) was used in this study to determine single PGN frequency. In a previous publication (Chang *et al.*, 1999; **Appendix X**), the dominant PGN frequency was determined from the autospectrum of the autocorrelogram envelope. The autocorrelogram of a neurone is an estimator of the firing probability density function given the condition that this neurone has fired. If the neurone discharges periodically a rhythm with the discharge frequency will appear on its autocorrelogram (Perkel *et al.*, 1967a) and this justifies the use of autospectrum of the autocorrelogram envelope to determine the dominant PGN frequency. It has an intuitive basis regarding evaluation of T-rhythm frequency by estimating the period of the rhythm shown on the autocorrelogram (Johnson & Gilbey, 1993; Johnson & Gilbey, 1996). These two approaches to determine the dominant rhythm of single PGNs, i.e. autospectrum of PGN event series and autospectrum of autocorrelogram envelope, are equivalent because the autocorrelogram is the estimator of autocorrelation function whose Fourier transformation is the

autospectrum (Rosenberg *et al.*, 1989; Rosenberg *et al.*, 1998). In fact, the difference of the PGN frequency determined by the two methods is not greater than 0.05 Hz which may be related to the resolution of the autospectrum (see below *3.2.1 Spectral analysis*). The autocorrelogram also provides additional information about the dispersion of PGN events around the dominant rhythm which may not be easily observed in the autospectrum. To determine the dominant frequency, the autocorrelogram was first generated to confirm the existence of a dominant rhythm and the frequency was read out from the autospectrum.

3.1.2 Synchrony of PGN activity

3.1.2A Population PGN activity

If a high degree of synchronization exists between single CVA PGNs, a prominent rhythmical activity at their common frequency will appear in VCN activity and high power density will concentrate at that frequency in the VCN autospectrum. Therefore, the power density at the dominant frequency was used as an indication of the degree of PGN synchrony. Synchronization between biological oscillators can be achieved through synchronization to a common periodic drive (Pavlidis, 1973; Winfree, 1980). One important purpose of this study is to examine how PGN synchronization changes in response to the changes of the driving forces such as CRD and LIC-related activity. The strength of coupling between VCN activity and these drives were evaluated in this study by squared coherence (abbreviated as coherence) spectrum. Generation of empirical autospectrum from real data is an estimation process to assign 'best fitted' power density to each harmonic frequency, i.e. the 'amplitude' of the rhythmical component is a random variable to be estimated. If

the 'amplitude' relationship between two activities at each harmonic frequency is evaluated by linear regression, the result is coherence spectrum. Therefore, coherence at a particular frequency provides a measure of the degree of linear correlation between two activities at that frequency (Priestley, 1981; Bendat & Piersol, 1986). It is a bounded parameter between zero, indicating completely unrelated processes, and one, indicating perfect correlation, in the sense of linear regression. It has been used in previous studies to evaluate the coupling of sympathetic nerve activity to various neural activities (Gebber *et al.*, 1994a,b; Kenney, 1994; Kocsis, 1994; Barman *et al.*, 1995; Cohen *et al.*, 1995; Gootman *et al.*, 1996).

3.1.2B Single PGN activity

Similar to that for the population activity, coupling strength of single PGN activity in response to frequency change of a modulatory input such as LIC-related activity was assessed using point process version of coherence spectrum (Rosenberg *et al.*, 1989; Rosenberg *et al.*, 1998). As a measure of linear correlation of rhythmical activity of two point process, it has been used to identify common periodic inputs between two neural spike trains (Rosenberg *et al.*, 1989; Farmer *et al.*, 1997; Rosenberg *et al.*, 1998).

A disadvantage of using coherence to evaluate the correlation between two activities is that shared non-periodic influences are not easily observed in the coherence spectrum and it does not provide phase information which is important for CVA PGNs regarding the functional significance of temporal convergence of their activity. Moreover, problems arise in using coherence to assess the correlation between two weakly coupled activities. This is because when coherence is low, the variance of the coherence estimation increases and

may augment the uncertainty in estimation (Bendat & Piersol, 1986). In Fig. 3.3, simulated PGN point processes that are weakly coupled through a common periodic input are used to illustrate this point. The event series of simulated PGN1 and PGN2 were generated by a stochastic model described in **Appendix I**. The shared input (trigger) had a regular rhythm with the ratio of event dispersion around its dominant frequency less than 15% (see **Appendix I**). The dominant frequencies for PGN1, PGN2 and trigger are 0.60 Hz, 0.70 Hz, and 0.85 Hz, respectively. Their autocorrelograms are shown in Fig. 3.3 Ai-iii. The input influence on the PGNs was simulated by insertion of trigger-related events, with peri-trigger intervals (lags) subject to stochastic variation, into PGN1 and PGN2 series (see Aertsen & Gerstein, 1985 and Christakos, 1994 for a similar procedure). The successful rate for input penetration was about 21% for PGN1 and 25% for PGN2. The coherence between the two PGNs at input trigger frequency (Fig. 3.3 B, asterisk) was low and not clearly distinguishable from the background sample fluctuation, casting uncertainty about this weak correlation.

An alternative to using frequency domain information based on coherence spectrum to assess synchrony between two spike trains is time domain analysis based on cross correlation functions which provide complementary information that may not be easily identified by spectral analysis (Farmer *et al.*, 1997). Cross correlation histogram or cross correlogram (or post-stimulus time histogram, Gerstein & Kiang, 1960), the estimator of cross correlation function, is a measure of the expected past and future firing probability of the output neurone relative to firing times of the input neurone (or trigger neurone). The peri-trigger interval with the maximal firing probability of the output neurone indicates the dominant phase difference of the input-output neurones.

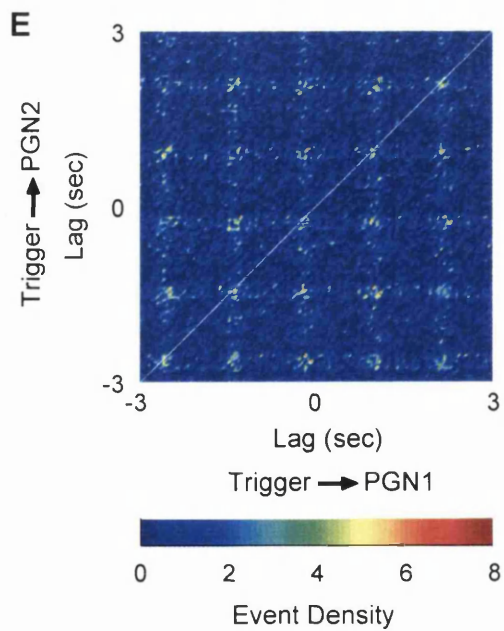
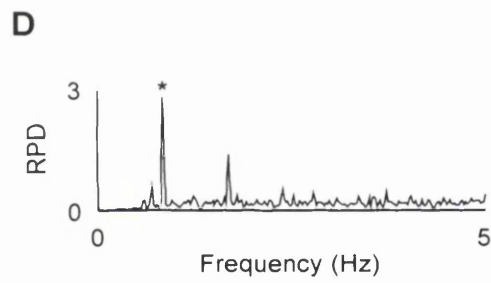
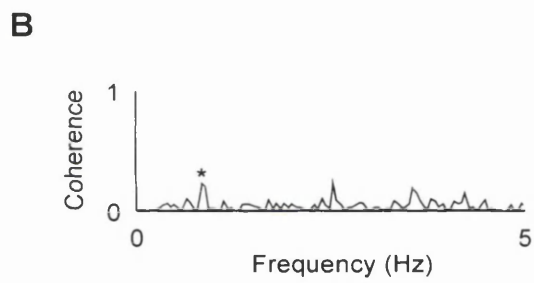
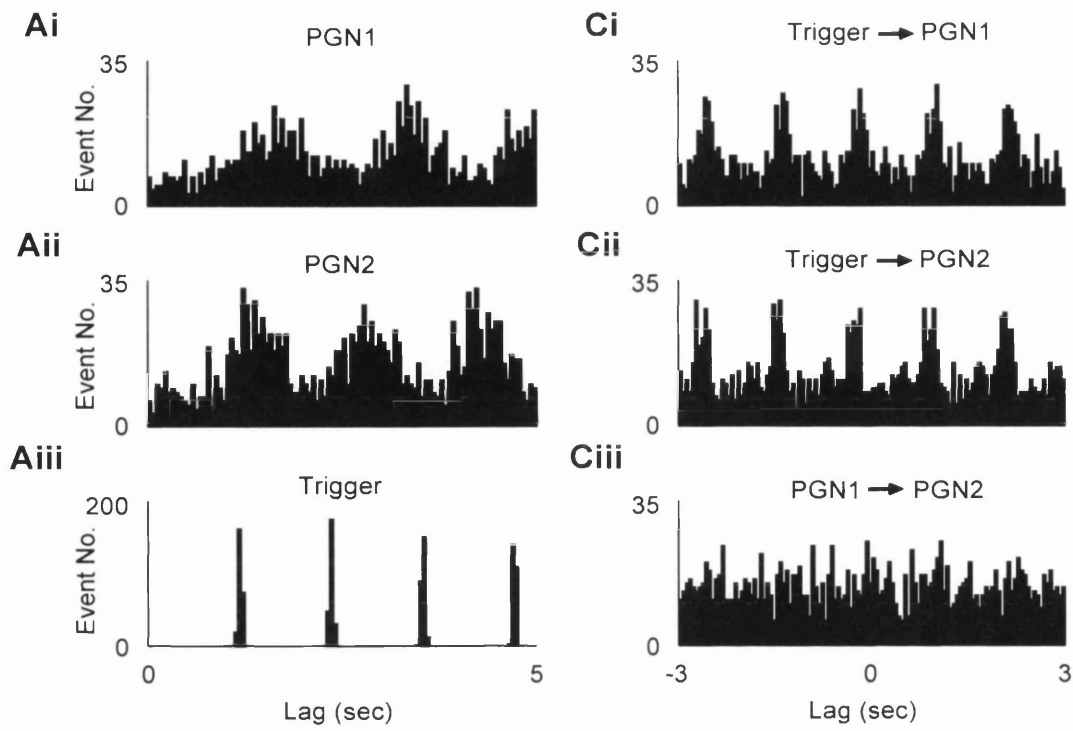


Fig. 3.3 Measurement of the coupling strength between two simulated single PGNs receiving a common input (trigger). Event series of PGN1, PGN2 and the trigger were generated using the stochastic model described in **Appendix I**. Some activity phase-locked to the trigger was inserted to the PGN1 and PGN2 event series (see text). *A_i, A_{ij}, A_{iii}*, The autocorrelograms of PGN1, PGN2 and the trigger, respectively. They had different dominant frequencies (0.6 Hz, 0.7 Hz, and 0.85 Hz for PGN1, PGN2 and the trigger, respectively). *B*, The coherence spectrum between the two PGNs. The small peak (asterisk) at the trigger frequency, which was not much different from the background stochastic fluctuations, suggests weak synchrony through coupling to a common drive, the trigger. *C_i, C_{ii}, C_{iii}*, The trigger→PGN1, trigger→PGN2 and PGN1→PGN2 cross correlograms. Some activity of the two PGNs was phase-locked to the trigger as revealed by the trigger→PGN cross correlograms. The PGN1→PGN2 cross correlogram had no prominent periodic pattern, which suggested periodic coupling between the two PGNs through the trigger was weak. *D*, The envelope autospectrum, scaled with relative power density (RPD), of PGN1→PGN2 cross correlogram. The weak coupling at the trigger frequency was easier to identify in the envelope autospectrum than in the PGN1→PGN2 coherence spectrum (see B) as the dominant peak at the trigger frequency (asterisk) stood out of the background. *E*, Colour-coded joint peri-stimulus scatter plot (JPSP). The detection of weak synchrony through coupling to the trigger was enhanced by JPSP (see text). The clusters of high-density cumulative events along the diagonal line (white) suggests that some activity of both PGNs was phase-locked to the trigger with nearly identical phase lag.

Cross correlation analysis has long been used as a tool to study the interaction between two neuronal activities (Perkel *et al.*, 1967b; Moore *et al.*, 1970; Bryant *et al.*, 1973). The direct effect of input activity on the output neurone was classified as the primary effect (Moore *et al.*, 1970). It was suggested that for a mono-synaptic or oligo-synaptic connection, the primary peak (or trough) around lag zero reflects the time course of the postsynaptic potential (Moore *et al.*, 1970; Knox, 1974; Kirkwood & Sears, 1978). These primary peaks can be observed in situations where input activity has periodic or non-periodic effect on the output neurones. In addition to the primary peaks, secondary peaks may appear in the cross correlogram and in general arise from statistical temporal features of the input and output neurones (Moore *et al.*, 1970). If the input and output neurones exhibit periodic activity, these periodicities may appear, sometimes with complex patterns, in the cross correlogram (Moore *et al.*, 1970; Bryant *et al.*, 1973). In particular, the rhythmicity of input activity will be mapped to both sides of lag zero of the cross correlogram if input activity has cyclic influences on the output neurones and this mapping reflects the strength of connection (Moore *et al.*, 1970). Furthermore, if two output neurones receive a shared periodic input, the cross correlogram of the output neurones will acquire the input periodicity (Moore *et al.*, 1970). It should be noted that periodicity at the input frequency can still emerge in the cross correlogram even though the probability of input penetration is low. This suggests that the rhythmicity on the PGN-PGN cross correlogram can be used as an indication of rhythmical synchronization between the PGNs.

To quantify the rhythmicity of the cross correlogram, the autospectrum of the correlogram envelope was generated and the maximal power density was

used as a measure of the degree of rhythmical synchronization between PGNs. Cross correlograms with envelope autospectra were used in this study to investigate synchrony between weak coupled neurones such as CVA PGNs (see **Chapters Four, Five**). The advantage of this approach is exemplified in the simulated event series in Fig. 3.3. The trigger→PGN1 and trigger→PGN2 (same activity used in Fig. 3.3 A, B) cross correlograms demonstrate that some discharges in the PGNs were phase locked to the triggers (Fig 3.3Ci, Cii). Although rhythmical synchronization was weak as evidenced by the lack of an obvious rhythmicity in PGN1→PGN2 cross correlogram (Fig. 3.3 Ciii), in contrast to its counterpart in the coherence spectrum (Fig. 3.3 B), its envelope spectrum reveals a clear peak activity, at the trigger frequency (asterisk, Fig. 3.3D), which suggests the existence of rhythmical synchronization driven by the trigger.

When the PGN coupling through phase locking to a common driving force was weak, the detection of this synchrony was further enhanced by examining the joint peri-stimulus scatter plot (JPSP). JPSP is used to assess the joint firing probability of two neurones in relationship to a trigger or stimulus (Gerstein & Perkel, 1969). Fig. 3.4 (adapted from Fig. 1 in Aertsen *et al.*, 1989) illustrates the underlying principle of JPSP generation. The abscissa and ordinate represent the peri-stimulus intervals (or lags) of discharges of the triggered neurones. Each dot in the scatter plot indicates the concurrence of discharges of the two neurones at the corresponding peri-stimulus intervals in relation to one stimulus. For example, Fig. 3.4A is the result after one stimulus was applied to two neurones (neurone1, neurone2) and the arrows indicate lag zero, i.e. where a stimulus is applied. For example, the existence of dot D suggests that discharges of the two neurones occur at peri-stimulus interval a and b,

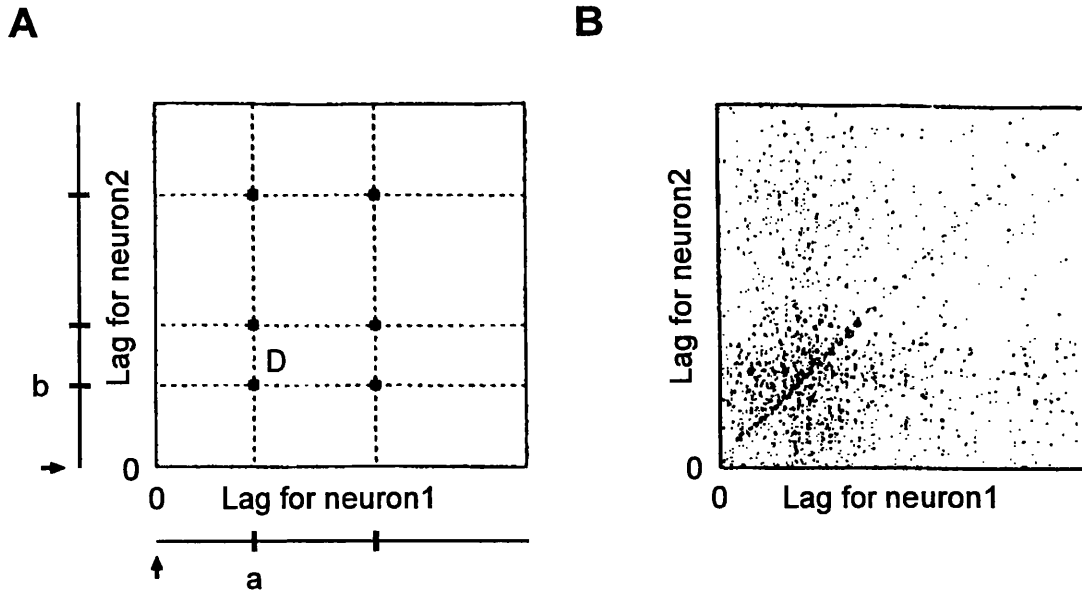


Fig. 3.4 Diagrammatic illustration of the principle to generate a joint peri-stimulus scatter plot (JPSP). Each dot in the JPSP represents the concurrence of discharges of the two neurons, neuron1 and neuron2, at the corresponding peri-stimulus intervals (or lags) in relation to the third activity (or the stimulus). *A*, The JPSP after one stimulus. In this example, the existence of dot D in the JPSP indicates that neuron1 and neuron2 discharges at lag a and b, respectively. The arrows indicate lag zero (i.e. coincidence of stimulation). *B*, The JPSP after repetitions of many stimuli. High probability of concurrent discharges in response to stimulation would appear as clusters with high event density at locations specified by the corresponding lags in the JPSP. In this example, there is high probability for the two neurons to discharge at the same time after stimulation. This was revealed by the high event density along the diagonal line of the JPSP. (adapted from Fig.1 in Aertsen *et al.*, 1989)

respectively. As this process is carried out for many repetitions of the stimuli, a scatter plot with varied event densities indicating concurrent joint firing probability is built up (Fig. 3.4B). If there is high event density along the diagonal band (Fig. 3.4B is an example), this would suggest that nearly zero lag synchrony arises from phase-lock to the stimulus. An example of the application of JPSP is its use in the behavioural neurosciences to study the detailed time structure between firings of cortical neurones and a behavioural marker (Vaadia *et al.*, 1995). The capability of JPSP to detect weak coupling through a common input is illustrated in Fig. 3.3E. The JPSP with colour-coded cumulative event density was generated for the simulated event series used in Fig. 3.3 A, B, C, D. The high density of cumulative events along the diagonal line suggests that some coincident PGN firings arose from phase-lock, with a similar time lag for both neurones, to the triggers. A checkerboard pattern like Fig. 3.3E reflects the fact that the firing probabilities of both neurones are periodically modulated by the periodic drive.

3.1.3 Stability of PGN activity

It should be emphasised that frequency domain spectral analysis and time domain correlation analysis are averaging procedures and any transient fluctuation will be significantly smoothed out. However, evidence is being accumulated that transient changes of the patterns of correlated firing between different neuronal assemblies is important in neural information processing (for review see Singer, 1996; Fetz, 1997) and this may be also true in the sympathetic nervous system (Gebber *et al.*, 1995b). This highlights the importance of studying the dynamic stability of coupling between PGNs using approaches other than the conventional techniques described above.

3.1.3A Population PGN activity

Time evolving autospectra were used to study temporal stability of synchronous firing of constituent PGNs in VCN activity. They were constructed by subdividing the whole data length into several sub-sections and then performing spectral analysis on these sections. The time evolving autospectrum was displayed by joining these sub-autospectra with their preserved temporal orders. The rationale behind this is that if there is a high degree of synchrony between single PGNs it will emerge as a prominent peak in the VCN autospectrum with high power density at the frequency common to these synchronous PGNs. Variation of the strength of synchrony or shift of the common frequency across time will be reflected in the time evolving autospectrum as a change of the power density or drift of the frequency associated with the dominant peak. From the time evolving autospectrum, the total variance of the power density, which includes variance both across the time axis and across the frequency axis, was taken as a measure to quantify temporal stability of synchrony of the constituent PGNs.

3.1.3B Single PGN activity

Along with the distribution of their frequencies, the stability and the distribution of phase differences in a pool of oscillators are major determinants of population rhythm, an output characteristic reflecting underlying synchronous process (Gath, 1974; Christakos, 1986). Temporal stability of phase difference between PGN-PGN or PGN-periodic drive such as CRD was evaluated using ordinary correlation raster plots (OCRPs). Like the cross correlogram, the OCRP shows the phase relationship between the triggers and the dependent

events, but differs because the peri-trigger event series are plotted against each trigger instead of being accumulated to produce a histogram. Each dot in the OCRP (represented by Cartesian coordinate: [time lag, Nth trigger]) indicates a PGN event occurring at the corresponding time lag relative to the associated trigger. If a group of PGN events are clustered in the OCRP, this indicates that these PGN events have a rather stable phase difference relative to the triggers. In particular, if a vertical dense band was present in OCRP, this suggests some PGN activity remains phase locked to the triggers across time, i.e. high temporal stability of synchrony. Furthermore, periodic appearance of the vertical bands is an indication of stability of rhythmical synchronization which occurs between stationary oscillators if a stable phase difference exists in some of their activity.

To quantify the degree of temporal stability of rhythmical synchronization, two factors were taken into consideration. Firstly, if the phase difference remains constant across time PGN events will concentrate on the vertical bands and produce high-density striations on the OCRP against a low-density background. Accumulation of these PGN events in the cross correlogram would result in prominent rhythmicity in its envelope. The maximal power density of the cross correlogram envelope autospectrum (see above) provides a measure of the density of the rhythmical vertical striations in the OCRP. The inverse of this power density is termed envelope spectral factor in this study. The higher this factor is, the less the tendency is that the PGN events would aggregate in periodic vertical bands in the OCRP. The second factor concerns inhomogeneous clustering of PGN events across time. The OCRP was divided into small quadrats and the number of events in each (the event density) was counted. The event density was normalised by the maximal event density in all

the quadrats. The sum of the normalised event density variance at each peritrigger time across the trigger occurrence represents the nonuniform phase change across time (termed density variance factor). It should be noted that the two factors might vary independently of each other. For example, periodic vertical bands with varied event density across time would produce a low envelope spectral factor but a high density variance factor. On the other hand, an OCRP with a uniformly distributed background will have a high spectral envelope factor but a low-density variance factor. The parameter, envelope spectral factor x density variance factor, termed the phase variation factor, is a measure of the level of unstable rhythmicity plus the degree of variation of phase difference across time and was used to assess the stability of rhythmical synchronization between two PGNs.

3.1.4 High order rational frequency-lock between single PGNs and LIC-related activity

The potential for biological oscillators to lock in a high order rational frequency ratio (or commensurate frequencies) other than 1:1 (e.g. 2:1, 3:1, 3:2, etc.) is a feature characterising non-linear interaction of two biologic oscillators (see **Chapter One**). These phenomena have been well described in modelling studies (Pavlidis, 1973; Petrillo & Glass, 1984; Hilborn, 1994). However, to decide whether two frequencies are commensurate in real data, problems arise from the difficulty in determining the exact frequency because any actual measurement of the frequencies has some finite precision dependent on the frequency resolution of the methodology (Hilborn, 1994). The problem of limited frequency resolution is illustrated in Fig. 3.5. Simulated event series (trigger, PGN1, PGN2) were generated according to the stochastic model described in

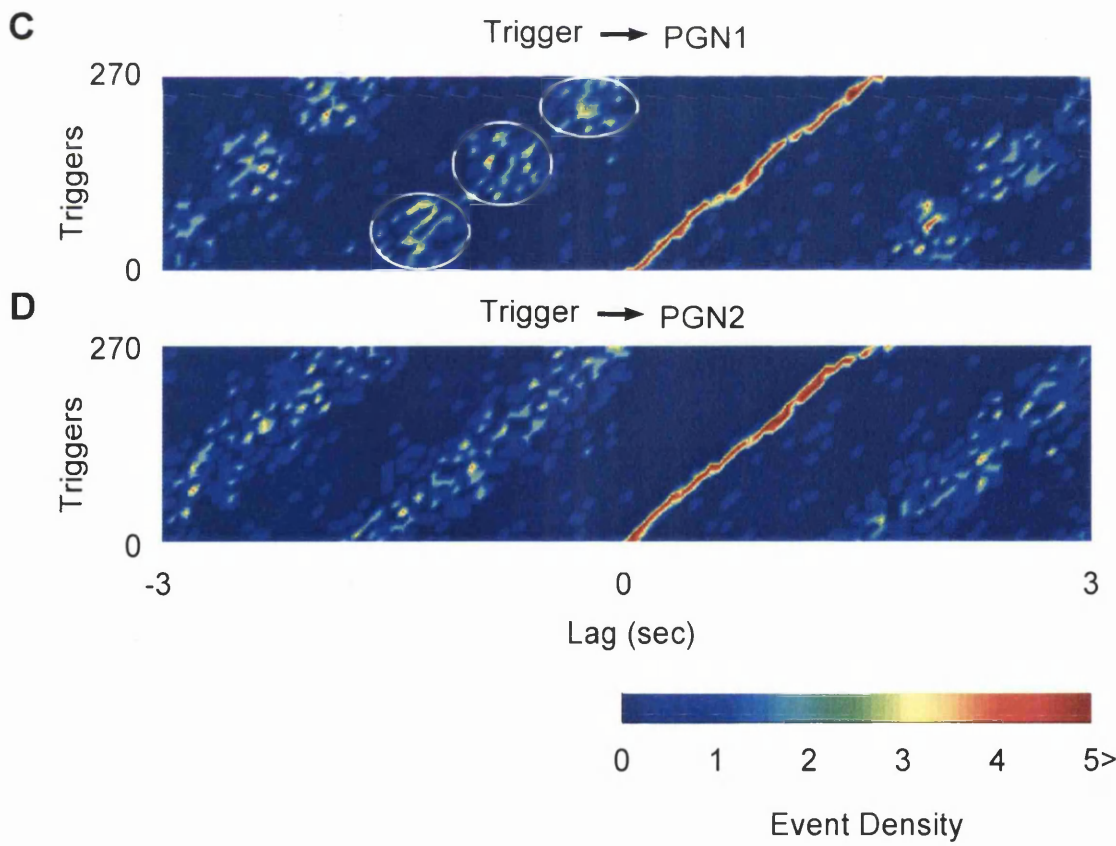
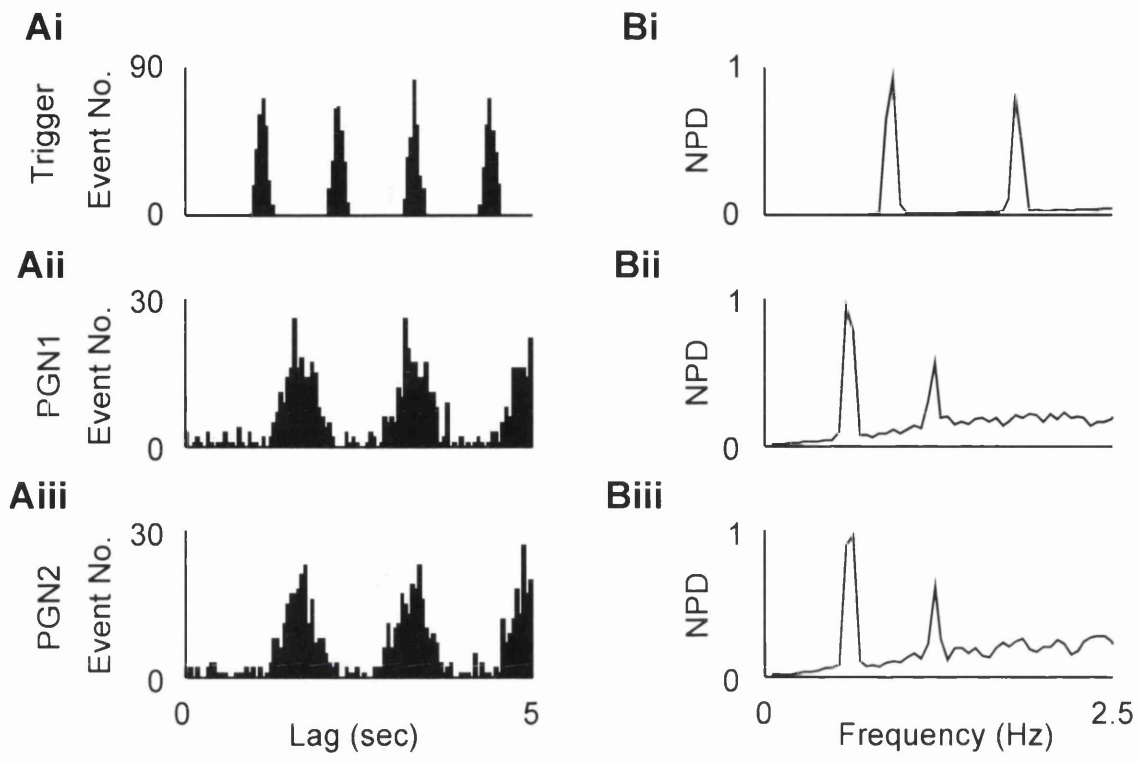


Fig. 3.5 Detection of higher order rational frequency lock by using the reordered correlation raster plot (RCRP). The simulated event series, the trigger, PGN1 and PGN2, were generated according to the stochastic model described in **Appendix I**. The dominant frequencies of the trigger, PGN1 and PGN2 were 0.91 Hz, $0.91 \times (2/3)$ Hz and $0.91 \times (2/3) + 0.005$ Hz, respectively. *Ai, Aii, Aiii*, The autocorrelograms of the trigger, PGN1 and PGN2, respectively. The time course of firing probability was virtually identical for PGN1 and PGN2 and it was difficult to determine whether their dominant frequencies were the same from the autocorrelograms. *Bi, Bii, Biii*, The autospectra (scaled by normalized power density, NPD) of the trigger, PGN1 and PGN2, respectively. The frequency difference of PGN1 and PGN2 was 0.005 Hz, which was beyond the spectral resolution (0.05 Hz) and consequently their frequencies difference could not be discriminated from the autospectra. *C*, Colour-coded trigger→PGN1 OCRP. The PGN1 events were grouped into three distinct clusters (white circles), which was consistent with the fact that the dominant frequencies of the trigger and PGN1 were locked in a simple ratio, 3:2 (see **Appendix IV**). *D*, Colour-coded trigger→PGN2 OCRP. The PGN2 events were clustered into slant bands each of which spanned the whole cycle of PGN2 activity without interruption. These findings suggest that no fixed phase difference was preferred and the frequencies of the trigger and PGN2 were not locked in a simple rational ratio.

Appendix I. The dominant frequencies of the Trigger, PGN1 and PGN2 were 0.91Hz, $0.91 \times (2/3)$ Hz, and $0.91 \times (2/3) + 0.005$ Hz. The frequencies of the trigger and PGN1 were locked in a 3:2 ratio but not the case for the trigger and PGN2. However, from the autocorrelograms (Fig. 3.5 Ai-Aiii) and autospectra (Fig. 3.5 Bi-Biii) it is hard to distinguish which PGN frequency is commensurate with that of the trigger at a 3:2 ratio because the real difference, 0.005 Hz, is beyond the spectral resolution used in this study (~ 0.05 Hz, see below 3.2.1 *Spectral analysis*). It must be emphasised that a difference as small as 0.005 Hz would have a major effect on the phase difference between the trigger and PGN. If their frequencies are not commensurate, even a small difference in the frequencies, i.e. small disparity of their periods, will cause continuous phase drift from cycle to cycle. When their frequencies are commensurate, the phase difference will alternate between some fixed values (see **Appendix IV**).

The different behaviours of phase drift were used to characterise commensurate and incommensurate frequencies in this study. This was achieved by reordered correlation raster plots (RCRPs). The RCRP was generated by reordering the OCRP, sorted by the first post-trigger interval. It should be noted that although the OCRP reveals the temporal order of the phase difference, RCRP does not. By doing this, PGN events with a similar phase difference to the trigger will be grouped into a cluster. The number of clusters depends on how many stable phase differences were observed across time. Continuous drift of phase difference between the trigger and PGN will appear in the RCRP as periodic dense slanting bands with the distance between them the same as the period of the PGN dominant rhythm (see **Appendix IV**). One important application for the RCRPs was to detect commensurate frequencies. It was found that if frequencies of the trigger and

PGN are locked in a $m:n$ ratio where m and n are relative prime positive integers (i.e. the greatest common divisor is 1), m clusters of PGN events (corresponding to m values of phase differences) in a peri-trigger interval identical to the period of the PGN will appear on the RCRP (**Appendix IV**). An exact frequency-lock can be decided by counting the number of discrete event clusters.

The average distance between any two adjoining clusters is the period of $\text{trigger}/n$ or the period of PGN/m (i.e. the greatest commensurate division of the period). In a population of oscillators with frequencies in a narrow range such as PGNs (Johnson & Gilbey, 1996; see also **Chapters Four, Five**), their periods are also bounded in a restricted range. It follows that when the order of rational frequency-lock is too high, i.e. high m and n , the greatest commensurate division of the period will become small and along with unavoidable 'jitters' or stochastic fluctuation of phase differences, the separation of distinct clusters will become difficult to identify. Therefore, this method is not sensitive for detection of frequency-lock with very high orders. However, under such conditions, the phase differences drift between many different values and from the functional point of view, the interaction behaves like that under conditions of incommensurate frequencies. Only low orders such as 2:1 or 3:1 were sought in this study to exemplify the non-linear interaction between PGNs and a periodic drive.

Fig. 3.5 C, D shows the capability of RCRP to differentiate 3:2 frequency-lock for the simulated trigger, PGN1 and PGN2 series (the same event series as in Fig. 3.5 A, B). The PGN events in $\text{trigger} \rightarrow \text{PGN1}$ RCRP (Fig. 3.5 C) were grouped into three clusters (white circles) and this was consistent with a 3:2 frequency-lock ratio. By contrast, no distinct event clusters were identified in the

trigger→PGN2 RCRP, which would suggest incommensurability or very high order commensurate frequency-lock.

3.2 Details of Analysis Methods

3.2.1 Spectral analysis: Autospectrum and coherence spectrum

Autospectra and cross spectra were generated in this study according to Welch method, i.e. averaged modified periodogram, and the algorithm was adapted from a standard textbook (Bendat & Piersol, 1986).

Steps:

1. Divide the data into several half-overlapped blocks. Each block contained 2048 data points. The block number for 8-min data was 45 and for 5-min data, 28. The linear trend was removed from each block unless absolute power density was calculated.
2. Finite Fourier transformation produces side-lobe leakage which may significantly distort the estimated spectrum. This distortion was suppressed by tapering both ends of each block with a Hanning taper defined by $0.5(1 - \cos(2\pi(t/T)))$ where T is the block length and t is time history $[0, \dots, T]$ in the block.
3. Fourier transform (discrete, DFT) each tapered block. For an N -point discrete time series, $\{x_1, x_2, \dots, x_N\}$, DFT is defined by:
$$X(f) = \sum x_k * e^{-i2\pi f k / N}$$
 where f is the discrete frequency (k/N , $k=1, 2, \dots, N$), e , is the Euler number, i is the unit imaginary number and the summation goes through $k=1, 2, \dots, N$. The actual DFT was carried out using a built-in Fast Fourier Transformation (FFT) algorithm in the mathematical software, Matlab (Mathwork, U.S.A.).
4. The tapering procedure to reduce side-lobe power leakage will cause loss of

power and reduce estimated power density. This was compensated by multiplying the result of DFT for each block with an adjust factor, $(8/3)^{1/2}$.

5. The squared norm of the output from step 4 at each discrete frequency was divided by the block length to produce the autospectrum of each block. The estimated autospectrum for the whole data length was obtained by averaging the autospectra from all the blocks.
6. For cross spectrum between two time series, X and Y, the Fourier components of each block, S_X and S_Y , were calculated separately for the two series proceeding through step 1 to step 4. The estimated cross spectrum for each block was given by $S_X S_Y^*$ / block length, where S_Y^* is the conjugate of S_Y . The estimated cross spectrum, C_{XY} , for the whole data length was obtained by averaging the cross spectra from all blocks.
7. The squared coherence (or coherence) at frequency f was given by: $\gamma^2(f) = |C_{XY}(f)|^2 / A_X(f) A_Y(f)$, where A_X and A_Y are the autospectra of series X and Y.

The Matlab script file to calculate the autospectrum and cross spectrum is given in **Appendix V**. The autospectrum was routinely displayed as relative power density or normalised power density (normalised by maximal power density) against frequency. This allowed frequencies with significant power density to stand out of the background. However, when it was necessary to compare PGN activity across experiments, the autospectrum was displayed as absolute power density against frequency (see **Chapter Five**).

To produce autospectra or cross spectra for single PGN activity, the event series are first converted to counting processes (Rosenberg *et al.*, 1989) with a bin size 10 ms, which is equivalent to a 100 Hz sampling rate. Spectral analysis is then carried out on the resultant event count series. The bin size (i.e. the

spectral resolution) for the autospectra in this study is equal to Nyquist frequency (i.e. the maximal frequency without the aliasing effect, see Bendat & Piersol, 1986) divided by the number of bins for the non-negative frequencies, i.e. $(\text{sampling rate}/2)/(\text{FFT size}/2) \approx 0.05 \text{ Hz}$.

The coherence was typically compared across different experimental conditions without specifying the confidence interval for the estimates. However, in order to demonstrate uncorrelation of simulated PGN activity in the modelling study of population activity (see **Chapter Four**), an asymptotic 95% confidence limit, $1-(0.05)^{1/(N-1)}$, where N is the number of blocks used in spectral analysis, was applied to gauge the degree of correlation (Halliday *et al.*, 1995). However, to use this confidence limit, the blocks must be disjointed and therefore no block overlapping was used in this particular case but block overlapping was otherwise routinely used in real data analysis in order to achieve a more consistent estimate (Bendat & Piersol, 1986).

Time evolving autospectra of VCN and PN activity were produced by dividing 8-min data into 12 segments followed by spectral analysis on each segment. The result was then colour-coded. The variance of power density across the time evolving autospectrum of VCN was calculated and taken as a measure of temporal stability of the VCN activity.

3.2.2 Cross correlogram and Autocorrelogram

The value of the tally at lag time λ (or peri-trigger interval) of the $A \rightarrow B$ cross correlogram for two event series, A and B, is given by:

$H(\lambda)_{A \rightarrow B} = \sum \#\{b | a_i + \lambda - \beta/2 < b \leq a_i + \lambda + \beta/2, b \in B\}$ summation over $i=1, 2, \dots, N$, where a_i s are the trigger events in A, N is the number of the triggers, $\#\{\cdot\}$ is the number of the members in the set, $\{\cdot\}$, and β is the binwidth of the histogram. The

histogram was generated by a built-in function in Matlab and the script file to calculate the autocorrelogram and the cross correlogram is given in **Appendix VI**. The binwidth used in this study was 50 ms. It should be noted that $H(\lambda)_{A \rightarrow B} = H(-\lambda)_{B \rightarrow A}$ (Perkel *et al.*, 1967a). It follows that the autocorrelogram ($A=B$) is symmetrical at lag zero and both sides of lag zero provide the same information. Therefore, although the cross correlogram for positive and negative lags was displayed, the autocorrelogram was only displayed for positive lags. An empirical 95% confidence interval was calculated to gauge if the tallies in the cross correlogram deviated significantly from the expected value if the trigger has no influence on the dependent activity (see **Appendix III**).

3.2.3 Envelope autospectrum of cross correlogram

When the autospectrum of the cross correlogram envelope was generated, the cross correlogram was calculated for 300 sec before and after the triggers, i.e. 600-sec peri-trigger interval. The sampling rate in this case was equivalent to 20 Hz because the binwidth was 0.05 sec and 1024 points were used as the block size in calculating the envelope autospectra.

3.2.4 Joint peri-stimulus scatter plot (JPSP)

JPSP was generated using the same approach mentioned in a previous paper (Aertsen *et al.*, 1989). For three event series, A, B, C, the number of coincident events at $[t_1, t_2]$ on the $C \rightarrow A$ vs. $C \rightarrow B$ JPSP, where t_1 and t_2 are the $C \rightarrow A$ and $C \rightarrow B$ peri-trigger intervals respectively, is determined by:

$$P(t_1, t_2)_{C \rightarrow A, C \rightarrow B} = \sum \# \{ (a, b) | a - c_i = t_1 \ \& \ b - c_i = t_2, \ a \in A, \ b \in B \}$$

summation over $i=1, 2, \dots, N$, where c_i s are the trigger events in C, N is the number of triggers.

The resultant JPSP is divided into small quadrats (size: 0.05 sec by 0.05 sec)

and the events in each quadrat are counted followed by colour encoding.

3.2.5 Ordinary correlation raster plot (OCRP) and reordered correlation raster plot (RCRP)

A→B OCRP was displayed as a raster plot, the order of trigger occurrences in A vs. peri-trigger interval. Whether a dot appears at the coordinate, [t, i], is determined by:

$C(t, i)_{A \rightarrow B} = \{b | b - a_i = t, b \in B\}$, where a_i is the i th event in A and t is peri-trigger interval.

If $C(t, i)_{A \rightarrow B}$ is not empty a dot is then assigned to the location [t, i], otherwise nothing is drawn. The procedure then runs from the first trigger with preserving order through all the trigger events in A to build up the raster plot. When OCRP was colour-coded, dots in small quadrats (0.05 sec by 10 triggers) were counted and the dot number was graded by colour. To calculate the density variance factor, quadrats of size, 0.1 sec by 10 triggers, were used to count the event density. The generation of RCRP is similar to that of OCRP except when displayed, the ordinate is not sorted by the order of trigger event occurrences but instead by the order of first post-trigger interval.

3.3 Statistics

Results are expressed as mean±S.D. when a parametric test was used or median and interquartile intervals (1st and 3rd quartiles) when a non-parametric test was used. Either one way analysis of variance (ANOVA) followed by Bonferroni multiple comparison test, Student t-test or Wilcoxon rank-sum test was used to assess statistical significance. In **Chapter Five**, the trend of change of parameters of nerve activity across a range of ventilation frequencies

was evaluated by linear regression. The comparison was considered to be significant if $p < 0.05$.

CHAPTER FOUR

DYNAMIC SYNCHRONIZATION OF MULTIPLE SYMPATHETIC OSCILLATORS

4.1 Introduction

It has been established in previous studies that activity of single CVA PGNs has a dominant rhythm, i.e. they are driven by neuronal oscillators (Johnson & Gilbey, 1994; Johnson & Gilbey, 1996). The purpose of this study is to determine whether different single CVA PGNs are driven by different oscillators and whether synchronization is an obligatory feature of them. This was achieved by studying the discharge behaviour of PGN activity under different conditions of CRD strength. Both population PGN activity and single PGN activity in response to CRD were examined. A stochastic model based on the findings from the single PGN experiments was used to explain the population PGN activity.

4.1.1 A single/common coupled PGN oscillator(s) vs. multiple autonomous PGN oscillators.

To examine the number of autonomous oscillators, the frequency of population PGN activity, i.e. VCN activity (see **Chapter Two**) was examined and frequencies of two single PGN activities recorded simultaneously were compared. If PGN activity is driven by a single/common coupled oscillator(s), periodic activity with a frequency similar to that of single PGN activity should be observed in the population activity and frequencies of simultaneously recorded PGNs should be identical. It is requisite to examine PGN frequencies in the absence of periodic driving forces which may synchronize PGN activity and

result in frequency-lock. For CVA PGN it is important to diminish the effects from CRD and LIC-related activity because previous studies have shown that both activities could modulate PGN activity (Johnson & Gilbey, 1994; Johnson & Gilbey, 1996). To prevent synchronization of PGNs by CRD the experiments were conducted under conditions of central apnea. The effect of lung inflation on PGN activity was minimised by cutting the vagi cut to interrupt afferent activity arising from pulmonary stretch receptors (Kaufman *et al.*, 1982).

Although it was found that stimulation of the aortic nerve could reset single PGN rhythm (Johnson & Gilbey, 1998a), the baroreceptors were not deafferented in these experiments because CVA PGN activity was not modulated by baroreflex activity at cardiac frequency (5-7 Hz in the anaesthetised rats) arising from arterial pulsation (Johnson & Gilbey, 1994; Johnson & Gilbey, 1996). However, this cannot rule out the possibility that CVA PGN activity may be modulated by slower baroreflex mediated periodic activity arising from ventilation-induced blood pressure undulation. This effect was minimised by thoracotomy to prevent cardiac output fluctuations due to ventilation. Furthermore, the rib cage was lifted to reduce phasic chest wall movement during ventilation and thus reduced the somato-sympathetic interaction which may originate from activation of intercostal sensory nerve endings (Dembowsky *et al.*, 1985; Zanzinger *et al.*, 1994).

4.1.2 Dynamics of synchronization between PGNs under conditions of different CRD.

Whether periodic CVA PGN activity originates from a common oscillatory source raises a question regarding synchronization of their activity. When the system is free from external influences, while synchrony is not an obligatory

feature in a population composed of multiple oscillators, the hypothesis of a common rhythm generator would imply that discharges of single PGNs are always synchronous. When the system is subjected to an 'external' driving force, if activity of single PGNs is generated from a common oscillator, they may still remain synchronous or the synchrony may be disrupted if there are differential influences on single PGNs. By contrast, if single PGNs are driven by multiple oscillators, the probability of synchronization may increase because it is known that synchronization can be achieved by coupling individual oscillators to a common drive (Winfree, 1980). In either case, the presence of a common drive may affect the synchrony of CVA PGNs.

In this study, CRD was used as a periodic driving force to examine synchrony of CVA PGNs. If most of the single PGNs are synchronized through coupling to CRD, rhythmicity at CRD frequency should be a prominent constant feature of population PGN activity. The dynamics of synchronization were studied by manipulating the strength of CRD. This was achieved by examining synchrony between PGNs under conditions of 1) absence of CRD (high PaO₂ and/or low PaCO₂) 2) normal control (normal PaO₂ and PaCO₂) 3) enhanced CRD (normal PaO₂ and high PaCO₂, St-John & Bianchi, 1985).

Some experiments were also carried out in spontaneously breathing animals to examine whether similar discharge behavior of PGNs can be observed under more natural conditions.

4.1.3 Modelling the discharge behavior of population PGN activity.

The findings of population PGN activity under different conditions of CRD were explained by using a stochastic model of single PGN activity. Data from single PGN experiments were used as a basis for modelling population activity.

4.2 Materials and Methods

4.2.1 Whole nerve experiments

VCN activity was recorded as population PGN activity from sixteen animals. Thirteen of these were ventilated artificially and the other three breathed spontaneously. In each experiment, nerve activity was recorded initially in control conditions. Of the thirteen artificially ventilated rats, eight animals were tested under enhanced CRD conditions and eight in the absence of CRD. Six of the thirteen animals were tested in all three conditions. The sympathetic nature of VCN activity was tested by applying a sympathetic ganglionic blocker, chlorisondamine, to the animals (N=10). Data was recorded for 8 minutes under each condition.

4.2.2 Single PGN experiments

Pairs of action potentials of single PGNs were recorded from seventeen animals. Twelve of these were ventilated artificially and the remainder breathed spontaneously. At least one pair of PGNs was recorded in each animal during control conditions. Six artificially ventilated and four spontaneously breathing subjects were tested under enhanced CRD conditions. Neuronal activity was also recorded in six artificially ventilated rats in the absence of CRD. Five of the eleven artificially ventilated animals were tested in all three conditions. Data was recorded for 5 minutes under each condition.

See **Chapter Two** for details of experimental preparations.

4.3 Data analysis

Autospectra were used to determine the frequency of PN and the dominant rhythm of single and population PGN activity. Autocorrelograms of single PGNs

were generated first to confirm the existence of rhythmicity. Autospectra were scaled with relative power density. Linear correlation between VCN and PN was assessed by coherence spectra. PN-single PGN and single PGN-single PGN cross correlograms were generated to examine the existence of rhythmical synchronization.

Time evolving VCN autospectra were used to evaluate temporal stability of the population rhythmical activity. The temporal stability was quantified by total variance of power density of this time evolving autospectrum. Stability of rhythmical phase lock between PN-single PGN or single PGN-single PGN was assessed by the ordinary cross correlograms (OCRP). To provide a quantitative measure of temporal stability of PGN-PGN phase difference, the phase variation factor under conditions of different CRD was calculated and compared. See **Chapter Three** for details of analysis.

4.4 Results

4.4.1 Condition of animals

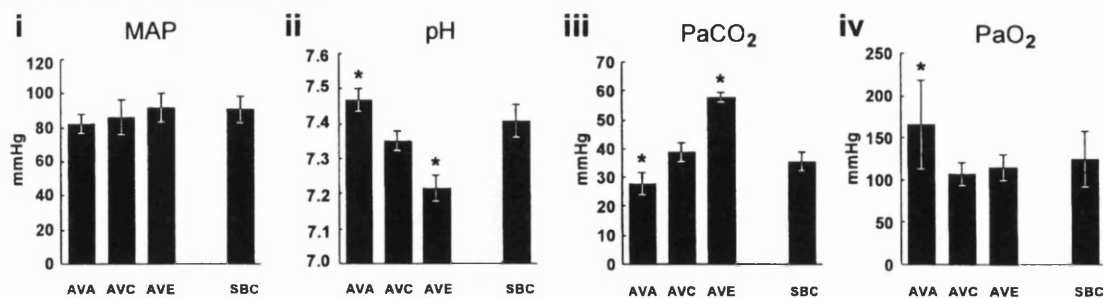
The animals were maintained in a consistent physiological state in each of the experimental conditions as indicated by measurements of four parameters. Fig. 4.1A summarises the mean arterial blood pressure (MAP) (Fig. 4.1Ai), pH (Fig. 4.1Aii), PaCO₂ (Fig. 4.1Aiii) and PaO₂ (Fig. 4.1Aiv) for the whole nerve recording experiments for four conditions; artificially ventilated, absence of CRD (AVA), artificially ventilated, control (AVC), artificially ventilated, enhanced CRD (AVE) and spontaneously breathing, control (SBC) animals. Fig. 4.1Bi-iv summarises the same parameters for the single PGN recording experiments for the four conditions stated above plus an additional condition; spontaneously breathing, enhanced CRD (SBE).

4.4.2 Whole nerve activity recorded from the VCN in artificially ventilated animals

4.4.2A Rhythmical and sympathetic nature of VCN activity

The nerve activity recorded from the VCN appeared as burst discharges with variable frequency and amplitude. A typical example (artificially ventilated, control) is shown in the neurogram in Fig. 4.2A. The major rhythmical component of the activity was revealed by the presence of a prominent peak at 0.63 Hz in the autospectrum (Fig. 4.2Bi). After application of chlorisondamine, this led to abolition of most of the activity and power in the autospectra in all cases (N=10) (see Fig. 4.2Bii and 4.2C). This indicated that activity recorded from the VCN was sympathetic in nature.

A Whole nerve experiments



B Single PGN experiments

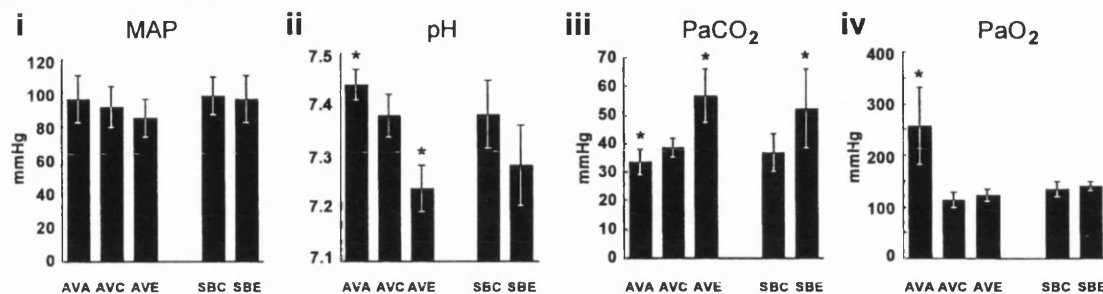


Fig. 4.1 Physiological parameters of experiments under different respiratory conditions. Conditions: AVA: artificially ventilated, absence of CRD; AVC: artificially ventilated, control; AVE: artificially ventilated, enhanced CRD; SBC: spontaneously breathing, control; SBE: spontaneously breathing, enhanced CRD. *A*, Whole nerve experiments. AVA: N=8; AVC: N=13; AVE: N=8; SBC: N=3. *B*, Single PGN experiments. AVA: N=6; AVC: N=13; AVE: N=6; SBC: N=6; SBE: N=4. *Ai*, *Bi*, Mean arterial pressure (MAP). *Aii*, *Bii*, pH. *Aiii*, *Biii*, PaCO₂. *Aiv*, *Biv*, PaO₂. Data are presented as mean±S.D. Statistical differences between the three subgroups of artificially ventilated animals were assessed using ANOVA followed by Bonferroni multiple comparison tests. A Student t-test was used to test the difference between the two subgroups in spontaneously breathing animals. Parameters that are significantly different from control conditions are indicated by an asterisk (*, p<0.05).

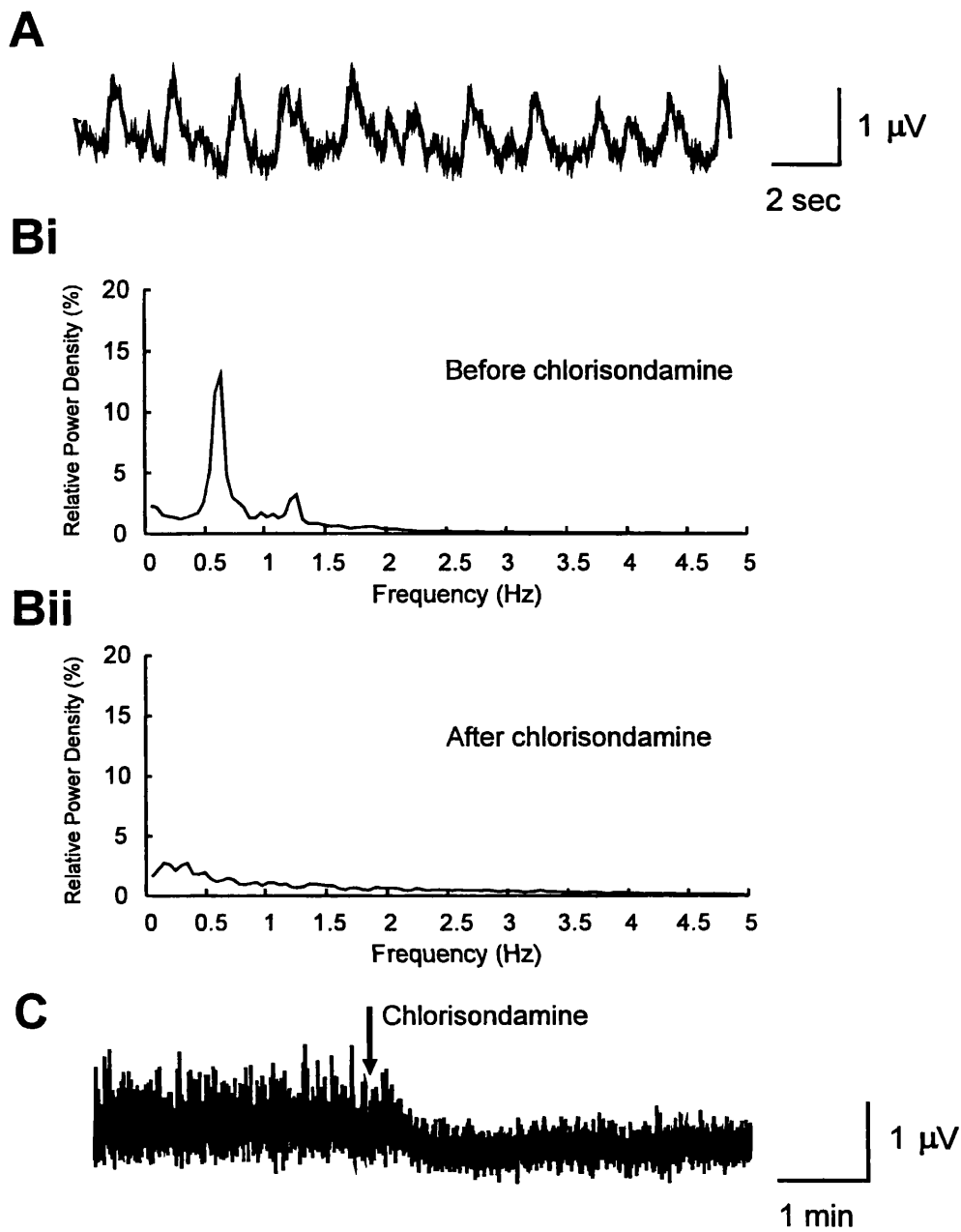


Fig. 4.2 The bursty and sympathetic nature of VCN activity in an artificially ventilated animal under a control CRD condition. *A*, Rectified and smoothed neurogram of VCN activity shows burst discharges with variable frequency and amplitude. *Bi*, Autospectrum of VCN activity shows a peak at 0.63 Hz with its 1st harmonic peak at 1.26 Hz. *Bii*, Autospectrum of activity of the same VCN in *Bi*, following chlorisondamine (3 mg kg⁻¹ I.V.), a sympathetic ganglionic blocker. The abolition of the peaks following this treatment shows that the nerve activity was sympathetic in nature. *C*, Real time neurogram of the same VCN activity before and after application of chlorisondamine.

4.4.2B Synchronous components in VCN activity become more prominent with increased CRD

VCN activity was recorded in animals under three different respiratory conditions, absence of CRD, control, and enhanced CRD. In each condition, autospectra for VCN and PN activity were generated and coherence spectra were produced to identify correlated components in their activity. Here, the results are presented first in the absence of CRD, then control and finally enhanced CRD, to emphasise the trend towards synchronization with increasing CRD.

In animals in which the CRD was abolished, a single prominent peak (median: 0.83 Hz, interquartile interval: 0.79-0.88 Hz) was observed in the VCN autospectra in all cases (N=8). This peak was in the frequency range of the T-rhythm (Johnson & Gilbey, 1994; Johnson & Gilbey, 1996) and it is referred as the T-peak. A typical example, in which the T-peak frequency is 0.82 Hz, is shown in Fig. 4.3Ai. The absence of CRD is indicated by the flatness of the autospectrum of the PN (Fig. 4.3Aii) and the lack of correlation between VCN and PN activity is shown by the coherence spectrum (Fig. 4.3Aiii).

Thirteen animals were examined under control conditions. In six (46%) of these, the VCN autospectra revealed a T-peak (median frequency: 0.79 Hz, interquartile interval: 0.74-0.82 Hz). Statistical comparisons between animals in the absence of CRD and in control conditions (where a discrete T-peak was present) demonstrated that the T-peak frequencies were not significantly different ($p=0.44$, Wilcoxon rank-sum test). In twelve (92%) of the animals, a peak at the CRD frequency was present (median frequency: 0.63 Hz, interquartile interval: 0.59-0.68 Hz). The coherence at the frequency of CRD between VCN and PN activity, revealed by the coherence spectrum, was high

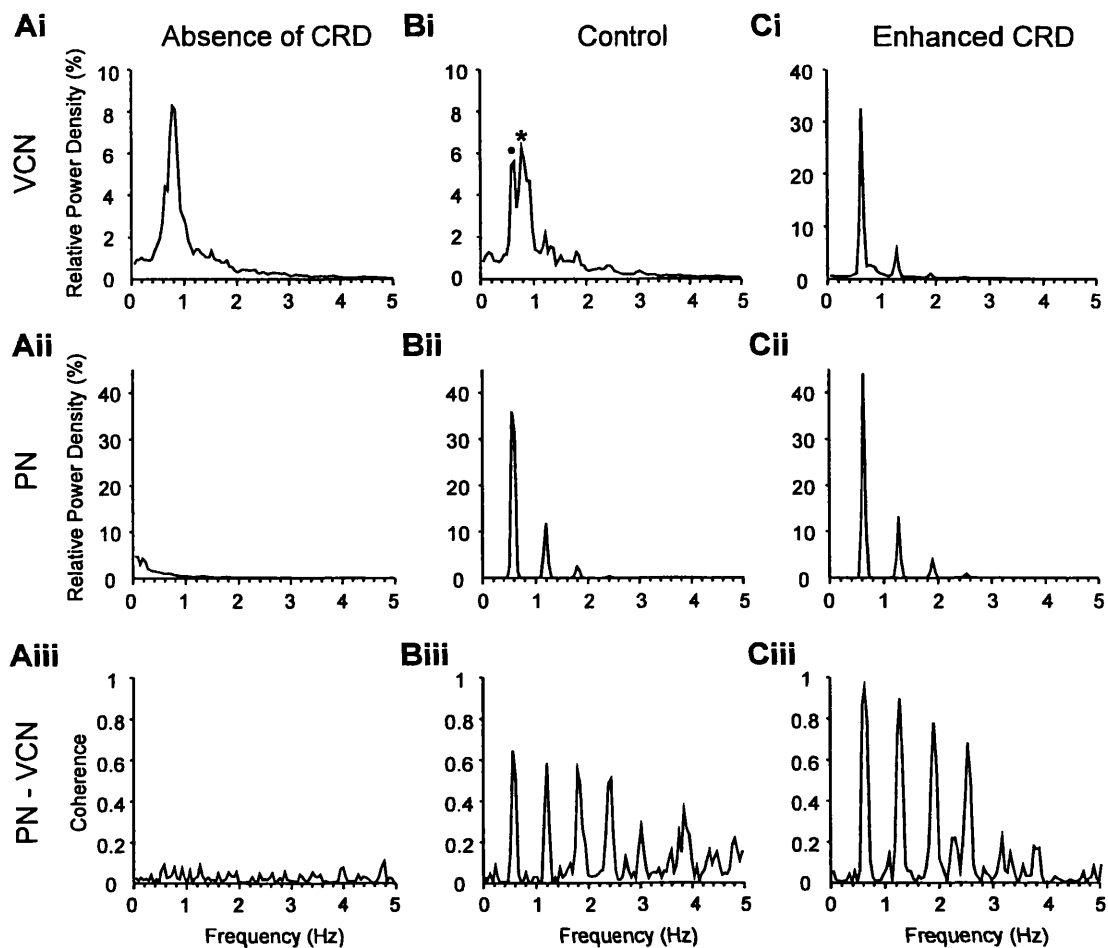


Fig. 4.3 The autospectra and coherence spectra of the VCN and PN in an artificially ventilated animal under three conditions of CRD. *A*, Absence of CRD. *Ai*, Autospectrum of VCN activity reveals a peak at 0.82 Hz. *Aii*, Autospectrum of PN activity shows no rhythmical components. *Aiii*, The coherence spectrum of VCN and PN shows lack of correlation between the two nerves. *B*, Control condition. *Bi*, Autospectrum of VCN activity shows two peaks, one (•) at 0.59 Hz was the same as the frequency of CRD, revealed in the autospectrum of the PN (see *Bii*) and a second, (*) at 0.79 Hz. *Bii*, Autospectrum of PN activity. *Biii*, The coherence spectrum between VCN and PN reveal high coherence at the frequency of CRD. *C*, Enhanced CRD. *Ci*, Autospectrum of VCN is dominated by a peak at 0.63 Hz (and its first harmonic component), which is the same as the frequency of CRD. Note the scale of relative power density is different from that in *Ai* and *Aii*. *Cii*, Autospectrum of PN activity. Comparison of the relative power density of the peak with control conditions shows that the level of CRD was increased. *Ciii*, VCN and PN activity show a high coherence.

(median: 0.73, interquartile interval: 0.63-0.88). The VCN autospectrum from one of the animals displaying both the T-peak and the respiratory-related peak is shown in Fig. 4.3Bi (this is the same animal as in Fig. 4.3A). The first peak at 0.59 Hz (•) corresponds to the main peak in the PN activity (Fig. 4.3Bii) and this was confirmed by the coherence spectrum shown in Fig. 4.3Biii. The additional peaks in the PN autospectrum were harmonics of the first peak and these also displayed high coherence with VCN activity. Lack of coherence between VCN and PN at the frequency of the second peak (*, 0.79 Hz) is also demonstrated in Fig. 4.3Biii.

A condition of enhanced CRD was induced in a subset of the animals (N=8) examined in control conditions. In all cases, there was a prominent respiratory-related peak in the VCN autospectra (median frequency: 0.59 Hz, interquartile interval: 0.53-0.63 Hz) which showed a very high coherence with the phrenic autospectra (median coherence: 0.90, interquartile interval: 0.76-0.92). In two (25%) of the animals there was also a separate T-peak (frequency: 0.73 and 0.68 Hz respectively). The RPD of the respiratory-related peak when the CRD was enhanced (median of the RPD: 14.2, interquartile interval: 9.75-19.8) was higher than that of the T-peak when CRD was abolished (median of the RPD: 4.14, interquartile interval: 3.7-6.4) ($p < 0.02$, Wilcoxon rank-sum test). This suggests that the dominant rhythmical activity became more prominent when the condition was switched from absence of CRD to enhanced CRD. A typical example of the VCN autospectrum in an animal with enhanced CRD is shown in Fig. 4.3Ci (this is the same animal as in Fig. 4.3A, 4.3B). There is a prominent peak at 0.63 Hz which has a high coherence with the PN discharge (Fig. 4.3Cii, 4.3Ciii); other peaks at harmonic frequencies of PN activity are also visible.

4.4.2C Stability of VCN rhythmical activity increases when the CRD is enhanced

VCN activity was also examined using colour-coded time-evolving autospectra, which provide information about the dynamics of the rhythmicity across time. When the CRD was abolished, VCN rhythmical activity was relatively unstable. The example shown in Fig. 4.4Ai (same animal as in Fig. 4.3), shows a band containing relatively high and low density components in the T-rhythm frequency range, indicating periods of strong and weak synchrony of rhythmical firing in the PGN population. No prominent bands were visible in the phrenic time-evolving autospectra confirming that CRD was abolished (see Fig. 4.4Aii). In control conditions, as shown in the example in Fig. 4.4Bi (same animal as in Fig. 4.3), part of the wide band with varied power density in VCN activity fell within the frequency range of the band observed in the phrenic time-evolving autospectra (see Fig. 4.4Bii). However, while the phrenic activity produced a dense, stable band, the VCN showed transient periods where band density was reduced, indicating periods of reduced rhythmical activity. It should be noted that the two peaks in the VCN autospectrum (indicated by • and * in Fig. 4.3Bi) did not correspond to separate stable bands in the time-evolving autospectrum (Fig. 4.4Bi). This indicates that the respiratory-locked activity in the PGN population underwent dynamic change. In conditions of enhanced CRD, the VCN time-evolving autospectra (example in Fig. 4.4Ci from the animal shown in Fig. 4.4A, 4.4B) was similar to the phrenic autospectra (Fig. 4.4Cii), exhibiting stable narrow bands at the phrenic frequency and its harmonics. This suggests that a substantial proportion of the PGNs were synchronized to phrenic activity throughout the time period examined. The level of stability in each condition was quantified using a measure of the power density variance across time (see

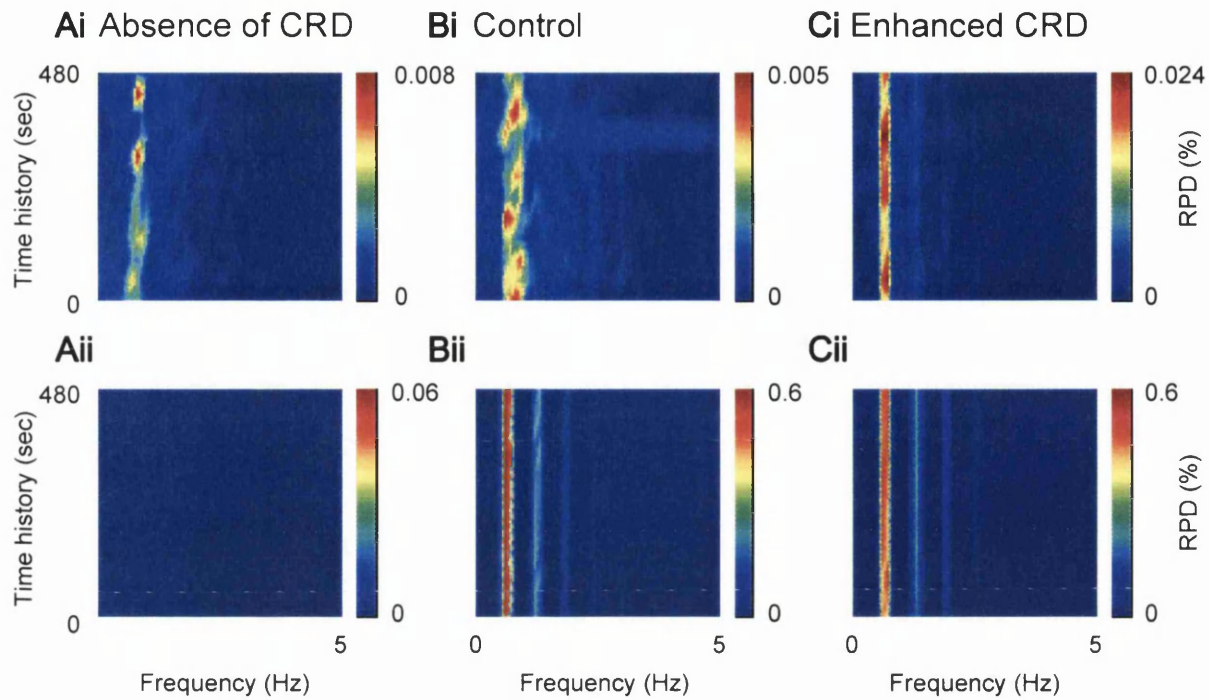


Fig. 4.4 Time evolving autospectra of VCN and PN under three conditions of CRD. Nerve activity was recorded from the same animal and across the same time periods as in Fig. 4.3. The data was divided into twelve 40 second subsections. Spectral analysis was performed on each subsection. The relative power density (RPD) across time is colour-coded (note the scale bar on right of each figure is different). *A*, Absence of CRD. *Ai*, VCN autospectrum shows that the power of the VCN was concentrated at a band around 0.82 Hz but the power density varied across time. *Aii*, PN autospectrum shows little or no power across time. *B*, Control condition. *Bi*, VCN autospectrum shows that the power of the VCN was concentrated in a relatively well-defined band between 0.54 and 1.05 Hz, including the frequency of CRD (0.59 Hz, see *Bii*). It should be noted that the two dominant peaks of the VCN autospectrum revealed in Fig. 4.3Bi were not constant across time; it was a feature arising from dynamic change of the power density within the narrow frequency band. *Bii*, PN autospectrum. *C*, Enhanced CRD. *Ci*, VCN autospectrum reveals that the relative power density of the VCN was very constant across time and centred at the frequency of CRD (0.63 Hz, see *Cii*). *Cii*, PN autospectrum.

Chapter Three). The data is summarised for the absence of CRD (N=8), control (N=13) and enhanced CRD (N=8) groups in Fig. 4.5. Comparisons between conditions of absent CRD and enhanced CRD revealed a significant difference ($p < 0.05$, Wilcoxon rank-sum test).

4.4.2D Heart rate- and LIC-related discharge in the VCN activity

Under all conditions, no spectral peak at cardiac frequency was observed in the VCN autospectra. On the other hand, a small peak at LIC frequency with high coherence (median of coherence: 0.68, interquartile interval: 0.50-0.81) was observed in the VCN autospectra in sixty two percent of whole nerve experiments (absence of CRD: 6/8; control: 7/13; enhanced CRD: 5/8). A typical example under control condition is shown in Fig. 4.6. In addition to the dominant peak at 0.63 Hz (arrow, Fig. 4.6 Ai), this VCN autospectrum had another small peak (*) at LIC frequency (1.61 Hz, Fig. 4.6 Aii). The high coherence (0.79) at LIC frequency demonstrated that this peak was highly correlated to LIC-related activity (Fig. 4.6 Aiii). It was not a spurious phenomenon arising from ventilatory movement artifacts because this LIC-related peak and the high coherence were abolished after sympathetic ganglionic blockade by giving chlorisondamine (Fig. 4.6 Bi-iii). The relationship between LICs and PGN activity will be addressed in **Chapter Five**.

4.4.3 Whole nerve activity recorded from the VCN in spontaneously breathing animals

Three animals were recorded under spontaneously breathing conditions to determine whether VCN activity behaved in a similar way to that seen in artificially ventilated animals. In all three, the VCN autospectra revealed a T-

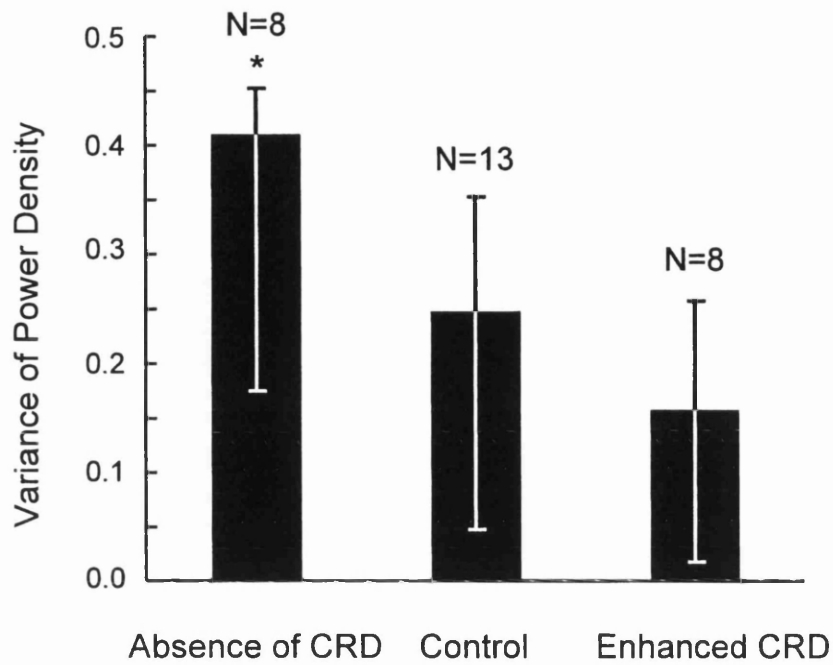


Fig. 4.5 Dynamic stability of rhythmical components evaluated by the variance of the relative power density of VCN activity across time in artificially ventilated animals under three conditions of CRD. Data are presented as medians and 1st and 3rd quartiles. The level of power density variance is inversely proportional to the level of stability. The asterisk, *, indicates that the power density variance in the absence of CRD was significantly higher than the variance in conditions of enhanced CRD (Wilcoxon rank-sum test, $p < 0.05$).

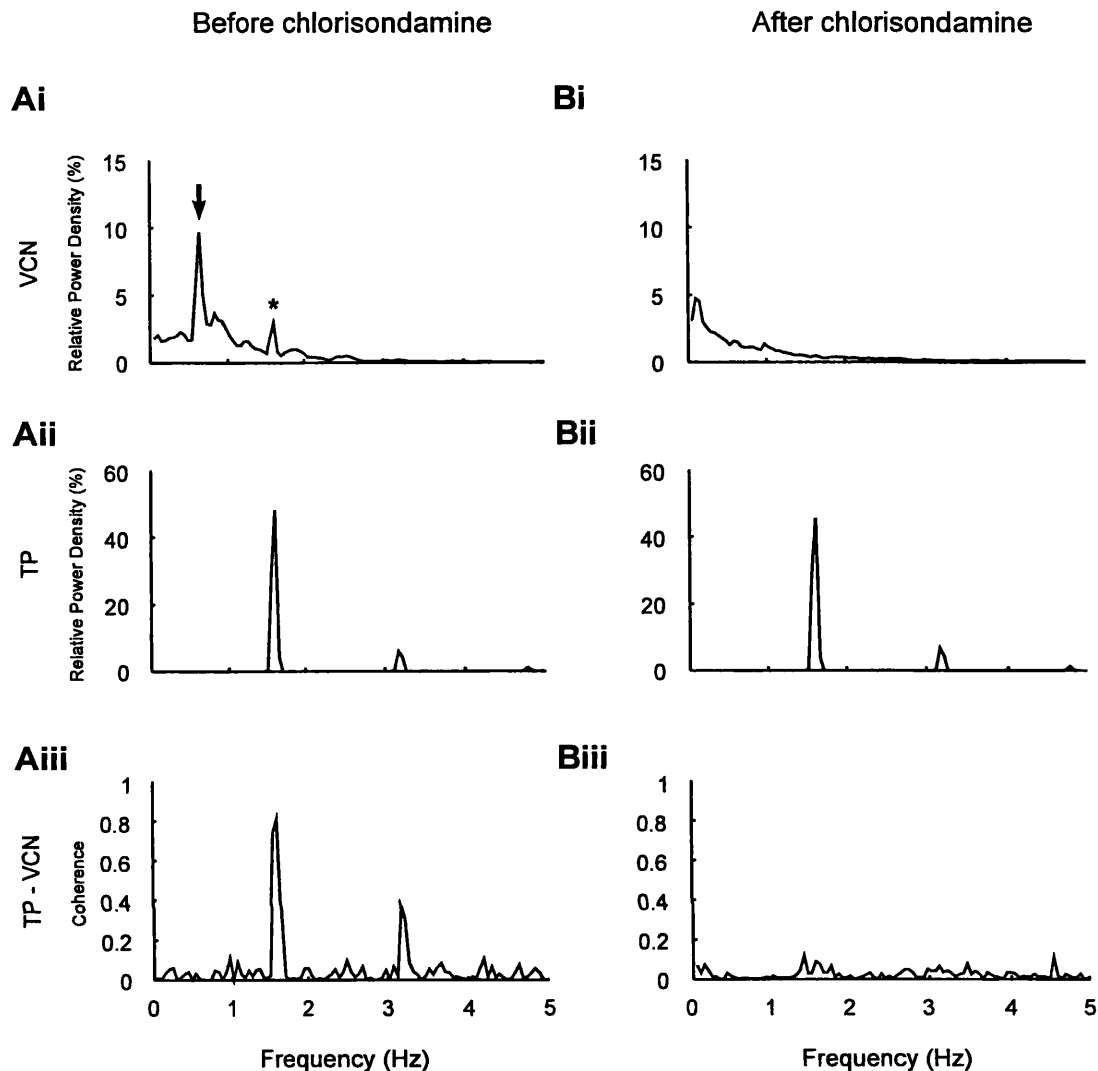


Fig. 4.6 Lung inflation cycle (LIC) related activity in VCN activity recorded from an artificially ventilated animal under a control CRD condition. *A*, Experiment before application of a sympathetic ganglionic blocker, chlorisondamine (3 mg kg⁻¹ I.V.). *Ai*, Autospectrum of VCN activity. In addition to the dominant peak at 0.63 Hz (↓), there was another minor peak at tracheal pressure (TP) frequency (*, 1.61 Hz). *Aii*, Autospectrum of TP. *Aiii*, Coherence spectrum between VCN activity and TP shows that the LIC-related activity in the VCN was correlated to TP with high coherence (0.79). *B*, Experiment after application of chlorisondamine. *Bi-Biii*, The abolishment of the VCN spectral peaks and the high coherence between VCN activity and TP demonstrates that the LIC-related activity in the VCN before application of chlorisondamine was not a movement-induced artifact.

peak with a median frequency of 0.60 Hz (interquartile interval: 0.56-0.66 Hz) and a second peak with a median frequency of 0.93 Hz (interquartile interval: 0.90-1.10 Hz), which showed high coherence with the PN activity (median: 0.52, interquartile interval: 0.51-0.62). This demonstrated that VCN activity of spontaneously breathing animals contained rhythmical components similar to those identified in artificially ventilated preparations.

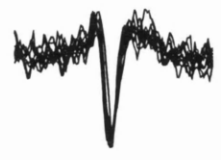
4.4.4 Paired recordings of PGNs innervating the CVA in artificially ventilated animals

4.4.4A In the absence of CRD the T-rhythms seen in PGNs recorded simultaneously show a low probability of synchronization

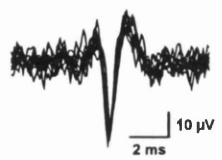
Activity of six pairs of PGNs (6 animals), each from separate electrodes, was recorded in the absence of CRD. The discharges of individual PGNs, examined by autocorrelograms and autospectra, were rhythmical in nature. The median frequency of the T-rhythm was 0.61 Hz (interquartile interval: 0.54-0.64 Hz). Although activity of all PGNs showed a dominant peak in the range of T-rhythm frequency in the autospectrum, neither of the PGNs in a pair had the same T-rhythm frequency and cross correlogram analysis revealed that no significant rhythmical synchronization was displayed in PGN→PGN activity.

Fig. 4.7Ai, Aii show ten superimposed action potentials for each of a pair of PGNs, illustrating the consistency of the spike shape and amplitude. A section of the real time neurograms of these two PGNs and PN is shown in Fig. 4.7Aiii. The autocorrelograms from these two PGNs, in the absence of CRD, are shown in Fig. 4.7Bi, 4.7Bii. These PGNs both exhibited characteristic rhythmicity, but the frequencies are different (0.54 Hz for PGN1, 0.69 Hz for PGN2). The PGN1→PGN2 cross correlogram shown in Fig. 4.8A, does not show a

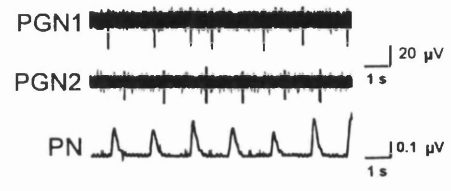
Ai PGN1 (10 spikes)



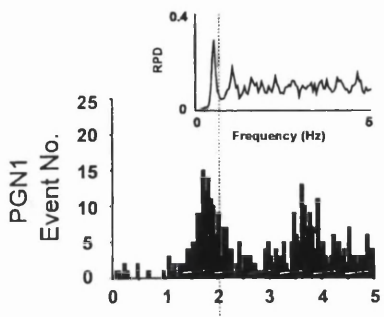
Aii PGN2 (10 spikes)



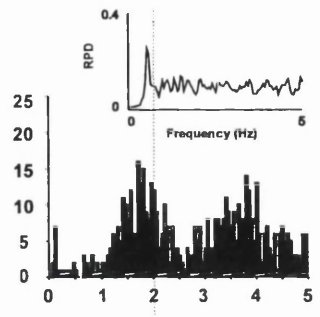
Aiii



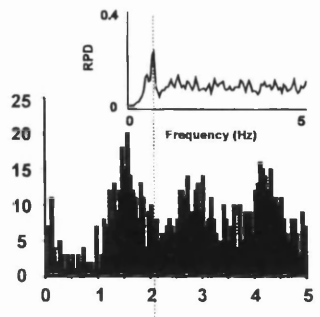
Bi Absence of CRD



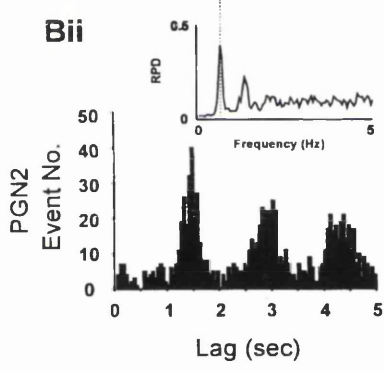
Ci Control



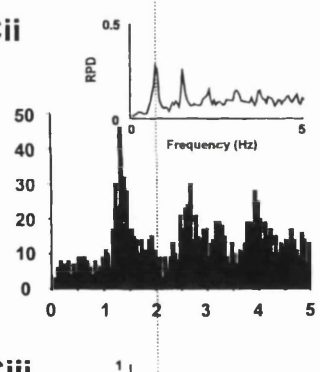
Di Enhanced CRD



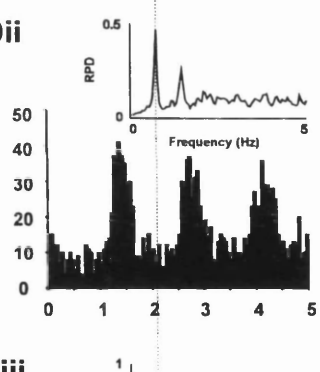
Bii



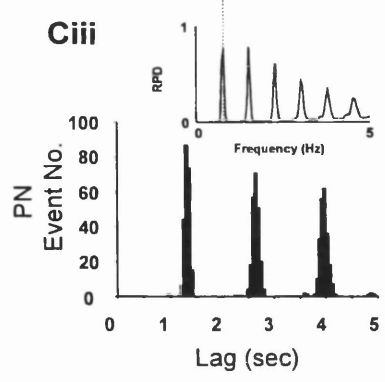
Cii



Dii



Ciii



Diii

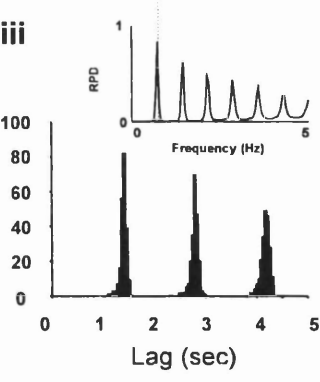


Fig. 4.7 Neurograms and frequency relationships of two PGNs and PN activity recorded simultaneously in an artificially ventilated animal under three conditions of CRD. *Ai, Aii*, Ten superimposed spikes recorded from the PGNs demonstrate the consistency of the shape and amplitude of the action potentials. *Aiii*, Typical example of a real time neurogram showing the temporal relationship between PGN and PN activity under control conditions. *B–D*: Autocorrelograms and autospectra (insets) of PGN and PN activity. The dashed lines across the autospectra allow comparisons between the frequencies of the T-rhythms and PN activity. *B*, Absence of CRD. *Bi*, PGN1 autocorrelogram (167 triggers) and autospectrum. *Bii*, PGN2 autocorrelogram (252 triggers) and autospectrum. *C*, Control condition. *Ci*, PGN1 autocorrelogram (199 triggers) and autospectrum. *Cii*, PGN2 autocorrelogram (298 triggers) and spectrum. *Ciii*, PN autocorrelogram (227 triggers) and autospectrum. *D*, Enhanced CRD. *Di*, PGN1 autocorrelogram (235 triggers) and autospectrum. *Dii*, PGN2 autocorrelogram (324 triggers) and autospectrum. *Diii*, PN autocorrelogram (215 triggers) and autospectrum.

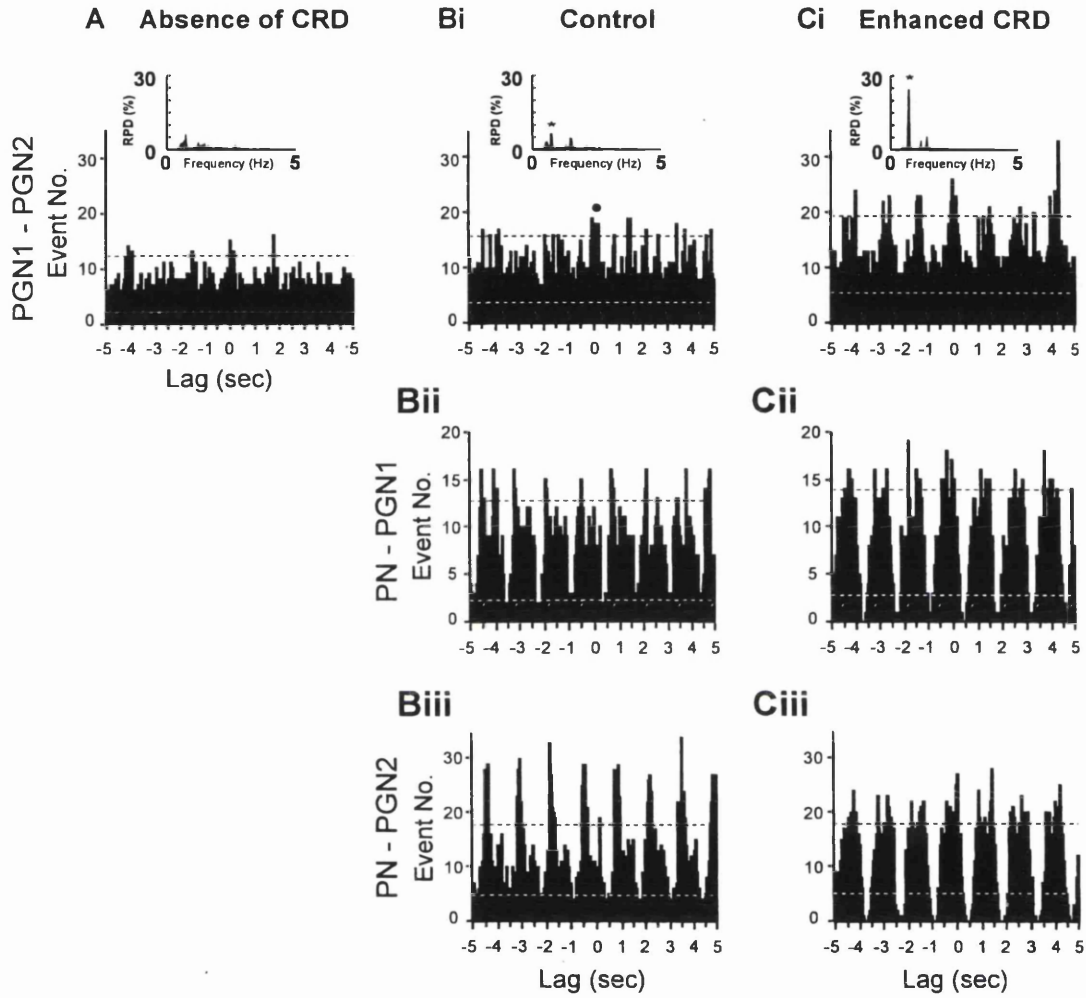


Fig. 4.8 Rhythmical PGN→PGN and PN→PGN synchronization revealed by cross correlograms under three conditions of CRD. The PGNs and the period of analysis are the same as in Fig. 4.7. If rhythmical synchronization exists between two neural activities, a periodic pattern should be observed in the cross correlogram. The dashed lines in the cross correlograms define the upper and lower limits of the 95% confidence interval. Significant rhythmical synchronization is indicated by the presence of periodic peaks (or troughs) over the 95% confidence interval. The degree of rhythmical synchronization was quantified by the autospectrum (scaled by relative power density, RPD) of the cross correlogram envelope (see **Chapter Three**). *A*, Absence of CRD. PGN1→PGN2 cross correlogram. No significant rhythmical synchronization was present. This was consistent with the absence of prominent peaks in the envelope autospectrum (inset). *B*, Control condition. *Bi*, PGN1→PGN2 cross correlogram. No significant rhythmical synchronization was present although some activity of both PGNs discharged at the same time as revealed by the small peak at lag zero (black circle). A small peak at CRD frequency in the envelope autospectrum (asterisk, inset) suggests a weak periodic modulation of correlated firings of both PGNs by CRD. *Bii*, PN→PGN1 cross correlogram and *Biii*, PN→PGN2 cross correlogram show that significant rhythmical synchronization was present. *C*, Enhanced CRD. *Ci*, PGN1→PGN2 cross correlogram, a significant periodic pattern appeared in the cross correlogram indicating rhythmical synchronization. The prominent peak at CRD frequency in the envelope spectrum (asterisk, inset) suggests that the rhythmical synchronization arose from coupling of both PGNs to CRD. *Cii*, PN→PGN1 cross correlogram and *Ciii*, PN→PGN2 cross correlogram show that the rhythmical synchronization between PGNs and PN are prominent.

significant rhythmicity (i.e. peaks passing through the 95% confidence level at regular intervals), indicating that the rhythmical component of the discharges of this pair of PGNs is not synchronized. The small peaks with low power density in the envelope spectrum of the cross spectrum (inset), a measure of degree of rhythmical synchronization (see **Chapter Three**), also suggest the periodic phase lock in the absence of CRD was weak.

4.4.4B In control conditions some pairs show PGN→PGN synchronization through coupling to CRD

Activity of pairs of PGNs (thirteen from twelve animals) was recorded in control conditions, either using separate electrodes (N=9) or discriminated from multiunit activity recorded through a single electrode (N=4). All the PGNs displayed a dominant rhythm with a median frequency of 0.73 Hz (interquartile interval: 0.64-0.76 Hz). In seven (54%) pairs of PGNs, each PGN had the same T-rhythm and there was significant PGN→PGN synchronization. The T-rhythm frequencies of these PGNs were the same as the frequency of CRD (median frequency: 0.73 Hz, interquartile interval: 0.73-0.74 Hz). The cross correlogram between PN and these PGNs (represented as PN→PGN) showed that they were significantly correlated. Six (46%) pairs of PGNs had different T-rhythm frequencies and no significant PGN→PGN synchronization. In four of these pairs, one PGN of each pair showed a T-rhythm frequency the same as CRD but the other did not. In the remaining two pairs, the frequencies of the T-rhythms of the PGNs in each pair were different from each other and from CRD. An example of the autocorrelograms of a pair of PGNs in control conditions is shown in Fig. 4.7Ci, 4.7Cii (these are the same units as in Fig. 4.7Bi, 4.7Bii). Fig. 4.7Ciii shows the PN autocorrelogram in this animal (CRD frequency: 0.74

Hz). The two PGNs have different T-rhythm frequencies (0.54 Hz for PGN1, 0.73 Hz for PGN2) and there is no significant PGN1→PGN2 rhythmical synchronization as revealed by the cross correlogram in Fig. 4.8Bi. PGN1 has a T-rhythm frequency which is different to the CRD frequency, but the PN→PGN1 cross correlogram shows a significant correlation (Fig. 4.8Bii). This arises from the dynamic nature of PN→PGN interaction (see section *The stability of rhythmical synchronization of PGNs increases when CRD is enhanced*). While some discharges of PGN1 are phase-locked to CRD, which produced the periodic pattern in the cross correlogram, the overall activity which produced the T-rhythm did not have a fixed phase difference to CRD. PGN2 has a T-rhythm which is at the same frequency as CRD and the cross correlogram reveals a significant rhythmical synchronization (Fig. 4.8Biii). The small peak around lag zero in the PGN→PGN cross correlogram (•, Fig. 4.8Bi) and the spectral peak with low power density in the envelope spectrum (*, inset) might result from the fact that some activity of the two PGNs became periodically synchronized through phase lock to CRD. This is more clearly demonstrated in the PN→PGN joint peri-stimulus scatter plot in Fig. 4.9. Although not a prominent feature, the clustering of PGN events along the diagonal line (arrows) indicates that some coincident activity of the two PGNs arises from phase-lock to CRD at the same time.

4.4.4C Enhanced CRD leads to PGN→PGN synchronization of T-rhythms

Six animals were recorded in conditions of enhanced CRD and six pairs of PGNs were recorded through separate electrodes. All the PGNs exhibited robust rhythmicity, as revealed by their autocorrelograms, with a median T-rhythm frequency of 0.68 Hz (interquartile interval: 0.63-0.69 Hz). Notably, in

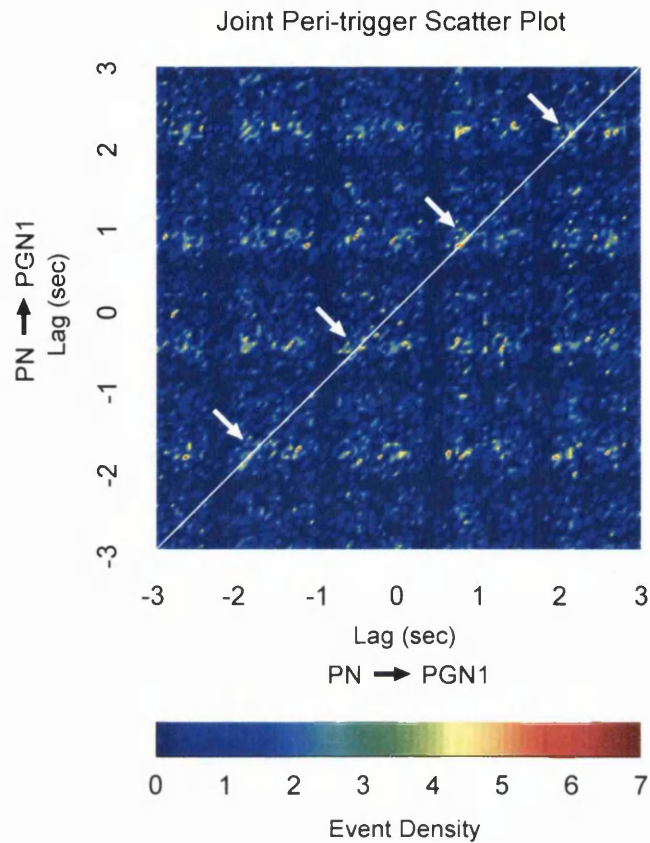


Fig. 4.9 Detection of weak coupling of PGNs through phase-lock to CRD. The colour-coded CRD→PNG1 vs. CRD→PNG2 joint peri-stimulus scatter plot (JPSP) was used to detect coincidence firings in relation to the CRD (see **Chapter Three**). The PGNs and the period of analysis (control condition) are the same as in Fig. 4.7C and Fig. 4.8B. The high-density clusters (arrows) along the diagonal line in the JPSP suggests that some coincident activity of the two PGNs arose from phase-lock to the CRD at the same time.

five (83%) of the pairs of PGNs, the activities of both PGNs had the same T-rhythm frequency and were significantly synchronized. These pairs were also locked in a 1:1 manner with CRD (median frequency: 0.68 Hz, interquartile interval: 0.64-0.71 Hz) and had significant PN→PGN synchronization. The dynamic nature of this synchronization is demonstrated by the fact that three (60%) pairs of PGNs synchronized during periods of enhanced CRD were not significantly synchronized in control conditions.

The same PGNs examined during the absence of CRD (Fig. 4.7B) and control conditions (Fig. 4.7C) are shown under enhanced CRD conditions in Fig. 4.7D. Both PGN1 and PGN2, and the PN show the same dominant frequency (0.72 Hz), as revealed by their autocorrelograms (Fig. 4.7Di, 4.7Dii, 4.7Diii) and autospectra (insets). These PGNs show significant PGN→PGN rhythmical synchronization (Fig. 4.8Ci). This synchronization as a result of coupling of both PGNs to CRD was suggested by the fact that the prominent peak (RPD: 24.9) in the envelope spectrum of the cross correlogram (inset) was associated with the CRD frequency (*). This was also supported by the findings that there was significant PN→PGN synchronization for both PGNs under conditions of enhanced CRD (Fig. 4.8Cii, 4.8Ciii).

4.4.4D Summary of the data from paired recordings under various respiratory conditions

The data presented here revealed a significant increase in the probability of synchronization of the rhythmical activity of PGN pairs as animals were moved from conditions where CRD was absent to conditions where CRD was enhanced. In the absence of CRD, PGN→PGN activity never showed rhythmical synchronization. Although all these PGNs showed a T-rhythm, the T-

rhythm frequency of each PGN of a pair was different as revealed in the scatter plot (Fig. 4.10A). During control conditions, where CRD was present, a proportion of PGN pairs (~55%) had the same T-rhythm frequency (Fig. 4.10B) which was also the same as that of CRD. The T-rhythms of PGNs of these pairs were phase-locked. Where the PGNs of a pair had different rhythms, there was no synchronization. In conditions of enhanced CRD, the majority of pairs (>80%) of PGNs had T-rhythms that were synchronized to each other at the frequency of the CRD. The T-rhythm frequencies of each PGN in each pair in this condition are shown in Fig. 4.10C. For all the synchronous pairs of PGNs either under control conditions or when the CRD was enhanced, the peak nearest to lag zero in the PGN→PGN cross correlograms always straddled the lag zero (as shown in Fig. 4.8Ci), indicating that statistically, the phase difference between synchronous PGNs was nearly zero (i.e. in-phase synchronization). Furthermore, PN→PGN cross correlograms reveal that activity of the two PGNs of a synchronous pair have similar phase differences relative to PN activity (see Fig. 4.8Cii, 4.8Ciii) and this, given the fact that the frequencies of the PGNs are the same as that of PN, strongly suggests that the in-phase synchrony of PGN discharges may arise from the synchronization through CRD.

The degree of rhythmical synchronization between PGNs, evaluated by the spectrum of the cross-correlogram envelope (see **Chapter Three**), was also significantly higher when CRD was enhanced than when CRD was absent ($p < 0.02$, Wilcoxon rank-sum test, Fig. 4.11).

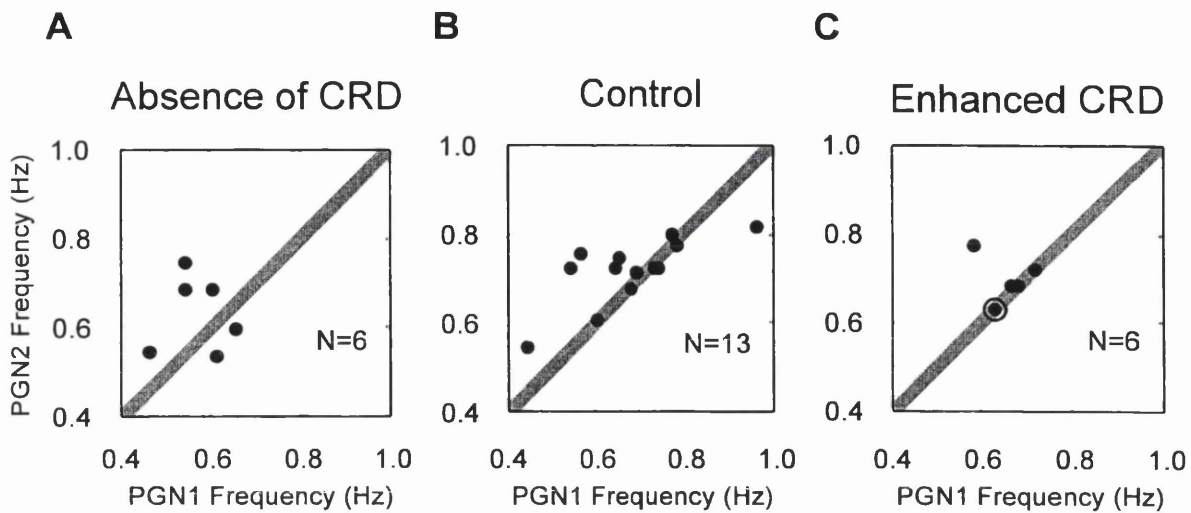


Fig. 4.10 Summary scatter plots showing T-rhythm frequencies of pairs of postganglionic neurons (PGN1 and PGN2) in three conditions of CRD. The shaded diagonal bands indicate where the T-rhythm of both PGNs have frequency differences less than 0.05 Hz, and by definition are considered to have the same frequency (see **Chapter Three**). *A*, Absence of CRD. 0/6 pairs of PGNs had the same frequency. *B*, Control condition. 7/13 pairs of PGNs (54%) had the same frequency. *C*, Enhanced CRD. 5/6 pairs of PGNs (83%, two pairs were superimposed as indicated by the circle) had the same frequency.

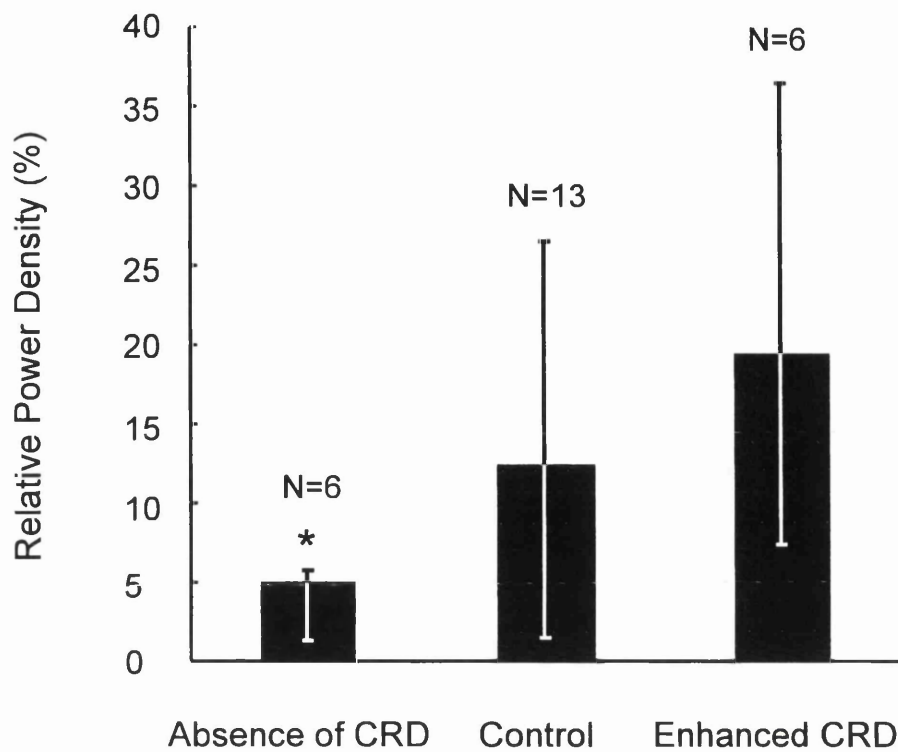


Fig. 4.11 Degree of rhythmical PGN → PGN synchronization in artificially ventilated animals under three conditions of CRD evaluated by the relative power density of the autospectrum of the cross correlogram envelope (see Chapter three). Data are presented as median and 1st and 3rd quartiles. The level of relative power density is proportional to the level of rhythmicity. The asterisk, *, indicates that the relative power density in conditions of enhanced CRD is significantly higher compared to that when CRD is absent (Wilcoxon rank-sum test, $p < 0.02$).

4.4.4E The stability of rhythmical synchronization of PGNs increases when CRD is enhanced

Time-evolving raster plots were used to investigate the temporal stability of the rhythmical synchronization in PGNs. The density of the striations on the raster plot, which are a measure of the stability of the phase relationship between two oscillators, were quantified by calculating the phase variation factor (**Chapter Three** for details).

When CRD was absent, raster plots of PGN→PGN activity displayed no obvious striations, indicating that no constant phase relationship existed between PGN firing activity, although occasionally transient phase-locked periods could be observed. A typical example is shown in Fig. 4.12A (this is the same animal shown in Fig. 4.7, 4.8). Three transient phase-locked periods are indicated by arrowheads. In control conditions, raster plots of PGN→PGN activity revealed a higher probability of striation, although this was not apparent for many of the pairs recorded. The example in Fig. 4.12Bi (from the animal in Fig. 4.7, 4.8) illustrates a raster plot with no evidence of a striated appearance. By contrast, time-evolving raster plots of PN→PGN activity revealed some striations, indicative of a relatively constant phase difference during these periods. In the typical examples shown in Fig. 4.12Bii, 4.11Biii, there are also periods of asynchrony (e.g. arrowhead in Fig. 4.12Bii) and changes in the phase difference (e.g. arrow in Fig. 4.12Biii), suggesting that the coupling to CRD is relatively dynamic. In conditions of enhanced CRD, the PGN→PGN raster plots of the PGN pairs showed some clear periods of striation, but also periods where a constant phase difference between the PGN activities was not so apparent. The example shown in Fig. 4.12Ci (from the animal in Fig. 4.7, 4.8) shows obvious striations (see period between arrows in Fig. 4.12Ci), suggesting

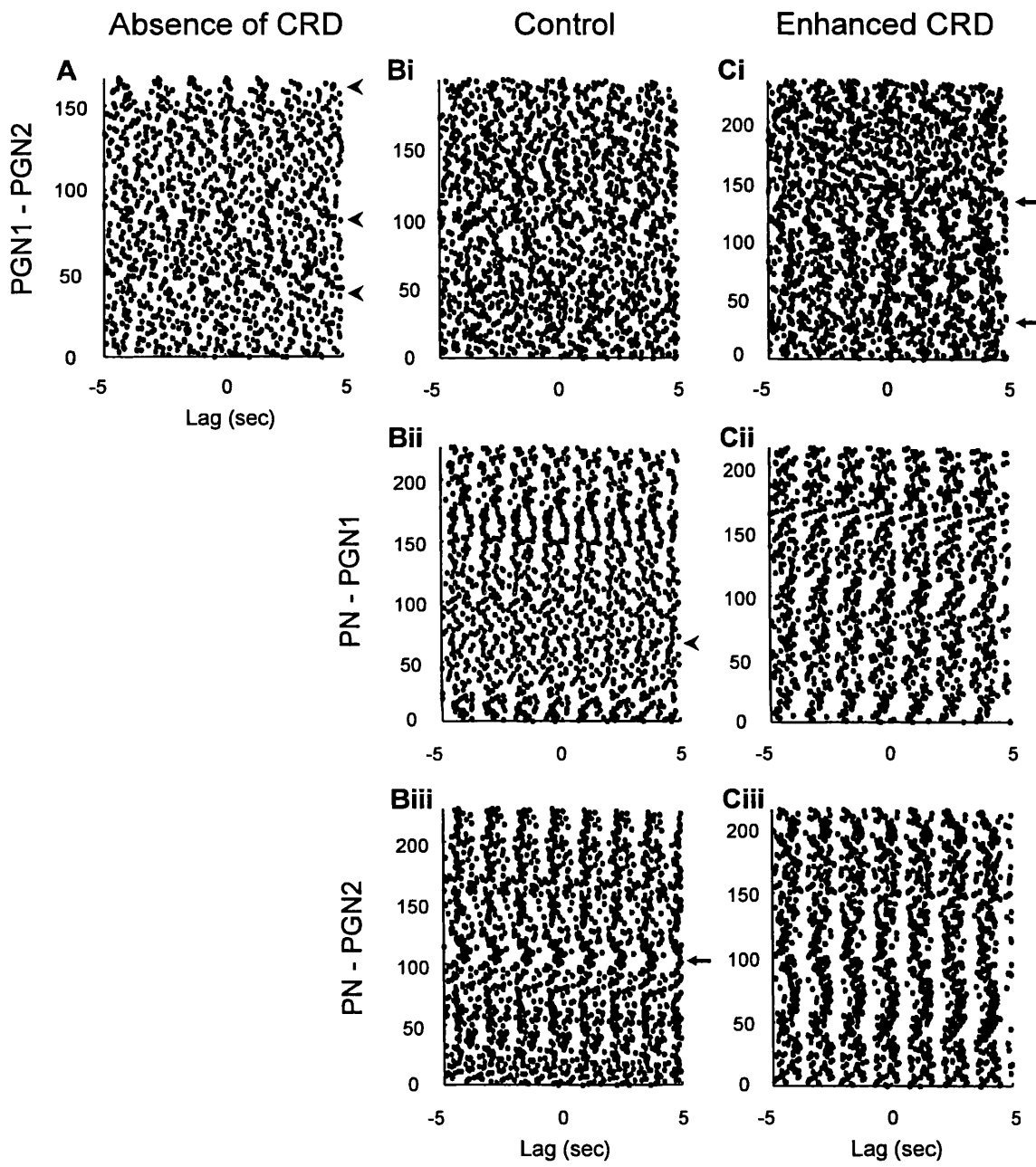


Fig. 4.12 Dynamic change of rhythmical PGN→PGN and PN→PGN synchronization evaluated by the ordinary correlation raster plot (OCRP) under three conditions of CRD. The two PGNs and the period of analysis are the same as those in Figs. 4.7, 4.8. If the phase difference between two activities is relatively constant across time, a vertical striation will be observed in the raster plot. *A*, Absence of CRD: no definite pattern was present in the PGN1→PGN2 OCRP although transient phase-locked periods can be observed (arrowheads). *B*, Control condition. *Bi*, PGN1→PGN2: the phase difference of the two units varied across time. *Bii*, PN→PGN1 and *Biii*, PN→PGN2, in some parts during data collection, the PGNs were synchronized with PN but periods of asynchrony (e.g. arrowhead, *Bii*) or changes of the phase difference (e.g. arrow, *Biii*) were also observed. *C*, Enhanced CRD. *Ci*, PGN1→PGN2: although phase drifting was still apparent (as in the absence of CRD and in control), there were also periods of rhythmical synchronization indicated by vertical striations (e.g. between arrows). *Cii*, PN→PGN1 and *Ciii*, PN→PGN2: Rhythmical synchronization between the PN and PGNs was more apparent across time than previously.

periods of strong phase locking, preceded and followed by periods where the synchronization is not so strong. The majority of PN→PGN raster plots in enhanced CRD conditions showed dense striations indicative of a constant phase relationship (see Fig. 4.12Cii, 4.11Ciii for typical examples). There was little evidence of phase hopping, suggesting that the synchronization to CRD was strong.

Comparison of the phase variation factor for PGN→PGN raster plots is shown in Fig. 4.13. The data illustrates that the phase variance was significantly lower in the condition of enhanced CRD versus absence of CRD ($p < 0.02$, Wilcoxon rank-sum test). This indicates that rhythmical synchronization was more stable during periods of enhanced CRD than in the absence of CRD.

4.4.5 Paired recordings of PGNs innervating the CVA in spontaneously breathing animals

Six pairs of PGNs were recorded from five spontaneously breathing animals under control conditions. Of the 12 PGNs recorded, only one unit did not show rhythmical discharges. The median frequency of the T-rhythm in the remainder was 0.65 Hz (interquartile interval: 0.50-0.84 Hz). One pair (8%) were synchronized and also showed 1:1 phase locking with the CRD (median frequency: 0.93 Hz, interquartile interval: 0.84-0.97 Hz).

Four pairs of PGNs were recorded from four animals in conditions of enhanced CRD. Rhythmical discharges were found in all the PGNs (T-rhythm median frequency: 0.68 Hz, interquartile interval: 0.63-0.74 Hz) and significant PGN→PGN synchronization was found in three (75%) of the pairs. All these PGNs were synchronized with CRD (median frequency: 0.92 Hz, interquartile interval: 0.71-1.18 Hz).

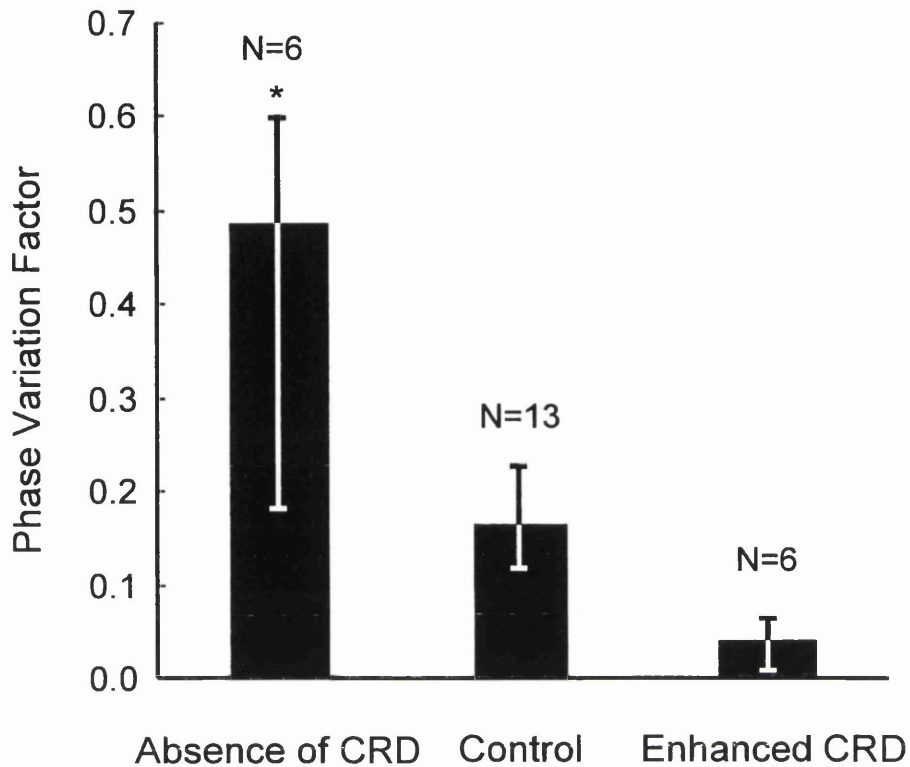


Fig. 4.13 Dynamic stability of rhythmical synchronization between PGNs evaluated by the phase variation factor in artificially ventilated animals under three conditions of CRD (see **Chapter Three**). Data are presented as medians and 1st and 3rd quartiles. The level of phase variation factor is inversely proportional to the level of stability. The asterisk, *, indicates that the phase variation factor in the absence of CRD was significantly higher than in conditions of enhanced CRD (Wilcoxon rank-sum test, $p < 0.02$).

The data presented here indicate that the rhythmical firing behavior in PGNs of spontaneously breathing animals was consistent with the findings from the artificially ventilated preparations.

4.4.6 The mean discharge rate of PGNs does not significantly change with increases in CRD

Unlike the dominant rhythm, which reflects the periodic change of firing probability given that a PGN spike has occurred, the mean discharge rate, which is more related to neuronal excitability, describes averaged firing rate (see **Chapter Three**). The discharge rate of the PGNs in each of the groups was calculated to test the hypothesis that synchronization of PGNs might be accompanied by change in their excitability. Since the mean discharge rate of single PGNs was highly variable, the median values with the range for each group are presented. Paired Wilcoxon signed-rank tests were used for statistical comparisons. In artificially ventilated rats, the median discharge rate of PGNs was 0.88 Hz in the absence of CRD (N=12, range: 0.42-1.33 Hz), 1.37 Hz in control (N=26, range: 0.51-4.19 Hz) and 0.91 Hz in conditions of enhanced CRD (N=12, range: 0.51-2.0 Hz). Paired statistical comparisons showed that the discharge rates were not significantly different between pairs in the absence of CRD versus conditions of enhanced CRD ($p=0.41$, paired Wilcoxon signed-rank test, N=10).

In spontaneously breathing rats, the median discharge rate of PGNs was 1.15 Hz in control conditions (N=12, range: 0.48-2.5 Hz) and 1.04 Hz in conditions of enhanced CRD (N=8, range: 0.49-3.18 Hz). A statistical analysis between pairs recorded in control and conditions of enhanced CRD revealed that the discharge rates were not significantly different ($p=0.14$, paired Wilcoxon

signed-rank test, N=4).

4.5 Simulation: Explanation of the discharge behavior of CVA PGN population activity

One apparently paradoxical observation in the experiments was that in the absence of CRD, while the autospectra of VCN activity revealed a rhythmical component, suggesting that some of the rhythmical discharges of PGNs were synchronized (Fig. 4.3Ai), no significant PGN→PGN rhythmical synchronization was observed (Fig. 4.8A). This paradox can be explained, however, as the autospectrum of a population composed of many weakly coupled or uncoupled oscillators with similar frequencies can still have a peak within the frequency range of its constituents. Theoretic consideration regarding the existence of population rhythmicity in spite of uncoupled constituent oscillators has been addressed by Christakos (see Christakos, 1986, Christakos, 1994). It can be proved mathematically that the autospectrum of stationary population activity is the sum of the autospectra of its components and the co-spectra (or coincidence spectra, the real part of cross spectra) between pairwise constituents. The proof is given in **Appendix II**. While the power density in an autospectrum at a particular frequency quantifies the 'strength' of rhythmicity at that frequency, the co-spectrum is a measure of in-phase or out-phase relationships of rhythmical components between two activities. Co-spectral intensity at a particular frequency can be positive (in-phase) or negative (out-phase) at that frequency (Bloomfield, 1976; Bendat & Piersol, 1986). For a population of uncoupled or weakly coupled oscillators with dominant frequencies within a similar range, the phase difference is expected to vary across pairwise oscillators at any particular frequencies. The annihilation of effect of phase lead and phase lag will lead to

diminishment in the sum of co-spectrum. However, a prominent peak within the dominant frequency range of its components will emerge out of the population autospectrum because any individual oscillator will contribute significant power within this frequency range.

A model of population PGN activity in the absence of CRD was used to illustrate this point. Using a stochastic model, five hundred uncorrelated event series representing activity of PGNs were generated by a computer using parameters estimated in the absence of CRD (see **Appendix I** for the stochastic model). Simulated population activity was provided by the superimposition of these simulated PGN activities followed by simple 11-point moving averaging. The moving averaging is used to simulate the integration and smoothing procedure for VCN activity signal processing (see **Chapter Two**). Fig. 4.14A, B, C show three examples of the simulated population PGN activity. Autocorrelograms of three simulated event series selected, each from the respective simulated population, are given in Fig. 4.14Ai, Bi, Ci. They are similar to the autocorrelograms of real data (compared with Fig. 4.7). The histograms of the frequencies with maximal power density (Fig. 4.14Aii, Bii, Cii) demonstrated that the dominant frequencies of the five hundred simulated PGN event series are concentrated in the range of T-rhythm. The uncorrelation between any pair of the simulated PGN event series is guaranteed by the randomness in selection of the parameters such as dominant frequency used for their generation (see **Appendix I**). Fig. 4.14Aiii, Biii, Ciii show the histograms of coherence at any frequency between any pair of PGN event series. Only thirty series selected randomly from each pool of PGN event series were used to generate these histograms because there was a limitation of computer memory to handle large amounts of data produced if the number of the event series is bigger. The

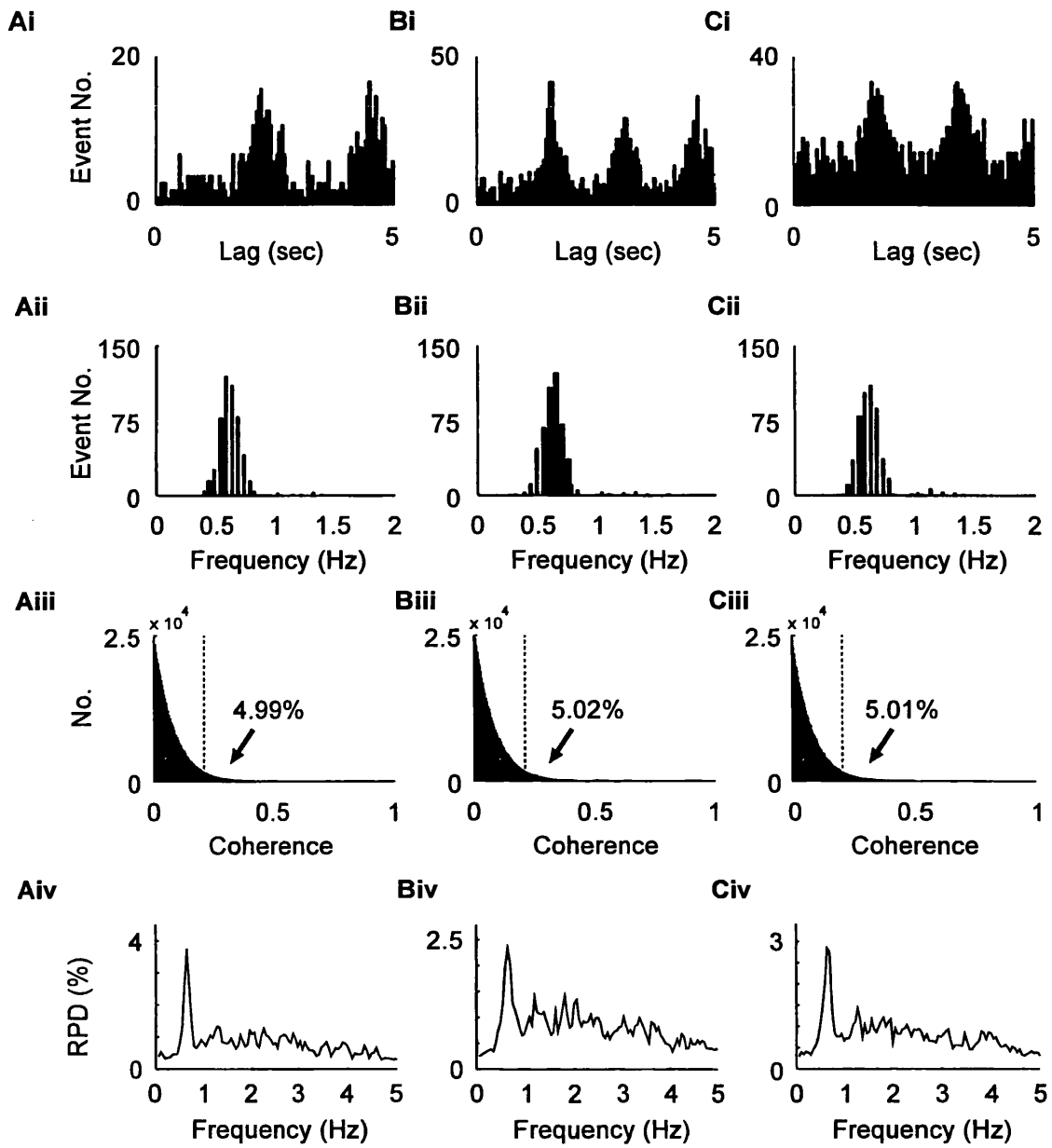


Fig. 4.14 Simulation of population activity composed of multiple PGN oscillators. The simulated population consisted of five hundred PGNs the event series of which were generated by the stochastic model described in **Appendix I**. Three examples of the simulation are illustrated in *A, B, C*. *Ai, Bi, Ci*, The autocorrelogram of a sampled single PGN from each population was similar to the autocorrelogram of real data (cf. Fig. 4.7Bi, 4.7Ci, 4.7Di). *Aii, Bii, Cii*, The frequency histogram from each population demonstrates that the dominant frequencies of the constituent simulated PGNs distributed in a frequency range similar to that of T-rhythm. *Aiii, Biii, Ciii*, The coherence histogram of thirty PGNs randomly selected from each population shows that the simulated PGNs were pairwise uncorrelated because the proportion of pairwise coherence at any frequency above the 95% confidence interval (dash line) was around 5% which was just a chance phenomenon. *Aiv, Biv, Civ*, The autospectrum of each simulated population activity clearly demonstrates a prominent peak centered in the frequency range of T-rhythm.

dashed lines represent the 95% confidence interval (Rosenberg *et al.*, 1989) for the coherence. These coherence histograms demonstrate that the simulated PGN event series are not correlated to each other because the proportion of coherence outside the 95% confidence interval was only about 5% (4.99% for Fig. 4.14Aiii, 5.02% for Fig. 4.14Biii, 5.01% for Fig. 4.14Ciii), which was just a chance phenomenon. Although these simulated PGN event series were not correlated to each other, it is clear from Fig. 4.14Aiv, 4.14Biv, 4.14Civ that a prominent peak within the frequency range of the dominant rhythms of its constituents appeared in the population activity.

This demonstrated the potential for the existence of a population rhythm centred within the dominant frequency range of its constituent oscillators. The conclusion that the population autospectrum is the sum of the component autospectra and the pairwise co-spectra also predicts that if a proportion of these oscillators are synchronized to a common frequency through a shared drive, a prominent peak at the driving frequency will emerge in the autospectrum of the population. This is because the power of the synchronous individuals would concentrate at that frequency and stands out from those components with dispersed frequencies. Furthermore, if these oscillators exhibit near zero lag (i.e. in-phase) synchronization, this will increase intensity of the co-spectrum at the driving frequency. The near zero lag synchronization in response to CRD (see **Results**) suggests that in-phase synchronization can happen when the single PGNs are subjected to a common drive. The same phenomenon was also observed when single PGNs were driven by LIC-related activity (see **Chapter Five**).

4.6 Discussion

4.6.1 Multiple CVA PGN oscillators

This study demonstrated that activity of PGNs innervating the CVA, originates from multiple sympathetic oscillators and these oscillators are capable of dynamic synchronization. The direct evidence of multiple oscillators came from experiments where two CVA PGNs were recorded simultaneously. It was found that dominant frequencies of single PGNs could be different and their activity was not necessarily synchronous. This suggests that the discharges of PGNs are driven by multiple oscillators. However, the existence of multiple oscillators does not necessarily imply that these oscillators are pacemakers, i.e. their rhythmical activity is self-generated without need of external input influences. In fact, considering the hierarchy of the SNS, it is more probable that sympathetic oscillatory activity originates from neural networks which receive inputs from different sources (Gebber & Barman, 1981; McAllen & Malpas, 1997; Malpas, 1998). One possible network may involve a common oscillator antecedent to CVA PGNs and the different dominant frequencies of single PGNs is a consequence of differential filtering processes by downstream neurones (Coote, 1988). In spite of this, it still suggests that at some level in the SNS, pathways destined to the single CVA PGNs differentiate to harbour oscillatory activity with different frequencies, i.e. multiple oscillators in a broad term. In the absence of CRD, the lack of significant rhythmical synchronization between single PGNs implies these oscillators are autonomous, i.e. they are not mutually synchronized to each other. The existence of dominant rhythmical activity at population level does not necessarily indicate that stable synchronization was present in some PGN oscillators. Synchronization could be switched from a pair of PGNs to another across time without a stable synchrony state in any of them. However, owing to

the relatively small sampling number in this study (Sittiracha *et al.*, 1987), it is inconclusive whether all the single PGNs are asynchronous in the absence of a common drive (i.e. 'free-run' conditions). In fact, indirect evidence from a recent study which compared coherence between bilateral VCNs in the absence of CRD suggested that both VCN received a common drive from the central nervous system (Smith & Gilbey, 1998a). This would indicate that activity of some PGNs innervating the CVA is correlated. However, the simulation study demonstrated that prominent population rhythmical activity can still emerge even though all the constituent oscillators are not pairwise correlated (see below section 4.6.3). This suggests that the statistical relationship between discharges of single PGN oscillators alone is capable of generating rhythmical burst activity in population activity. If some PGNs are correlated under 'free-run' conditions, it is expected that the dominant periodicity in the population activity will become more conspicuous.

4.6.2 Synchronization of CVA PGNs

Although activity of single PGNs may not be synchronous under 'free-run' conditions, this study clearly demonstrated that they could become synchronized when they are subjected to a common driving force, in this case, the CRD. Previous studies have shown that respiratory modulation in PGN activity became more prominent during hypercapnia (Bachoo & Polosa, 1986). At the preganglionic sympathetic neurone (SPN) level, hypercapnia could induce recruitment of silent SPNs or increase discharge rate of active SPNs in acute spinal cats (Zhang *et al.*, 1982). It is possible that similar mechanisms may operate at the PGN level and so account for the increase of the respiratory modulation observed in the postganglionic sympathetic nerves during hypercapnia. Synchrony by summation of PGN activity phase locked to CRD

provides another possibility for the increase of respiratory modulation. Although it has been shown that respiratory modulation of single PGNs becomes more prominent during hypercapnia (Boczek *et al.*, 1992; Habler *et al.*, 1993), by recording two single PGNs simultaneously, this study provided direct evidence indicating that enhancement of synchronization between single PGNs without significant change of discharge rate could result in prominent respiratory related activity in sympathetic nerves. The degree of synchronization depends on the strength of CRD. This conclusion was reached through some key findings in experiments where the strength of CRD was manipulated. In the absence of CRD, the phase difference between single PGNs drifted across time and consequently, synchronization was not a feature although transient phase lock periods may occur as revealed by OCRP (Fig. 4.12). Increase of synchronization was observed under control conditions where CRD was present. The fact that the synchronized pairs had a dominant frequency the same as the respiratory frequency and they were phase locked to CRD suggested that this synchronization was a consequence of coupling of PGNs to CRD. However, synchronization was not obligatory under such conditions. Some units were synchronized to CRD but some pairs were not. This further indicated that the PGN oscillators may have different intrinsic properties and, therefore, substantiated the existence of multiple autonomous sympathetic oscillators.

The interaction between PGNs was dynamical in nature. This was demonstrated by the findings that even in pairs of asynchronous PGNs, transient phase lock through coupling to CRD was possible (Fig. 4.9). When CRD was enhanced, the temporal stability of the phase difference between PGNs increased and this resulted in a high probability of PGN synchronization. Thus, the adjustment of coupling strength to a common drive may provide an important

mechanism for the SNS to regulate the degree of synchronization in a pool of autonomous sympathetic oscillators. Changes in the level of synchronization without simultaneous significant changes in the mean discharge rate of PGNs also supports the idea that in addition to the mean discharge rate, the temporal pattern of neuronal discharges may provide another mechanism for information coding in the nervous system (Fetz, 1997; Farmer, 1998).

4.6.3 Explanation of the population discharge behaviour

The dual approach of examining correlation both in whole nerve (VCN) activity and in PGN→PGN activity allowed us to explore the relationship between the activity profile of a neuronal population and its individual components. Importantly, the comparisons indicate that the emergent properties of multiunit activity can be different from those that would be predicted from PGN→PGN relationships. In the absence of CRD, VCN activity has a dominant rhythmical activity although individual single PGNs did not reveal significant rhythmical synchronization. The simulation and theoretical study (**Appendix II**) suggests that this population rhythm arises from the fact that the dominant frequencies of single PGNs are restricted in a narrow range and in the VCN autospectrum, each single PGN contributes significant power density to the spectral peak centred within this range. The power density of the peak depends on the number of units in the population, the strength of correlation between units and the distribution of phase difference (Christakos, 1986; Christakos, 1994). The dominant population rhythm, however, does not exhibit high temporal stability under 'free-run' conditions. This is because the rhythms of single PGNs are not constant across time themselves (see **Chapter Three, Introduction**) and although the global feature of single PGNs is not synchronous, fluctuation of

correlation is possible on account of the potential for transient synchronization. These factors can explain the temporal variation of power density of the wide band around the T-rhythm frequency range in the time evolving autospectrum. Under control conditions, some PGNs were synchronized through coupling to CRD and this contributed to the respiratory related activity observed in VCN activity. However, the CRD related activity in VCN activity was not a stable feature across time as shown in the time evolving autospectrum (Fig. 4.4Bi). The instability of the CRD related activity at the population level arose from the fact that the phase difference between single PGN and CRD underwent considerable temporal variation. One important feature for the interaction of single PGNs and CRD is that single PGNs cannot be absolutely dichotomised to two distinct groups based on whether they are synchronous to CRD. Synchronization or asynchronization might not always be a constant phenomenon (cf. Fig. 4.12Bii, Biii). A consequence of this was that synchronization between PGNs at CRD frequency did not exhibit absolute temporal stability either. The dynamic characteristic of the interaction at single neuronal level resulted in the varied power density along the dominant band in the time evolving VCN autospectrum (Fig. 4.4Bi). It also demonstrated that the two peaks, one related to CRD and the other did not, in the VCN autospectrum did not necessarily imply existence of two distinct groups of single PGNs (Fig. 4.3Bi). When CRD was enhanced, a higher proportion of single PGNs were synchronized to CRD and the phase difference between single PGNs and CRD became more stable across time. This explains the narrow band with less varied power density in the time evolving VCN autospectrum (Fig. 4.4Ci), and, therefore the sharp peak in the autospectrum (Fig. 4.3Ci), at CRD frequency.

4.6.4 Conclusion

This study demonstrated:

1. Activity of PGNs innervating the CVA of the rat's tail is driven by multiple oscillators.
2. Synchronization between single PGNs is not obligatory but it can be modified by adjustment of the strength of a common driving force, CRD. Enhanced CRD increased the probability of PGN synchronization.
3. Population PGN activity (VCN activity) should not be considered as one distinct oscillator but instead, should be considered as superimposed activity of multiple oscillators. The discharge behavior of the population activity is a direct reflection of the dynamic interaction at single oscillator level.

Chapter Five

Dynamics of periodically driven multiple sympathetic oscillators

5.1 Introduction

The previous study (**Chapter Four**) established that PGNs innervating the CVA of the rat's tail are driven by multiple oscillators. When the strength of a common driving force such as CRD was changed, these PGN oscillators might undergo dynamic synchronization. In the present study, the discharge behaviour of PGN activity in response to frequency changes of another periodic drive, LIC-related activity was examined from both the population (VCN activity) and the single neurone levels.

5.1.1 Dynamics of PGN activity in response to frequency changes of the LIC-related activity (f_{LIC})

Periodically driven biological oscillators frequently exhibited complex dynamics and oscillators with different intrinsic frequencies (f_{INT}) may differ in their responses when subjected to frequency change of the driving forces (Glass & Mackey, 1988). In particular, the ability of the periodic driving force to 1:1 entrain the driven oscillator when their frequencies are similar is a common observation in biological oscillators (Winfree, 1980; Glass & Mackey, 1988; Kelso, 1995). This provides an important mechanism to coordinate individual oscillators to produce stable population rhythms in response to the external drives. The findings in the previous study (**Chapter Four**) are consistent with this concept. However, the observations under conditions when driving

frequency and f_{INT} of driven oscillators are similar cannot be extended directly to the conditions when the frequency of the driving oscillator is moved away from f_{INT} . This is because at such driving frequencies, the interaction between driving and driven oscillators may display complex dynamics such as high order rational frequency-lock (i.e. commensurate frequencies) other than 1:1 (e.g. 2:1, 3:1, 3:2, etc.), chaotic or asynchronous coupling, or intermittency of phase locking (Glass & Mackey, 1988; Kelso, 1995).

In the previous study (**Chapter Four**), the frequency of the driving force, CRD, of the vagotomized and anaesthetised rats only operated in a range close to the f_{INT} of the PGN activity. The median of CRD frequency (pooled data from conditions of control and enhanced CRD) was 0.70 Hz (interquartile interval: 0.63-0.77 Hz) which was within the frequency range of T-rhythm (see **Chapter Four** and Johnson & Gilbey, 1994, Johnson & Gilbey, 1996). It is not clear whether CVA PGN oscillators exhibit dynamics consistent with that of periodically driven oscillators across a wide range of driving frequencies. To examine this, LIC-related activity, whose periodic modulatory effect on the sympathetic nerve activity is well documented (Lipski *et al.*, 1977; Gerber & Polosa, 1978), was used as the driving force instead of CRD because it is easier to change f_{LIC} while keeping other physiological parameters constant. During these experiments the tidal volume (V_{T}) of ventilation was kept approximately constant except during periods of f_{INT} determination (see **Materials and Methods**). The purpose of this was to maintain a steady strength of LIC-related activity while changing its frequency so that the frequency dependent nature of PGN activity could be examined.

5.1.2 Comparison of the discharge behaviours of single PGN and population PGN activity

The observations from single PGN experiments were compared with those from population PGN experiments. From the functional point of view, it is important to consider the difference because the discharge pattern of VCN activity is more important than that of single PGNs in determining the neurogenic regulation of tail circulation. This is because the arterial wall can be considered as syncytium of smooth muscle cells connected by gap junctions through which depolarising currents can spread rapidly over relatively large distances in vascular tissues (Christ *et al.*, 1996). The muscular syncytium would thus behave like an integrator in the sense that any 'local' fluctuation of single PGN discharges would be summated and smoothed out at the population level allowing population activity to stand out as the paramount factor for neurogenic contraction.

The changes of the degree of PGN synchronization in response to the changes of driving frequencies may have a direct impact on the neurogenic contraction of the CVA. If the discharge behaviours of PGN oscillators are consistent with that predicted by nonlinear dynamics of periodically driven oscillators, it would be expected that different PGNs may exhibit distinct responses to LICs because the diversity of their intrinsic frequencies. Mutual entrainment through a common driving force would be jeopardised by different coupling dynamics of individual oscillators to the driving force and consequently the probability of synchronization should be greatly reduced. Without mutual entrainment of constituent oscillators, the question remains as to whether the population can still maintain stable rhythmical activity coupled to the periodic drive.

5.2 Materials and Methods

The experiments were carried out on 18 male Sprague Dawley rats. All the animals were ventilated artificially. Population PGN activity was recorded from VCN and single PGN activity was recorded from the surface of CVA. Experiments started with determination of the f_{INT} of PGNs during periods of low V_T and high ventilation rate, i.e. 'free-run' conditions. The idea of 'free-run' is to unlock PGN activity from LICs. A low V_T would reduce the strength of LIC-related activity and therefore minimise its effect on the PGNs. Furthermore, unlocking was likely to achieve when f_{LIC} was much higher than PGN f_{INT} because for nonlinear coupled oscillators, stable 1:1 entrainment is only observed when the frequency of the driving oscillator is close to the intrinsic frequency of the driven oscillator. (Glass & Mackey, 1988). V_T was then increased and the ventilation rate was brought close to the f_{INT} to see if LIC-related activity and PGN activity could establish stable 1:1 coupling. The ventilation rate was then subsequently changed stepwise away from the f_{INT} while keeping V_T constant. All the experiments were carried out in the absence of CRD. Central apnea was maintained by giving the rats inspiratory gas with high concentration of oxygen. However, it was difficult to maintain apneic state when ventilation rate was too low even under conditions of hyperoxemia. Therefore, in all the experiments f_{LIC} was kept above 0.49 Hz.

5.2.1 Whole nerve experiments

VCN activity was recorded from six animals. When the f_{LIC} was high PaCO_2 dropped as a result of hyperventilation (see **Results**). Although all the experiments were conducted during central apnea, the possibility remains that CO_2 may influence sympathetic nerve activity even in the absence of CRD

(Trzebski & Kubin, 1981). To test whether in the absence of CRD low PaCO₂ will change the discharge pattern of PGN activity, half of the animals were given CO₂ (<5%) and O₂ gas mixture during periods of high minute ventilation volume to maintain a state with relatively constant PaCO₂. These results were compared with those obtained in experiments where PaCO₂ was not clamped. During each episode of f_{LIC} changes, 8-minute data was collected.

5.2.2 Single PGN experiments

Twenty one single PGNs were recorded focally from the surface of the CVA of twelve animals. Simultaneous paired recordings were performed in ten of these (5 pairs). Some single PGNs (N=8) were not carried through the whole frequency range of f_{LIC} (see **Chapter Two**) because of difficulties in maintaining stable recording conditions. Five-min data was collected for each episode of f_{LIC} changes.

See **Chapter Two** for further details of experimental preparations and procedures.

5.3 Data analysis

Autospectra were used to determine f_{LIC} and the dominant rhythm of single and population PGN activity. For single PGNs, autocorrelograms were generated first to confirm the existence of rhythmicity. Autospectra were routinely normalised by the maximal power density for direct comparison of the dominant frequency across different experiments. However, when autospectra were used to evaluate actual activity of VCN, they were scaled by absolute power density normalised by total power under 'free-run' conditions. Linear correlation between LIC-population PGN, LIC-single PGN or single PGN-single PGN was

assessed by coherence spectra.

Time evolving VCN autospectra were used to evaluate temporal stability of rhythmical activity in the PGN population. The temporal stability was quantified by total variance of power density of this time evolving autospectrum. Stability of rhythmical phase lock between two single PGNs was assessed by the envelope spectrum of their cross correlograms and the ordinary cross correlation raster plot (OCRP). To provide a quantitative measure of temporal stability of phase difference, the phase variation factor under conditions of different f_{LIC} was calculated and compared. When two single PGNs exhibited strong coupling through phase locking to LICs, this phenomenon could be easily detected in the presence of strong rhythmicity at f_{LIC} in the PGN→PGN cross correlogram. However, when the phase lock of two single PGNs to LICs was weak, detection of coincidence of events of two single PGNs in relation to LICs was enhanced by examining LIC triggered joint peri-stimulus scatter plots (JPSP).

The dynamic patterns of interaction between single PGNs and LICs were classified by studying the LIC triggered OCRP, which provides information about the stability of phase difference, and the reordered correlation raster plot (RCRP), which groups single PGN events into different clusters based on LIC-PGN phase difference. See **Chapter Three** for details.

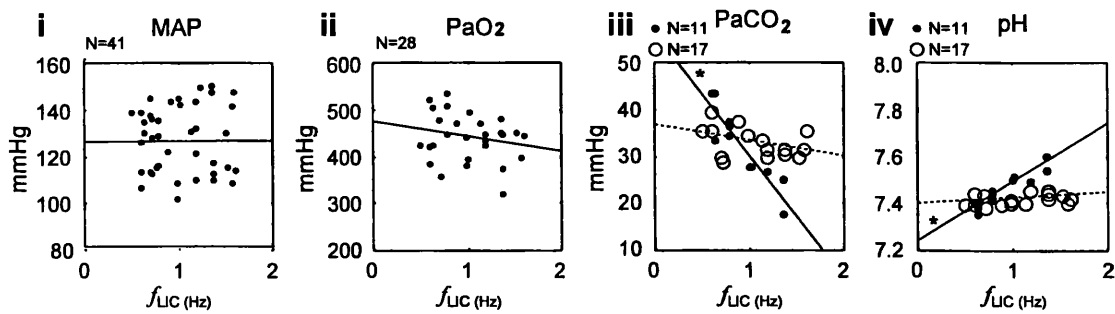
5.4 Results

5.4.1 Conditions of animals

The general circulatory and respiratory conditions of the animals were assessed by four physiological parameters. Fig. 5.1 summarises the mean arterial blood pressure (MAP), PaO₂, PaCO₂ and pH for whole nerve experiments (Fig.5.1A) and single PGN experiments (Fig. 5.1). The trends of change of these parameters as f_{LIC} varied were evaluated by linear regression test. The solid and dotted lines represent linear regression lines. Significant deviation of the slope from zero was indicated by an asterisk. There was no significant change of MAP (Fig. 5.1Ai, Bi). No significant change of PaO₂ was present in whole nerve experiments (Fig. 5.1Aii) although a borderline negative trend was observed in single PGN experiments ($p=0.048$, Fig. 5.1Bii). When f_{LIC} was high, respiratory alkalosis developed due to pulmonary alveolar hyperventilation. Under such conditions, PaCO₂ dropped and pH increased (Fig. 5.1Aiii, Aiv and Fig. 5.1Biii, Biv). In the whole nerve experiments, half of the animals were given PCO₂ to counteract respiratory alkalosis (○, dash regression line, Fig. 5.1Aiii, Aiv). These experiments were compared with those from which animals were not given CO₂ (●, solid regression line, Fig. 5.1Aiii, Aiv).

Although there was no significant trend of MAP change when f_{LIC} varied, the effect of ventilation on the phasic fluctuation of blood pressure (BP) diminished as f_{LIC} increased. Fig. 5.2 shows the dependence of the LIC-related undulation of the BP waves on f_{LIC} . When f_{LIC} was low there was prominent BP oscillation correlated to tracheal pressure (TP) (f_{LIC} : 0.49 Hz, Fig. 5.2A). By contrast, when f_{LIC} was high the LIC-related BP oscillation was markedly reduced (f_{LIC} : 1.51 Hz, Fig. 5.2B). The degree of LIC-related BP fluctuations was quantitated by the relative power density (RPD) at f_{LIC} in BP autospectra. Fig. 5.2B shows the

A Whole nerve experiments



B Single PGN experiments

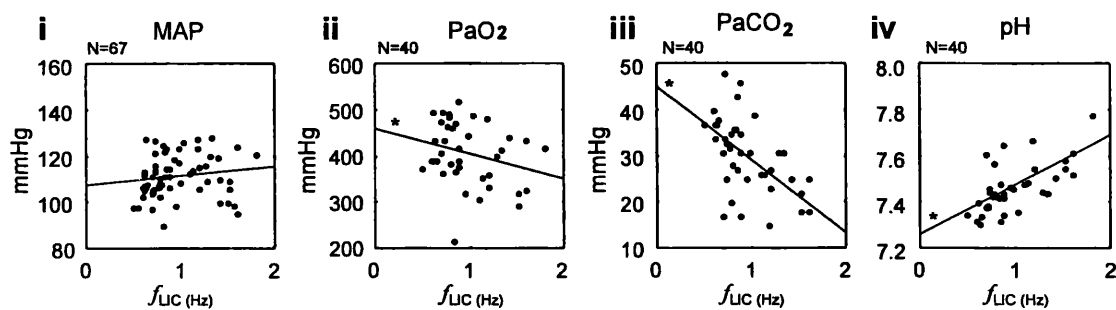


Fig. 5.1 Scatter plots of physiological parameters of experiments under conditions of different f_{LUC} . Significant deviation of the slope of the regression line from zero when f_{LUC} was changed is indicated by an asterisk (t-test, $p < 0.05$). *A*, Whole nerve experiments. *A_i*, *A_{ii}*, No significant linear trend was present in the mean arterial pressure (MAP) and PaO₂ as f_{LUC} varied. *A_{iii}*, *A_{iv}*, When f_{LUC} was high without adding CO₂ into the inspiratory gas (black circles, solid line), respiratory alkalosis developed with low PaCO₂ and high pH (t-test for zero slope, $p < 0.001$ for both). There was no significant linear trend in the PaCO₂ and pH in experiments where CO₂ was added (open circles, dash line). *B*, Single PGN experiments. *A_i*, No significant linear trend was present in MAP as f_{LUC} was changed. *A_{ii}*, A borderline negative linear trend (t-test for zero slope, $p = 0.048$) in PaO₂ was observed when f_{LUC} was increased. *A_{iii}*, *A_{iv}*, Respiratory alkalosis developed with low PaCO₂ and high pH (t-test for zero slope, $p < 0.001$ for both) during periods of high f_{LUC} .

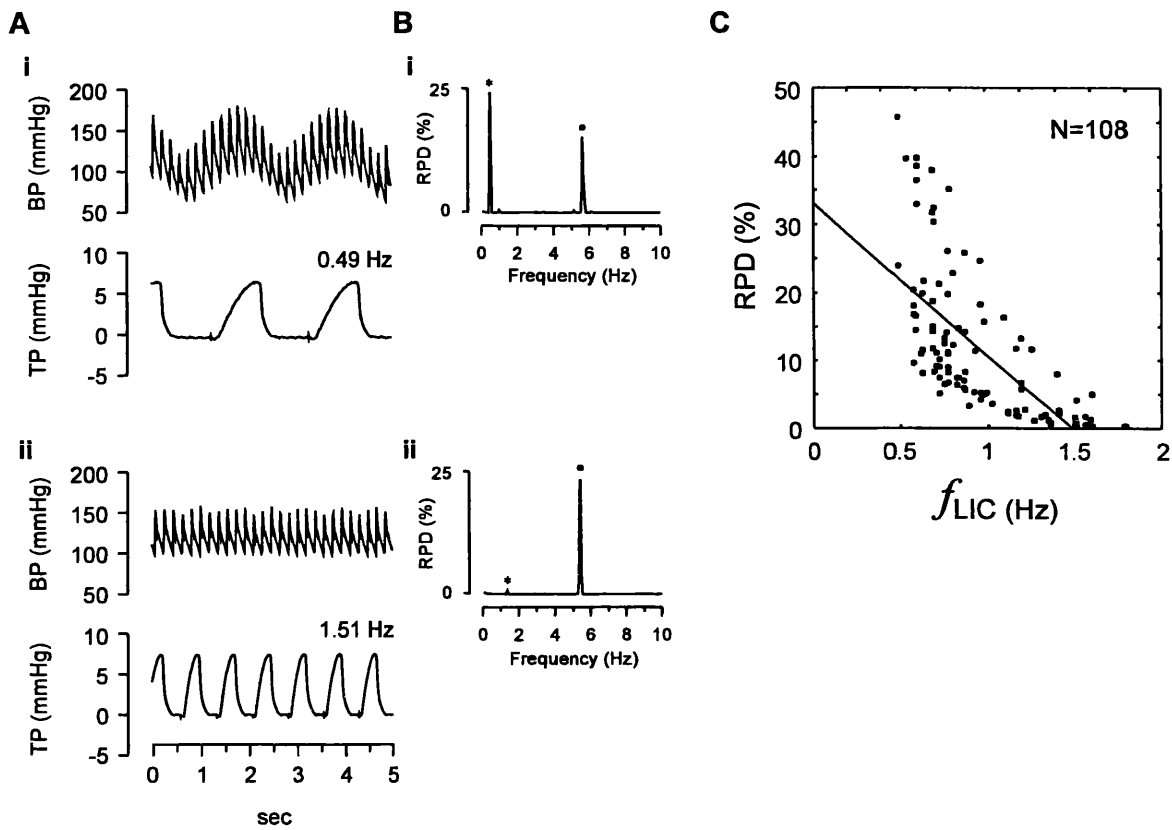


Fig. 5.2 f_{LIC} dependent LIC-related oscillations of BP. **A**, Real time BP and TP waves. Although the mean BP was similar under conditions of low f_{LIC} (0.49 Hz, *Ai*) and high f_{LIC} (1.51 Hz, *Aii*), prominent LIC-related BP oscillations were only observed when f_{LIC} was low but not when f_{LIC} was high. **B**, Autospectrum of BP. The degree of the LIC-related BP oscillations were evaluated by the relative power density (RPD) at f_{LIC} in the BP autospectrum. *Bi*, When f_{LIC} was high (the same experiment as in *Ai*) there was a prominent peak at f_{LIC} (asterisk, RPD: 24.02%). *Bii*, RPD of the peak at f_{LIC} (asterisk, RPD: 0.53%) dropped when f_{LIC} was high (the same experiment as in *Aii*). The additional peak at cardiac frequency is indicated by a black circle for both autospectra. **C**, Summary scatter plot of RPD at f_{LIC} in the BP autospectrum when f_{LIC} varied. RPD of the peak at f_{LIC} declined precipitously as f_{LIC} was increased (t-test for zero slope, $p < 0.001$).

corresponding BP autospectra (f_{LIC} and heart rate were indicated by asterisks and dots, respectively) for data in Fig. 5.2A. The RPD at f_{LIC} under conditions of low f_{LIC} (RPD: 24.02%, Fig. 5.2 Bi) was much higher than that under conditions of high f_{LIC} (RPD: 0.53%, Fig. 5.2Bii). Fig. 5.2C summarises the results (data from whole nerve and single PGN experiments were pooled). There was strong negative correlation (t-test for zero slope of regression line, $p < 0.001$) between RPD of BP at f_{LIC} and f_{LIC} .

5.4.2 Population PGN activity in response to f_{LIC} changes

5.4.2A The dominant frequency of population PGN activity is 1:1 locked to LIC-related activity across a broad f_{LIC} range

Except for the periods during ‘free-run’ conditions (see below), population PGN activity (VCN activity) in response to f_{LIC} changes was examined in a f_{LIC} range extending from 0.49 Hz to 1.6 Hz. VCN activity under conditions without PaCO₂ clamp and with PaCO₂ clamp during hyperventilation had similar discharge patterns in response to f_{LIC} changes. Fig 5.3 shows examples of results under the two experimental conditions (Fig.5.3A, without PaCO₂ clamp; Fig.5.3B, with PaCO₂ clamp). Sample segments of neurograms and autospectra of VCN activity and the TP waves are shown on the left and right panels of each activity, respectively (VCN: orange; TP: black). Under ‘free-run’ conditions (i.e. low V_T , 1.0 ml, and high f_{LIC} , 1.94-2.00 Hz), spectral analysis of VCN activity revealed a broad peak reflecting the f_{INT} range emergent from the oscillator pool (median frequency, 0.78 Hz. Interquartile range, 0.67-0.78). The existence of a modal f_{INT} in VCN activity was exemplified by the wide spectral peak in Fig. 5.3 (f_{LIC} : 1.97 Hz and f_{INT} : 0.64 Hz in Fig. 5.3Ai; f_{LIC} : 1.95 Hz and f_{INT} : 0.78 Hz in Fig. 5.3Bi). This peak was within the frequency range of the T-rhythm of single

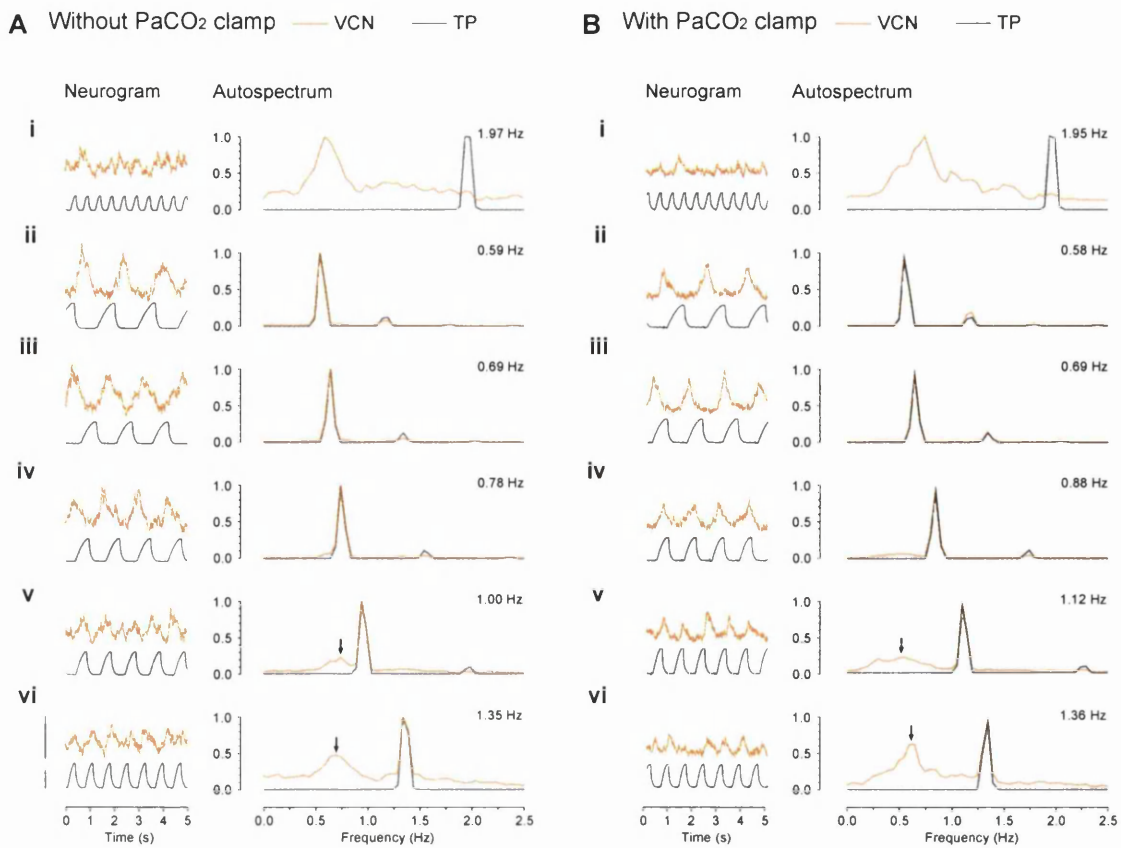


Fig. 5.3 Neurograms and superimposed autospectra of VCN activity (orange) and LICs (black) showing frequency dependent synchronization of VCN activity to LICs. To test the influence of respiratory alkalosis on PGN activity during periods of high f_{LIC} , the frequency response of VCN activity to f_{LIC} changes was examined under conditions, A, without and B, with adding CO_2 to the inspiratory gas when the f_{LIC} was high (see text). The discharge pattern of VCN activity was similar under both conditions. *Ai, Bi*, During 'free-run' conditions (f_{LIC} , *Ai*, 1.97 Hz; *Bi*, 1.95 Hz) the VCN activity reveals a broad peak (modal f_{NT} , *Ai*, 0.64 Hz; *Bi*, 0.78 Hz) representing the spread of f_{NT} within the population. *Aii-Aiv, Bii-Biv*, Moving ventilation frequency into this range (f_{LIC} , *Aii-Aiv*, 0.59-0.78 Hz; *Bii-Biv*, 0.58-0.88 Hz) resulted in a single narrow peak at f_{LIC} , indicating that most of the single PGNs discharged in synchrony at f_{LIC} . *Av-Avi, Bv-Bvi*, At higher ventilation frequencies (f_{LIC} , *Av-Avi*, 1.00-1.35 Hz; *Bv-Bvi*, 1.12-1.36 Hz) a narrow peak at f_{LIC} was still preserved although some PGNs 'escape' 1:1 entrainment as indicated by minor peaks in the f_{NT} range (arrows). Sample neurograms of VCN activity and TP waves under each condition are shown on the left. Calibration, 0.5 μV (VCN), 10 mmHg (TP).

PGNs found in previous studies (see Johnson & Gilbey, 1994; Johnson & Gilbey, 1996 and **Chapter Four**). Moving f_{LIC} while keeping V_T constant (2.0-2.5 ml) into this f_{INT} range resulted in prominent LIC-related activity in VCN and yielded a single narrow peak in the VCN autospectra, suggesting that most PGNs in the population were entrained 1:1 with f_{LIC} (f_{LIC} : 0.59-0.78 Hz in Fig. 5.3Aii-Aiv and 0.58-0.88 Hz in Fig. 5.3Bii-Biv). The LIC-related activity of VCN was not a ventilation movement artefact because it was abolished after infusion of chlorisondamine, accompanied with a drop of blood pressure (Fig. 5.4A; detailed contours of VCN activity, TP and BP using expanded time scale are shown in Fig. 5.4B and 5.4C). At high f_{LIC} , the narrow peak at f_{LIC} , was well preserved (f_{LIC} : 1.00, 1.35 Hz in Fig. 5.3Av, Avi and 1.12, 1.36 Hz in Fig. 5.3Bv, Bvi) although some PGNs must have escaped 1:1 entrainment, as suggested by the appearance of minor peaks in f_{INT} range (arrows, Fig. 5.3Av, Avi and Bv, Bvi). These dominant spectral peaks showed high coherence to LIC-related activity. This is revealed in Fig. 5.5 (same VCN activity and same data recording time as in Fig. 5.3, f_{LIC} was indicated by •). During 'free-run' conditions there was low coherence between VCN activity and LIC-related activity (coherence at f_{LIC} : 0.21 in Fig. 5.5Ai; 0.07 in Fig. 5.5Bi). Although at high f_{LIC} coherence dropped a little (coherence at f_{LIC} : 0.67 in Fig. 5.5Avi; 0.80 in Fig. 5.5Bvi), high coherence at f_{LIC} with its harmonic components was a prominent feature for all the f_{LIC} tested (coherence at f_{LIC} : 0.88, 0.85, 0.91, 0.90 in Fig. 5.5 Aii, Aiii, Aiv, Av, respectively; 0.98, 0.98, 0.97, 0.93 in Fig. 5.5 Bii, Biii, Biv, Bv, respectively). This demonstrates that under conditions of high V_T , population PGN activity has a rhythmical component highly correlated to LIC-related activity independent of f_{LIC} across a rather broad range.

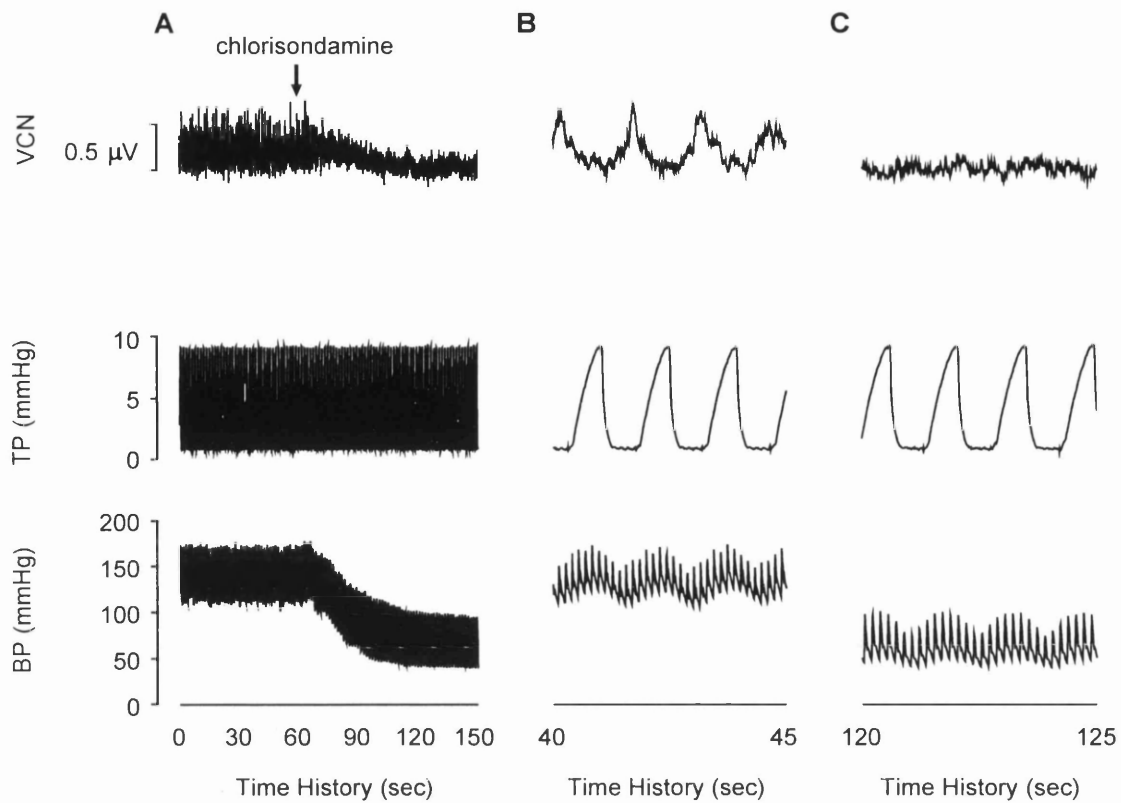


Fig. 5.4 The effect of chlorisondamine (3 mg kg^{-1} I.V.), a sympathetic ganglionic blocker, on LIC-related activity in VCN activity and BP. A, Real time data of integrated VCN activity, TP waves and BP waves before and after application of chlorisondamine. VCN activity and BP dropped after application of chlorisondamine. B, Real time data with expanded time scale before application of chlorisondamine shows LIC related activity in VCN activity and BP. C, Real time data with expanded time scale after application of chlorisondamine shows abolishment of LIC-related activity in VCN activity but its persistence in BP.

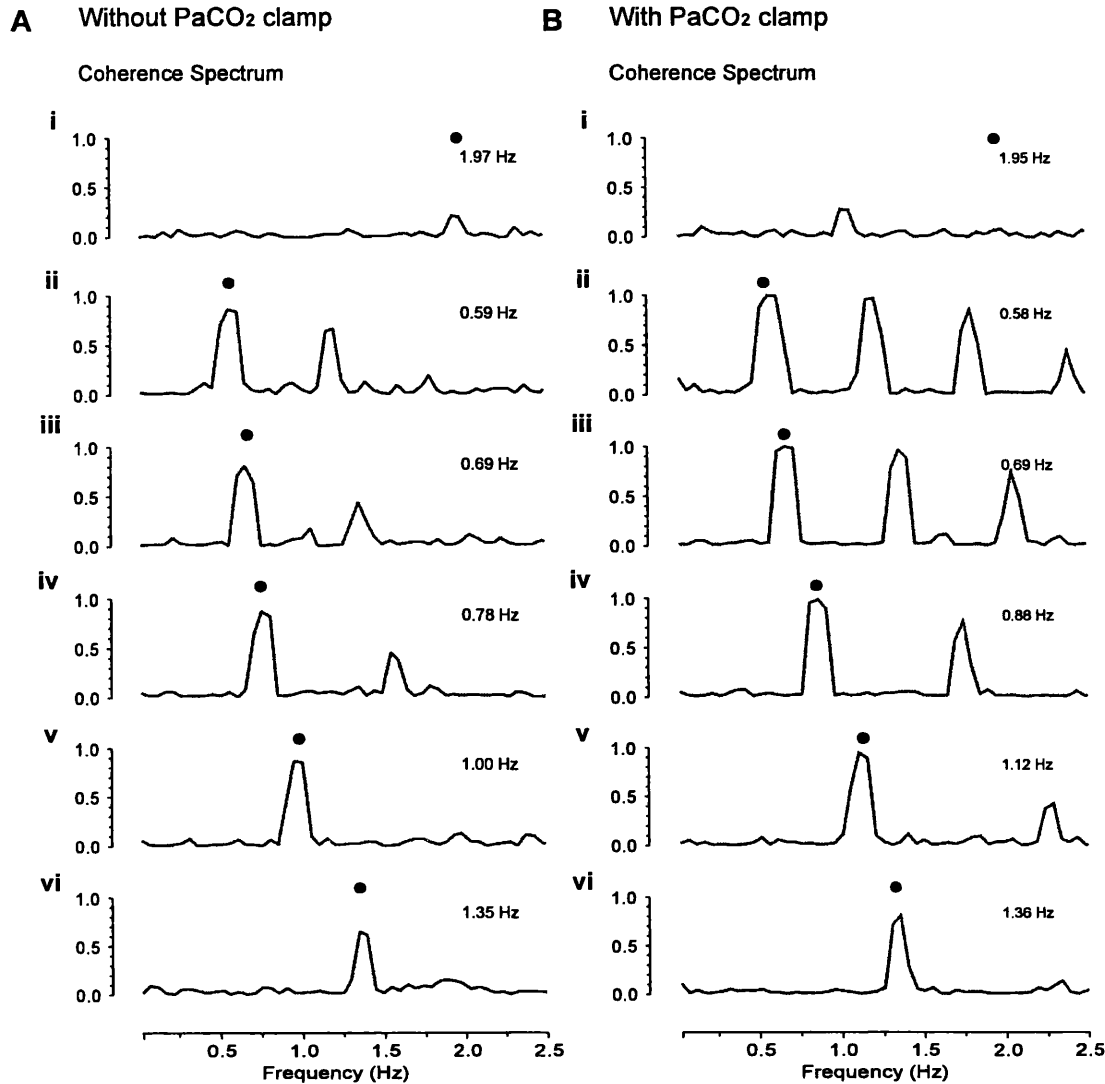


Fig. 5.5 Change of strength of LIC-VCN activity linear correlation in response to f_{LIC} changes. The linear correlation was evaluated by coherence spectrum between LIC-related activity and VCN activity. The coherence was evaluated both under the condition, *A*, without and under the condition, *B*, with PaCO₂ clamp when the f_{LIC} was high (see text). The VCN activity and period of data analysis are the same as in Fig. 5.3. The changes of the coherence were similar under both conditions when f_{LIC} , indicated by a black circle, was changed. *Ai, Bi*, During periods of 'free-run', the coherence at f_{LIC} was low. *Aii-Av, Bii-Bv*, high coherence at f_{LIC} was maintained close to unity across wide range of f_{LIC} (coherence at f_{LIC} , 0.88, 0.85, 0.91, 0.90 in *Aii, Aiii, Aiv, Av*, respectively; 0.98, 0.98, 0.97, 0.93 in *Bii, Biii, Biv, Bv*, respectively). *Avi, Bvi*, A moderate drop was observed when f_{LIC} increased further but high coherence was still maintained (coherence at f_{LIC} , 0.67 in *Avi*; 0.80 in *Bvi*).

5.4.2B Moving f_{LIC} away from f_{INT} the temporal stability of population PGN

rhythmical activity decreased

Although the dominant rhythmicity in VCN activity can maintain 1:1 frequency-lock to LIC-related activity across a broad f_{LIC} range, its temporal stability decreased as f_{LIC} was moved away from f_{INT} . Time evolving autospectra were used to illustrate this phenomenon. An example is given in Fig. 5.6 (same VCN activity as in Fig.5.3A, 5.5A). Under 'free-run' conditions (Fig. 5.6 A, same data recording time as in Fig. 5.3Ai, 5.5Ai), the power density of the dominant peak shown in Fig. 5.3Ai underwent considerable variation across time indicating temporal instability of synchrony of PGN activity. This is similar to previous findings from the experiments in the previous studies where VCN activity was recorded in the absence of CRD (see **Chapter Four**, cf. Fig. 4.4Ai), i.e. synchronization of PGNs was unstable under conditions without a periodic entraining force. When f_{LIC} was brought close to f_{INT} (same data recording time as in Fig. 5.3Aiii, 5.5Aiii) the power density of the LIC-related spectral band was rather stable (Fig. 5.6B), which resulted in the prominent spectral peak and high coherence at f_{LIC} in Fig. 5.3Aiii and Fig. 5.5Aiii, respectively. When f_{LIC} was moved away from f_{INT} (Fig. 5.6C, same data recording time as in Fig. 5.3Avi, 5.5Avi), although considerable power still concentrated at f_{LIC} , the power density was not as stable as that during the periods when f_{LIC} was close to f_{INT} . This may account for the moderate drop of the coherence at f_{LIC} shown in Fig. 5.5Avi. Despite the fact that the power density at f_{LIC} was not invariable across time, when the rhythmical activity at this frequency was prominent the spectral band was narrow, suggesting that during these periods the lock to LICs was stable without constantly phase drifting. This could explain how, in spite of a moderate drop, high coherence could still be maintained during periods of high f_{LIC} . The

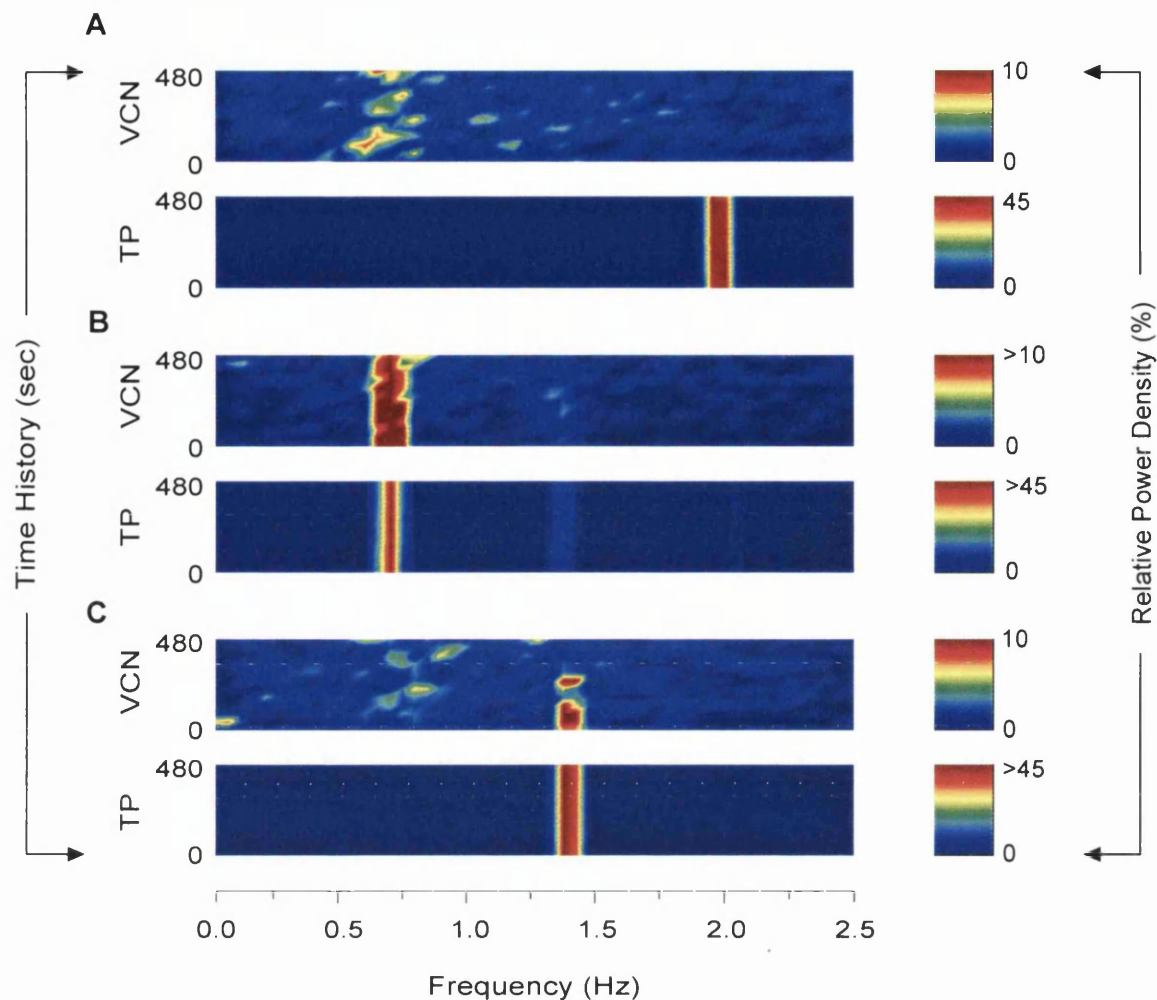


Fig. 5.6 Dynamic stability of synchronous rhythmical activity in VCN activity and TP evaluated by colour-coded time evolving autospectra. The VCN activity is the same as in Fig. 5.3A and Fig. 5.5A. *A*, Under 'free-run' conditions (the same period of data analysis as in Fig. 5.3Ai and Fig. 5.5Ai), the power density of the dominant peak shown in Fig. 5.3Ai underwent considerable variation across time indicating temporal instability of synchrony of PGN activity. *B*, When f_{LIC} was brought close to the f_{NT} of the PGN activity (the same period of data analysis as in Fig. 5.3Aiii and Fig. 5.5Aiii), the power density of the LIC-related spectral band became rather stable. *C*, When f_{LIC} was increased further (the same period of data analysis as in Fig. 5.3Avi and Fig. 5.5Avi), considerable power still concentrated at f_{LIC} but it was not as stable as that when f_{LIC} was close to PGN f_{NT} . Emergence of spectral peaks with variable power density in the range of PGN f_{NT} suggests instability of synchrony in those PGNs which escaped 1:1 entrainment to LIC-related activity.

appearance of highly variable power density across time near the f_{INT} , which gave rise to the minor broad peak in Fig. 5.3Ai (arrow) suggested instability of synchrony in those PGNs which escaped 1:1 entrainment to LIC-related activity. The temporal stability of rhythmical VCN activity was quantitated by calculating the variance of power density across time (see **Chapter Three**). Fig. 5.7 summarises the result (data from experiments without PaCO₂ clamp and with PaCO₂ clamp during hyperventilation were pooled together because they showed similar behaviour in response to f_{LIC} changes). A strong positive correlation between the increase of power density variation and difference of f_{LIC} and f_{INT} was observed (t-test for zero slope of the regression line, $p < 0.001$). This suggests that stable synchronization of PGNs was strongest when they were driven by LIC-related activity with a frequency near the PGN f_{INT} .

5.4.2C LIC-related rhythmical activity diminished without drop of total population

PGN activity when f_{LIC} was moved away from f_{INT}

Although the dominant rhythm of VCN activity exhibited strong 1:1 coupling to LICs across a wide range of f_{LIC} , this rhythmical activity diminished as f_{LIC} increased. This is demonstrated in Fig. 5.8. The absolute power density normalised by absolute total power under conditions of 'free-run' was used as a measure of the actual activity. The normalisation is a necessary procedure to minimise the effect of unequal number of recorded nerve fibres across experiments. This is because the VCN is a mixed nerve composed of sympathetic and somatic nerve fibres (see **Chapter Two**) and the number of the sympathetic nerve fibres that contact the recording electrode may differ from one experiment to another. The solid and open circles in Fig 5.8 represents the normalised absolute power density at f_{LIC} (scaled by left ordinate) and the

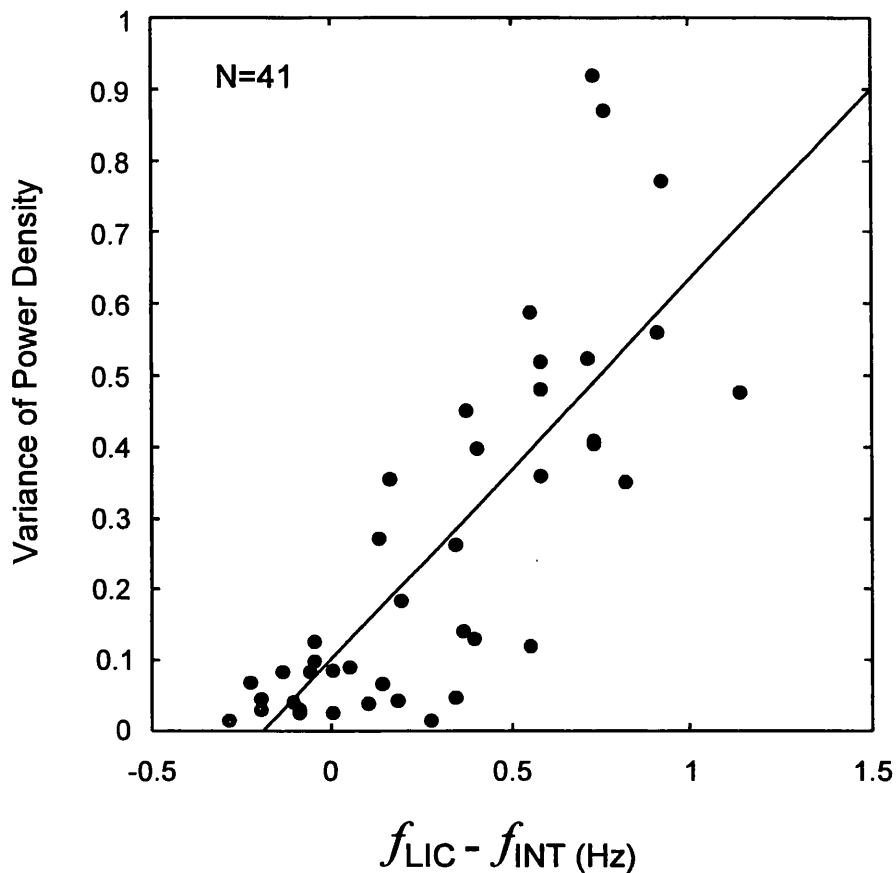


Fig. 5.7 Summary scatter plot of the changes of temporal stability of rhythmical components in VCN activity in response to f_{LIC} changes. The temporal stability was quantitated by variance of power density in the VCN time evolving autospectrum. High variance of power density suggests instability of distribution of power density in the time evolving autospectrum (see Chapter three). There was a strong positive linear trend of variance of power density when f_{LIC} was moved away from PGN f_{INT} (t-test for zero slope, $p < 0.001$), indicating that synchronous rhythmical activity in VCN activity became unstable when the difference between f_{LIC} and PGN f_{INT} was great.

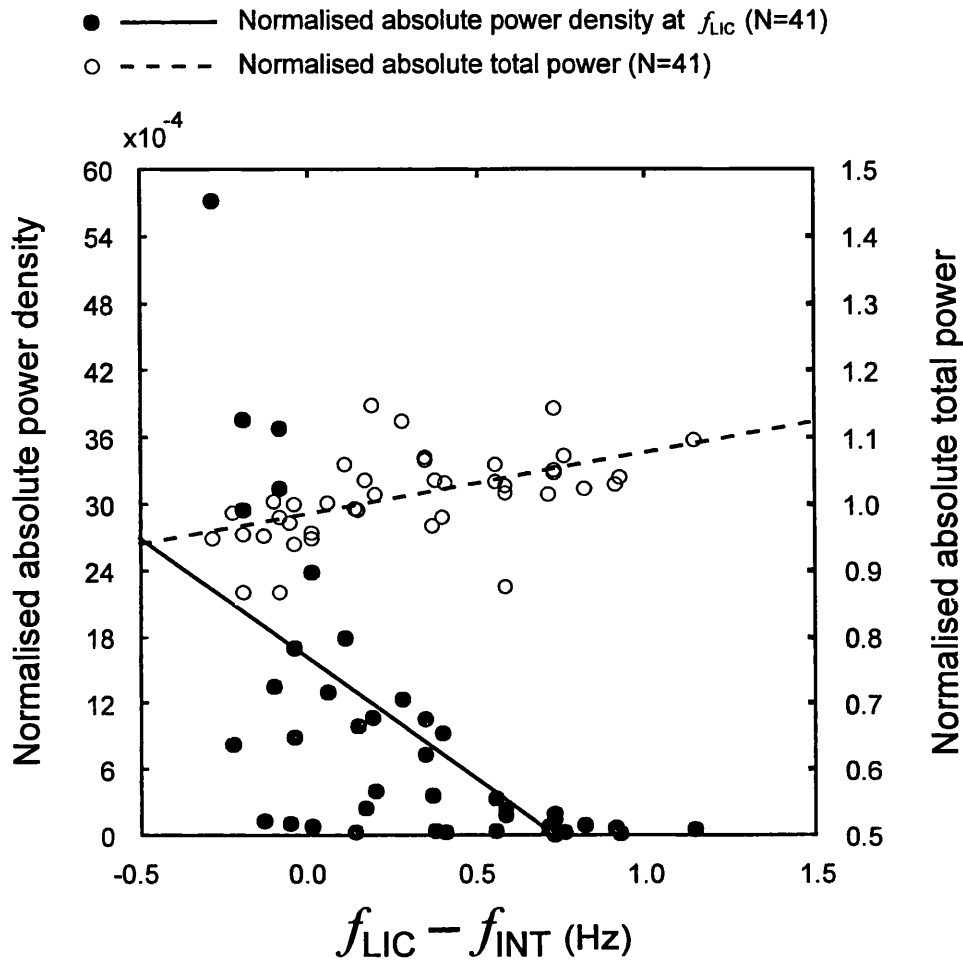


Fig. 5.8 Relationship between the power density at f_{LIC} and the total power in VCN activity in response to f_{LIC} changes. The absolute power density or total power was normalised by the total power in VCN activity measured under 'free-run' conditions (see text). When f_{LIC} was moved away from PGN f_{INT} , the normalised absolute power density at f_{LIC} (left Y axis, filled circles, solid line) dropped (t-test for zero slope, $p < 0.0001$). By contrast, the normalised absolute total power (right Y axis, open circles, dash line) had a positive linear trend (t-test for zero slope, $p < 0.01$). It should be noted although there was a positive trend, across all the f_{LIC} tested, the variation of the normalised absolute total power was small (1.01 ± 0.06 , mean \pm S.D.) and the difference from 1 is not significant (t-test, $p = 0.90$).

normalised absolute total power (scaled by right ordinate) of VCN activity, respectively. In spite of the fact that increases of f_{LIC} had a positive trend effect on the total power (dash regression line, t-test for zero slope <0.01), the effect seemed minimal because the deviation from 1 (normalised absolute total power, 1.01 ± 0.06 , mean \pm S.D.), i.e. deviation from total power under 'free-run' conditions, was not significant (t-test, $p=0.90$). By contrast, there was remarkable reduction of power density at f_{LIC} (solid regression line, t-test for zero slope <0.0001) as f_{LIC} was moved away from f_{INT} . This effect could be observed by comparing the VCN neurograms under conditions of different f_{LIC} in Fig. 5.3A, 5.3B. In summary, the decline of rhythmical activity at f_{LIC} was not accompanied by a reduction of total population PGN activity.

5.4.3 Single PGN activity in response to f_{LIC} changes

5.4.3A 1:1 frequency-lock of the dominant rhythm of single PGNs to LIC-related activity only occurs within a narrow range of f_{LIC}

Change of discharge patterns of single PGNs was examined in a f_{LIC} range (0.49-1.79 Hz) similar to that tested for population PGN activity. Fig. 5.9 shows an example of results from experiments where single PGN activity was recorded (left panel: neurograms; right panel: overlapping autospectra of PGN activity and TP waves). In this example two PGNs were recorded simultaneously (PGN1: red line, PGN2: blue line, TP waves: black line). Under 'free-run' conditions (V_T : 1-1.2 ml; f_{LIC} : 1.9-2.5 Hz), single PGNs exhibited an intrinsic dominant rhythm in their discharges (f_{INT} , median frequency, 0.69 Hz; interquartile range, 0.66-0.73 Hz). This is illustrated in Fig. 5.9A (f_{LIC} : 2.00 Hz; f_{INT} of PGN1, 0.78 Hz; f_{INT} of PGN2, 0.69 Hz). Neither of the PGNs simultaneously recorded in a pair (5 pairs) had the same f_{INT} . This result was

— PGN1 — PGN2 — TP

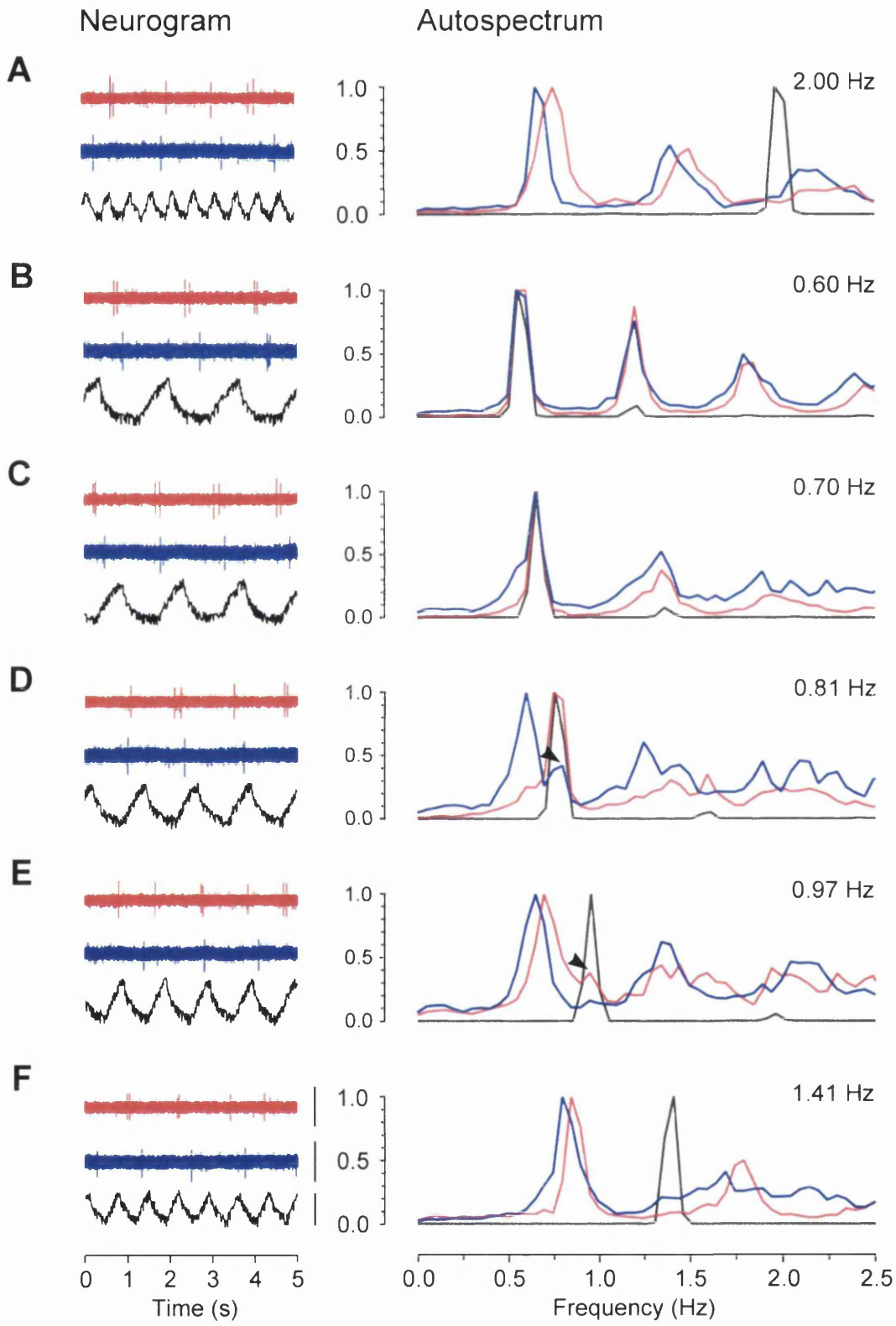


Fig. 5.9 Neurograms and superimposed autospectra of PGN activity, PGN1(red), PGN2 (blue) and LICs (black) showing frequency dependent synchronization of single PGNs to LICs. *A*, Under 'free-run' conditions (f_{LIC} , 2.00 Hz), both neurones show an intrinsic dominant rhythm (f_{INT} , 0.78 and 0.69 Hz for PGN1 and PGN2, respectively). *B*, *C*, When f_{LIC} was moved into f_{INT} range (0.60 Hz in *B* and 0.70 Hz in *C*), stable 1:1 entrainment between the two PGNs and LICs resulted. *D*, At 0.81 Hz, the PGN with the higher f_{INT} was still entrained to LICs but the other unit failed to lock. *E*, *F*, At higher f_{LICs} (0.97 in *E* and 1.41 Hz in *F*) single units were not entrained to LICs. The small peak at f_{LIC} in *D* and *E* (arrowhead) might arise from intermittent phase-lock of single PGNs to LICs (relative coordination, see text). Sample neurograms of PGN1 and PGN2 activity and TP wave under each condition are shown on the left. Calibration, 25 μ V (PGN), 10 mmHg (TP).

similar to those observed in the absence of CRD in the previous study (see **Chapter Four**). Moving f_{LIC} while maintaining constant V_T (2-2.5 ml) into f_{INT} range led to 1:1 frequency-lock between PGNs and LIC-related activity and, in cases where two PGNs were recorded simultaneously, this also resulted in frequency-lock of the two units at f_{LIC} (f_{LIC} : 0.6 Hz in Fig. 5.9B). LIC-PGN 1:1 entrainment was retained through a range of different f_{LICs} (eg. f_{LIC} : 0.70 Hz in Fig. 5.9C) above which 1:1 frequency-lock probability started to decline. The frequency-locking range of different PGNs was rarely the same, presumably reflecting the spread of f_{INTs} within the population. In the illustrative example, while PGN1 (higher f_{INT}) was still frequency-locked to LIC-related activity, PGN2 (lower f_{INT}) was not (f_{LIC} : 0.81 Hz in Fig. 5.9D). In contrast to the observations in the whole nerve experiments, at higher f_{LICs} , the dominant rhythms of single PGNs were not frequency-locked to LICs and they were different from each other (f_{LIC} : 0.97, 1.41 Hz in Fig. 5.9 E, F, respectively). Although the dominant rhythm of PGNs was not locked to LIC when f_{LIC} was high, a less prominent rhythmical component at f_{LIC} was frequently observed (e.g. arrowheads: PGN2 in Fig. 5.9D and PGN1 in Fig. 5.9E). The presence of such a minor LIC-related rhythmical activity could be explained by intermittency of phase locking between PGNs and LIC (see section **Dynamic patterns of interaction between PGNs and LIC**). The dissociation of the dominant frequencies of PGNs and f_{LIC} when f_{LIC} shifted away from f_{INT} was accompanied by a decline in coherence. This is demonstrated in Fig. 5.10 (same PGNs and same data recording time as in Fig. 5.9, f_{LIC} is indicated by •). Coherence spectra between LIC-PGN1 (red), LIC-PGN2 (blue) and PGN1-PGN2 (purple) was superimposed. Under 'free-run' conditions, coherence between them was low (coherence at f_{LIC} : LIC-PGN1, 0.08; LIC-PGN2, 0.21; PGN1-PGN2, 0.04, Fig. 5.10A). As f_{LIC} was brought near

— TP to PGN1 — TP to PGN2 — PGN1 to PGN2

Coherence Spectrum

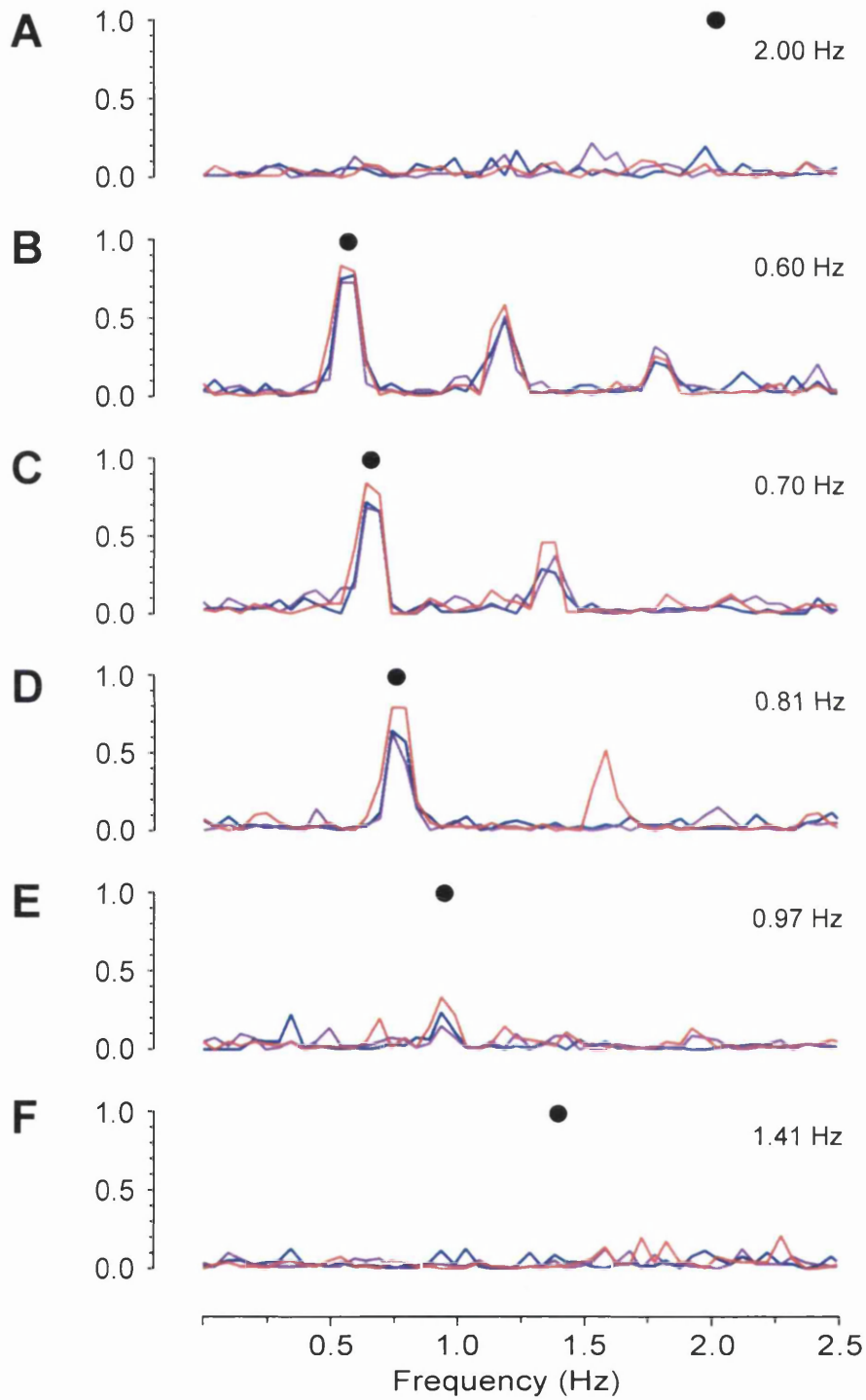


Fig. 5.10 Change of strength of LIC-single PGN and single PGN-single PGN linear correlation, evaluated by coherence spectrum, in response to f_{LIC} changes. Coherence spectra between LIC-PGN1 (red), LIC-PGN2 (blue) and PGN1-PGN2 were overlapped. f_{LIC} is indicated by a black circle. The PGNs and period of data analysis are the same as in Fig. 5.9. *A*, Under 'free-run' conditions, coherence between them was low (coherence at f_{LIC} , LIC-PGN1, 0.08; LIC-PGN2, 0.21; PGN1-PGN2, 0.04). *B, C, D*, When f_{LIC} was brought close to PGN f_{INT} , high coherence emerged (coherence at f_{LIC} , LIC-PGN1, 0.87, 0.88, 0.83; LIC-PGN2, 0.80, 0.76, 0.67; PGN1-PGN2, 0.75, 0.71, 0.67, in *B, C, D*, respectively). *E, F*, When f_{LIC} was moved further away from PGN f_{INT} , coherence at f_{LIC} dropped (coherence at f_{LIC} , LIC-PGN1, 0.36, 0.01; LIC-PGN2, 0.25, 0.08; PGN1-PGN2, 0.16, 0.04, in *E, F*, respectively).

f_{INT} , high coherence emerged (coherence at f_{LIC} : LIC-PGN1, 0.87, 0.88, 0.83; LIC-PGN2, 0.80, 0.76, 0.67; PGN1-PGN2, 0.75, 0.71, 0.67, in Fig. 5.10B, C, D, respectively). When f_{LIC} was moved further away from f_{INT} , coherence at f_{LIC} declined abruptly (coherence at f_{LIC} : LIC-PGN1, 0.36, 0.01; LIC-PGN2, 0.25, 0.08; PGN1-PGN2, 0.16, 0.04, Fig. 5.10E, F, respectively). The drop of coherence between PGNs and LIC at high f_{LIC} suggested that if the difference between f_{LIC} and f_{INT} was great tight coupling between them was lost and synchrony between single PGNs diminished as a result of loss of entrainment to a common drive. Consequently, PGNs could not maintain a synchronous state.

5.4.3B Temporal stability of phase difference between PGNs decreased when f_{LIC} was moved away from f_{INT}

Fig. 5.11 illustrates PGN→PGN phase relationship subjected to different conditions of LIC-related activity (same PGNs as in Fig. 5.9, 5.10). Under ‘free-run’ conditions, rhythmical synchronization between the two PGNs was not prominent in their cross correlogram (Fig. 5.11Ai, same data recording time as in Fig. 5.9A, 5.10A, dot lines: 95% confidence interval), which suggested phase lock was not a dominant feature. The lack of evident periodic phase lock could also be observed by the fact that no prominent peak was present in the envelope spectrum of the cross correlogram (Fig. 5.11Aii, f_{LIC} is indicated by •, see **Chapter Three**). The absence of apparent vertical striation in the PGN1→PGN2 OCRP (Fig. 5.11Aiii) suggested that the phase difference between the two PGNs drifted across time. By contrast, when f_{LIC} was close to f_{INT} (Fig. 5.11Bi, same data recording time as in Fig. 5.9B, 5.10B), the PGN1→PGN2 cross correlograms revealed conspicuous rhythmicity indicating strong rhythmical synchronization. The rhythm on the cross correlogram had a

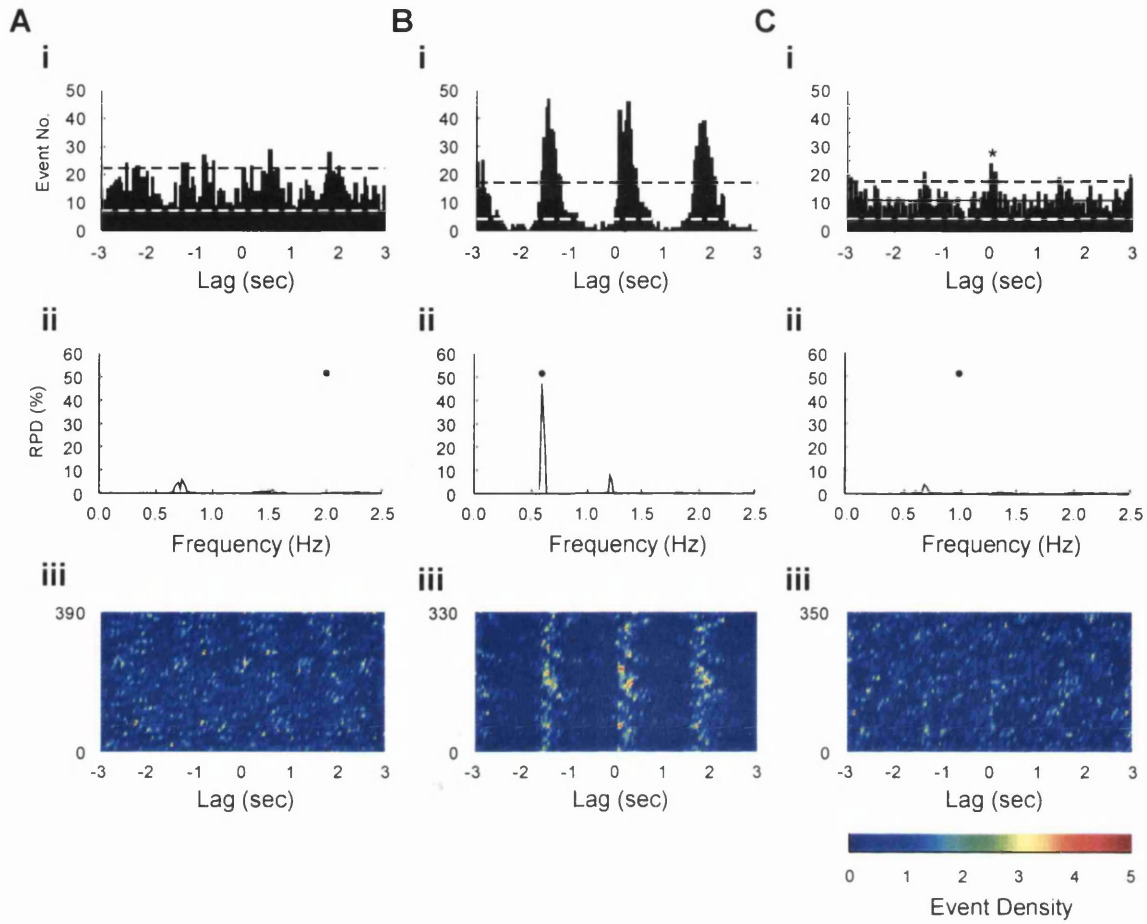


Fig. 5.11 Rhythmical synchronization between single PGNs in response to f_{LIC} changes. The PGNs are the same as in Fig. 5.9 and Fig. 5.10. *A*, 'Free-run' conditions (the same period of analysis as in Fig. 5.9A and Fig. 5.10A). *Ai*, Rhythmical synchronization was not a prominent feature as revealed by the PGN1→PGN2 cross correlogram (dash lines, 95% confidence interval). *Aii*, The lack of rhythmical synchronization was also suggested by the absence of a prominent spectral peak in the envelope autospectrum (scaled by relative power density, RPD) of the cross correlogram. f_{LIC} is indicated by a black circle. *Aiii*, Under 'free-run' conditions, there was no stable phase relationship between the two PGNs as revealed by the absence of vertical striations in the ordinary correlation raster plot (OCRP). *B*, Conditions when f_{LIC} was close to PGN f_{INT} (the same period of analysis in Fig. 5.9B and Fig. 5.10B). *Bi*, *Bii*, Prominent rhythmical synchronization through coupling to LICs emerged as revealed by the conspicuous periodic pattern in the cross correlogram and the dominant spectral peak at f_{LIC} in its envelope autospectrum. *Biii*, There was high temporal stability of phase difference between the two PGNs as suggested by the striking vertical striations in OCRP. *C*, Conditions when f_{LIC} was moved away from PGN f_{INT} (the same period of analysis as in Fig. 5.9E and Fig. 5.10E). *Ci*, *Cii*, No rhythmical synchronization was present as revealed by the absence of a significant periodic pattern in the cross correlogram and by the lack of a prominent spectral peak in the envelope autospectrum. However, a small peak (asterisk) near lag zero in the cross correlogram suggests that some activity of both PGNs discharged at the same time. *Ciii*, The lack of vertical striations in the OCRP suggests that there was no stable phase difference between the two PGNs.

frequency the same as f_{LIC} . This suggests that the rhythmical synchronization between the two PGNs was achieved through coupling of both PGNs to LICs. Under these strong coupling conditions, the cross correlograms showed that the interval between lag zero and the peak nearest to lag zero was short (median, 0.04 sec, interquartile range, 0.01-0.11 sec, N=13), indicative of near zero synchronization. The prominent peak at f_{LIC} in the envelope spectrum (Fig. 5.11Bii) demonstrates that this periodic phase locking occurred at f_{LIC} . High temporal stability of PGN1→PGN2 phase difference was revealed by the distinct vertical striations in the correlation raster plot (Fig. 5.11Biii). When f_{LIC} was moved away from f_{INT} , rhythmical synchronization did not dominate PGN1→PGN2 interactions as evidenced by the lack of obvious rhythmicity in the cross correlogram and no prominent peak in its envelope spectrum (Fig. 5.11Ci, Cii, same data recording time as in Fig. 5.9E, 5.10E). The phase difference between them underwent considerable drift across time as revealed by the random distribution of event density in the cross correlation raster plot (Fig. 5.11Ciii). Although rhythmical synchronization was not the dominant feature, a small peak around zero lag was frequently observed (Fig. 5.11Ci, asterisk). This arose from intermittent phase-lock of PGN1 and PGN2 to a common drive, LIC-related activity. LIC triggered JPSPs, which measure the probability of concurrence of two triggered events in relation to triggers (see **Chapter Three**), were used to clarify this phenomenon. This is shown in Fig. 5.12 (same PGNs and same data recording time as in Fig. 5.9E, 5.9E, 5.11C). Although not conspicuous, clustering of concurrent events along the diagonal (arrows) suggested that some discharges of the two PGNs occurred around the same time in relation to LICs (• indicated where the inflation phase of TP

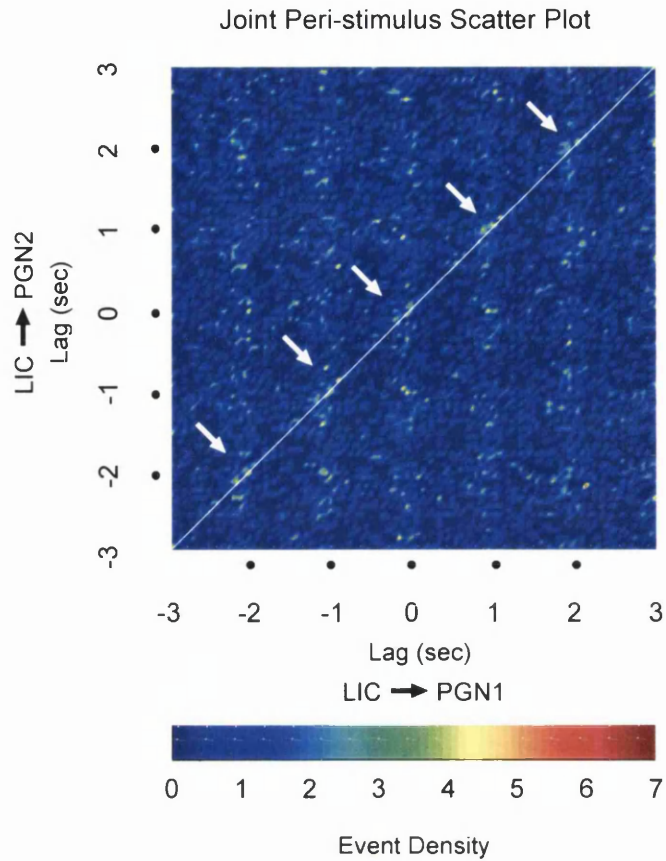


Fig. 5.12 Detection of PGN-PGN weak coupling through LIC-related activity by the joint peri-stimulus scatter plot (JPSP). The PGNs and the period of data analysis are the same as in Fig. 5.9E, Fig. 5.10E and Fig. 5.11C. The clusters with high event density (arrows) along the diagonal line suggest that coincidence of some activity from PGN1 and PGN2 arose from phase-lock to LICs with the same phase difference.

occurred). This implies phase lock of these PGN events resulted from the fact that both were phase locking to LICs.

The temporal stability of rhythmical synchronization between PGNs was quantified by the phase variation factor (see **Chapter Three**). Fig. 5.13 summarises the results. When f_{LIC} was close to the f_{INT} range of PGNs (frequency range: 0.46-0.88 Hz, shaded area), there was a high probability that both PGNs were frequency-locked to LICs (○) and phase variation was minimal. By contrast, when f_{LIC} was moved away from f_{INT} , the PGNs failed to follow f_{LIC} (●) and the phase difference between them became unstable (t-test for zero slope of regression line: $p < 0.0001$).

5.4.3C The change of PGN discharge patterns in response to change of f_{LIC} is not accompanied by a significant change of the mean discharge rate of single PGNs

The mean discharge rate (MDR) of single PGNs under different ventilation conditions was normalised by MDR under 'free-run' conditions because of the wide range of MDR of single PGNs (range: 0.75-2.71 Hz; see also **Chapter Four** and Johnson & Gilbey, 1996). Fig. 5.14 shows the scatter plot of normalised MDR under conditions of different f_{LIC} . Although there was a moderate positive trend when f_{LIC} increased, it was not significant (t-test for zero slope of the regression line, $p = 0.055$). This demonstrates that change of single PGN discharge patterns in response to increase of f_{LIC} was not associated with significant change of their discharge rates.

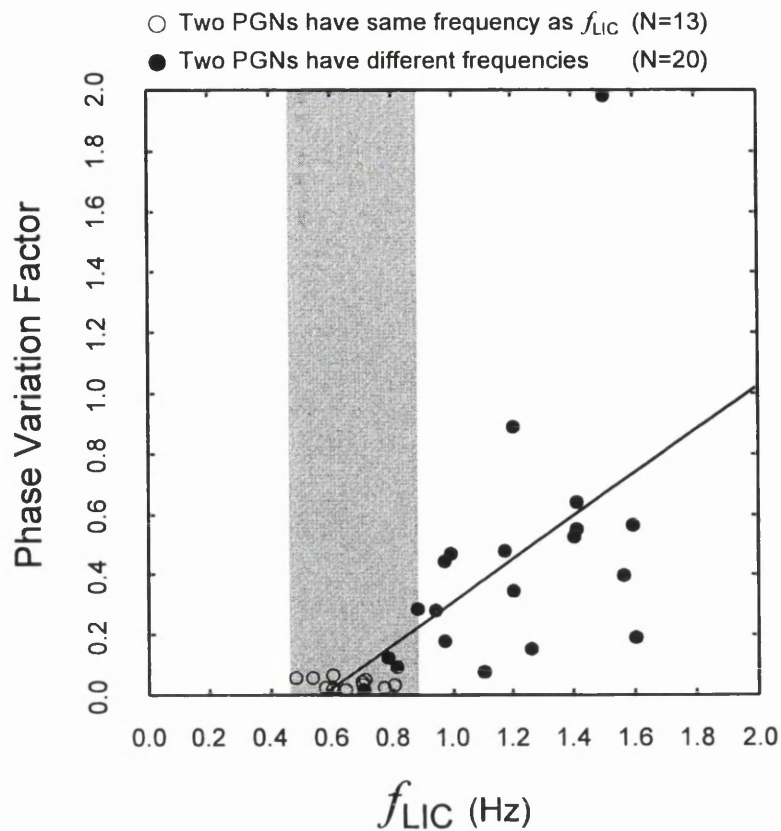


Fig. 5.13 Summary scatter plot for the temporal stability of rhythmical synchronization between two PGNs in response to f_{LIC} changes. The temporal stability of rhythmical synchronization was evaluated by the phase variation factor (see Chapter three). A low phase variation factor would suggest a stable state of rhythmical synchronization. When f_{LIC} was close to the range of PGN f_{NT} (0.45-0.88 Hz, shaded area), there was a high probability both PGNs were 1:1 frequency locked to LICs (open circles) and the rhythmical synchronization between them was rather stable. When f_{LIC} was moved out of the PGN f_{NT} range, the dominant frequencies of the two PGNs differed and stable rhythmical synchronization was not a dominant feature (filled circles). The phase variation factor increased significantly as f_{LIC} was increased (t-test for zero slope, $p < 0.0001$).

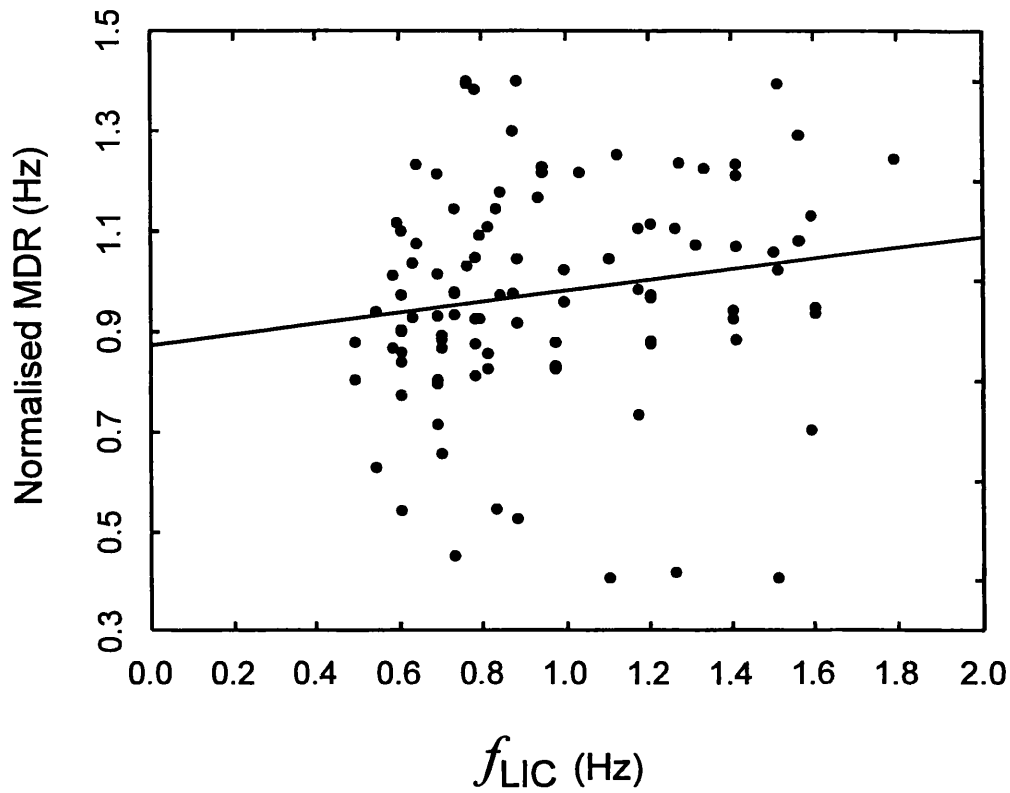


Fig. 5.14 Changes of the mean discharges rate (MDR) of single PGNs in response to f_{LIC} changes. In order to compare the results across different PGNs, the MDR of single PGNs was normalised by the MDR under 'free-run' conditions because of the wide range of MDR of single PGNs. There was no significant linear trend in the normalised MDR as f_{LIC} varied.

5.4.4 Summary for difference of discharge behaviours of population and single PGN activity in response to f_{LIC} changes

The difference in single and population PGN behaviour in response to changes of f_{LIC} are summarised in Fig. 5.15. Fig. 5.15A shows the frequency response range of PGN activity when the ventilation rate changed. When f_{LIC} increased, the dominant frequency of PGNs could maintain 1:1 frequency-lock to f_{LIC} only within a narrow f_{LIC} range (~ 0.5 - 1.0 Hz) which was close to the range of f_{INT} (0.46 - 0.88 Hz, Fig. 5.15A, shaded area). When f_{LIC} was high the dominant frequency of the PGNs remained near the range of f_{INT} . In contrast to the frequency response of single PGNs, the dominant frequency of population PGN activity could follow f_{LIC} faithfully over a much wider range (up to ~ 1.5 Hz). Fig 5.15B relates the frequency ratio of PGN activity and LICs to the difference between f_{LIC} and f_{INT} . 1:1 entrainment (Fig 5.15B, lower dash line) between single PGNs and LICs occurred only when the difference of f_{LIC} to f_{INT} was less than ~ 0.2 Hz (shaded area). When the frequency difference was out of that range, the dominant frequency of single PGNs dissociated from f_{LIC} although higher order rational frequency-lock (other than 1:1) such as 2:1 (upper dash line) was possible. By contrast, the dominant frequency of population PGN activity could maintain 1:1 frequency-locked to f_{LIC} even when f_{LIC} was ~ 1.0 Hz above f_{INT} . Fig 5.15C displays the changes of coherence between PGN activity and LICs when f_{LIC} was moved away from f_{INT} . In both cases, coherence dropped significantly as f_{LIC} was moved away from f_{INT} (t-test for zero slope of the regression lines, single PGNs: $P < 0.001$, population PGNs: $P < 0.001$). However, the decline in coherence was more moderate at the population level than at single unit level (t-test for equal slope of the regression lines, $P < 0.001$).

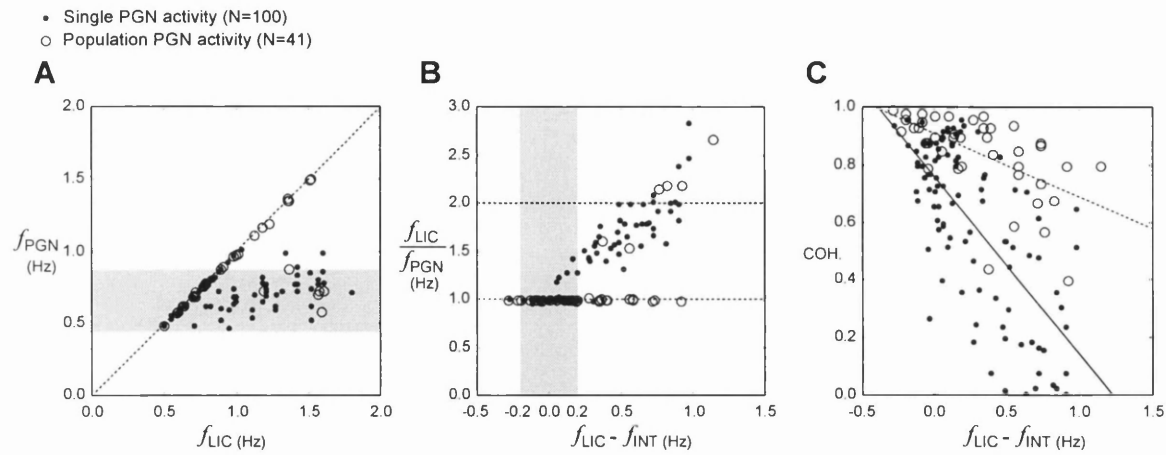


Fig. 5.15 Summary scatter plots showing frequency responses of single PGN activity (filled circles) and population PGN activity (open circles) to changes of f_{LIC} . **A**, Dominant frequency (f_{PGN}) for single PGNs and population PGN plotted against f_{LIC} illustrates the difference in distribution of f_{PGN} s when f_{LIC} changed. While f_{PGN} of population activity could maintain 1:1 frequency-lock to LICs when f_{LIC} was increased, f_{PGN} of most single unit activity remained in the range of f_{INT} (shaded area, 0.46-0.88 Hz). **B**, The frequency ratio, $f_{\text{LIC}} / f_{\text{PGN}}$, plotted against the difference between f_{LIC} and PGN f_{INT} , $f_{\text{LIC}} - f_{\text{INT}}$, provides evidence for frequency-lock at 1:2 as well as 1:1 (dash lines). f_{PGN} to f_{LIC} 1:1 entrainment for single PGNs was only possible when $f_{\text{LIC}} - f_{\text{INT}}$ was less than ~ 0.2 Hz (shaded area), while population f_{PGN} could follow f_{LIC} faithfully over a broader range. **C**, Coherence at f_{LIC} (COH.) plotted as a function of $f_{\text{LIC}} - f_{\text{INT}}$ shows significant decline of coherence at single neuron and population level (t-test for zero slope, $p < 0.001$ for both single PGN activity, solid regression line, and population PGN activity, dash regression line). The coherence drop was more moderate for population PGN activity than single PGN activity when f_{LIC} was moved away from PGN f_{INT} (t-test for equal slope, $p < 0.001$).

In summary, there was strong evidence indicating that 1:1 frequency coupled to LIC-related activity was a stable feature of population PGN activity across a wide range of f_{LIC} despite this property declining rapidly at single PGN level as f_{LIC} increased.

5.4.5 PGN activity at cardiac frequency

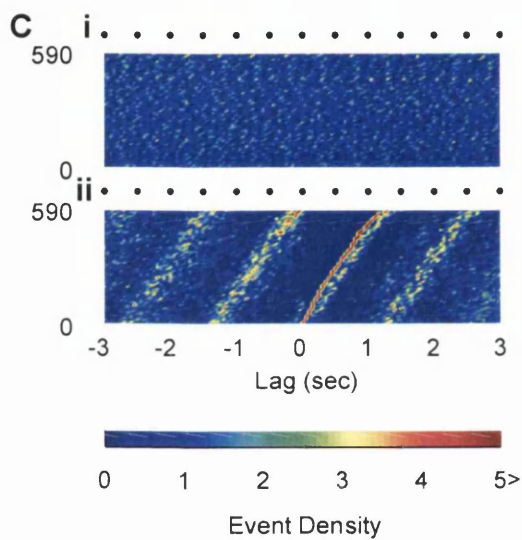
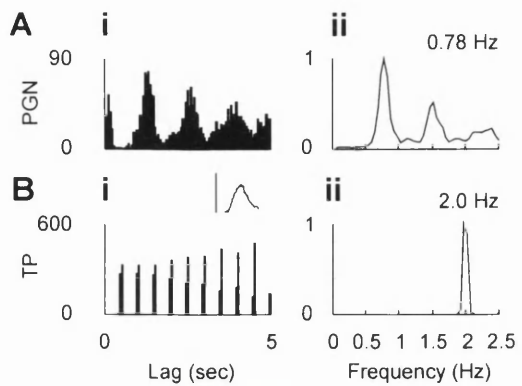
No spectral peak at cardiac frequency was observed in any of the VCN autospectra. In all cases, the dominant frequencies of single PGNs were different from the heart rate and BP→PGN cross correlograms triggered by systolic phase of BP waves did not exhibit significant correlation.

5.4.6 Dynamic patterns of interaction between PGNs and LIC

Fig. 5.16 – 5.18 show the dynamic patterns of LIC-single PGN phase difference under different ventilation conditions. The dynamic patterns were classified based on OCRP and RCRP between LICs and single PGNs. The autocorrelograms and autospectra were also displayed to provide information of the emergent dominant features across time. Since not all the patterns could be observed across the range of f_{LIC} tested in any experiment, single PGNs from different experiments are used for illustration. Moreover, it must be emphasised that a dynamic pattern did not necessarily persist across the whole data recording time. In many cases different patterns were mixed, especially when f_{LIC} was moved away from the PGN f_{INT} . For example, in some cases, although LIC→PGN 2:1 frequency-lock was the dominant feature, 1:1 relationship was observed in brief periods of the whole data recording time (for example, Fig. 5.18A-C). An exact incidence for each pattern is therefore not specified here.

1. 'Free-run' (Fig. 5.16A-C): During periods of 'free-run', the autocorrelogram (Ai) of single PGNs exhibited a dominant rhythm with the corresponding spectral peak in the autospectrum (0.78 Hz, Aii). The nature of high f_{LIC} and low V_T during 'free-run' is revealed in the TP autocorrelogram with the inset showing the magnitude of the TP (Bi) and its autospectrum (2.0 Hz, Bii). The TP-triggered LIC→PGN OCRP and RCRP were used to study the temporal stability of phase difference and the clustering of phase difference, respectively (see **Chapter Three**). Lack of vertical striations in OCRP (Ci, • denotes the occurrences of TP inflation phase) indicates that no stable phase difference existed. The RCRP was dominated by periodic diagonal bands, reflecting the rhythmical nature of the single PGN. Spanning of each of these diagonal bands across a whole cycle of the single PGN rhythm suggests constant LIC→PGN phase drift. These observations were consistent with asynchronization between PGN activity and LICs.
2. 1:1 entrainment (Fig. 5.16D-F): When f_{LIC} was brought close to f_{INT} (0.58 Hz in this single PGN) with high V_T (Ei inset), there was high probability that single PGN activity was 1:1 entrained to LICs. The frequency-lock phenomenon (f_{LIC} : 0.63) could be easily observed by comparing the autocorrelograms (Di, Ei) and the autospectra (Dii, Eii) of single PGN activity and LICs. The striking vertical striations in OCRP (Fi) and in RCRP (Fii) indicated that there was only one stable TP→PGN phase difference across time.
3. Asynchrony (or phase walk-through, Ermentrout & Rinzel, 1984) (Fig. 5.17A-C): Although complete TP→PGN asynchrony throughout the whole data recording time under conditions of high V_T was uncommon, it was observed in some experiments. One example is shown on the left panel of Fig. 5.17.

'Free Run' $f_{INT} = 0.78$ Hz



1:1 Entrainment $f_{INT} = 0.58$ Hz

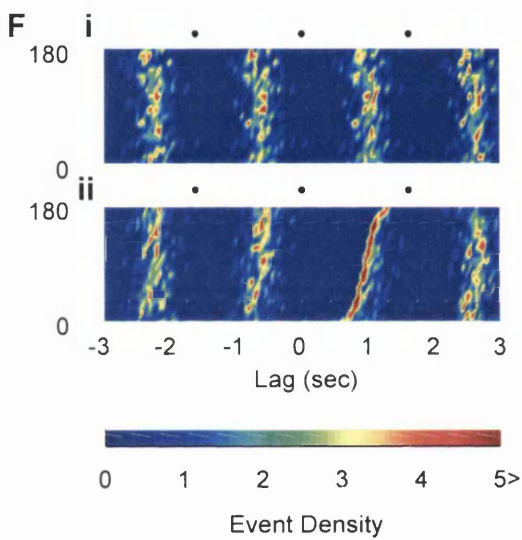
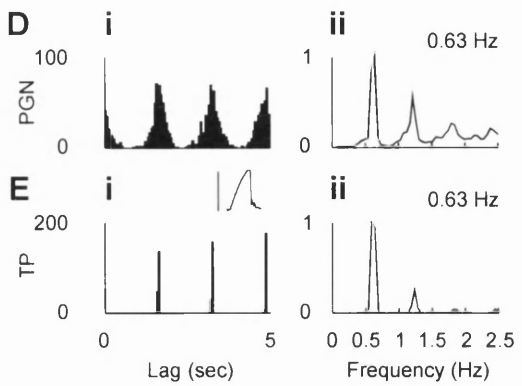
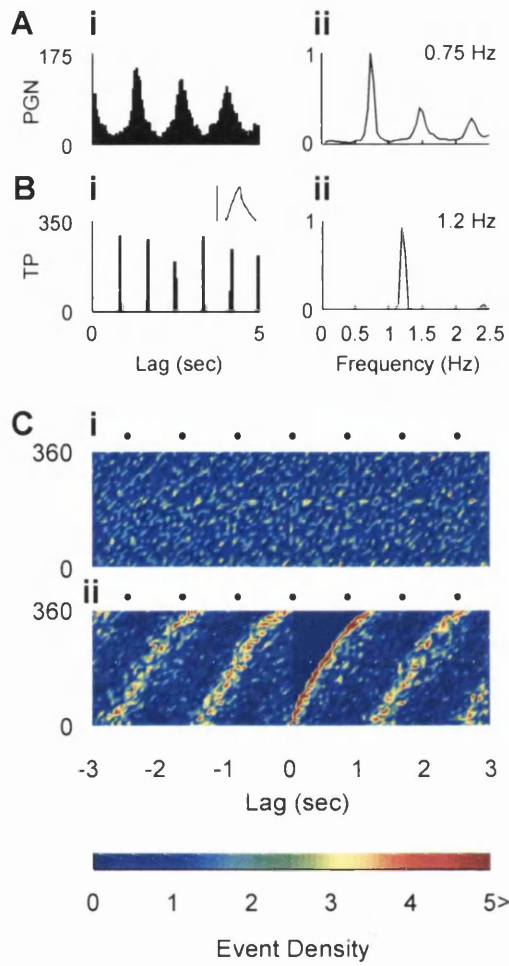


Fig. 5.16 Interaction under 'free-run' conditions and 1:1 entrainment between LICs and single PGN activity. *A, B, C*, An example of LIC-PGN interaction when the tidal volume (V_T) was low and f_{LIC} (2.00 Hz) was high, i.e. 'free-run' condition. *Ai, Bi*, Autocorrelograms of the single PGN and LICs. The inset shows the amplitude of the TP was relatively low. *Aii, Bii*, Autospectra, scaled by normalised power density, of the single PGN and LICs. The f_{INT} of the single PGN (0.78 Hz) was different from that of LICs. *C*, The LIC→PGN ordinary correlation raster plot (OCRP) and reordered correlation raster plot (RCRP). The black circles denote the occurrences of TP inflation phase. *Ci*, The lack of vertical striations in the OCRP indicates constant phase drift between LICs and single PGN activity. *Cii*, The RCRP shows that the phase differences spanned the whole cycle of the single PGN rhythm without interruption. Note the periodic slant bands repeated with a period equivalent to that of the PGN dominant rhythm. These findings suggest asynchronization between them. *D, E, F*, An example of LIC- PGN 1:1 entrainment when V_T was high and f_{LIC} was close to PGN f_{INT} . *Di, Ei*, The autocorrelograms of the single PGN and LICs (inset showing relative high amplitude of TP). *Dii, Eii*, The autospectra of the single PGN and LICs. The single PGN was frequency-locked to f_{LIC} (0.63 Hz) which was close to the PGN f_{INT} (0.58 Hz). *F*, LIC→PGN OCRP and RCRP. *Fi, Fii*, There was only one stable phase difference between LIC and the single PGN activity as revealed by the vertical striations in the LIC→PGN OCRP and RCRP, indicating 1:1 entrainment relationship. Calibration for TP, 10 mmHg.

Asynchrony $f_{INT}: 0.72 \text{ Hz}$



Relative Coordination $f_{INT}: 0.78 \text{ Hz}$

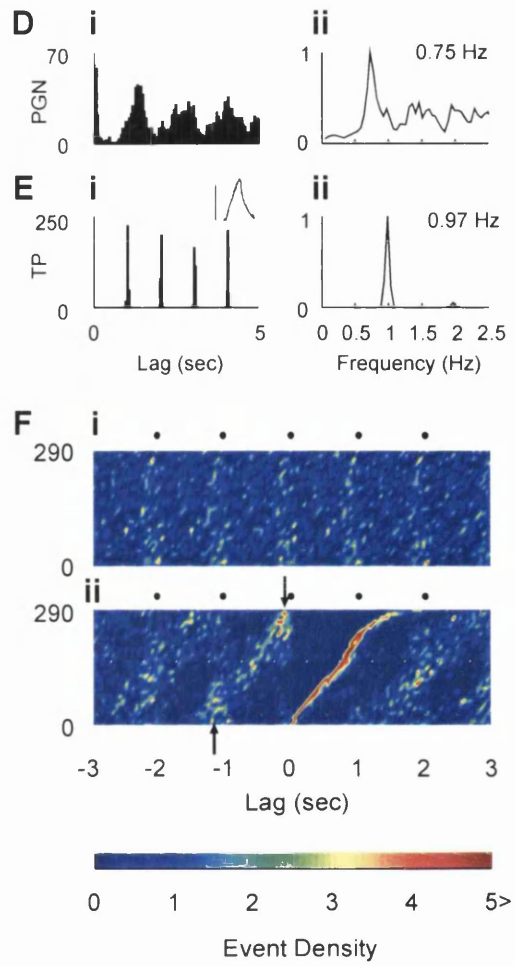


Fig. 5.17 Asynchrony (or phase walk-through) and relative coordination between LICs and single PGN activity. *A, B, C*, An example of asynchrony between single PGN activity and LICs when both V_T and f_{LIC} (1.2 Hz) were high. *Ai, Bi*, Autocorrelograms of the single PGN and LICs (inset showing relative high amplitude of TP). *Aii, Bii*, Autospectra of the single PGN and LICs. The dominant frequency of the single PGN (0.75 Hz) was close to its f_{INT} (0.72 Hz) but different from that of LICs. *C*, The LIC→PGN ordinary correlation raster plot (OCRP) and reordered correlation raster plot (RCRP). The black circles denote the occurrences of TP inflation phase. *Ci, Cii*, Similar to those under conditions of 'free-run' (cf. Fig. 5.16Ci, 5.16Cii), the absence of vertical striations in the OCRP and uninterrupted whole-cycle spanning phase differences in the RCRP are consistent with constant phase drift, i.e. complete asynchrony. *D, E, F*, An example of relative coordination between LICs and single PGN activity when both V_T and f_{LIC} (0.97 Hz) were high. *Di, Ei*, The autocorrelograms of the single PGN and LICs (inset showing relative high amplitude of TP). *Dii, Eii*, The autospectra of the single PGN and LICs. The dominant frequency of the single PGN (0.75 Hz) was similar to its f_{INT} (0.78 Hz) but was different from f_{LIC} . *F*, LIC→PGN OCRP and RCRP. *Fi*, Vertical striations with variable event density in the OCRP suggest intermittent phase-lock between LICs and single PGN activity. *Fii*, The whole-cycle spanning slant bands mixed with short vertical striations in the RCRP were consistent with phase-lock of some PGN activity to LICs in spite of a phase drifting background. These findings suggest relative coordination between LICs and single PGN activity (see text). Calibration for TP, 10 mmHg.

In this case, the f_{INT} was 0.72 Hz. When f_{LIC} was changed to 1.2 Hz, this PGN retained a dominant frequency (0.75 Hz), similar to its f_{INT} , as revealed in its autocorrelogram (Ai) and autospectrum (Aii). The autocorrelogram and the autospectrum of LICs are shown in Bi (inset, TP) and Bii. The OCRP and RCRP were similar to those observed under conditions of 'free-run' (cf. Fig. 5.16Ci, Cii) suggesting complete asynchrony.

4. Relative coordination (Fig. 5.17D-F): A more common finding during periods of high f_{LIC} and high V_T was phase drift alternating with intermittency of phase lock, i.e. relative coordination, a term used to contrast absolute coordination where stable phase lock is present (von Holst, 1939). The case shown in the right panel of Fig. 5.17 characterises this phenomenon. The f_{INT} was 0.78 Hz in this single PGN. During the period illustrated (high V_T , Ei inset), the dominant rhythm of this PGN had a frequency (0.75 Hz, Di, Dii) different from that of LICs (0.97 Hz, Ei, Eii). The LIC→PGN OCRP shows periodic LIC-locked vertical bands with varied event densities (Fi). This suggests that the phase lock to LICs was not a stable feature of this PGN. The slant bands with short vertical striations in the RCRP (arrows, Fii) indicates that some single PGN events were locked to LICs in spite of a phase drifting background.
5. 2:1 frequency-lock (Fig. 5.18A-C): The existence of high order rational frequency-lock, other than 1:1, is exemplified by 2:1 frequency-lock. During the period shown in the left panel of Fig. 5.18, this PGN had a dominant frequency (0.80 Hz) similar to its f_{INT} (0.88 Hz). The dominant frequency was half of f_{LIC} (1.60 Hz) as revealed by comparing the periods in their autocorrelograms (Ai, Bi) and by the fact that the spectral peak at f_{LIC} (Bii) coincided with the first harmonic of the dominant rhythm of this PGN (Aii). A

2:1 frequency lock $f_{INT}: 0.88 \text{ Hz}$

3:1 frequency lock $f_{INT}: 0.82 \text{ Hz}$

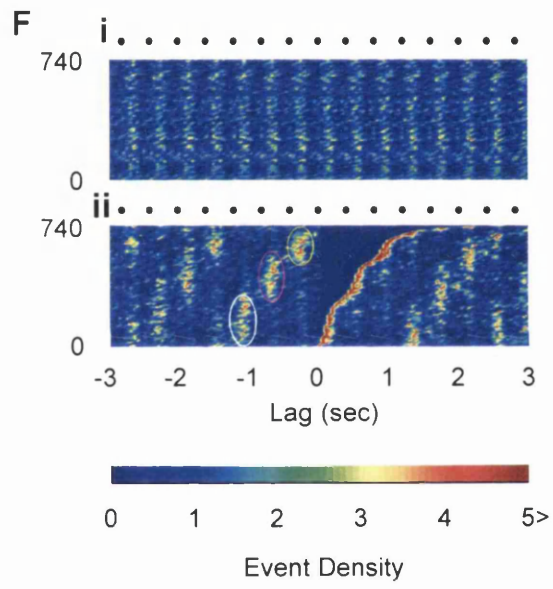
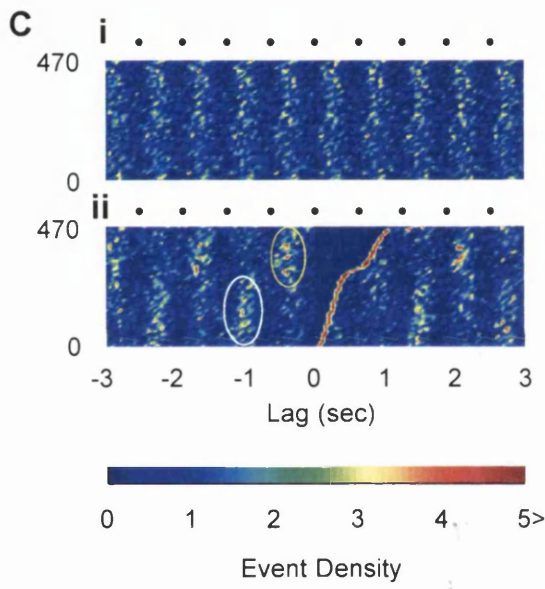
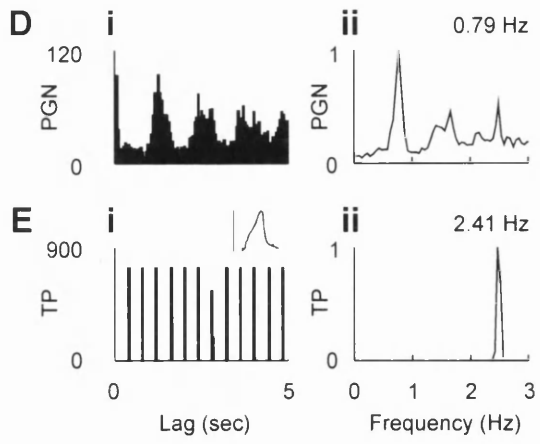
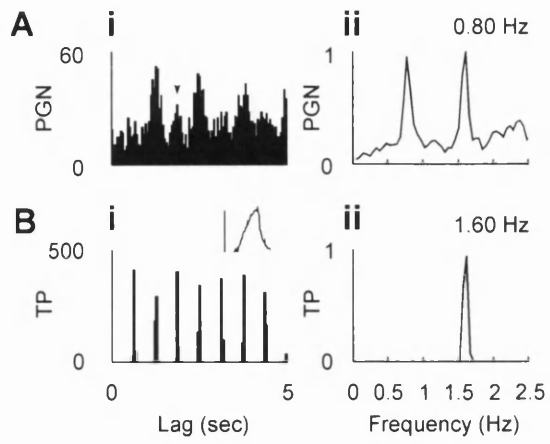


Fig. 5.18 High order rational frequency lock between LICs and single PGN activity. *A, B, C*, An example of 2:1 LIC→PGN frequency lock when V_T and f_{LIC} (1.60 Hz) were high. *Ai, Bi*, The autocorrelograms of the single PGN and LICs (inset showing relative high amplitude of TP). The first dominant peak in the PGN autocorrelogram is lined up with the second peak in the LIC autocorrelogram, indicating a 2:1 frequency lock relationship. Some PGN activity was locked 1:1 to LICs as indicated by the small peak (arrowhead). *Aii, Bii*, The autospectra of the single PGN and LICs. The dominant frequency of the single PGN (0.80 Hz) was similar to its f_{INT} (0.88 Hz) and was half of f_{LIC} . The prominence of the first harmonic peak in the single PGN autospectrum was due to 1:1 frequency-lock to LICs in some PGN activity. *C*, The LIC→PGN ordinary correlation raster plot (OCRP) and reordered correlation raster plot (RCRP). The black circles denote the occurrences of TP inflation phase. *Ci*, The vertical striations in the OCRP suggests that phase-lock was a stationary feature. *Cii*, The RCRP shows that the stationary phase differences were grouped into two clusters (grouped by white and yellow circles). These findings are consistent with a 2:1 frequency lock relationship between LICs and single PGN activity. *D, E, F*, An example of 3:1 LIC→PGN frequency lock when V_T was high and f_{LIC} (2.41 Hz) was exceptional high (see text). *Di, Ei*, The autocorrelograms of the single PGN and LICs (inset showing relative high amplitude of TP). The first peak in the PGN autocorrelogram was lined up with the third peak in the LIC autocorrelogram, indicating a 3:1 frequency-lock relationship. *Dii, Eii*, The autospectra of the single PGN and LICs. The dominant frequency of the single PGN (0.79 Hz) was similar to its f_{INT} (0.82 Hz) and was approximately one third of f_{LIC} . The exactness of frequency determination was limited by the spectral resolution but a 3:1 frequency-lock could be determined by the RCRP (see **Chapter three**). *F*, LIC→PGN OCRP and RCRP. *Fi*, The vertical striations in the OCRP suggests that phase-lock was a stationary feature. *Fii*, The RCRP shows that the stationary phase differences were grouped into three clusters (grouped by white, yellow and pink circles). These findings are consistent with a 3:1 frequency lock relationship between LICs and single PGN activity. Calibration for TP, 10 mmHg.

single TP wave was shown in Bi, inset. Some PGN activity was locked 1:1 to LICs as indicated by the small peak (Ai, PGN autocorrelogram, arrowhead) coincident with the peak in the LIC autocorrelogram and the prominence of the first harmonic peak of the PGN autospectrum. The vertical striations in the TP→PGN OCRP indicated that phase-lock was a stationary feature across time. A further analysis by RCRP revealed that these phase differences clustered into two fixed values (grouped by white and yellow circles). This finding is consistent with phenomenon of 2:1 frequency-lock, where the activities alternate between two distinct phase differences.

6. 3:1 frequency-lock (Fig. 5.18D-F): 3:1 frequency-lock was not observed under conditions of high V_T and the f_{LIC} used in the standard experiment procedure. The reason for this might be partly attributed to the fact that the f_{LIC} used in the experiment protocol was not high enough for 3:1 frequency-lock because most of the single PGNs had a f_{INT} about 0.7 Hz and for 3:1 frequency-lock to occur, f_{LIC} should be around 2 Hz, a high frequency not used under conditions of high V_T . However, in one experiment (Fig. 5.18 right panel, this data was not included in the pooled data illustrated above because the high f_{LIC} was exceptional) the f_{LIC} was increased to 2.41 Hz (Eii) while maintaining high V_T (Ei inset), 3:1 frequency-lock was observed in a single PGN (f_{INT} : 0.82 Hz). Three to one frequency-lock was suggested by the fact that the first peak in the PGN autocorrelogram (Di) lined up with the third peak in the LIC autocorrelogram (Ei). Their frequency relationship was clearly demonstrated in the autospectra: the spectral peak at f_{LIC} (Eii) coincided with the second harmonic of the dominant frequency of this PGN (0.79 Hz, Dii). The LIC→PGN OCRP showed that the constancy of phase difference was a stationary feature. However, clustering of the PGN events

into three groups (yellow, pink and white circles) in RCRP suggested the phase difference shifted between three fixed values; a finding consistent with 3:1 frequency-lock.

5.5 Discussion

This study has demonstrated that a dominant population rhythm coupled to a periodic drive can emerge from a pool of CVA PGN oscillators across a wide range of driving frequencies although an individual oscillator can only maintain 1:1 frequency lock over a restricted frequency range. Although lung inflation has a significant depressive effect on the cardiovascular system (Daly & Robinson, 1968; Ashton & Cassidy, 1985; Cheng *et al.*, 1989) in dogs, it was less prominent in cats and rats (Marshall, 1994). The finding that there was no significant change of MBP across the range of f_{LIC} tested was consistent with observations from a previous study in rats (Marshall & Metcalfe, 1988).

5.5.1 Afferent pathways involved in the interaction between LIC-related activity and CVA PGN activity

Although the detail anatomy is not clearly understood, the interaction between LICs and PGNs probably involves multiple afferent inputs. These include activity arising from pulmonary stretch receptors in response to lung volume change (Daly, 1985), from thoracic blood-volume and pressure sensitive cardiopulmonary receptors (Hainsworth, 1991) due to ventilatory cyclic changes of venous returns and from sympathetic afferents (Daly *et al.*, 1967). Muscle spindle afferent activity arising from chest movement (Critchlow & von Euler, 1963; De Troyer, 1996) through intercostal nerves may also be involved because stimulation of the intercostal nerve can influence sympathetic activity (Zanzinger *et al.*, 1994).

In addition, the ventilation-related BP fluctuations may contribute to ventilation-related sympathetic modulation through baroreceptors (McAllen, 1987; Habler *et al.*, 1996). Although pulse related activity was not a feature in the CVA PGN activity (see **Result, Chapter Four** and Johnson & Gilbey, 1996),

the baroreceptor pathway probably operates in the tail circulation because stimulation of the aortic nerve can reset the dominant rhythm of CVA PGNs (Johnson & Gilbey, 1998a). The prominent LIC-related BP undulations at low f_{LIC} (Fig. 5.2Ai, 5.2C) suggested the baroreflex mediated responses could at least account for part of the origin of PGN rhythmical activity at f_{LIC} . However, it is unlikely that it was the only factor because when BP LIC-related oscillations became inconspicuous at high f_{LIC} (Fig. 5.2Aii, 5.2C), modulatory effects of LICs on CVA PGN activity such as relative coordination and high order commensurate frequency-lock could still be observed. Although most of the effects of lung inflation on sympathetic activity is relayed through vagi (Daly, 1985), circuits localised to the spinal cord may also be involved because the LIC-related sympathetic activity was still found after transection of spinal cord at upper thoracic level in neonatal swine (Sica *et al.*, 1997). This can explain the existence of LIC-related activity after vagotomy in some of previous experiments (see **Chapter Four**). The present study followed a 'black-box' approach and the relative contributions of different afferent pathways to the LIC-related activity of CVA PGNs were not determinable from the present findings.

5.5.2 Comparison of discharge behaviours of single PGN and population

PGN activity in response to f_{LIC} changes

The f_{LIC} used in this study was biased towards the direction where ventilation rate was higher than f_{INT} of CVA PGNs. This is because in spite of hyperoxemia a state of central apnea could not be sustained if f_{LIC} was too low (see **Materials and Methods**). However, it is clear from the present study that stable 1:1 entrainment between LICs and single PGNs can only be maintained when the f_{LIC} is close to the f_{INT} of single PGNs. When the f_{LIC} was increased and

moved away from f_{INT} , the dominant frequencies of single PGNs still remained close to the range of f_{INT} (Fig. 5.15A) and the phase difference between them became unstable (Fig. 5.13). Different single PGNs may have different responses (e.g. Fig. 5.9D) when f_{LIC} is changed, reinforcing the conclusion (see **Chapter Four**) that CVA PGN activity is generated by multiple oscillators. The evidence indicates that strong coupling between LICs and single PGNs diminished precipitously as f_{LIC} shifted away from the range of PGN f_{INT} (Fig. 5.15C).

By contrast, the dominant rhythmical activity in the population PGN activity was 1:1 locked to LIC-related activity with high coherence across a much wider range of f_{LIC} (Fig. 5.3, 5.5, 5.15A). However, the persistence of the dominant frequency at f_{LIC} in the population activity does not necessarily imply that the underlying processes responsible for generating this rhythmical component were similar across the range of f_{LIC} tested. The possible involvement of different mechanisms was suggested by several findings from whole nerve experiments. First, in addition to the dominant peak at f_{LIC} , the emergence of a wide spectral peak within the range of PGN f_{INT} in the VCN autospectrum when f_{LIC} was increased (Fig. 5.3Av-Avi, 5.3Bv-B-vi) suggested that there was a difference in power distribution under conditions of low and high f_{LIC} and at least some single PGNs were not 1:1 entrained to LICs at high f_{LIC} . Second, unlike the tight coupling observed under conditions where f_{LIC} was close to PGN f_{INT} (Fig. 5.6B), the temporal stability of the rhythmical activity at f_{LIC} decreased as f_{LIC} was moved away from the PGN f_{INT} range (Fig. 5.6C). Third, although not as drastic as that observed in single PGN activity, the reduction of the LIC-VCN coherence at f_{LIC} (Fig. 5.15C) also indicated that the strength of coupling at high f_{LIC} was less than that when f_{LIC} was close to PGN f_{INT} . The drop of the power

density of the spectral peak at f_{LIC} in the VCN autospectrum further supported the idea that synchronization at f_{LIC} diminished when f_{LIC} was shifted away from PGN f_{INT} (Fig. 5.8 filled circles).

However, the drop of the rhythmical activity at f_{LIC} was not accompanied by a decline of the total power (Fig. 5.8 open circles), suggesting that it was an effect of desynchronization rather than a reduction of CVA PGN excitability. The finding that the mean discharge rate of single PGNs did not have a significant trend of change as f_{LIC} increased was consistent with the observation at the population level and a previous study in humans (Seals *et al.*, 1990). In conclusion, although the PGN population could maintain a dominant rhythmical activity coupled to LICs across a wider range of f_{LIC} , the stability of this coupling was different at different f_{LIC} . The possible underlying processes for generating this phenomenon are discussed in the next section.

The discharge behavior of single PGNs in response to LIC-related activity is consistent with the theory of non-linear coupled oscillators. This is supported by several key observations. First, we have deliberately tested and confirmed that 1:1 entrainment did not occur only at just one f_{LIC} . If single PGNs and LICs were linearly coupled, the output from PGNs should consist of two components: one is f_{LIC} and the other is f_{INT} of PGNs (Pavlidis, 1973; Bendat & Piersol, 1986). 1:1 entrainment at just one f_{LIC} cannot rule out the possibility that the frequency equality is pure coincidence of but if it happens at more than one f_{LIC} , this strongly suggests non-linearity of underlying processes. Second, the input-output relationship of a linear system should be frequency invariant (Bendat & Piersol, 1986) and the existence of high order rational frequency-lock between LICs and PGN activity is against the assumption of linearity. Third, if the system is stationary, which was presumed to be valid in this study because

physiological parameters were kept stable, intermittent phase lock (relative coordination) can be explained through nonlinear dynamics (Kelso, 1995) and it is hard to reconcile with the idea of linear dynamics. By contrast, behavior of population activity appeared as a mixture of linear and non-linear dynamics. When f_{LIC} was close to f_{INT} of CVA PGNs, strong 1:1 coupling was observed at many f_{LIC} (cf. Fig. 5.3 Aii-Aiv, Bii-Biv), which suggests 'entrainment' arising from non-linear coupling. However, when f_{LIC} was high, a mixture of f_{LIC} and f_{INT} appeared in the VCN autospectrum (cf. Fig. 5.3 Av-Avi, Bv-Bvi), suggesting that f_{LIC} was transmitted to otherwise undisturbed PGNs as predicted by linear coupling.

5.5.3 Explanation of the population discharge behaviour in response to f_{LIC} changes

When f_{LIC} was close to the range of PGN f_{INT} , the near zero lag synchronization (see Result) between single PGNs occurred through tight 1:1 coupling with stable phase difference to the common periodic drive, LIC-related activity (e.g. Fig. 5.16D, E, F). This synchronization enabled the PGN population to generate a prominent rhythmical activity with high coherence to LICs at f_{LIC} . When f_{LIC} was moved away from the range of PGN f_{INT} , although activity of some single PGNs might completely dissociate from LIC-related activity (Fig. 5.17A, B, C), there were at least three mechanisms to maintain the LIC-population PGN coupling. When f_{LIC} is close to the frequency range of PGN f_{INT} , the spread of f_{INT} within the oscillator population allowed a proportion of the pool to remain 1:1 entrained over a much wider driving frequency range than any single oscillator.

However, the above mechanism could not account for the persistence of a dominant population rhythm at f_{LIC} when f_{LIC} was above the upper limit of PGN

f_{INT} range (>1.2 Hz) because 1:1 coupling was not found in any single PGN at such f_{LIC} (see Fig. 5.15A). Under conditions where f_{LIC} was out of the PGN f_{INT} range, two other mechanisms, relative coordination and high rational frequency-lock, may help to stabilise the phase difference and preserve frequency-lock between LICs and population PGN activity. Relative coordination describes interactions where oscillators are not synchronized but nevertheless exhibit occasional instances of phase-lock (von Holst, 1939; Ayers & Selverston, 1979; Rosenblum & Turvey, 1988). Transient phase-lock would become a relatively stable feature at the population level, since at any given moment, there would be a high probability that a sub-population of PGNs would be phase-locked to LIC. Despite the dominant frequency of any single PGN being different from f_{LIC} , the summation of the phase-locked activity would produce a rhythm at f_{LIC} .

In addition, high order rational frequency-lock such as those exemplified in Fig. 5.18. might also occur when f_{LIC} was out of PGN f_{INT} range. This would tend to channel single PGNs into a finite number of phase differences, which would prevent continuous phase drift and contribute to the stabilising of LIC-single PGN phase difference. Although states like relative coordination and high order rational frequency-lock might help stabilise phase differences between LICs and PGNs, the strength of coupling was not as strong as that under conditions of 1:1 entrainment. Therefore, despite the PGN population still maintaining a dominant frequency the same as f_{LIC} , the coherence dropped. The wide range of PGN dynamics including complete asynchrony, 1:1 entrainment, relative coordination and high order rational frequency-lock cannot be explained based on a simple linear model for the interaction between LIC and PGN. A model of non-linear coupled oscillators is more appropriate to describe the behaviours of the single PGNs in response to f_{LIC} changes (Glass & Mackey, 1988; Kelso, 1995).

5.5.4 Conclusion

This study demonstrated:

1. The f_{LIC} range for PGN activity to maintain 1:1 coupling was much wider for population activity than that for single units.
2. Coupling strength at f_{LIC} between PGN and LICs dropped as f_{LIC} was moved away from PGN f_{INT} but the drop was more moderate at the population level than at single unit level.
3. When subjected to f_{LIC} changes, single PGN exhibit complex dynamics including complete asynchrony, 1:1 entrainment, relative coordination and high order rational frequency-lock, which was consistent with non-linear interaction.
4. In spite of the rapid decrease of synchronization at single PGN level with the consequent decline of the rhythmical population activity at the driving frequency (f_{LIC}), the tendency for the population PGN activity to maintain a 1:1-locked dominant feature provided a mechanism to coordinate sympathetic output in response to a periodic input across a wide frequency range.
5. The findings in the present study substantiate the conclusion in **Chapter Four** that the although population PGN activity exhibits oscillatory activity, it should not be conceived as one distinct oscillator but instead, its behavior should be considered and explained as superimposition of activity from multiple single PGN oscillators.

CHAPTER SIX

GENERAL DISCUSSION

My study demonstrated that CVA PGN activity is driven by multiple oscillators and when subjected to a driving force, they are capable of synchronization. The coupling to a periodic drive may display features compatible with non-linear dynamics of coupled oscillators. I also gave evidence showing that the robust discharge behavior of population PGN activity might not be the same as that of single PGNs but rather could be explained based on the underlying dynamic interaction between single PGNs.

6.1 The existence of independent sympathetic oscillators

No satisfactory mechanism has yet been proposed to explain the generation of sympathetic rhythms (McAllen & Malpas, 1997; Malpas, 1998). The theory of independent sympathetic oscillators for sympathetic rhythmogenesis as proposed by Gebber (see **Chapter One** and Gebber, 1980; Gebber *et al.*, 1994a,b; Zhong *et al.*, 1997) was supported by observations from experiments where sympathetic nerve activity was studied under conditions of baroreceptor denervation and/or central apnea. Under such conditions, i.e. free from periodic driving forces, it has been found in a number of animal species that the autospectrum of sympathetic nerve activity frequently contained peaks indicating rhythmical activity (cat: Taylor & Gebber, 1975; dog: Camerer *et al.*, 1977; goat: Toda *et al.*, 1996). The whole nerve activity contained burst discharges with variable amplitudes and its spectral peaks spread across a broad frequency range, which indicated the burst discharges in the sympathetic nerve were only quasi-periodic. Moreover, similar to that shown in the present study

(Chapters Four, Five), the peak amplitude under 'free-run' conditions was lower than that when sympathetic nerve activity was locked to the driving forces. The seemingly aperiodic behavior with drop of power during 'free-run' sometimes caused difficulty in determination of whether rhythmical activity existed. For example, Connelly and Wurster showed that in α -chloralose anaesthetised cats, a respiratory related peak was a prominent feature of the autospectrum of the inferior cardiac sympathetic nerve but it disappeared under conditions of hyperventilation apnea. The authors concluded that the respiratory related sympathetic rhythm derived from the CRD input into the SNS and an independent sympathetic oscillator was not consistent with the absence of rhythmicity during apnea (Connelly & Wurster, 1985). However, a close examination of their results revealed that during episodes of central apnea, sympathetic burst discharges still existed (their Fig. 4) and the autospectrum of the sympathetic nerve had substantial power concentrated in the low frequency range although the power was distributed across a broad range and the peak amplitude was lower than that when CRD was present (their Fig.3). These findings might just as well indicate that some rhythmical activity was present in sympathetic activity although the rhythmicity was not as prominent as that observed under the influence of CRD. In fact, the dispersion of power in the autospectrum under 'free-run' conditions has been used as an argument against the existence of a well-defined sympathetic oscillator (Bachoo & Polosa, 1987a).

Malpas extended the theory of independent sympathetic oscillators to include a layer of gating neurones, for example gated by chemoreceptor input, to account for the amplitude variation of sympathetic rhythms (Malpas, 1995). Thus, the 'upper-stream' sympathetic activity generated by central oscillators is gated by these neurones and the amplitude of the outflow activity can be adjusted by

'opening' or 'closing' these gates. However, it still does not offer a satisfactory explanation for why power of sympathetic burst activity distributes across a wide frequency range and there is no evidence indicating the on-off states of gating neurones should fluctuate so drastically as to produce moment to moment change of amplitude.

The findings from the present study offer an alternative explanation for the discharge behavior of whole nerve sympathetic activity. The experimental and simulated data showed that the discharge patterns of population CVA PGN activity during 'free-run' can be described as a superimposition of multiple oscillators with distinct frequencies, restricted to a limited range. In a population composed of multiple oscillators, power of the autospectrum will concentrate in the frequency range of the constituent individual oscillators and the peak amplitude and the degree of power dispersion depends on the distribution of their dominant frequencies and phase differences (**Chapter Four, Appendix II** and see also Christakos, 1986). A consequence of this is that population activity may not necessarily appear very regular and its amplitude may have substantial temporal fluctuation dependent on the moment to moment interaction of individual oscillators. Another important feature of this model is that discharge behavior of population activity can be different from that of its components and the population should not be considered as a well-defined single oscillator.

It is interesting to note that the conclusion from a recent study on activity of single fibres teased from the VCN of the rats was different from that of the present study (Häbler *et al.*, 1999). In their study, Häbler, Bartsch and Jänig showed that the discharge behaviours of single fibres and multi-fibre (2-7 single units) were similar because most of them revealed CRD or LIC-related activity and only rarely a dominant rhythm different from that of CRD or LICs was observed in single fibre

activity (2/51). They concluded that it was justified not to distinguish between single fibre and population rhythmicity. However, the experimental conditions were not the same in that study and in the present study. In their study, the f_{LIC} was at the upper limit (1.25 Hz) of T-rhythm frequency range and the V_T (2-3 ml)-to-weight (200-280 gm) ratio was higher than that used in the present study and this would suggest a stronger LIC-related drive was used in that study. Although the distribution of $PaCO_2$ was not given, from its range (35-50 mmHg), it would be expected that CRD in some of their experiments might be strong because of hypercapnia. The enhancement of LIC-related and CRD might account for the predominance of ventilation and respiration frequencies in the PGN activity. From the present study, it was found that 'local' similarity between population and single unit activities could occur if there was high probability of synchronization of single units through coupling to a strong common driving force (cf. Fig. 4.3 C vs. Fig. 4.7 D and Fig. 5.3 Aii, Bii vs. Fig. 5.9B). The variance between the two studies emphasised the necessity to manipulate the driving force, especially diminish its strength and/or move its frequency away from f_{INT} of single PGNs, in order to observe the difference between single unit and population activities.

6.2 Sympathetic oscillators in other vascular beds

Dominant rhythms similar to the T-rhythm in the CVA PGNs have also been observed in the PGNs innervating the lateral tail vein of the rats (Johnson & Gilbey, 1998b). If the principle of multiple oscillators governing the sympathetic outflow to the rat's tail circulation is crucial to understand the regulation of sympathetic nerve activity, it is important to know if the similar principle can be applied to different vascular beds. As described above, the population PGN activity may be different from that of single PGNs and therefore the semi-

periodic rhythm present in the whole nerve activity cannot be used as direct evidence of the existence of single PGN oscillators in vascular beds other than the rat's tail.

Most studies on single PGNs come from Jänig's group. Using the teased fibre technique, Jänig and his colleagues have examined the discharge behavior of single or multi-fibre activity in a number of different vascular beds. (for review see Jänig, 1988). However, the purposes of most of those experiments were to study the discharge patterns in response to an input activity and the dominant rhythms of single PGNs were not examined under 'free-run' conditions. The existence of independent PGN oscillators in other vascular beds in different animals is still open to question.

However, some inferences can be made by comparing population PGN activity in other vascular beds and the findings from the present study. Similar to VCN activity, peripheral sympathetic nerve activity recorded from other vascular beds exhibited quasi-periodic burst discharges (McAllen & Malpas, 1997) and as mentioned above, in many cases this robust rhythm still existed under 'free-run' conditions. This suggests that a model of multiple PGN oscillators may also be applied to describe the population behavior in those vascular beds. However, there are important qualitative and quantitative differences in the rhythmical components recorded from different vascular beds of different animal species. The present and previous studies (Johnson & Gilbey, 1994; Johnson & Gilbey, 1996) clearly demonstrated that the dominant frequency in the CVA PGN activity is within a narrow range, 0.4-1.2 Hz and this is also reflected in the VCN autospectrum. Although aortic nerve stimulation could reset the T-rhythm (Johnson & Gilbey, 1998a), cardiac related activity was minimal if present at all in the CVA PGNs. By contrast, two rhythmical components of sympathetic

activity with frequencies much higher than those of CVA PGNs, could be frequently identified in different nerves such as inferior cardiac nerve, vertebral nerve, splanchnic nerve and renal nerve in the cats. In the autospectrum, one appeared as a wide peak or complex configuration spreading between 2 and 6 Hz (2-to 6-Hz rhythm) (Taylor & Gebber, 1973; Gebber & Barman, 1980) and the other, while not necessarily appeared as a sharp peak, concentrated around 10 Hz (10-Hz rhythm) (Green & Heffron, 1967; Cohen & Gootman, 1970; Barman *et al.*, 1992). The two rhythmical activities may coexist or exist in the absence of the other in the same preparation (Barman *et al.*, 1992). The 2-to-6 Hz rhythm has also been identified in the renal nerve, splanchnic nerve (Zhong *et al.*, 1993) and lumbar sympathetic nerve in the rats (Allen *et al.*, 1993). Unlike the observations from the VCN, cardiac related activity was a prominent feature in the frequency range of the 2-to-6 Hz rhythm in these nerves in baroreceptor intact animals (for review see Malpas, 1998). The underlying mechanism for generation of these rhythms are presently not clear (McAllen & Malpas, 1997; Malpas, 1998).

Based on the findings from series of experiments, Gebber proposed that the 2-to-6 Hz and 10 Hz rhythms in nerves to different vascular beds are generated by distinct sympathetic oscillators whose oscillatory activity may originate from the brainstem (Barman *et al.*, 1992; Huang *et al.*, 1992; Zhong *et al.*, 1992; Gebber *et al.*, 1994a,b; Barman *et al.*, 1995). The key findings which would suggest the existence of the proposed sympathetic oscillators were: when the brainstem was stimulated with different frequencies, the responding discharge behaviours of sympathetic nerves were consistent with those predicted by the theory of periodically driven oscillators (Huang *et al.*, 1992). The coupling dynamics included 1:1 entrainment when the stimulation

frequency was centred in the inherent (or intrinsic) frequency range of 2-to-6 Hz or 10 Hz rhythm. When the stimulation frequency was moved away from the inherent frequency range, the 'entrainment' became weak and sometimes, lower order rational frequency-lock emerged (for example, stimulation frequency : sympathetic frequency: 1:3, 1:2).

A close examination of Fig. 3 (an experiment concerning 10 Hz rhythm) and Fig. 8 (an experiment concerning 2-to-6 Hz rhythm) in their study (Huang *et al.*, 1992) reveals striking similarity to the coupling behavior between VCN and LIC-related activity (see Fig. 5.3 **Chapter Five**). One similarity was that when the driving frequency was close to the f_{INT} range of the sympathetic oscillators, stable 1:1 entrainment appeared. Furthermore, when the driving frequency was moved away, a broad spectral peak re-emerged in the f_{INT} range but a sharp peak at the driving frequency remained, although its amplitude dropped. As shown in **Chapter Five**, these driving-frequency dependent behaviours can be readily explained in terms of a population of multiple oscillators if their f_{INT} ranges are those of 2-to-6 Hz rhythm or 10 Hz rhythm. In their papers based on bivariate spectral analysis of coherence, Gebber and his colleagues further suggested that the sympathetic oscillators for nerves innervating different targets are capable of dynamic and differential synchronization (Gebber *et al.*, 1994a; Gebber *et al.*, 1994b; Gebber *et al.*, 1995a). They found that significant coherence existed between a paired sympathetic nerve activities and this was still true even when the coherence was partialised by removing the effect predicted by linear correlation to a common drive, cardiac related activity. These observations do not necessarily imply that sympathetic activity in one nerve is generated by **one single oscillator**. They might just as well be consistent with the hypothesis that activity from different nerves is generated by distinct groups

of **multiple oscillators**. This is because coherence between two activities at a particular frequency measures how strong, in the sense of linear regression, one activity can be predicted from the other (see **Chapter Three** and Bendat & Piersol, 1986). If a proportion of the two oscillator pools receive a common periodic drive and/or are coupled, there can be substantial coherence at the driving frequency or coupling frequency. This possibility is consistent with the finding that activity of the bilateral VCNs was significantly correlated in the absence of CRD (Smith & Gilbey, 1998a).

Finally, the prominent cardiac related activity in cats, which is absent in CVA PGNs, can also be explained in terms of the multiple oscillator model. The difference of f_{INT} between the CVA PGNs (0.4-1.2 Hz) and the PGNs (2 to 6 Hz and/or 10 Hz, inferior cardiac, vertebral, renal nerves) of cats may reflect their different intrinsic properties. The different intrinsic properties may explain the difference in the propensity to be entrained by cardiac related activity. If the coupling dynamics between cardiac activity and PGNs also obey the theory of non-linear driven oscillators (see below *Discharge behavior of PGNs in response to a periodic driving force*), as shown in the relationship between LIC-related activity and CVA PGNs (**Chapter Five**), then it would be expected that probability of entrainment is high only when cardiac frequency is close to PGN f_{INT} . CVA PGN cannot be entrained by cardiac related activity because cardiac frequency (~7-8 Hz) is much higher relative to CVA PGN f_{INT} . The frequency dependent entrainment to cardiac related activity was supported by the findings that the dominant frequency of single CVA PGNs could be reset by slow aortic nerve stimulation (1 per 7 sec, Johnson & Gilbey, 1998a) and this suggests that entrainment may occur if the frequency of baroreceptor afferent activity was brought into the f_{INT} range of CVA PGNs. For the PGNs in sympathetic nerves

of the cats, stable entrainment occurs in the frequency range of 2-to-6 Hz rhythm because the cardiac frequency of cats is close to this range.

In summary, the observations from the experiments performed by Gebber's group can be explained based on a model of multiple oscillators. The latter model can also explain the power dispersion across the f_{NT} range in the absence of an external drive, which is hard to reconcile with a model involving a single oscillator.

6.3 Discharge behavior of PGNs in response to a periodic driving force

The mechanisms underlying the coupling dynamics between sympathetic whole nerve activity and respiratory-, cardiac- or LIC-related activity is still under considerable debate (Malpas, 1998). Two principal hypotheses have been proposed to explain the coupling dynamics. One regards the sympathetic neurones simply as followers which acquire the input rhythm through the imposition of periodic driving activity (i.e. phase-editing effect). For example, a common cardiorespiratory oscillator has been suggested to account for the respiratory related rhythm of sympathetic activity (Richter & Spyer, 1990; Richter *et al.*, 1991). Influences of lung inflation on the CRD, which in turn modulates sympathetic nerve activity, has been proposed as the mechanism for generation of LIC-related sympathetic rhythms (Gerber & Polosa, 1978). The other hypothesis, an extension of Gebber's independent sympathetic oscillator theory, considers the interaction between sympathetic neurones and the periodic drive as a manifestation of non-linear coupled oscillators.

The most usual approach to distinguish the two proposed mechanisms is to manipulate the driving frequency and analyse the change of discharge behavior of sympathetic activity in response to the frequency perturbation. If the

interaction is simply a 'phase-editing' effect, it would be expected that the phase difference between the driving activity and the sympathetic activity should be reasonably constant as a reflection of the conduction delay between them and invariance of frequency response should be observed across a wide range of the driving frequency. By contrast, in a system of non-linear coupled oscillators, the phase difference may vary when the frequency of the driving oscillator is changed and 1:1 frequency-lock can only occur over a limited range of the driving frequencies (Pinsker, 1977b; Guevara *et al.*, 1986).

By manipulating the driving frequency, the studies from Bachoo and Polosa on the respiratory modulation (Bachoo & Polosa, 1987b) and from Hedman, et al., on cardiac modulation (Hedman *et al.*, 1994) supported the 'phase-editing' theory. The analysis methods used in these studies to detect constancy of the phase difference were based on either the neurogram of whole nerve activity (Bachoo & Polosa, 1987b) or triggered average of whole nerve activity (Hedman *et al.*, 1994). As the present study has shown, the population may consist of multiple oscillators and when the driving frequency changed, some PGNs might be transiently phase-locked to the drive. The phase-locked components identified by the above analysis methods might only consist of a part of the population. Therefore, their findings do not necessarily imply that constant phase difference was a ubiquitous feature with high temporal stability in all the constituents when the driving frequency changed. Second, it should be noted that these experiments did not explore the effect of drive strength which may have considerable effect on coupling dynamics (Winfree, 1980; Glass & Mackey, 1988). It is not clear whether non-linear coupling behavior may become obvious when other drive strengths are used. Furthermore, when extending the conclusion from the studies at neuronal level to the studies at

system level, one should be cautious about the sensitivity of analysis to detect the difference of conduction delay because a small phase shift may become inconspicuous in the output activity along a poly-synaptic pathway.

In contrast to these findings, studies from Gebber and his colleagues supported the non-linear coupled oscillator theory for respiratory modulation (Zhong *et al.*, 1997) or cardiac modulation (Gebber *et al.*, 1997). They used spectral analysis as the basic tool to extract the frequency domain information and strong evidence of non-linear coupling came from the presence of high order rational frequency-lock in these studies. However, as has already been pointed out (**Chapter Three**), the accuracy of determination of the high order rational frequency-lock is subject to the limitation of spectral resolution. Thus, for example in one of their studies (Gebber *et al.*, 1997), in order to isolate one rhythmical component through digital filtering to construct Lissajous diagrams for frequency-lock analysis, the centre frequency of that rhythm must be read first from the autospectrum and this might introduce measurement error (spectral resolution: 0.1 Hz) and affect the appearance of Lissajous diagrams.

In summary, a conclusive remark about the underlying mechanisms for the coupling between sympathetic activity and respiratory or cardiac activity is still not attainable at present. Whether 'phasic editing' or non-linear oscillatory coupling is the mechanism for the effect of CRD on CVA PGNs cannot be answered in the present study either because the frequency dependent nature was not examined. However, this study clearly demonstrated that interaction between single PGNs and LICs could be described as dynamics arising from non-linear coupled oscillators. When f_{LIC} was high, a dominant frequency the same as f_{LIC} persisted at population level despite the fact that 1:1 entrainment was no longer a feature between single PGNs. These observations provided an

alternative to mutual entrainment, which has been proposed as the mechanism for the cardiac (Jalife, 1984; Michaels *et al.*, 1986) and circadian (Liu *et al.*, 1997) rhythms, for generating a stable rhythm in a population composed of multiple oscillators.

6.4 Physiological significance of synchronization

This study has demonstrated that dynamic synchronization of CVA PGN activity may occur in the absence of obvious change of the discharge rate. Synchronous sympathetic activity coupled to other biological rhythms is a common phenomenon. In addition to respiratory, cardiac and ventilation rhythms, peripheral sympathetic nerve activity may be locked to movements in intermittent isometric exercise (Victor *et al.*, 1995) and in pathologic conditions such as epileptiform discharges (Lathers *et al.*, 1987). Under many different stress conditions, the synchronous burst discharges were found to be enhanced (Callister *et al.*, 1992; Nordin & Fagius, 1995; Morgan *et al.*, 1996; Katragadda *et al.*, 1997).

The functional significance of these phenomena is not clear (McAllen & Malpas, 1997). However, it has been suggested that burst synchronous discharges lead to more efficient synaptic transmission in the central nervous system (Lisman, 1997; Abeles, 1991). Indirect evidence from *in vitro* studies suggests that this mechanism may also operate at the periphery in sympathetic neuroeffector transmission and influence the efficacy of neurogenic contraction of arteries. In many arteries in a diverse range of animal species ATP and noradrenaline are co-released from the sympathetic nerve endings (Morris & Gibbins, 1992). The excitatory junctional potentials (EJPs) and smooth muscle contraction induced by ATP release are typically characterised by a fast onset

and rapid decline time profile (Brock & Cunnane, 1992). By contrast, adrenergic mediated membrane potential changes and muscle contraction are much slower in onset and associated with a prolonged time course (Morris & Gibbins, 1992; Stjärne & Stjärne, 1995) although membrane depolarisation is not absolutely necessary for the adrenergic related contraction (Hirst & Edwards, 1989).

When weak single electric stimulation was applied to the perivascular sympathetic nerve, which activated only a few fibres, EJPs were evoked without concomitant muscle contraction. Stronger stimulation activates more fibres and muscle contraction might arise from summation of EJPs. With further increase of the stimulation strength, adrenergic mediated contraction began to emerge and higher and prolonged muscle tension developed. See Hirst & Edwards, 1989 for review of the electro-mechanical coupling sequence. Although arterial smooth muscle contraction is not necessarily accompanied with generation of action potentials (Harder, 1982), the vasomotor response only occurs when the membrane potential exceeds a threshold (Xia & Duling, 1995) and the generation of action potentials help to develop higher muscle tension (Hirst & Edwards, 1989).

These studies suggest that simultaneous activation of sympathetic fibres is important for the generation of arterial vasomotor tone. One possible usage of synchronous burst discharges is through the summation of fast response EJPs. For example, in the rat's tail circulation, although single CVA PGNs frequently discharge in doublets or triplets, the effect of temporal summation perhaps is not enough to induce effective contractile response (Stjärne & Stjärne, 1995) and the EJPs will diminish rapidly before the next burst arrives (compare T-rhythm frequency and the time course of EJPs, see Cheung, 1982). When

activity from many CVA PGNs is synchronized, the temporal summation effect will be added by spatial summation, which is possible in vascular tissue because the smooth muscle cells are connected through low resistance, high conductance gap junctions (Christ *et al.*, 1996). This will cause rapid and large membrane depolarisation even with generation of action potentials and, consequently, fast contraction of the smooth muscles. This perhaps provides an important mechanism for rapid redistribution of blood flow under stress, for example, hypercapnia. A prolonged time course of synchronization may bring out the slow reactive adrenergic contractile response as well.

Direct *in vivo* evidence supporting the above mechanism is, as yet, unavailable. However, I propose that synchronous sympathetic activity may play a substantial role in maintaining perfusion pressure of vital organs during hypercapnia. It is well known that systemic arteries have auto-regulation ability and many vessels dilate in response to hypercapnia (Levick, 1995). However, BP is well-maintained or even increases during hypercapnia (Lioy *et al.*, 1984). Ample evidence indicates that the BP response, in spite of the local vasodilatation effect of CO₂, arises from sympatho-activation (Lioy *et al.*, 1984; Fukuda *et al.*, 1989; Trzebski *et al.*, 1995). This helps to re-distribute blood flow to vital organs such as the brain where sympathetic innervation is less dense (Dodge *et al.*, 1994). In muscular and renal vascular beds the increase of sympathetic nerve activity is probably due to the increase of neuronal discharge rate (Fukuda *et al.*, 1989; Trzebski *et al.*, 1995). In view of the fact that the cutaneous circulation is one of the largest reservoirs of blood (O'Leary & Johnson, 1989), the re-allocation of blood from the cutaneous vascular bed may be also important to prevent BP drop during hypercapnia. However, in cutaneous circulation which has high sympathetic tone (O'Leary & Johnson,

1989), modulation of the temporal patterns of nerve discharge may provide a more efficient way to enhance the sympathetic effect instead of increasing the discharge rate. The findings of the present study, i.e. increased synchrony without concomitant change of CVA PGN discharge rate during hypercapnia, are consistent with the above hypothesis.

If synchronization of PGN activity is a reflection of synchrony of upstream neural activity in the central nervous system, this implies that facilitated synaptic transmission along sympathetic pathways may also occur centrally and may provide an important mechanism to coordinate outflow from different neurone groups. Accumulated evidence has indicated that in addition to changes of the discharge rate, neural assemblies may use synchronous discharges to provide another mechanism for information encoding in sensory processing and motor programming (Singer, 1993; Singer, 1996; Fetz, 1997). Correlated firings provide a neural mechanism for the binding problem: how are different characteristics of an object perceived to generate a gestalt image? (von der Malsburg, 1990; von der Malsburg, 1995). Neurones are bound through synchronous discharges to form a functional unit in response to a demand.

Similar to the somatic motor and sensory systems, different neurones in the autonomic nervous system are activated under different situations. Many nuclei have been identified to be important for cardiovascular regulation in the central nervous system and they form an intricate network with divergent and convergent connection pathways (Dampney, 1994). This provides the anatomical basis for the autonomic neurones to coordinate and synchronize their discharges. If dynamic synchronization is also a feature between different autonomic neurone pools, this may provide a mechanism to channel preferential pathways and activate different neurones to form a functional unit to respond to a challenge. For example, the

rostral ventral lateral medulla (RVLM) is the most important source of inputs to the preganglionic sympathetic neurones (SPN) and it also receives inputs from other nuclei important for sympathetic regulation (Guyenet, 1990). The RVLM is important for maintaining sympathetic tone but little is known about the influence of discharge patterns of its neurones on the sympathetic response. Regulation of the discharge patterns in these neurones is possible as revealed in a recent *in vivo* intracellular study. Lipski, et al. showed that most neurones in the RVLM were tonically active with irregular on-going activity and no identifiable pacemaker potentials (Lipski et al., 1996). However, the irregular discharge pattern can be converted to a regular one in the presence of DC input. Furthermore, they also found some neurones which were not baro-sensitive but had pacemaker properties and their rhythms could be reset by short depolarising currents. This may provide the RVLM with the potential to generate synchronous output in response to input activity and therefore modulate the sympathetic outflow. Synchronization of sympathetic activity can also occur at the spinal cord level. The discovery of gap junctions between SPNs raises the possibility that the SNS coordinates discharges at this location before preganglionic fibres exit the central nervous system (Logan et al., 1996). Even at the periphery the extensive convergent and divergent arrangement of the ganglionic neurones provides the potential for modulation of the sympathetic outflow at the level of the sympathetic ganglia (Bulygin, 1983). These anatomical and physiological studies indicate that synchronization of neural activity may potentially occur at many different levels in the autonomic nervous system.

6.5 Conclusion

In this study, the findings of multiple sympathetic oscillators controlling a well-defined target organ, the CVA, provide a dynamic model for cardiovascular regulation. In comparison to a model involving only one single oscillator, multiple oscillators have the capability for dynamic synchronization in response to external challenges. First, if individual PGNs are absolutely synchronized and behave like one single oscillator, it cannot provide too much stability for the organisms to adapt to environmental changes. This is because as a single oscillator it would respond drastically when the input parameters (or challenge characteristics) change as predicted by non-linear coupled oscillator theory (cf. single PGN behavior in response to f_{LIC} changes in **Chapter Five**). By contrast, a population of multiple oscillators with different intrinsic properties is capable of generating graded output coupled to an external driving force by fine tuning the discharge pattern of each individual oscillator (cf. population PGN behavior in response to f_{LIC} changes in **Chapter Five**). Second, it has been suggested that in the cortex the broad band fast oscillations (or γ rhythms) can also be easily desynchronized, and thus the network can be prevented from entering global synchronization which would be inappropriate for information processing (Singer, 1993). Similarly, if PGNs behave as a single oscillator, which indicates a persistent global synchronous state, it would be detrimental to the survival of the organisms in view of the steady enhanced neuroeffector transmission arising from synchronous prejunctional activity.

This study does not disregard the importance of information encoding by discharge rate in the SNS, which may be especially important in maintaining vascular tone in the absence of a driving force. Although a functional correlate is not yet available, this study shows that some stable (e.g. maintain a dominant

frequency-lock to f_{LIC}) and unstable features (e.g. drop of coherence at f_{LIC}) of the population, could coexist due to reordering PGN spike trains in response to a driving force (e.g. LIC-related activity). The metastability of the population discharge pattern suggests that temporal coding may also be important in the SNS similar to its proposed role in cortical information processing.

Prospects:

1. It is important to know if changes of the PGN discharge pattern can effectively modulate the post-junctional responses. Temporal encoding through synchronous discharges in the cortical neurones is considered to be important in sensory processing or motor programming. However, the functional significance of synchrony in the SNS is still not clear. For the SNS, one of its most important functions is to regulate the regional blood flow through modulating the vascular tone. This is particularly important under situations of emergency when an appropriate pattern of rapid redistribution of blood supply to different organs is needed because non-neurogenic smooth muscle contraction mediated by humoral factors is too slow. As discussed above, synchronization of PGN activity may enhance the efficacy of junctional transmission. This effect can be examined by studying the PGN discharge patterns and neurogenic vascular contraction simultaneously. The vascular tone can be measured directly by recording the muscular tension or indirectly by measuring the local vascular resistance. An intracellular recording from the smooth muscle cells will help delineate the subthreshold effect of the prejunctional nerve discharge patterns.
2. It is necessary to examine the discharge patterns of PGNs innervating other vascular beds. As discussed above, the principle of dynamic synchronization of multiple sympathetic oscillators may be important in the sympathetic

regulation of cardiovascular responses because it confers the SNS with metastability to pattern the sympathetic outflow. Although this principle can be used to explain some observations from studies on sympathetic nerves innervating vasculatures other than the rat's tail circulation (see above), direct evidence of its ubiquitousness is still lacking. Single PGN studies under 'free-run' are particularly important to confirm if sympathetic activity in other vascular beds is also generated by multiple oscillators. Examination of activity recorded simultaneously from two or more single units is necessary to establish the principle governing the genesis of population activity.

3. Theoretical studies through neural network modelling for rhythmogenesis of the SNS will help to understand puzzling features arising from underlying dynamic processes. Sympathetic activity is generated from an intricate complex neural network receiving influences from numerous areas in the central nervous system. It will be extremely difficult if not impossible to conduct experiments where these areas are examined simultaneously when system parameters are varied. A model of sympathetic rhythmogenesis can be constructed by fitting observations from 'piecewise' experiments, where only few variables are tested at one time, into a concrete and consistent hypothesis. Currently there is not enough detail knowledge for constructing a satisfactory model but advances towards this goal may be provided by combining evidence from neural anatomy, neuronal physiology and system physiology.

Appendix I

A stochastic model for simulated CVA PGN event series

Using a similar strategy in previous papers (Gath, 1974; Aertsen & Gerstein, 1985), the modelling of spike trains in this study involved a black-box type approach, operating in terms of stochastic point processes with parameters estimated from experimental data. No attempt was made to incorporate the biochemical mechanism underlying the generation of action potentials.

These simulated PGN event series have mean discharge rates (MDR, spikes/sec) and T-rhythm frequencies (bursts/sec) similar to the observations in the real experiments. The distribution of MDR was assumed to be uniform because of the wide variation of real data. On the other hand, the T-rhythm frequency was assumed to be normally distributed because of its central clustering tendency. Also, the time of the first event was chosen randomly to specify the beginning of the PGN event series.

The sample space from which the values of the two variables were selected:

MDR: uniform distribution between 0.42 Hz and 1.33 Hz.

T-rhythm frequency: normal distribution with mean, 0.61 Hz, and standard deviation, 0.08 Hz.

The first event time uniform distribution between 0.11 sec and 1.87 sec.

These parameters with the presumed distributions were estimated from experimental data in the absence of CRD (N=12).

Although there was a dominant rhythm in single PGN activity, the discharge was not absolutely periodic and the autocorrelograms most frequently displayed broad peaks rather than sharp ones. The mechanism of the spread of

events around the dominant frequency was unknown and was assumed to arise from stochastic processes in this simulation. The diagrammatic autocorrelogram in Fig. A1.1 is used to illustrate how this feature is simulated. The half of the width of the first peak in the autocorrelogram (a) and the period of the dominant rhythm (b) were measured. The ratio, a/b , (called event dispersion ratio) was taken as a measure of the extent of event dispersion around the dominant frequency. This ratio was assumed to have a normal distribution with mean, 0.29 and standard deviation, 0.08 based on experimental data.

Steps for generation of simulated PGN event series

1. Choose MDR, T-rhythm frequency, the first event time and event dispersion ratio randomly from their sample spaces according to the estimated distribution of these parameters described above.
2. Generate an event series beginning at the first event time with a perfect T-rhythm frequency.
3. Shift each event randomly around its original occurrence time (i.e. when the rhythm is absolutely periodic). The extent of this shift depends on event dispersion ratio.
4. Add more events with random occurrence time if necessary according to MDR.

All the random numbers used in this simulation were produced by an IBM compatible computer using built-in pseudorandom number generators in a mathematical software, Matlab (MathWorks, USA). The following algorithm is the Matlab script file used to generate the simulated data.

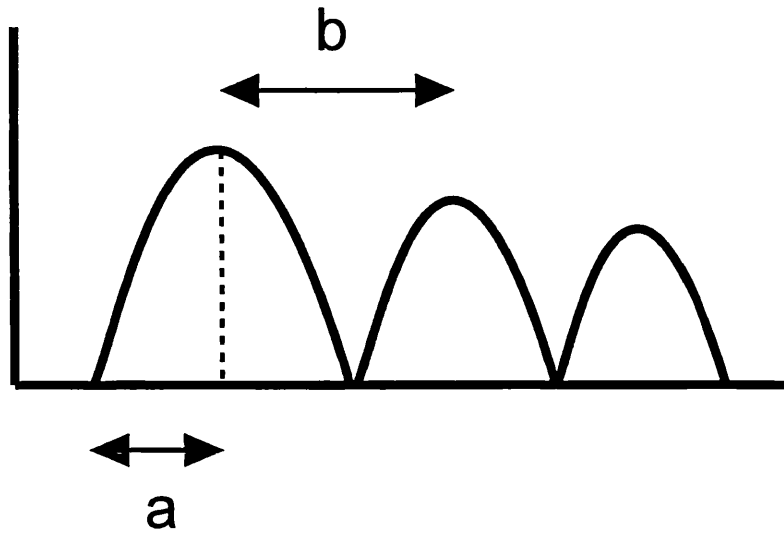


Fig. A1.1 Diagrammatic illustration of the calculation for the event dispersion ratio (see text). This figure represents the envelope of a PGN autocorrelogram. The half width of the first peak (a) divided by the period (b) of the dominant rhythm is the event dispersion ratio.

```

function x=simpgn(et)
%X=SIMPGN(ET) returns a simulated PGN event series.
%ET: End time of the event (sec).
if st==0 %Avoid event occurrence time is zero and 0.0001 sec was used
    st=0.0001 %because the ADC rate in experiment is 10000 Hz.
end
st=unifrnd(0.11,1.87,1,1); %generate occurrence time of the first event
f=normrnd(0.61,0.08,1,1); %generate dominant frequencies
dr=unifrnd(0.42,1.33,1,1); %generate mean discharge rate
evr=normrnd(0.29,0.08,1,1); %generate event dispersion ratio
x=(st:1/f:et)'; %generate an event series with perfect periodicity
rp=((1/f)*evr)*rand([length(x)-1,1]);
sig=randchoose([1,-1],1,2);
x=[x(1);x(2:length(x))+sig*rp]; %shift events around the original occurrence
                                %time.
k=length(x);
if k<dr*(et-st)
    dr=dr;
else
    dr=k/(et-st);
end
rn=fix(dr*(et-st))-k;
rnx=randevent(st,et,0.001,rn);
x=[x;rnx]; %add more events with random occurrence time if needed according
                                %to MDR
x=sort(x);

```

Appendix II

Autospectrum of population activity

To prove that the autospectrum of stationary population activity is the sum of the autospectra of its components and the real part of pairwise cross spectra, it is more convenient to calculate the autospectrum by Fourier-transforming the autocorrelation function. This approach is equivalent to the Welch's method, i.e. averaged modified periodogram, used in this study (Bendat & Piersol, 1986). The first part of this proof will be the calculation of the autocorrelation function of population activity by mathematical induction. The second part will be the Fourier transform of this autocorrelation function.

Notation: $E(x)$: the expectation of X .

$R_{X,X}$: the autocorrelation function of X .

$R_{X,Y}$: the cross correlation function for X and Y .

$S_{X,X}$: the autospectrum of X .

$S_{X,Y}$ and $S^*_{X,Y}$: the cross spectrum and its conjugate, respectively, for X and Y . If $\text{Re}(S)$ and $\text{Imag}(S)$ represent the real and imaginary part of the cross spectrum,

$$S_{X,Y} = \text{Re}(S_{X,Y}) + \text{Imag}(S_{X,Y}) \text{ and}$$

$$S^*_{X,Y} = \text{Re}(S_{X,Y}) - \text{Imag}(S_{X,Y})$$

The real part of cross spectrum is called coincidence spectrum or co-spectrum.

The imaginary part of cross spectrum is called quadrature spectrum or quad-spectrum.

Γ : Fourier transform operator.

$$\Gamma \text{ is defined by: } \Gamma(f) = \int_{-\infty}^{\infty} f(k) \cdot e^{-2\pi i \omega \cdot k} dk$$

A. Symmetrical properties of cross correlation function and cross spectrum.

Assume that $X(t)$ and $Y(t)$ are two stationary time series. For stationary processes, by definition, the cross correlation function for X and Y is:

$$\begin{aligned} R_{X,Y}(k) &= E[X(t) \cdot Y(t+k)] \\ &= E[X(s-k) \cdot Y(s)] \\ &= R_{Y,X}(-k) \end{aligned} \tag{Eq. 3.1}$$

According to Wiener-Khinchine relations, autocorrelation function/autospectrum and cross-correlation function/cross spectrum are Fourier transform pairs (Bendat & Piersol, 1986):

$$\Gamma(R_{XX}) = S_{XX} \tag{Eq. 3.2}$$

$$\Gamma(R_{XY}) = S_{XY} \tag{Eq. 3.3}$$

The cross spectrum, S_{YX} , is given by:

$$\begin{aligned} S_{YX}(\omega) &= \Gamma(R_{YX}) \text{ (By Eq. 3.3)} \\ &= \int_{-\infty}^{\infty} R_{YX}(k) \cdot e^{-2\pi i \cdot \omega \cdot k} dk \\ &= \int_{-\infty}^{\infty} R_{XY}(-k) \cdot e^{-2\pi i \cdot \omega \cdot k} dk \text{ (By Eq. 3.1)} \\ &= \int_{-\infty}^{\infty} R_{XY}(k) \cdot e^{2\pi i \cdot \omega \cdot k} dk \\ &= S_{XY}^*(\omega) \end{aligned} \tag{Eq. 3.4}$$

Thus,

$$\begin{aligned} S_{XY} + S_{YX} &= S_{XY} + S_{XY}^* \\ &= 2\text{Re}(S_{XY}) \\ &= \text{Re}(S_{XY} + S_{YX}) \end{aligned} \tag{Eq. 3.5}$$

B. Autocorrelation function of population activity

Assume activity, $Z(t)$, is the sum of two stationary activities, $X(t)$ and $Y(t)$ and $W(t)$ is another stationary activity. By definition, for stationary processes, the

cross correlation function for W and Z is:

$$\begin{aligned}
 R_{W,Z}(k) &= E(W(t) \cdot Z(t+k)) \\
 &= E[W(t) \cdot \{X(t+k)+Y(t+k)\}] \\
 &= E[W(t) \cdot X(t+k)] + E(W(t) \cdot Y(t+k)) \\
 &= R_{W,X} + R_{W,Y} \qquad \qquad \qquad (\text{Eq. 3.6})
 \end{aligned}$$

Similarly,

$$R_{Z,W}(k) = R_{X,W}(K) + R_{Y,W}(K) \qquad \qquad \qquad (\text{Eq. 3.7})$$

From Eq. 3.6 and Eq. 3.7 it is easy to establish that if Z(t) is an activity composed more than two components, i.e. $Z(t) = \sum Z_i(t)$, the following equations are true:

$$R_{W,Z}(k) = \sum R_{W,Z_i}(K) \qquad \qquad \qquad (\text{Eq. 3.8})$$

$$R_{Z,W}(k) = \sum R_{Z_i,W}(k) \qquad \qquad \qquad (\text{Eq. 3.9})$$

The autocorrelation function of Z(t), composed of two components, X(t) and Y(t), is:

$$\begin{aligned}
 R_{Z,Z}(k) &= E[Z(t) \cdot Z(t+k)] \\
 &= E[\{X(t)+Y(t)\} \cdot \{X(t+k)+Y(t+k)\}] \\
 &= E[X(t) \cdot X(t+k)] + E[X(t) \cdot Y(t+k)] + E[Y(t) \cdot X(t+k)] + E[Y(t) \cdot Y(t+k)] \\
 &= R_{X,X} + R_{X,Y} + R_{Y,X} + R_{Y,Y} \qquad \qquad \qquad (\text{Eq. 3.10})
 \end{aligned}$$

The next part will prove that the autocorrelation function of population activity is the sum of 1) autocorrelation functions of individual components and 2) pairwise cross-correlation functions.

Assume A is the sum activity composed of n components, i.e.,

$$A(t) = \sum B_i(t) \quad (i=1,2,\dots,n, n \geq 2)$$

Then, its autocorrelation function is:

$$R_{A,A}(k) = \sum R_{B_i, B_i}(k) + \sum R_{B_i, B_j}(K) \quad (i=1,2,\dots,n; j=1,2,\dots,n; i \neq j) \quad (\text{Eq. 3.11})$$

Proof

For $n=2$, Eq. 3.11 is true by Eq. 3.10.

Now assume Eq. 3.11 is true for $n=m$ ($m \geq 2$), the following argument will show that Eq. 3.11 is also true for $n=m+1$.

Let $C = \sum B_i$ ($i=1,2,\dots,m$)

$A(t) = \sum B_i(t)$ ($i=1,2,\dots,m,m+1$) = $C(t) + B_{m+1}(t)$

$$\begin{aligned} R_{A,A}(k) &= E\{[\sum B_i(t)] \cdot [\sum B_i(t+k)]\} \\ &= E\{[C(t) + B_{m+1}(t)] \cdot [C(t+k) + B_{m+1}(t+k)]\} \\ &= R_{C,C}(k) + R_{C,B_{m+1}}(k) + R_{B_{m+1},C}(k) + R_{B_{m+1},B_{m+1}}(k) \quad (\text{By Eq. 3.10}) \\ &= R_{C,C}(k) + R_{B_{m+1},B_{m+1}}(k) + \sum R_{B_i,B_{m+1}}(k) + \sum R_{B_{m+1},B_i}(k) \quad (i=1,2,\dots,m) \\ &\quad (\text{By Eq. 3.8 and Eq. 3.9}) \\ &= \sum R_{B_i, B_i}(k) + \sum R_{B_i, B_j}(K) + R_{B_{m+1}, B_{m+1}}(k) + \sum R_{B_i, B_{m+1}}(k) + \sum R_{B_{m+1}, B_i}(k) \\ &\quad (\text{By assumption, } i=1,2,\dots,m; j=1,2,\dots,m; i \neq j) \\ &= \sum R_{B_i, B_i}(k) + \sum R_{B_i, B_j}(K) \quad (i=1,2,\dots,m+1; j=1,2,\dots,m+1; i \neq j) \end{aligned}$$

Q.E.D.

C. Autospectrum of population activity

Assume A is a population activity arising from n components:

$A(t) = \sum B_i(t)$ ($i=1,2,\dots,n$, $n \geq 2$), then,

$$S_{A,A} = \sum S_{B_i, B_i} + \text{Re}(\sum S_{B_i, B_j}) \quad (i=1,2,\dots,n; j=1,2,\dots,n; i \neq j) \quad (\text{Eq. 3.12})$$

Proof

The autospectrum of A is the Fourier transform of its autocorrelation function:

$$\begin{aligned} S_{A,A} &= \Gamma(R_{A,A}) \\ &= \Gamma(\sum R_{B_i, B_i} + \sum R_{B_i, B_j}) \quad (i=1,2,\dots,n; j=1,2,\dots,n; i \neq j) \quad (\text{By Eq. 3.11}) \end{aligned}$$

$$=\Sigma\{\Gamma(R_{B_i,B_i})\} + \Sigma\{\Gamma(R_{B_i,B_j})\} \quad (\Gamma \text{ is a linear operator})$$

$$=\Sigma S_{B_i,B_i} + \Sigma S_{B_i,B_j}$$

$$=\Sigma S_{B_i,B_i} + \text{Re}(\Sigma S_{B_i,B_j}) \quad (\text{By Eq. 3.5})$$

Q.E.D.

Appendix III

Empirical confidence interval for cross correlogram

The underlying procedure to generate the empirical confidence interval follows the idea suggested in a previous paper (p208, suggestion 3, Bryant *et al.*, 1973). The confidence interval is calculated for a single peri-trigger bin. When there are N triggers, the random variable, X_{ij} ($i=1, 2, \dots, N$ and $j=1, 2, \dots, M$), where M is the number of bins, represents the number of dependent events in the jth peri-trigger bin after the ith trigger. In total, there are $M \cdot N$ random variables. The null hypothesis is that all the X_{ij} random variables are independent and identically distributed with finite variance. The random variable,

$$Y_j = \sum_{i=1}^N X_{ij}$$

represents the number of events in the jth bin in the cross correlogram. If $N > 30$, the distribution of Y_j is approximately normal according to the central limit theorem (Freiwald *et al.*, 1995). The parameters to be estimated are the expectation and the variance of Y_i .

$$E(Y_j) = E(\sum_{i=1}^N X_{ij}) = \sum_{i=1}^N E(X_{ij})$$

$$\text{Var}(Y_j) = \text{Var}(\sum_{i=1}^N X_{ij}) = \sum_{i=1}^N \text{Var}(X_{ij})$$

The estimators of $E(X_{ij})$ and $\text{Var}(X_{ij})$, sample mean, m_x , and variance, s_x^2 , were calculated from the empirical data: $M \cdot N$ samples,

$$x_{ij}, i=1, 2, \dots, N; j=1, 2, \dots, M$$

The 95% confidence interval for Y_j is

$$[-1.96 \cdot (N \cdot s_x^2)^{1/2} + N \cdot m_x, 1.96 \cdot (N \cdot s_x^2)^{1/2} + N \cdot m_x]$$

This confidence interval is applied to all the Y_j s since the distributions of the Y_i ($i=1, \dots, M$) are identical under the null hypothesis. It should be noted that it is

possible for the event number in several bins (5% of M) to exceed the 95% confidence interval by chance. In this study we defined significant rhythmical synchronization between two neural activities as the existence of rhythmicity in the envelope of the cross correlogram where the peaks and/or troughs exceed the 95% empirical confidence interval. It should be noted that the confidence interval is empirical because it is applied only to the specific data under consideration. For this reason, the result based on this empirical confidence interval in **Chapter Four** was double-checked with an asymptotic confidence interval for squared root transformation of cross intensity function given by Brillinger (Brillinger, 1976) and the conclusion was the same. The A→B squared root transformed cross intensity function with the significant level was given below:

cross intensity function: $m(\lambda)_{A \rightarrow B} = \{(C(\lambda)_{A \rightarrow B} / \beta N_A) + |\lambda| N_B / T^2\}^{1/2}$

mean: $\mu_m = p^{1/2} N_B$

upper limit of 95% confidence interval: $UL = \mu_m + (\beta N_A)^{1/2}$

lower limit of 95% confidence interval: $LL = \mu_m - (\beta N_A)^{1/2}$, where:

A and B: trigger and dependent event series respectively

λ : peri-trigger interval (or time lag)

N_A and N_B : number of events in A and B

T: data time length

$m(\lambda)_{A \rightarrow B}$: cross intensity function, centred at λ

β : binwidth

$C(\lambda)_{A \rightarrow B}$: cross correlation function histogram estimator (number of B events falling in a tally, centred at λ)

p_B : mean discharge rate of B

Appendix IV

Detection of commensurate frequency-lock by reordered correlation raster plot (RCRP)

Suppose the frequency ratio of two periodic event series, **E1** and **E2**, is **m1:m2**, where **m1** and **m2** are positive integers and relative prime (commensurate frequencies). The periods for **E1** and **E2** are thus **p.m2** and **p.m1** for some **p** respectively, where **p** is the greatest commensurate division of the periods. For time variable $t \geq 0$, let the two event series be represented by:

$$\mathbf{E1: } g(t) = \sum \delta(t-t_i), i=1 \dots N1$$

$$\mathbf{E2: } g(t) = \sum \delta(t-t_j), j=1 \dots N2$$

where $\delta(t)$ is Dirac delta function (i.e. impulse function) and **N1** and **N2** are the number of events in **E1** and **E2** and suppose the event series are long enough so that **N1** > **m1** and **N2** > **m2**. t_i ($i=1 \dots N1$) and t_j ($j=1 \dots N2$) are the occurrence time of events in **E1** and in **E2** respectively. For simplicity, here assume that events in **E1** and **E2** are coincident at time zero (By shifting time, the same argument can be applied if they are not coincident at time zero) It follows that:

$$t_k = (i-1) \cdot p \cdot m2, i=1 \dots N1$$

$$t_j = (j-1) \cdot p \cdot m1, j=1 \dots N2$$

Now the set of time differences between any event occurrences in the two series is:

$$\mathbf{D} = \{x \mid x = p \cdot [(i-1) \cdot m2 - (j-1) \cdot m1], i=1 \dots N1, j=1 \dots N2\}$$

or its normalised form:

$$\mathbf{D}' = \{x \mid x = [(i-1) \cdot m2 - (j-1) \cdot m1], i=1 \dots N1, j=1 \dots N2\}$$

D and **D'** are related by:

if $x \in D \Rightarrow x/p \in D'$ & if $x \in D' \Rightarrow x.p \in D$

Now we prove that D' can be partitioned into m_1 non-overlapping subsets (modulo m_1).

First we define congruence and least residue:

Definition A4.1

Let a and b be integers and let n be positive integer. a is said to be congruent to b modulo n , denoted by

$$a \equiv b \pmod{n}$$

if only if n is a common divisor of $a - b$.

It is easy to see that congruence is a reflective, symmetrical and transitive relationship (P55, Redmond, 1996).

Definition A4.2

Let n be a positive integer. If $x \equiv a \pmod{n}$, then a is called a residue of x modulo n . If $0 \leq a \leq n-1$, then a is called the least residue of x modulo n .

It is clear the set of all possible least residues (mod n) is $[0, 1, \dots, n-1]$ and any integer is congruent to one and only one of the least residues modulo n .

Lemma A4.1

D' can be partitioned into m_1 non-overlapping subsets under congruence relationship (modulo m_1) in the sense that all the members in any subset are congruent to one and only one of the least residues modulo m_1 .

Proof

Suppose D' is partitioned to k different subsets, D'_1, D'_2, \dots, D'_k under the congruence relationship (mod m_1). The first part is to prove that the intersection of any pair of these subsets is empty.

Assume the intersection of some D'_i and D'_j ($i, j \in [1 \dots k]$ & $i \neq j$) is not empty and

$\mathbf{a} \in \mathbf{D}'_i \cap \mathbf{D}'_j$ and suppose

$\forall \mathbf{x} \in \mathbf{D}'_i, \mathbf{x} \equiv \mathbf{r}_i \pmod{\mathbf{m}_1}$ & $\forall \mathbf{y} \in \mathbf{D}'_j, \mathbf{y} \equiv \mathbf{r}_j \pmod{\mathbf{m}_1}$ \mathbf{r}_i and \mathbf{r}_j are two different least residues
 $\pmod{\mathbf{m}_1}$

This implies $\mathbf{a} \equiv \mathbf{r}_i \pmod{\mathbf{m}_1}$ & $\mathbf{a} \equiv \mathbf{r}_j \pmod{\mathbf{m}_1}$. Since congruence is symmetrical and transitive, it follows that,

$$\mathbf{r}_i \equiv \mathbf{r}_j \pmod{\mathbf{m}_1},$$

which is against the assumption that they are different least residues. This proves any subsets in such a partition is disjointed.

The second part will prove that \mathbf{k} equals \mathbf{m}_1 .

It is obvious that \mathbf{k} cannot be bigger than \mathbf{m}_1 because the maximal number of possible least residues is \mathbf{m}_1 .

We now prove that it is impossible for \mathbf{k} to be less than \mathbf{m}_1 .

Suppose $\mathbf{x} \in \mathbf{D}'$, i.e. $\mathbf{x} = [(\mathbf{i}-1) \cdot \mathbf{m}_2 - (\mathbf{j}-1) \cdot \mathbf{m}_1]$ for some $\mathbf{i}, \mathbf{j}, \mathbf{i} \in [1, \dots, \mathbf{N}_1]; \mathbf{j} \in [1, \dots, \mathbf{N}_2]$

It is only necessary to consider the cases when $\mathbf{i} = 1, \dots, \mathbf{m}_1$ because for any $\mathbf{i} > \mathbf{m}_1$, \mathbf{x} is congruent to some value $\pmod{\mathbf{m}_1}$ with \mathbf{i} between $1, \dots, \mathbf{m}_1$.

If $\mathbf{k} < \mathbf{m}_1$, this implies that when \mathbf{i} runs through $[1, \dots, \mathbf{m}_1]$, there are at least two \mathbf{x} s, said \mathbf{x}_1 ($\mathbf{i} = \mathbf{i}_1$) and \mathbf{x}_2 ($\mathbf{i} = \mathbf{i}_2$), which are congruent $\pmod{\mathbf{m}_1}$. Therefore,

$$(\mathbf{i}_1 - 1) \cdot \mathbf{m}_2 \equiv (\mathbf{i}_2 - 1) \cdot \mathbf{m}_2 \pmod{\mathbf{m}_1}, \mathbf{i}_1, \mathbf{i}_2 \in [1, \dots, \mathbf{m}_1] \text{ and } \mathbf{i}_1 \neq \mathbf{i}_2. \text{ This follows that,}$$

$$(\mathbf{i}_1 - \mathbf{i}_2) \cdot \mathbf{m}_2 \equiv 0 \pmod{\mathbf{m}_1}, \text{ but the fact that } \mathbf{m}_1 \text{ and } \mathbf{m}_2 \text{ are relative prime implies}$$

$$(\mathbf{i}_1 - \mathbf{i}_2) \equiv 0 \pmod{\mathbf{m}_1}, \text{ which is impossible because } \mathbf{m}_1 \text{ cannot be a divisor of } (\mathbf{i}_1 - \mathbf{i}_2).$$

Therefore, \mathbf{k} equals to \mathbf{m}_1 and the proof is completed.

Q.E.D.

An extension of Lemma A4.1 to \mathbf{D} establishes that \mathbf{D} can be partitioned to \mathbf{m}_1 subsets under a congruence relationship $\pmod{\mathbf{p} \cdot \mathbf{m}_1}$. Specifically, any

phase differences between **E1** and **E2** has the following form:

$n \cdot p \cdot m_1 + r \cdot p$, where n is an integer and $r \in [0, \dots, m_1 - 1]$. It should be noted that the phase differences between **E1** and **E2** can also be represented as $n \cdot p \cdot m_2 + r \cdot p$, where n is an integer and $r \in [0, \dots, m_2 - 1]$. Along the same argument, It can be shown that the phase differences may be partitioned into m_2 congruent subsets (mod $p \cdot m_2$). Selecting $p \cdot m_1$ or $p \cdot m_2$ as the basis for the congruent partition of the phase differences is equivalent to choosing **E1** or **E2** as the trigger event series. To see this, consider a minimal period of data where all possible phase differences (mod $p \cdot m_1$ or $p \cdot m_2$) may occur. In this case, it is $m_1 \cdot m_2 \cdot p$ because during this period, **E1**, **E2** repeats m_1 , m_2 cycles, respectively and the events in both series become coincident again (the first coincidence is at time zero under the assumption). It follows that subsequent events cycle through the same pattern identical to this minimal period. Furthermore, this period must exhaust all the possible phase differences (mod $p \cdot m_1$ or $p \cdot m_2$) because outside this period the phase differences (mod $p \cdot m_1$ or $p \cdot m_2$) just repeat. In this period, there are m_1 distinct **E1**→**E2** first post trigger intervals. Each of these intervals belongs to one and only one of the m_1 congruent partition sets of phase difference (modulo $p \cdot m_1$). After or before the first post trigger **E2** event, the **E2** events just repeat with its frequency. Therefore, each data segment with length equal to $m_1 \cdot m_2 \cdot p$ will produce m_1 event clusters with a period of $m_1 \cdot p$. If the events are lined up, sorted by the order of the first post-trigger intervals, a slanting band including m_1 discrete vertical event clusters appears and spans an interval equal to $m_1 \cdot p$. This band would repeat with a period equal to $m_1 \cdot p$ (the period of **E2**) in the RCRP. Same argument can be applied if **E2** is chosen as the trigger event series.

The structure of RCRP is detailed in Fig. A4.1 using an example produced from

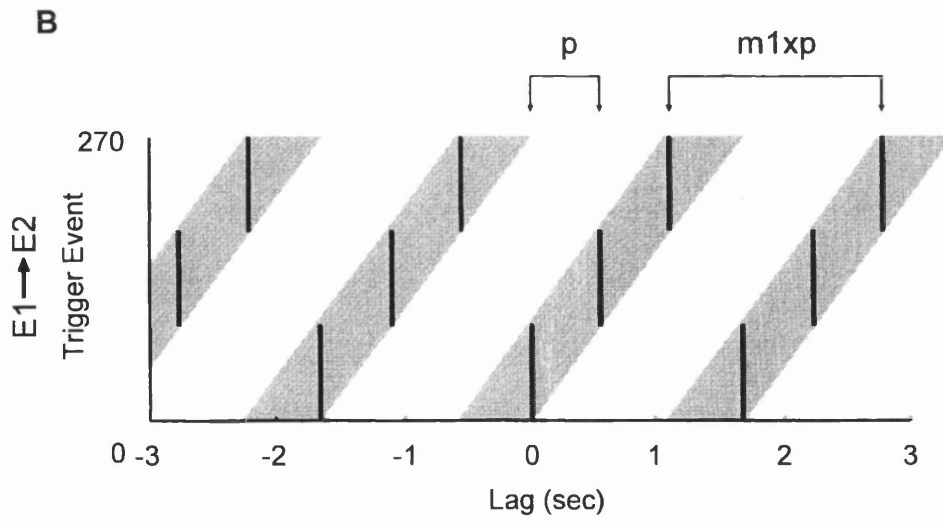
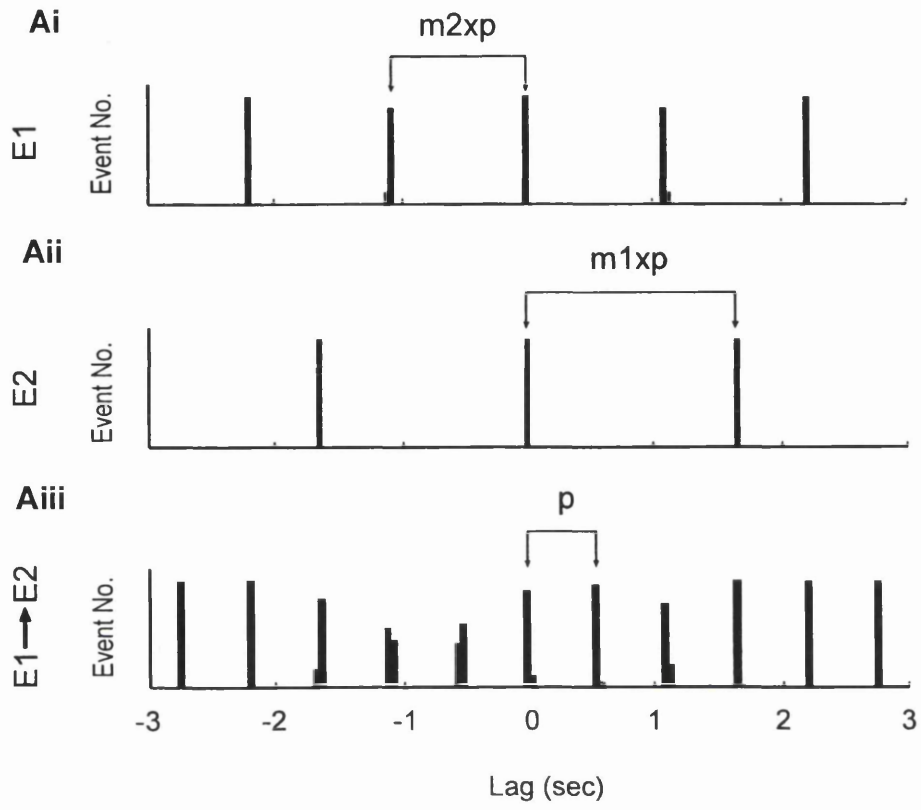


Fig. A4.1 Diagrammatic illustration of the structure of the reordered correlation raster plot (RCRP) for a pair of periodic event series locked in a simple high rational frequency ratio. Two idealised event series, E1 and E2, with perfect rhythms (frequency, 0.9 Hz for E1; 0.6 Hz for E2), are used to illustrate the structure of E1→E2 RCRP. The E1 to E2 frequency ratio is $m_1:m_2=3:2$, where m_1 and m_2 are relative prime integers, and the greatest commensurate period, p , equals to $1/0.9/2=1/0.6/3=5/9$ sec (see text). *A_i*, *A_{ij}*, The autocorrelograms of E1 and E2. Their periods are $m_2xp=10/9$ sec and $m_1xp=5/3$ sec for E1 and E2, respectively. *A_{iii}*, E1→E2 cross correlogram. The periodic pattern in the envelope has a period equal to the greatest commensurate period, $p=5/9$ sec (see text). *B*, E1→E2 RCRP. The RCRP consists of periodic slant bands repeating with a period equal to the period of E2, i.e., m_1xp (shaded bands). Each band is composed of $m_1=3$ vertical event clusters with the distance between adjacent clusters equal to the greatest commensurate period $p=5/9$ sec (see text for details).

two ideal event series, **E1** and **E2**, with perfect rhythmicity. In this example, the frequency of **E1** was 0.9 Hz and **E2** is 0.6 Hz. Therefore, $m_1=3$ and $m_2=2$. The greatest commensurate division of period was $1/0.9/m_2$ or $1/0.6/m_1$, i.e. $p=1/1.8=5/9$ sec. The periods of **E1** and **E2** were $m_2.p=10/9$ sec and $m_1.p=5/3$ sec, respectively (autocorrelograms of **E1** and **E2**, Fig. A4.1Ai, Aii). **E1**→**E2** RCRP was shown in Fig. A4.1B. Within a segment equal to the period of **E2** ($m_1.p$), there was a slant band (shaded area) composed of $m_1=3$ event clusters with inter-cluster distance equal to $p=5/9$ sec. This pattern repeated every $m_1.p=5/3$ sec.

The above analysis uncovers an interesting phenomenon: under conditions of high order rational frequency-lock, it is possible for the cross correlogram to exhibit periodicity with a frequency different from those of the trigger and dependent activity. Previous studies classified interaction between input-output neurones into primary effects, a direct influence and secondary effects, a statistical property arising from periodicity inherent to input or output neurones. The secondary effect frequently maps the rhythms of input and output neurones into the cross correlogram (Moore *et al.*, 1970; Bryant *et al.*, 1973). However, frequencies different from those of input or output neurones can appear in the cross correlogram simply as a result of a statistical process, i.e. secondary effect. For example, the envelope of cross correlogram (Fig. A4.1Aiii) between the simulated event series, **E1** and **E2**, had a periodic pattern with a frequency equal to $1/p$ which is different from those of **E1** and **E2**.

Appendix V

Matlab script file, SPECTRUM, for autospectrum and coherence spectrum

```
function p=spectrum(x,y,s,ft,wo)

% P=SPECTRUM(X, Y, S, FT, WO) returns the autospectrum and coherence
% coherence spectrum of two time series.

% Input: [X, Y, S, FT, WO]

% X: First time series.

% Y: Second time series.

% S: Sampling rate (Hz).

% FT: FFT size for one block

% WO: Size of block overlapping.

% Output: P=[Px, Py, Coherence]

% Px: X autospectrum.

% Py: Y autospectrum.

% Coherence: X-Y coherence spectrum.

n=max(size(x)); % number of data points
k=fix((n-wo)/(ft-wo)); % number of blocks
block=1:ft; % indexes of data points in one block
w=0.5*(1-cos(2*pi*(linspace(0,1,ft)))); % weighing function: Hanning taper
m=ft/s; % block length
px=zeros(ft,1); py=px;pxy=px; % pre-assigned empty autospectrum and cross
```

```

for i=1:k
wx=w.*detrend(x(block)); wy=w.*detrend(y(block)); % remove linear trend from
% each block followed by
% windowing

block=block+(ft-wo); % recursive definition of 'block'

fx=fft(wx)/s; fy=fft(wy)/s; % fast Fourier transformation of each block

fx=sqrt(8/3)*fx; fy=sqrt(8/3)*fy; % scaling factor to compensate power loss due
% to tapering

psdx=abs(fx).^2/m; psdy=abs(fy).^2/m; % estimated autospectrum in each block

cpsdxy=(fy.*conj(fx))/m; % estimated cross spectrum in each block

px=px+psdx; py=py+psdy; % summation of autospectra from all blocks

pxy=pxy+cpsdxy; % summation of cross spectra from all blocks

end

px=px/k; py=py/k; % average of autospectra

pxy=pxy/k; % average of cross spectra

f=[1:ft/2+1]; % select components with non-negative frequencies

px=px(f); py=py(f); pxy=pxy(f);

coherence=(abs(pxy).^2)./(px.*py); % calculation of coherence

p=[px,py,coherence]; % assign output

```

Appendix VI

Matlab script file, COEVENT, for the autocorrelogram and the cross correlogram

```
function h=coevent(ex,ey,b,t1,t2)

% COEVENT(EX,EY,B,T1,T2): Correlogram of point processes
% Input: [EX, EY, B, L1, L2, T1, T2, TRIGGER Number]
% EX & EY: The trigger & the dependent event series
% B: Binwidth (sec).
% T1 and T2: The pre- and post-triggering intervals (second).
% Note: Set the trigger and dependent event series to be the same for
% autocorrelogram

m=length(ex); % trigger number
f1=fix(t1/b); f2=fix(t2/b); f=f2-f1; % bin number
sy=[]; % pre-assigned empty set
n=1;
while n<=m; % recursive on the trigger events
shy=ey-ex(n); % phase differences between dependent events and the trigger
vy=shy(find(shy>=t1 & shy<=t2)); % restrict the phase differences into the
                                % specified peri-trigger interval
sy=[sy;vy]; % collect all the restricted phase differences while the trigger runs
                                % through all its events
n=n+1;
end;
hist(sy,f); % generate histogram with specified bin number
```

Rhythmic sympathetic activity recorded from the ventral collector nerve (VCN) innervating the rat tail

Hong-Shiu Chang & Michael P. Gilbey

Autonomic Neuroscience Institute, Dept. Physiology, Royal Free Hospital School of Medicine, London NW3 2PF

Previous studies from our laboratory have shown that on-going activity recorded from single postganglionic sympathetic neurones (PSNs) innervating the caudal ventral artery (CVA) or lateral tail vein (LV) has a characteristic dominant rhythm (T-rhythm, around 0.8 Hz; Johnson & Gilbey, 1995, 1996). In the present study we examined whether sympathetic activity recorded from the whole VCN, which innervates various targets in the tail, also displays the T-rhythm.

Experiments were conducted on thirteen male Sprague-Dawley rats (275-355g) that were anaesthetized with pentobarbitone (60 mg kg⁻¹, I.P.) and supplemented with α -chloralose (5-10 mg, I.V.) when required, paralysed with gallamine (16 mg kg⁻¹ h⁻¹) (see Johnson & Gilbey, 1996), ventilated artificially, vagotomized and given a pneumothorax. The cauda equina was cut to remove somatic motor activity from the VCN. Phrenic nerve activity was recorded as an indicator of central respiratory rate (CRR). Nerve activity was filtered, rectified and smoothed. CRR was adjusted by altering PaCO₂ &/or PaO₂ (by changing pump rate &/or O₂ content of inspired gas).

Under control conditions (PaO₂ and PaCO₂, 107.6 ± 14.0 (mean ± S.D.) and 38.6 ± 3.6 mm Hg, respectively, MABP, 86.4 ± 10.5 mm Hg), spectral analysis (sampling rate 100 Hz, FFT block size 2048; 45 blocks) in 12/13 animals revealed a peak in the autospectrum of sympathetic activity at the same frequency as the CRR (0.67 ± 0.12 Hz) (coherence 0.71 ± 0.2). Another peak, at 0.82 ± 0.13 Hz, was observed in 6/13 animals. When the CRR was slowed to 0.35 ± 0.03 Hz in seven animals, a sympathetic peak at this frequency was seen in 2 animals (coherence 0.33 ± 0.06 Hz, significantly different from control; t test, P<0.05),

however in all seven animals another sympathetic peak was seen at 0.80 ± 0.11 Hz. When apnoea was induced by hyperventilation, a sympathetic peak remained at 0.81 ± 0.12 Hz in the eight animals tested. Peaks in the autospectra at around 0.8 Hz were not significantly different in the 3 conditions tested (one-way ANOVA).

The data shows that sympathetic activity recorded from the whole VCN has a rhythmical component with a similar frequency to that recorded from single PSNs innervating the CVA or LV. In addition, although single unit activity recorded from CVA or LV does not frequently show prominent respiratory-related activity, sympathetic activity recorded from the VCN under control conditions commonly displayed a separate 'respiratory peak'. The difference between single PSN & whole VCN activity might reflect the functional heterogeneity of the latter or it might be a statistical population property of the activity of PSNs projecting through the VCN.

Supported by the Wellcome Trust & Chang Gung Memorial Hospital.

References

- Johnson, C. D. & Gilbey, M. P. (1995). *J. Physiol.* **483**, P, 103-104P.
Johnson, C. D. & Gilbey, M. P. (1996). *J. Physiol.* **497**, 241-259.

Multiple "oscillators" and the discharges of sympathetic neurons innervating the rat caudal ventral artery

H-S. Chang, J.E. Smith, K. Staras, B.A. Cotsell and M.P. Gilbey

(Sponsor: A.G.Ramage)

Autonomic Neurosci. Inst., Dept. Physiol., Royal Free Hosp. Sch. Med.,
London NW3 2PF, UK.

We have previously shown, using a focal recording technique, that the discharges of single sympathetic postganglionic neurons (PGNs) innervating the caudal ventral artery (CVA) have a dominant rhythm (T-rhythm: Johnson, C.D. and Gilbey, M.P. (1996). *J. Physiol.* 497. 241-259). In this study we examined whether all PGNs are driven by the same "oscillator" or whether multiple "T-rhythm oscillators" regulate the sympathetic outflow to the CVA. Rats were anaesthetized (60 mg/kg I.P. Na pentobarbitone, supplemented with chloralose 5-10 mg I.V.), paralysed, artificially ventilated and vagotomized. Simultaneous recordings were made of the discharges of pairs of PGNs. It was observed that although the frequency of the T-rhythm displayed by pairs of PGNs could be the same and demonstrate a constant phase relationship (N=5), such a relationship was not obligatory. The discharges of pairs of PGNs could demonstrate periods of uncoupling. We conclude that multiple "T-rhythm oscillators" exist.

Wellcome Trust 05115, BHF FS/96009. Chang Gung Memorial Hospital.

Synchronous and asynchronous rhythmical discharges of postganglionic sympathetic neurones innervating an identified blood vessel in the rat.

H-S. Chang, J.E. Smith, K. Staras and M.P. Gilbey

Autonomic Neuroscience Institute, Department of Physiology, Royal Free Hospital School of Medicine, London NW3 2PF

In vitro studies have indicated that the nature of neuroeffector transmission is influenced by the pattern of sympathetic discharges. Synchronous and asynchronous models of sympathetic activity have been used to study neuroeffector transmission in the caudal ventral artery (CVA) of the rat *in vitro* using either electrical stimulation (synchronous, Bao & Stjarne, 1993) or ciguatoxin (asynchronous, Brock *et al*, 1997). Using a focal recording technique, we have previously shown *in vivo* that the discharges of single sympathetic postganglionic neurones (PGNs) innervating the CVA are rhythmical (dominant rhythm: T-rhythm, Johnson & Gilbey, 1996). In this study by recording activity from pairs of PGNs, we sought to determine whether the rhythmical discharges can be synchronous and/or asynchronous.

Sprague-Dawley rats (n=10) were anaesthetized (60 mg/kg I.P. pentobarbitone, supplemented with chloralose 5-10 mg I.V. as required, see Johnson & Gilbey, 1996), pneumothoracotomized, paralysed, ventilated artificially and vagotomized. Activity of PGNs was recorded focally from CVA through glass microelectrodes (internal diameter, 20-100 μ m). The action potentials of pairs of PGNs were either recorded through separate electrodes or discriminated from multiunit activity recorded through one electrode. Eleven pairs were analysed. Under control conditions (pH, 7.38 \pm 0.04, PaO₂, 115.6 \pm 14 mmHg, PaCO₂, 38.2 \pm 3.5 mmHg, mean \pm S.D.), frequencies of T-rhythms were the same in three pairs (mean frequency, 0.7 \pm 0.06 Hz, n=6) but they were significantly different (paired *t*-test, *p*<0.05) in eight pairs (mean frequency, 0.7 \pm 0.13 Hz, n=16). Cross-correlation analysis (5 mins data set) showed a

rhythmical pattern in four pairs and no prominent peaks in the remaining seven pairs. However, when time evolving cross correlograms (1 min/each subdivision) were inspected, periods of correlation and noncorrelation could be observed in both groups. Hypercapnia (pH, 7.24 ± 0.04 , PaO₂, 121.7 ± 12.5 mmHg, PaCO₂, 57 ± 9.3 mmHg) was induced in six experiments and strong synchronization was observed in five pairs (mean frequency, 0.66 ± 0.03 Hz, n=10).

This study indicates that multiple T-rhythm generators underlie activity of PGNs innervating the CVA and the rhythmical discharges can be either synchronous or asynchronous with a high probability of synchrony during hypercapnia. This suggests that the temporal relationship of activity between the different rhythm generators is relatively plastic and is capable of undergoing dynamic change.

Supported by the Wellcome Trust, British Heart Foundation FS/96009 and Chang Gung Memorial Hospital.

References

- Bao, J. & Stjarne, L. (1993). *Br. J. Pharmacol.* **110**, 1421-1428.
- Brock, J.A., McLachlan, E.M. & Rayner, S.E. (1997). *Br. J. Pharmacol.* **120**, 1513-1521.
- Johnson, C. D. & Gilbey, M. P. (1996). *J. Physiol.* **497**, 241-259.

Sympathetic Neuronal Oscillators are Capable of Dynamic Synchronization

Hong-Shiu Chang, Kevin Staras, Julia E. Smith, and Michael P. Gilbey

Autonomic Neuroscience Institute, Department of Physiology, Royal Free and University College Medical School, University College London, London NW3 2PF, United Kingdom

In this paper we show that the discharges of sympathetic neurons innervating an identified peripheral target are driven by multiple oscillators that undergo dynamic synchronization when an entraining force, central respiratory drive (CRD), is increased. Activity was recorded from postganglionic sympathetic neurons (PGNs) innervating the caudal ventral artery of the rat tail: (1) at the population level from the ventral collector nerve (VCN); and (2) from pairs of single PGNs recorded simultaneously using a focal recording technique. Autospectral analysis of VCN activity revealed a more prominent rhythmical component in the presence of CRD than in its absence, suggesting that (1) multiple oscillators drive the discharges of PGNs and (2) these oscillators can be entrained and therefore synchronized by CRD. This interpretation was supported by analysis of the firing behavior of PGN pairs. Autocorrelation and

cross-correlation analysis showed that pairs were not synchronized in the absence of CRD but showed significant synchronization when CRD was enhanced. Time-evolving spectral analysis and raster plots demonstrated that the temporal stability of PGN-to-PGN and CRD-to-PGN interactions at a given level of CRD were also dynamic in nature, with stable constant phase relationships predominating as CRD was increased. This is the first reported example of dynamic synchronization in populations of single postganglionic sympathetic neurons, and we suggest that, as in sensory processing and motor control, temporal pattern coding may also be an important feature of neuronal discharges in sympathetic pathways.

Key words: postganglionic sympathetic neuron; central respiratory drive; neural oscillator; synchronization; entrainment; blood vessel; in vivo; Sprague Dawley rat

Recent evidence indicates that the nervous system may use transient periods of synchronization as an information-encoding mechanism (for review, see Fetzi, 1997; Farmer, 1998). This poses questions about the functional importance of synchrony and the nature of the underlying neuronal circuitry. Although this phenomenon has been studied in the CNS, particularly with regard to sensory processing and skeletal muscle motor control (Farmer, 1998), synchronous firing has not been examined in a functionally defined sympathetic pathway where it is likely to have important implications for neuroeffector transmission and consequently the end organ response (Sneddon and Burnstock, 1984; Sjöblom-Widfelt et al., 1990; see also, McAllen and Malpas, 1997). In this paper, using an application of a focal recording technique developed in this laboratory, we test the idea that synchronous neuronal firing is a feature of postganglionic sympathetic neurons (PGNs) innervating an identified blood vessel [the caudal ventral artery (CVA) of the rat tail].

Our previous work revealed that CVA PGN activity exhibits a dominant rhythm (frequency range, 0.4–1.2 Hz): this was given the generic term, T-rhythm (Johnson and Gilbey, 1996). It was observed that the frequency of the T-rhythm could be the same or different from that of the CRD. Importantly, when CRD was absent, the T-rhythm persisted, indicating that it could be gener-

ated by autonomous oscillator or oscillators (defined here as an entity or entities with periodic activity) that could be entrained by CRD. This raises important questions about whether the discharges of PGNs are driven by single oscillator obligatorily coupled oscillators or multiple independent oscillators and whether these discharges can be synchronized through entrainment by CRD. The oscillator substrate might be the PGNs themselves or antecedent neuronal oscillators and/or oscillating neural networks (for review, see Selverston and Moulins, 1985; Marder and Calabrese, 1996). In this study, by recording both population and single PGN activity, we sought to discriminate between a single/obligatorily coupled versus multiple oscillator model of T-rhythm generation and investigated the temporal relationship of PGN to PGN and CRD to PGN activity.

Population activity was recorded from the ventral collector nerve (VCN), which contains ~80% of the PGN axons that innervate the CVA (Sittiracha et al., 1987). The absence of a rhythmical component would be consistent with the idea that the discharges of PGNs are driven by separate oscillators with little or no global synchronization. We also recorded from pairs of PGNs using the focal recording technique, which enabled the findings of the whole-nerve analysis to be tested at the level of "target identified" PGNs. In both whole-nerve and paired recordings we manipulated CRD to investigate whether dynamic synchronization of rhythmical PGN activity can occur through entrainment.

The findings of this study demonstrate that the rhythmical discharges of PGNs innervating a blood vessel can arise from multiple oscillators that can be entrained by a periodic neural activity, CRD. These results show for the first time that like, for example, cortical neurons in the CNS, rhythmical discharges of PGNs are capable of dynamic synchronization. In the same way

Received Oct. 14, 1998; revised Jan. 28, 1999; accepted Feb. 1, 1999.

H.-S.C. was supported by Chang Gung Memorial Hospital, K.S. and work was supported by Wellcome Grant 05115, and J.E.S. was supported by British Heart Foundation Grant FS/96009. We thank Bruce Cotsell for his excellent technical support.

Correspondence should be addressed to Dr. Michael P. Gilbey, Autonomic Neuroscience Institute, Department of Physiology, Royal Free Hospital School of Medicine, Rowland Hill Street, London NW3 2PF, UK.

Copyright © 1999 Society for Neuroscience 0270-6474/99/193183-15\$05.00/0

that temporal coding in the CNS is thought to be important in sensory processing and skeletal muscle motor control, we suggest that dynamic synchronization of PGN activity may have significant functional implications for sympathetic cardiovascular control.

Part of this work has been published previously as abstracts (Chang and Gilbey, 1998; Chang et al., 1998a,b).

MATERIALS AND METHODS

General preparation and maintenance

Experiments were conducted on 33 male Sprague Dawley rats (255–355 gm) anesthetized initially with sodium pentobarbitone (60 mg/kg, i.p.) supplemented with α -chloralose (5–10 mg, i.v.) when required. Anesthetic level was monitored, and an appropriate depth was indicated by the stability of blood pressure and phrenic nerve (PN) activity and the absence of both corneal and paw-pinch withdrawal reflexes. The femoral artery and vein were cannulated for recording blood pressure and infusing drugs, respectively. The trachea was cannulated. The oesophageal temperature was monitored and maintained at 36.5–37°C using a heating blanket (and/or a lamp). The urinary bladder was cannulated to ensure an unobstructed urine flow. Figure 1 summarizes the main surgical procedures performed.

In experiments in which rats were artificially ventilated ($n = 25$), vagotomies and pneumothoracotomies were performed (Fig. 1), and an end-expiratory pressure (2–3 cm H₂O) was applied to prevent atelectasis. During periods of data collection, animals were paralyzed (gallamine triethiodide, 15 mg · kg⁻¹ · hr⁻¹), and the depth of anesthesia was assessed by monitoring the stability of the blood pressure and phrenic discharges. Blood gas samples were taken immediately before data were collected. In experiments performed on spontaneously breathing rats ($n = 8$), the vagi were left intact, and the animals were supplied continuously with O₂-enriched room air.

In all animals, peak expiratory CO₂ was monitored in every breath using a CO₂ meter (model FM1; The Analytical Development Company). Arterial blood gases were sampled regularly (0.5–1 hr) using a blood gas analyzer (model M238; Ciba-Corning Ltd.), and if necessary sodium bicarbonate (1 M) was given to counter metabolic acidosis. PN activity was recorded routinely in all preparations, and the inspiratory-related activity was taken as an indication of CRD (Johnson and Gilbey, 1994, 1996).

Recording from the VCN

The VCNs are mixed nerves that contain both sympathetic and somatic sensory-motor axons. The central connection of somatic motor efferents projecting through the VCNs were interrupted by cutting the cauda equina at the L5 level, thereby leaving only sympathetic efferents intact (Sittiracha et al., 1987; Smith and Gilbey, 1998a; Smith et al., 1998). A VCN was then exposed, cut, and desheathed. Monophasic activity was recorded differentially by placing the central and peripheral nerve ends on bipolar platinum electrodes in a paraffin oil-filled bath (Fig. 1). The peripheral nerve end was crushed. In ten experiments, the sympathetic nature of VCN activity was confirmed by the abolition of ongoing nerve activity after intravenous injection of the ganglionic blocker chlorisondamine (3 mg/kg).

Focal recording of the activity of PGNs

Glass microelectrodes (internal diameter of the tip, 20–100 μ m), filled with Krebs' solution, were placed on the surface of the CVA, and gentle suction was applied to "seal" the tip (Johnson and Gilbey, 1994, 1996). The discharges of two PGNs were either recorded simultaneously through two independent electrodes or discriminated from multiunit activity recorded through one electrode. Previous studies have confirmed that all units recorded from the surface of the CVA are sympathetic in nature with characteristic discharge patterns (Johnson and Gilbey, 1994, 1996). Activity from single PGNs was identified by a consistent spike waveform and amplitude. In each experiment in which paired recordings were made, we were careful to establish that the latency between the firing of the two PGNs was not constant, because this would be evidence that both recordings arose from the same PGN (either its axon or branches). Although constant latency firing was occasionally seen in single-patch recordings between pairs of "PGNs" (and these were therefore discarded), the latency between PGNs recorded from separate electrodes (physical separation, 2.5–5.5 cm) was always variable.

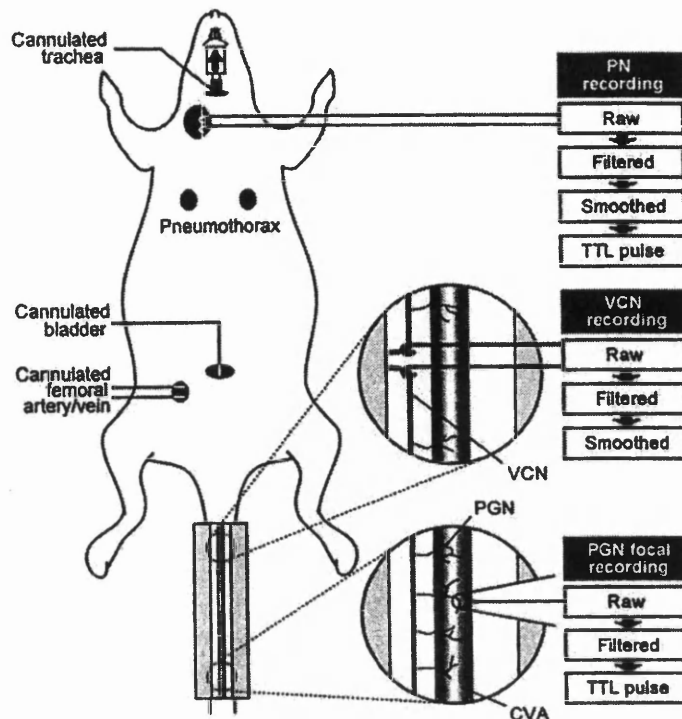
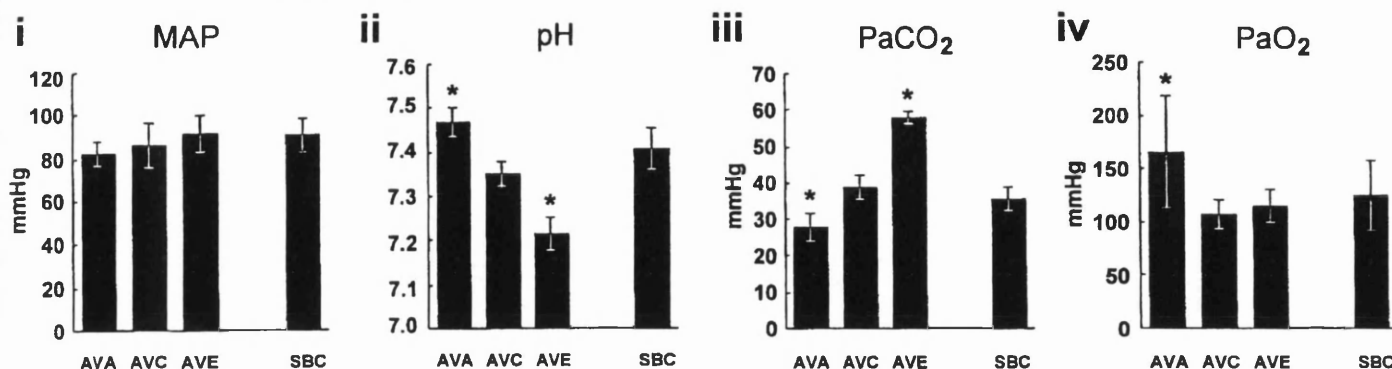


Figure 1. The experimental preparation and signal processing procedures used for recording neural activities. The femoral artery/vein, trachea, and urinary bladder of the rats were cannulated. A pneumothoracotomy was performed, and the vagi were cut (not shown) in the experiments in which animals were ventilated artificially. Whole-nerve activity of PN was recorded from the neck. Activity was recorded from the VCN in the tail by cutting the nerve and placing the cut ends on bipolar electrodes (*top insert*). The cauda equina was transected in the VCN whole-nerve experiments (not shown). It should be noted there is one VCN on either side of the tail, but only the right one is shown here for simplicity. Single PGN activity was recorded from the surface of the CVA through a focal suction glass microelectrode (*bottom insert*). Two focal electrodes were used simultaneously in most experiments in which two PGNs were recorded, but only one is shown here for simplicity. For PN and VCN activity, the raw activity was filtered, rectified, and smoothed, and spectral analysis was performed on this smoothed data. TTL pulses representing the rising (inspiratory) phase of PN activity were generated from the smoothed data using a low-frequency threshold trigger interface. For PGN activity, the raw signal was filtered and passed through a window preset in a spike processor to generate TTL pulses. For further details, see Materials and Methods.

Data collection

All neuronal activity was recorded using high impedance headstages (model NL100; Neurolog, Digitimer Ltd), amplified (model NL104; Neurolog) and filtered (bandpass 300–1 kHz; model NL125; Neurolog). PN activity and VCN activity were rectified and smoothed (Fig. 1) with a "leaky integrator" (time constant: PN, 0.1 or 0.2 sec; VCN, 0.1 sec; model NL703, Neurolog). Such narrow-band filtering followed by rectification and smoothing (or integration) is a well established procedure for generating an envelope of the activity (for examples, see Haselton and Guyenet, 1989; Czyzyk-Krzeska and Trzebski, 1990). One of the main advantages is that it removes movement-related artifacts that frequently appear as slow wave activity (Kenney and Fedde, 1994). However, the filtering causes little attenuation of individual action potentials because the instantaneous frequency of single fiber activity is higher than the high-pass cutoff value (see Fig. 7*Ai, Aii, Aiii*). All data were stored on tape using a video recorder (model V-404B; Toshiba) for off-line analysis. In addition, the blood pressure, tracheal pressure, smoothed phrenic and VCN activity, and single PGN activity were converted into digital signals via an analog-to-digital converter interface (model 1401, Cambridge Electronic Design; sampling frequency: 13.3 kHz for PGN activity; 100 Hz for VCN and PN activity) and sent to a computer for analysis.

A Whole nerve experiments



B Single PGN experiments

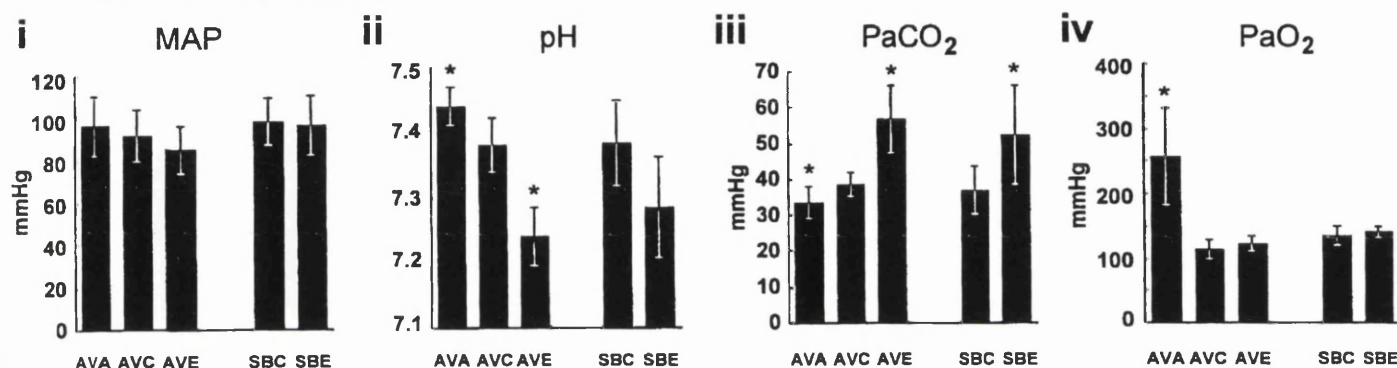


Figure 2. Physiological parameters under different experimental conditions. Conditions: AVA, AVC, AVE, SBC, and SBE. *A*, Whole-nerve experiments. AVA, $n = 8$; AVC, $n = 13$; AVE, $n = 8$; and SBC, $n = 3$. *B*, Single PGN experiments. AVA, $n = 6$; AVC, $n = 13$; AVE, $n = 6$; SBC, $n = 6$; SBE, $n = 4$. *Ai*, *Bi*, MAP. *Aii*, *Bii*, pH. *Aiii*, *Biii*, PaCO₂. *Aiv*, *Biv*, PaO₂. Data are presented as mean \pm SD. Statistical differences between the three subgroups of artificially ventilated animals were assessed using ANOVA followed by Bonferroni multiple comparison tests. A Student's *t* test was used to test the difference between the two subgroups in spontaneously breathing animals. Parameters that are significantly different from control conditions are indicated by an asterisk ($*p < 0.05$).

A spike processor (model D130; Digitiser) and an interface (model NLS15; Neurolog) were used to generate transistor-to-transistor logic (TTL) pulses from single PGN action potentials and the rising phase of rhythmical (inspiratory) PN activity, respectively (Fig. 1). These TTL pulses were also sent to the computer and used to generate autocorrelograms, cross-correlograms, and correlation raster plots of PGNs and PN activity (SPIKE2, Cambridge Electronic Design; MATLAB, MathsWorks).

Whole-nerve analysis

Spectral analysis of VCN and PN activity. The presence of rhythmical components in VCN and PN activity and the degree of correlation between them were assessed using spectral analysis. A 480 sec data set of integrated nerve activity was sampled at 100 Hz and divided into 45 half-overlapped subsections with 2048 data points in each. The linear trend was removed in each subsection. The autospectrum and cross-spectrum averaged from these subsections were calculated according to the Welch Method (size of fast Fourier transformation, 2048) (Bendat and Piersol, 1986). The autospectrum, plotted as relative power density (RPD) against harmonic frequencies, was only displayed between 0 and 5 Hz because the power at frequencies above this level was negligible. The coherence spectrum was used to investigate the linear correlation between PN and VCN activity at different frequencies. The squared coherence coefficient (abbreviated as coherence) at each harmonic frequency was estimated by normalizing the cross-spectrum between the PN and VCN activity (Bendat and Piersol, 1986).

Assessing temporal changes in VCN activity. Time-evolving autospectra were generated to examine temporal changes in VCN and PN activity. A 480 sec data set was divided into twelve 40 sec segments, and spectral analysis was performed on each. The magnitude of the RPD for each

segment was then coded using a 64-grade gray scale. The time-evolving spectrum was plotted as harmonic frequency against time history. Changes in the gray scale represent the change of the RPD across both the recording time and frequency range. To quantify the dynamic change of the RPD, the time evolving autospectrum was normalized by its maximal value, and the sum of RPD variance of all the frequencies across the twelve 40 sec segments was taken as a measure of the stability of VCN activity.

Single-unit analysis

T-rhythm frequency determination. For event series composed of PGN or PN occurrences, the event-triggered cumulative histograms, correlograms, were used to assess the correlation of occurrences between neural activities (Perkel et al., 1967a,b). For autocorrelograms the histograms are self-triggered, and for cross-correlograms the trigger events and the dependent events come from different event series. Series of 300 sec data sets of neuronal activity were used to generate autocorrelograms and cross-correlograms. The 5 sec post-trigger period in the autocorrelogram was inspected visually to establish the presence of a dominant rhythmicity. The exact frequency was determined from the spectrum of the envelope of the autocorrelogram across the 300 sec post-trigger interval as follows: the envelope of the autocorrelogram (bin width, 0.05 sec; duration, 300 sec) was first smoothed using a moving average method [weight factor, (0.15, 0.2, 0.3, 0.2, 0.15)]. The gain of the frequency response function of this moving average process was monotonically decreased, and there was no net phase shift in the frequency range in which we were primarily interested (0–5 Hz). Consequently, the rhythmical components in the envelope are not artifacts arising from the smoothing process ("Slutsky effect", see Koopmans, 1995). The smoothed envelope of the autocorrelogram was subjected to spectral

analysis using a similar method to that described for VCN and PN activity (sampling rate, 20 Hz; fast Fourier transformation size, 1024). Because the bin width of the discrete spectrum is 0.02 Hz, the frequencies of two PGN T-rhythms were considered to be the same if the difference between them was <0.02 Hz.

Evaluation of synchronization between two PGNs (represented by PGN→PGN). By definition, synchronization is a state of constant phase difference between two activities (Winfree, 1980). If the phase difference between two rhythmic activities, such as PGNs, is constant, a periodic pattern will appear on their cross-correlogram. Thus, in this study, the state of PGN→PGN synchronization, termed rhythmical synchronization, is assessed by the cross-correlogram (divided into 200 bins, bin-width, 0.05 sec). To quantify the degree of synchronization, the spectrum of the envelope of the cross-correlogram was generated using a method analogous to that described for autocorrelogram spectral analysis. The RPD of the dominant peak shown on the envelope spectrum was taken and used as a measure of synchronization. As a gauge of the significance of the rhythmicity in each cross-correlogram, we calculated a 95% confidence interval, based on a novel analysis method described below.

The confidence interval is calculated for a single peritrigger bin. When there are N triggers, the random variable, X_{ij} ($i = 1, 2, \dots, N$ and $j = 1, 2, \dots, 200$) represents the number of dependent events in the j th peritrigger bin after the i th trigger. In total, there are $200 \times N$ random variables. The null hypothesis for the statistical inference is: all the X_{ij} random variables are independent and identically distributed with finite variance. The random variable, $Y_i = \sum X_{ij}$ ($j = 1, \dots, N$), represents the number of events in the i th bin in the cross-correlogram. If $N > 30$, the distribution of Y_i is approximately normal according to the central limit theorem (Papoulis, 1991). The parameters to be estimated are the expectation and the variance of Y_i . $E(Y_i) = E(\sum X_{ij}) = \sum E(X_{ij})$ ($j = 1, \dots, N$). $\text{Var}(Y_i) = \text{Var}(\sum X_{ij}) = \sum \text{Var}(X_{ij})$ ($j = 1, \dots, N$). The estimators of $E(X_{ij})$ and $\text{Var}(X_{ij})$ are the unbiased sample mean, m_x , and variance, s_x^2 , calculated from the empirical data ($200 \times N$ samples, x_{ij} , $i = 1, 2, \dots, N$; $j = 1, 2, \dots, 200$). The 95% confidence interval for Y_i is $[-1.96 * (N * s_x^2)^{1/2} + N * m_x, 1.96 * (N * s_x^2)^{1/2} + N * m_x]$. This confidence interval is applied to all the Y_i s because the distributions of the Y_i ($i = 1, \dots, 200$) are identical under the null hypothesis. It should be noted that it is possible for the event number in several bins (5% of 200) to exceed the 95% confidence interval by chance. In this study we were concerned primarily with the rhythmical T-rhythm oscillator or oscillators, and we define significant synchronization between two neural activities as the existence of rhythmicity in the envelope of the cross-correlogram in which the peaks and/or troughs exceed the 95% confidence interval.

Assessing temporal changes in synchronization. PGN→PGN correlation raster plots were used to elucidate dynamic temporal changes in synchronization between PGNs. The raster plot, as with the cross-correlogram, shows the temporal relationship between the triggers and dependent activity, but differs because the peritrigger event series are plotted against each trigger. To quantify the stability of the phase relation between two PGNs, the raster plot was divided into small quadrats (0.1 sec \times 10 trigger events), and the number of events in each (the event density) was counted. The event density was normalized by the maximal event density in all the quadrats. The sum of the normalized event density variance at each peritrigger time across the trigger occurrences represents the inhomogeneous phase change across time (termed density variance). If the phase difference remains relatively constant across time, a dense vertical striation will be present on the raster plot against a low-density background. The RPD of the cross-correlogram envelope (spectral density) provides a measure of the density of the rhythmical vertical striation. The parameter, density variance/spectral density, termed the phase variation factor, is a measure of the level of unstable rhythmicity plus the degree of variation of phase difference across time and was taken to assess the stability of rhythmical synchronization between two PGNs.

Experiment protocol

Manipulating CRD. Activity of the PGNs innervating the CVA was recorded under three conditions, absence of CRD, control, and enhanced CRD. The control condition was achieved by maintaining the blood gas parameters within a normal physiological range (see Results). The absence of CRD (apnea) was induced either by raising the oxygen concentration (60–90%) of the inflow and/or by hyperventilation hypocapnia. CRD was enhanced by raising inspired CO_2 to 5% and inducing a hypercapnic state (St-John and Bianchi, 1985).

Whole-nerve experiments. VCN activity was recorded from sixteen

animals. Thirteen of these were ventilated artificially, and the other three breathed spontaneously. In each experiment, nerve activity was recorded initially in control conditions. Of the thirteen artificially ventilated rats, eight animals were tested under enhanced CRD conditions and eight in the absence of CRD. Six of the thirteen animals were tested in all three conditions.

Single PGN experiments. Action potentials of single PGNs were recorded from seventeen animals. Twelve of these were ventilated artificially, and the remainder breathed spontaneously. At least one pair of PGNs was recorded in each animal during control conditions. Six artificially ventilated and four spontaneously breathing subjects were tested under enhanced CRD conditions. Neuronal activity was also recorded in six artificially ventilated rats in the absence of CRD. Five of the eleven artificially ventilated animals were tested in all three conditions.

Statistics

Results are expressed as mean \pm SD when a parametric test was used or median and interquartile intervals (first and third quartiles) when a nonparametric test was used. Either one-way ANOVA followed by Bonferroni multiple comparison test, Student's t test, or Wilcoxon rank-sum test was used to assess statistical significance. The comparison was considered to be significant if $p < 0.05$.

RESULTS

Condition of animals

The animals were maintained in a consistent physiological state in each of the experimental conditions, as indicated by measurements of four parameters. Figure 2*A* summarizes the mean arterial blood pressure (MAP) (Fig. 2*Ai*), pH (Fig. 2*Aii*), PaCO_2 (Fig. 2*Aiii*), and PaO_2 (Fig. 2*Aiv*) for the whole-nerve recording experiment for four conditions: artificially ventilated, absence of CRD (AVA); artificially ventilated, control (AVC); artificially ventilated, enhanced CRD (AVE); and spontaneously breathing, control (SBC) animals. Figure 2, *Bi–Biv*, summarizes the same parameters for the single PGN recording experiments for the four conditions stated above plus an additional condition: spontaneously breathing, enhanced CRD (SBE).

Whole-nerve activity recorded from the VCN in artificially ventilated animals

Rhythmical and sympathetic nature of VCN activity

The nerve activity recorded from the VCN appeared as burst discharges with variable frequency and amplitude. A typical example (artificially ventilated, control) is shown in the neurogram in Figure 3*A*. The major rhythmical component of the activity is revealed by the presence of a prominent peak at 0.63 Hz in the autospectrum (Fig. 3*Bi*). To establish the sympathetic nature of VCN activity, we tested the effect of the sympathetic ganglionic blocker chlorisondamine on the activity ($n = 10$). In all cases, this led to abolition of most of the activity and power in the autospectra (Fig. 3, *Bii, C*).

Synchronous components in VCN activity become more prominent with increased CRD

VCN activity was recorded in animals under three different respiratory conditions, absence of CRD, control, and enhanced CRD. In each condition, autospectra for VCN and PN activity were generated, and coherence spectra were produced to identify correlated components in their activity. Here, the results are presented first in the absence of CRD, then control, and finally enhanced CRD, to emphasize the trend toward synchronization with increasing CRD.

In animals in which the CRD was abolished, a single prominent peak (median, 0.83 Hz; interquartile interval, 0.79–0.88 Hz) was observed in the VCN autospectra in all cases ($n = 8$). This peak is in the frequency range of the T-rhythm (Johnson and Gilbey,

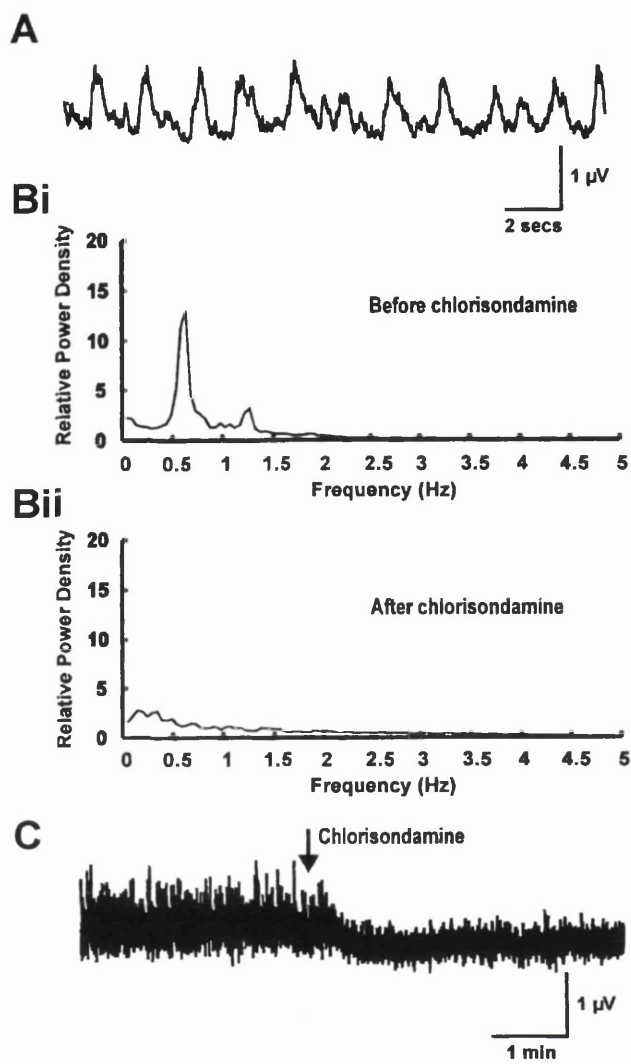


Figure 3. The bursty and sympathetic nature of the VCN activity in an artificially ventilated animal under control conditions. *A*, Rectified and smoothed neurogram of VCN activity shows burst discharges with variable frequency and amplitude. *Bi*, Autospectrum of VCN activity shows a peak at 0.63 Hz with its first harmonic peak at 1.26 Hz. *Bii*, Autospectrum of activity of the same VCN in *Bi*, after chlorisondamine (3 mg/kg, i.v.), a sympathetic ganglionic blocker. The abolition of the peaks after this treatment shows that the nerve activity was sympathetic in nature. *C*, Real time neurogram of the same VCN activity before and after application of chlorisondamine.

1996), and we refer to it in this paper as the T-peak. A typical example, in which the T-peak frequency is 0.82 Hz, is shown in Figure 4*Ai*. The absence of CRD is indicated by the flatness of the autospectrum of the PN (Fig. 4*Aii*), and the lack of correlation between VCN and PN activity is shown by the coherence spectrum (Fig. 4*Aiii*).

Thirteen animals were examined under control conditions. In six (46%) of these, the VCN autospectra revealed a T-peak (median frequency, 0.79 Hz; interquartile interval, 0.74–0.82 Hz). Statistical comparisons between animals in the absence of CRD and in control conditions (in which a discrete T-peak was present) demonstrated that the T-peak frequencies were not significantly different ($p = 0.44$; Wilcoxon rank-sum test). In twelve (92%) of the animals, a peak at the CRD frequency was present (median frequency, 0.63 Hz; interquartile interval, 0.59–

0.68 Hz). The coherence at the frequency of CRD between VCN and PN activity, revealed by the coherence spectrum, was high (median, 0.73; interquartile interval, 0.63–0.88). The VCN autospectrum from one of the animals displaying both the T-peak and the respiratory-related peak is shown in Figure 4*Bi* (this is the same animal as in Fig. 4*A*). The first peak at 0.59 Hz (filled circle) corresponds to the main peak in the PN activity (Fig. 4*Bii*), and this is confirmed by the coherence spectrum shown in Figure 4*Biii*. The additional peaks in the PN autospectrum are harmonics of the first peak, and these also display high coherence with VCN activity. Lack of coherence between VCN and PN at the frequency of the second peak (asterisk, 0.79 Hz) was also demonstrated in Figure 4*Biii*.

A condition of enhanced CRD was induced in a subset of the animals ($n = 8$) examined in control conditions. In all cases, there was a prominent respiratory-related peak in the VCN autospectra (median frequency, 0.59 Hz; interquartile interval, 0.53–0.63 Hz) that showed a very high coherence with the phrenic autospectra (median coherence, 0.90; interquartile interval, 0.76–0.92). In two (25%) of the animals there was also a separate T-peak (frequency, 0.73 and 0.68 Hz, respectively). The RPD of the respiratory-related peak when the CRD was enhanced (median of the RPD, 14.2; interquartile interval, 9.75–19.8) was higher than that of the T-peak when CRD was abolished (median of the RPD, 4.14; interquartile interval, 3.7–6.4) ($p < 0.02$; Wilcoxon rank-sum test). This suggests that the dominant rhythmical activity became more prominent when the condition was switched from absence of CRD to enhanced CRD. A typical example of the VCN autospectrum in an animal with enhanced CRD is shown in Figure 4*Ci* (this is the same animal as in Fig. 4*A,B*). There is a prominent peak at 0.63 Hz that has a high coherence with the PN discharge (Fig. 4*Cii,Ciii*); other peaks at harmonic frequencies of PN activity are also visible.

Stability of VCN rhythmical activity increases when the CRD is enhanced

VCN activity was also examined using time-evolving autospectra, which provide information about the dynamics of the rhythmicity across time. When the CRD was abolished, VCN rhythmical activity was relatively unstable (see below). The example shown in Figure 5*Ai* (same animal as in Fig. 4), shows a band containing relatively high- and low-density components at the T-rhythm frequency, indicating periods of strong and weak synchrony of rhythmical firing in the PGN population. No prominent bands were visible in the phrenic time-evolving autospectra confirming that CRD was abolished (Fig. 5*Aii*). In control conditions, as shown in the example in Figure 5*Bi* (same animal as in Fig. 4), the VCN band was dense and more stable across time than in CRD-abolished conditions. Part of the prominent dense band in VCN activity fell within the frequency range of the band observed in the phrenic time-evolving autospectra (Fig. 5*Bii*). However, although the phrenic activity produced a dense, stable band, the VCN showed transient periods in which band density was reduced, indicating periods of frequency drifting. In conditions of enhanced CRD, the VCN time-evolving autospectra (example in Fig. 5*Ci* from the animal shown in Fig. 5*B,C*) was similar to the phrenic autospectra (Fig. 5*Cii*), exhibiting stable dark bands at the phrenic frequency and its harmonics. This suggests that a substantial proportion of the PGNs were entrained with phrenic activity throughout the time period examined. The level of stability in each condition was quantified using a measure of the power density variance across time (see Materials and Methods).

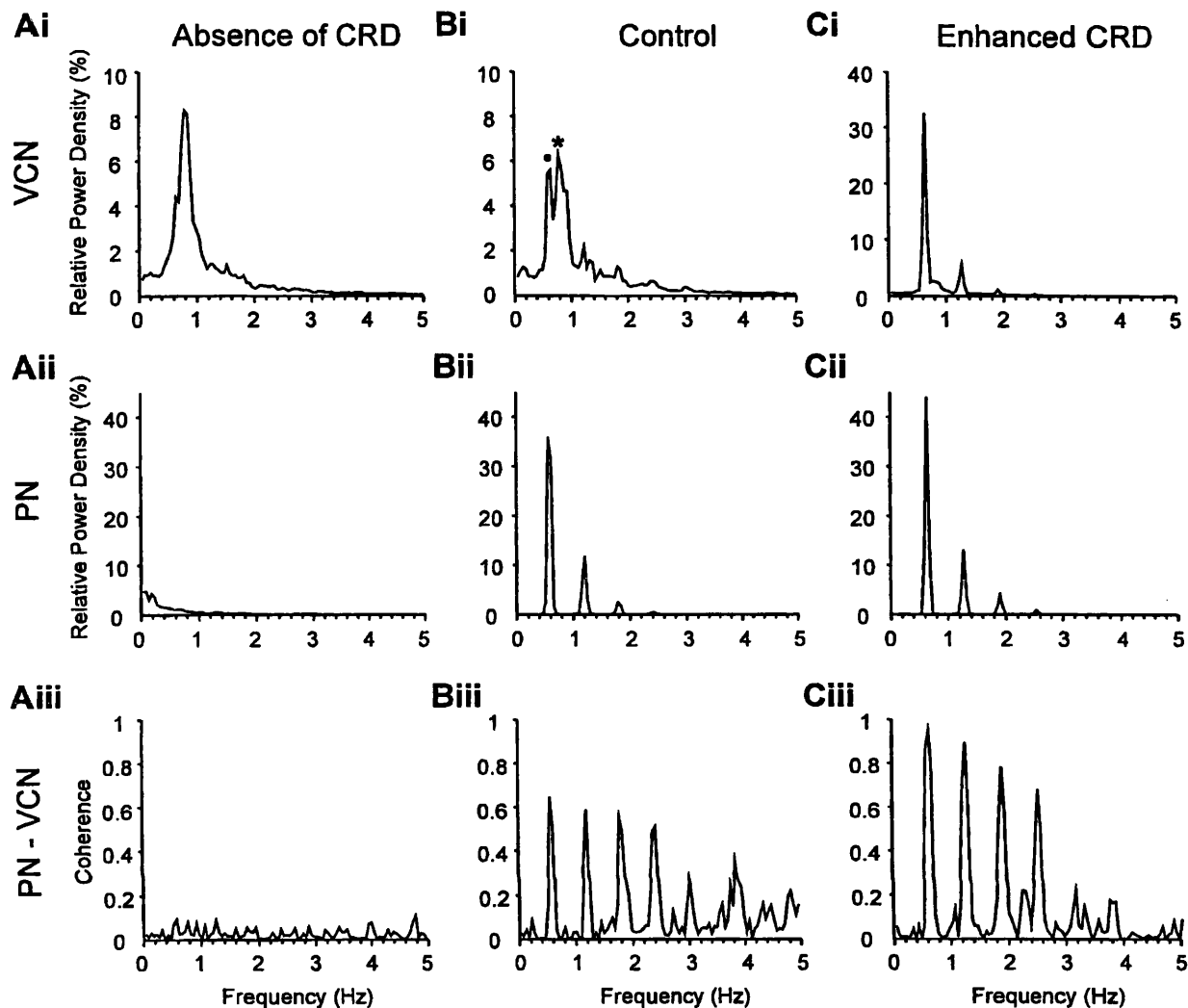


Figure 4. The autospetra and coherence spectra of the VCN and PN in an artificially ventilated animal under three conditions of CRD. *A*, Absence of CRD. *Ai*, Autospetrum of VCN activity reveals a peak at 0.82 Hz. *Aii*, Autospetrum of PN activity shows no rhythmic components. *Aiii*, The coherence spectrum of VCN and PN shows lack of correlation between the two nerves. *B*, Control condition. *Bi*, Autospetrum of VCN activity shows two peaks, one (filled circle) at 0.59 Hz was the same as the frequency of CRD, revealed in the autospetrum of the PN (*Bii*) and a second, (asterisk) at 0.79 Hz. *Bii*, Autospetrum of PN activity. *Biii*, The coherence spectrum between VCN and PN reveal high coherence at the frequency of CRD. *C*, Enhanced CRD. *Ci*, Autospetrum of VCN is dominated by a peak at 0.63 Hz (and its first harmonic component), which is the same as the frequency of CRD. Note the scale of relative power density is different from that in *Ai* and *Aii*. *Cii*, Autospetrum of PN activity. Comparison of the relative power density of the peak with control conditions shows that the level of CRD was increased. *Ciii*, VCN and PN activity show a high coherence.

The data are summarized for the absence of CRD ($n = 8$), control ($n = 13$), and enhanced CRD ($n = 8$) groups in Figure 6. Comparisons between conditions of absent CRD and enhanced CRD revealed a significant difference ($p < 0.05$; Wilcoxon rank-sum test).

Whole-nerve activity recorded from the VCN in spontaneously breathing animals

Three animals were recorded under spontaneously breathing conditions to determine whether VCN activity behaved in a similar way to that seen in artificially ventilated animals. In all three, the VCN autospetra revealed a T-peak with a median frequency of 0.6 Hz (interquartile interval, 0.56–0.66 Hz) and a second peak with a median frequency of 0.93 Hz (interquartile interval, 0.9–1.1 Hz) that showed high coherence with the PN activity (median, 0.52; interquartile interval, 0.51–0.62). We concluded that in spontaneously breathing animals, VCN activity

included rhythmic components similar to those identified in artificially ventilated preparations.

Paired recordings of PGNs innervating the CVA in artificially ventilated animals

In the absence of CRD, the T-rhythms seen in PGNs recorded simultaneously show a low probability of synchronization

The activity of six pairs of PGNs (six animals), each from separate electrodes, were recorded in the absence of CRD. The discharges of individual PGNs, examined by generating autocorrelation plots, were rhythmic in nature. The median frequency of the T-rhythm was 0.61 Hz (interquartile interval, 0.55–0.68 Hz). Although the activity of all PGNs showed a dominant peak in the range of T-rhythm frequency in the envelope spectrum (median of RPD, 4.9; interquartile interval; 3.7–5.8), neither of the PGNs in a pair had the same T-rhythm frequency, and cross-

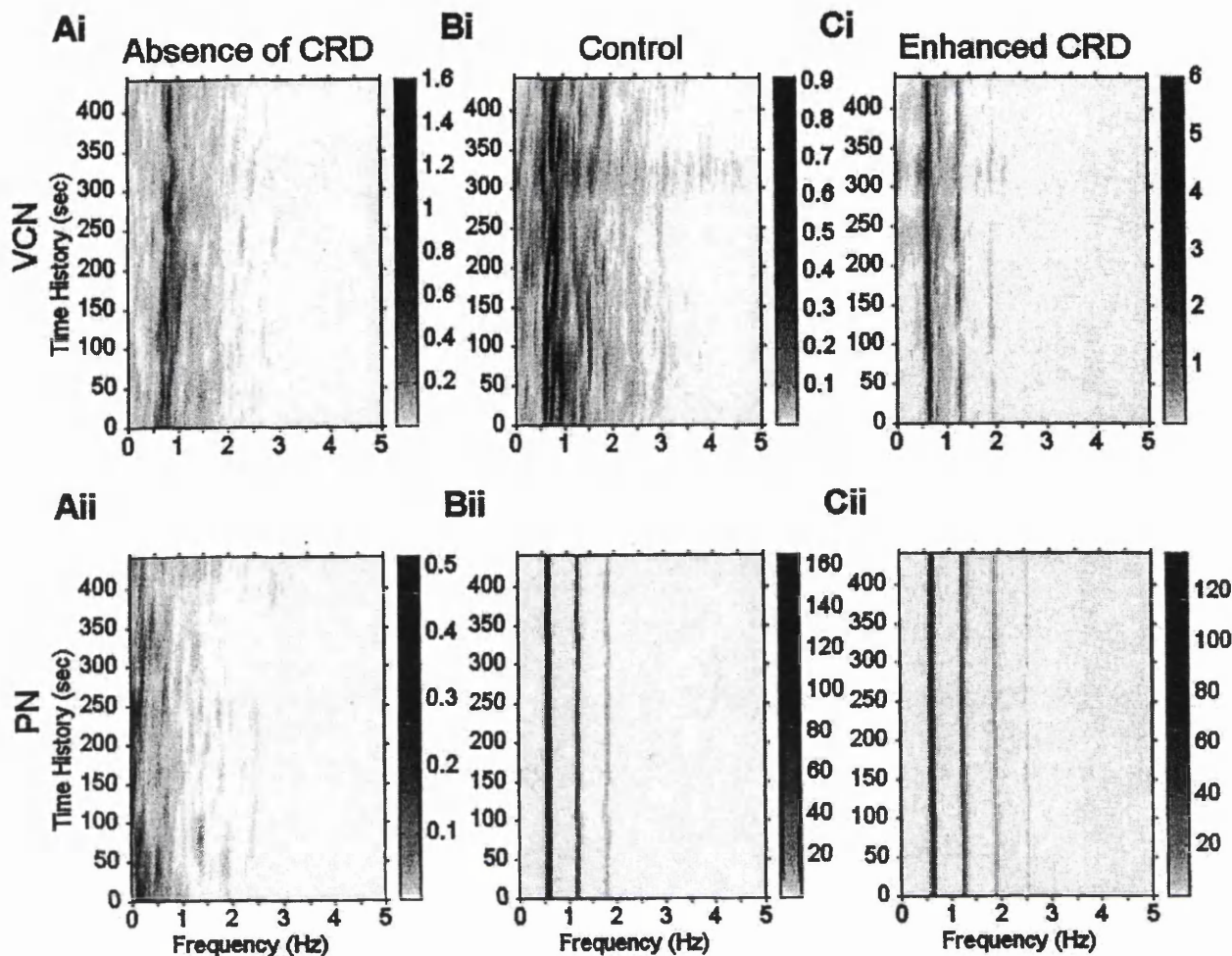


Figure 5. Time-evolving autospectra of the VCN and PN under three conditions of CRD from the same animal and across the same time periods as in Figure 4. The data were divided into twelve 40 sec subsections. Spectral analysis was performed on each subsection. The relative power density across time is coded by a 64 grade gray scale (note scale bar on right of each figure is different). *A*, Absence of CRD. *Ai*, VCN autospectrum shows that the relative power of the VCN was concentrated at a band around 0.82 Hz, but the power density varied across time. *Aii*, PN autospectrum shows little or no power across time. *B*, Control condition. *Bi*, VCN autospectrum shows that the power of the VCN is concentrated in a relatively well defined band between 0.54 and 1.05 Hz, including the frequency of CRD (0.59 Hz, see *Bii*). It should be noted that the two dominant peaks of the VCN autospectrum revealed in Figure 4*Bi* are not constant across time; it is a feature arising from dynamic change of the power density within the narrow frequency band. *Bii*, PN autospectrum. *C*, Enhanced CRD. *Ci*, VCN autospectrum reveals that the relative power density of the VCN is very constant across time and centered at the frequency of CRD (0.63 Hz; *Cii*). *Cii*, PN autospectrum.

correlogram analysis revealed that no significant synchronization was displayed in PGN→PGN activity.

Figure 7, *Ai* and *Aii*, shows ten superimposed action potentials for each of a pair of PGNs, illustrating the consistency of the spike shape and amplitude. A section of the real time neurograms of these two PGNs and PN is shown in Figure 7*Aiii*. The autocorrelograms from these two PGNs, in the absence of CRD, are shown in Figure 7, *Bi* and *Bii*. These PGNs both exhibit characteristic rhythmicity, but the frequencies are different (0.55 Hz for PGN1; 0.70 Hz for PGN2). The PGN1→PGN2 cross-correlogram shown in Figure 8*A* does not show a significant rhythmicity (i.e., peaks passing through the 95% confidence level at regular intervals), demonstrating that the rhythmical component of the discharges of this pair of PGNs is not synchronized.

In control conditions some pairs show PGN→PGN synchronization through entrainment by CRD

The activity of pairs of PGNs (thirteen from twelve animals) were recorded in control conditions, either using separate electrodes

($n = 9$) or discriminated from multiunit activity recorded through a single electrode ($n = 4$). All the PGNs displayed a T-rhythm with a median frequency of 0.72 Hz (interquartile interval, 0.66–0.75 Hz). The spectra of the envelope of cross-correlograms in all pairs showed a dominant peak (median of RPD, 12.5; interquartile interval, 11.0–26.4). In seven (54%) pairs of PGNs, each PGN had the same T-rhythm, and there was significant PGN→PGN synchronization. The T-rhythm frequencies of these PGNs were the same as the frequency of CRD (median frequency, 0.73 Hz; interquartile interval, 0.68–0.77 Hz). The cross-correlogram between PN and these PGNs (represented as PN→PGN) showed that they were significantly correlated. Six (46%) pairs of PGNs had different T-rhythm frequencies and no significant PGN→PGN synchronization. In four of these pairs, one PGN of each pair showed a T-rhythm frequency the same as CRD but the other did not. In the remaining two pairs, the frequencies of the T-rhythms of the PGNs in each pair were different from each other and from CRD. An example of the autocorrelograms of a

pair of PGNs in control conditions is shown in Figure 7, *Ci* and *Cii* (these are the same units as in Fig. 7*Bi, Bii*). Figure 7*Ciii* shows the PN autocorrelogram in this animal (CRD frequency, 0.74 Hz). The two PGNs have different T-rhythm frequencies (0.53 Hz for PGN1; 0.74 Hz for PGN2), and there is no PGN→PGN synchronization as revealed by the cross-correlogram in Figure 8*Bi*. PGN1 has a T-rhythm frequency that is different to the CRD frequency, but the PN→PGN1 cross-correlogram shows a significant correlation (Fig. 8*Bii*). This arises from the dynamic nature of PN→PGN interaction (see section “The stability of rhythmical synchronization of PGNs increases when CRD is enhanced”). Although some discharges of PGN1 are phase-locked to CRD, which produced the periodic pattern in the cross-correlogram, the overall activity that produced the T-rhythm did not have a fixed phase difference to CRD. PGN2 has a T-rhythm that is at the same frequency as CRD, and the cross-correlogram reveals a significant 1:1 synchronization (Fig. 8*Biii*).

Enhanced CRD leads to PGN→PGN synchronization of T-rhythms

Six animals were recorded in conditions of enhanced CRD, and six pairs of PGNs were recorded through separate electrodes. All the PGNs exhibited robust rhythmicity, as revealed by their autocorrelograms, with a median T-rhythm frequency of 0.67 Hz (interquartile interval, 0.64–0.7 Hz). The dominant peak in the envelope of the cross-correlogram ($n = 6$) had a median RPD of 19.4 (interquartile interval, 12.0–36.5). Notably, in five (83%) of the pairs of PGNs, the activities of both PGNs had the same T-rhythm frequency and were significantly synchronized. These pairs were also locked in a 1:1 manner with CRD (median frequency, 0.67 Hz; interquartile interval, 0.64–0.69 Hz) and had significant PN→PGN synchronization. The dynamic nature of this synchronization is demonstrated by the fact that three (60%) pairs of PGNs synchronized during enhanced CRD were not significantly synchronized in control conditions.

The same PGNs examined during the absence of CRD (Fig. 7*B*) and control conditions (Fig. 7*C*) are shown under enhanced CRD conditions in Figure 7*D*. Both PGN1 and PGN2 and the PN show the same frequency (0.71 Hz) as revealed by their autocorrelograms (Fig. 7*Di, Dii, Diii*). These PGNs show significant PGN→PGN (Fig. 8*Ci*) and PN→PGN synchronization (Fig. 8*Cii, Ciii*).

Summary of the data from paired recordings under various respiratory conditions

The data presented here revealed a significant increase in the probability of synchronization of the rhythmical activity of PGN pairs as animals were moved from conditions when CRD was absent to conditions with enhanced CRD. In the absence of CRD, PGN→PGN activity never showed rhythmical synchronization. Although all these PGNs showed a T-rhythm, the T-rhythm frequency of each PGN of a pair was different as revealed in the scatter plot (Fig. 9*A*). During control conditions, in which CRD was present, a proportion of PGN pairs (~55%) had the same T-rhythm frequency (Fig. 9*B*) that was also the same as that of CRD. The T-rhythms of PGNs of these pairs were phase-locked. When the PGNs of a pair had different rhythms, there was no synchronization. In conditions of enhanced CRD, the majority of pairs (>80%) of PGNs had T-rhythms that were synchronized to each other at the frequency of the CRD. The T-rhythm frequencies of each PGN in each pair in this condition are shown in Figure 9*C*. For all the synchronous pairs of PGNs either under

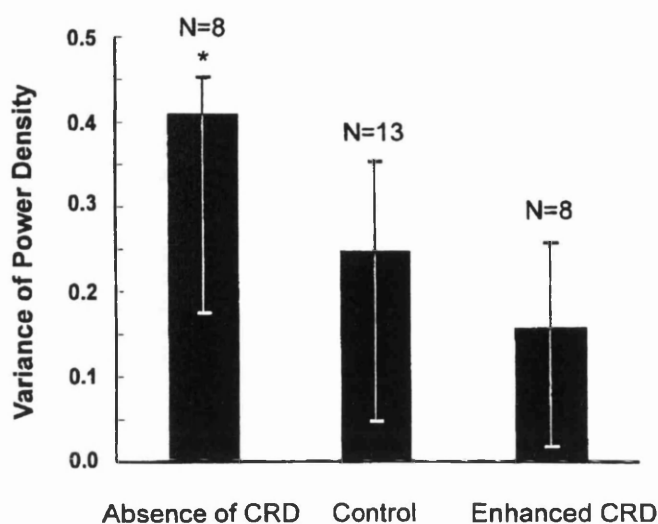


Figure 6. Dynamic stability of rhythmical components evaluated by the variance of the relative power density of VCN activity across time in artificially ventilated animals under three conditions of CRD. Data are presented as medians and first and third quartiles. The level of power density variance is inversely proportional to the level of stability. The asterisk indicates that the power density variance in the absence of CRD is significantly higher than the variance in conditions of enhanced CRD (Wilcoxon rank-sum test; $p < 0.05$).

control conditions or when the CRD was enhanced, the peak nearest to lag zero in the PGN→PGN cross-correlograms always straddled the lag zero (as shown in Fig. 8*Ci*), indicating that statistically, the phase difference between synchronous PGNs was nearly zero. Furthermore, PN→PGN cross-correlograms reveal that activity of the two PGNs of a synchronous pair have similar phase differences relative to PN activity (Fig. 8*Cii, Ciii*) and this, given the fact that the frequencies of the PGNs are the same as that of PN, strongly suggests that the in-phase synchrony of PGN discharges may arise from the synchronization through CRD.

The degree of synchronization, as evaluated by the spectrum of the cross-correlogram envelope (see Materials and Methods), was also significantly higher when CRD was enhanced than when CRD was absent ($p < 0.02$; Wilcoxon rank-sum test; Fig. 10).

The stability of rhythmical synchronization of PGNs increases when CRD is enhanced

Time-evolving raster plots were used to investigate the temporal stability of the rhythmical synchronization in PGNs. The density of the striations on the raster plot, which are a measure of the stability of the phase relationship between two oscillators, were quantified by calculating the phase variation factor (see Materials and Methods for details).

When CRD was absent, raster plots of PGN→PGN activity displayed no obvious striations, indicating that no constant phase relationship existed between PGN firing activity, although occasionally transient phase-locked periods could be observed. A typical example is shown in Figure 11*A* (this is the same animal shown in Figs. 7, 8). Three transient phase-locked periods are indicated by arrowheads. In control conditions, raster plots of PGN→PGN activity revealed a higher probability of striation, although this was not apparent for many of the pairs recorded. The example in Figure 11*Bi* (from the animal in Figs. 7, 8) illustrates a raster plot with no evidence of a striated appearance. By contrast, time-evolving raster plots of PN→PGN activity revealed some striations, indicative of a relatively constant phase

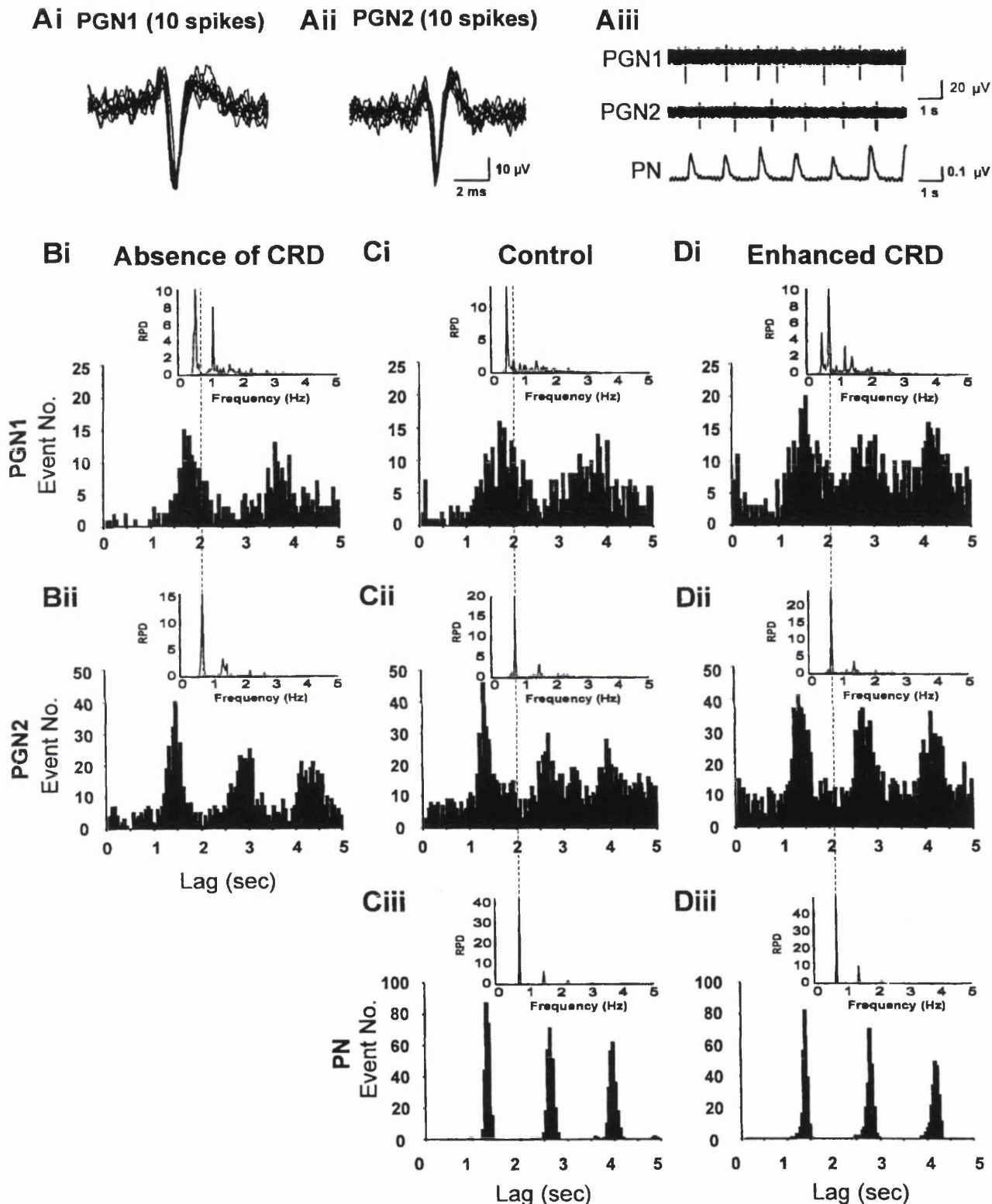


Figure 7. Neurograms and frequency relationships of two PGNs and PN activity recorded simultaneously in an artificially ventilated animal under three conditions of CRD. *Ai, Aii*, Ten superimposed spikes recorded from the PGNs demonstrate the consistency of the shape and amplitude of the action potentials. *Aiii*, Typical example of a real time neurogram showing the temporal relationship between PGN and PN activity under control conditions. *B–D*, The autocorrelograms and the spectra of the autocorrelogram envelopes (*insets*) of the PGN and PN activity. The envelope spectra, displayed as frequency versus RPD, were used to assess the frequency of the T-rhythm (see Materials and Methods). The *dashed lines* across the spectra allow comparisons between the frequencies of the T-rhythms and PN activity. *B*, Absence of CRD. *Bi*, PGN1 autocorrelogram (167 triggers) and spectrum. *Bii*, PGN2 autocorrelogram (252 triggers) and spectrum. *C*, Control condition. *Ci*, PGN1 autocorrelogram (199 triggers) and spectrum. *Cii*, PGN2 autocorrelogram (298 triggers) and spectrum. *Ciii*, PN autocorrelogram (227 triggers) and spectrum. *D*, Enhanced CRD. *Di*, PGN1 autocorrelogram (235 triggers) and spectrum. *Dii*, PGN2 autocorrelogram (324 triggers) and spectrum. *Diii*, PN autocorrelogram (215 triggers) and spectrum.

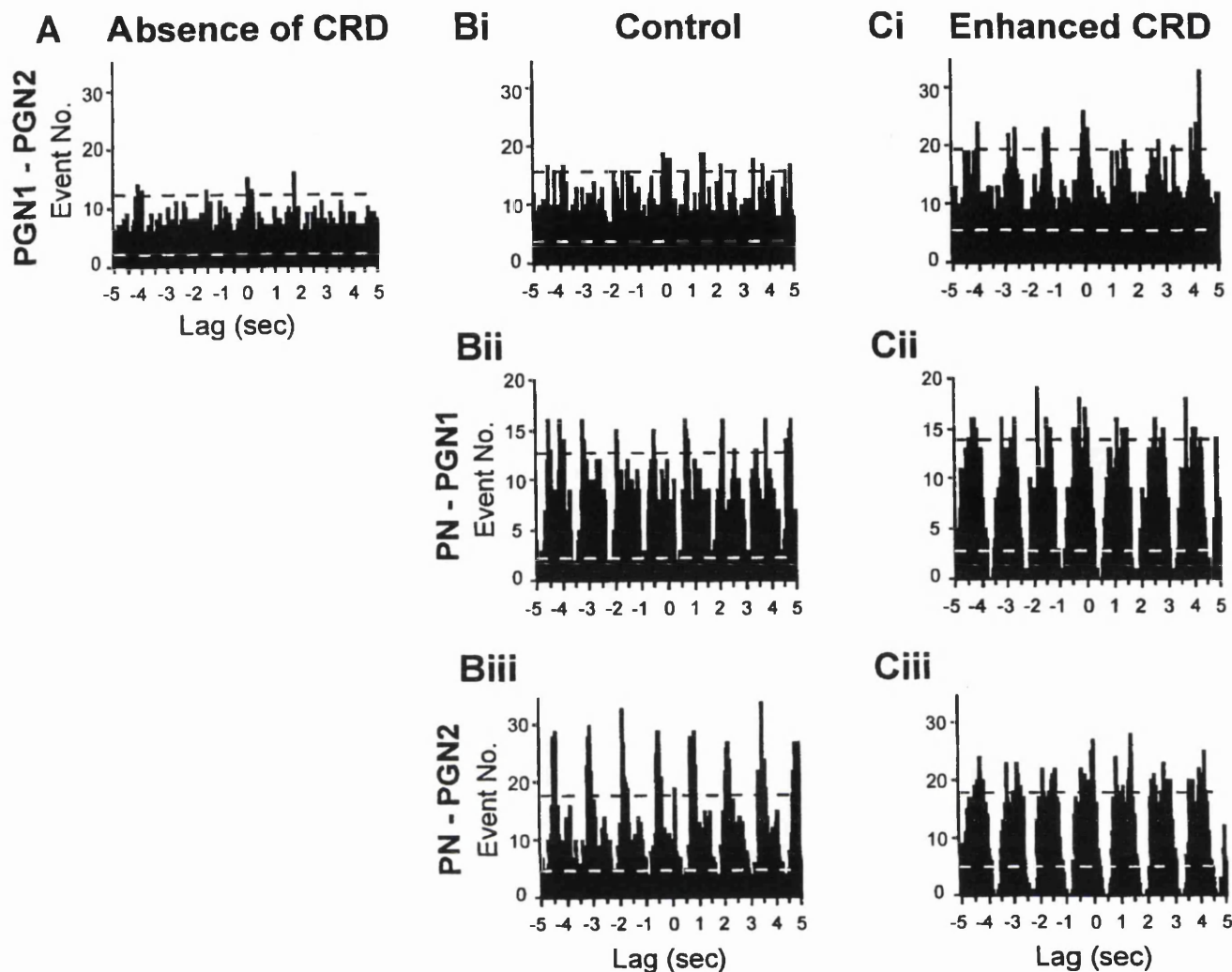


Figure 8. Rhythmic PGN→PGN and PN→PGN synchronization revealed by cross-correlograms under three conditions of CRD. The PGNs and the period of analysis are the same as in Figure 7. If rhythmic synchronization exists between two neural activities, a periodic pattern should be observed in the cross-correlogram. The dashed lines in the cross-correlograms define the upper and lower limits of the 95% confidence interval. In this study, we were interested in the significance of correlation only when there was a periodic pattern in the cross-correlogram because uncorrelated activities may occasionally exceed the confidence interval by chance (see Materials and Methods). *A*, Absence of CRD. PGN1→PGN2 cross-correlogram, no rhythmic synchronization was present in the absence of the CRD. *B*, Control condition. *Bi*, PGN1→PGN2 cross-correlogram, no rhythmic synchronization was present. *Bii*, PN→PGN1 cross-correlogram and *Biii*, PN→PGN2 cross-correlogram show that significant rhythmic synchronization was present. *C*, Enhanced CRD. *Ci*, PGN1→PGN2 cross-correlogram, a significant periodic pattern appeared in the cross-correlogram, indicating rhythmic synchronization. *Cii*, PN→PGN1 cross-correlogram and *Ciii*, PN→PGN2 cross-correlogram show that the rhythmic synchronization between PGNs and PN are prominent.

difference during these periods. In the typical examples shown in Figure 11, *Bii* and *Biii*, there are also periods of asynchrony (Fig. 11*Bii*, arrowhead) and changes in the phase difference (Fig. 11*Biii*, arrow), suggesting that the entrainment to CRD is relatively dynamic. In conditions of enhanced CRD, the PGN→PGN raster plots of the PGN pairs showed some clear periods of striation, but also periods in which a constant phase difference between the PGN activities was not so apparent. The example shown in Figure 11*Ci* (from the animal in Figs. 7, 8) shows obvious striations (Fig. 11*Ci*, period between arrows), suggesting periods of strong phase locking, preceded and followed by periods in which the synchronization is not so strong. The majority of PN→PGN raster plots in enhanced CRD conditions showed dense striations indicative of a constant phase relationship (Fig. 11*Cii*, *Ciii*). There was little evidence of phase hopping, suggesting that the entrainment by CRD was strong.

Comparison of the phase variation factor for PGN→PGN raster plots is shown in Figure 12. The data illustrates that the phase variance is significantly lower in the condition of enhanced CRD versus absence of CRD ($p < 0.02$; Wilcoxon rank-sum test).

Paired recordings of PGNs innervating the CVA in spontaneously breathing animals

Six pairs of PGNs were recorded from five spontaneously breathing animals under control conditions. Of the 12 PGNs recorded, only one unit did not show rhythmic discharges. The median frequency of the T-rhythm in the remainder was 0.67 Hz (interquartile interval, 0.5–0.8 Hz). One pair (8%) were synchronized and also showed 1:1 phase locking with the CRD (median frequency, 0.91 Hz; interquartile interval, 0.85–0.98 Hz).

Four pairs of PGNs were recorded from four animals in conditions of enhanced CRD. Rhythmic discharges were found in

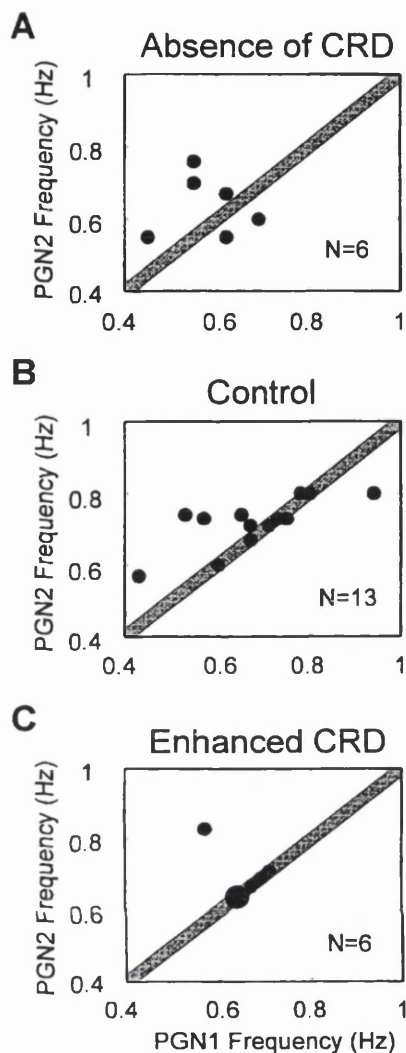


Figure 9. Summary scatter plots showing T-rhythm frequencies of pairs of postganglionic neurons (PGN1 and PGN2) in three conditions of CRD. The shaded diagonal bands indicate where the T-rhythm of both PGNs have frequency differences < 0.02 Hz and by definition are considered to have the same frequency (see Materials and Methods). *A*, Absence of CRD. Zero of six pairs of PGNs had the same frequency. *B*, Control condition. Seven of 13 pairs of PGNs (54%) had the same frequency. *C*, Enhanced CRD. Five of six pairs of PGNs (83%, two pairs were superimposed as indicated by the circle) had the same frequency.

all the PGNs (T-rhythm median frequency, 0.68 Hz; interquartile interval, 0.64–0.71 Hz), and significant PGN→PGN synchronization was found in three (75%) of the pairs. All these PGNs were synchronized with CRD (median frequency, 0.92 Hz; interquartile interval, 0.71–1.18 Hz).

The data presented here indicate that the rhythmical firing behavior in PGNs of spontaneously breathing animals is consistent with the findings from the artificially ventilated preparations.

The mean discharge rate of PGNs does not significantly change with increases in CRD

The discharge rate of the PGNs in each of the groups was calculated to test the hypothesis that entrainment of PGNs might be accompanied by changes in their excitability. Because the mean discharge rate of single PGNs was highly variable, the median values with the range for each group are presented.

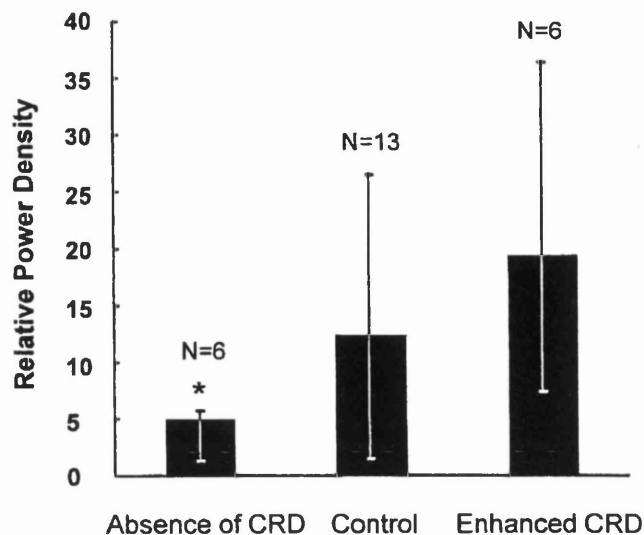


Figure 10. Degree of rhythmical PGN→PGN synchronization in artificially ventilated animals under three conditions of CRD evaluated by the relative power density of the spectrum of the cross-correlogram envelope (see Materials and Methods). Data are presented as median and first and third quartiles. The level of relative power density is proportional to the level of rhythmicity. The asterisk indicates that the relative power density in conditions of enhanced CRD is significantly higher compared to that when CRD is absent (Wilcoxon rank-sum test; $p < 0.02$).

Paired Wilcoxon signed-rank tests were used for statistical comparisons. In artificially ventilated rats, the median discharge rate of PGNs was 0.88 Hz in the absence of CRD ($n = 12$; range, 0.42–1.33 Hz), 1.37 Hz in control ($n = 26$; range, 0.51–4.19 Hz), and 0.91 Hz in conditions of enhanced CRD ($n = 12$; range, 0.51–2.0 Hz). Paired statistical comparisons showed that the discharge rates were not significantly different between pairs in the absence of CRD versus conditions of enhanced CRD ($p = 0.41$; paired Wilcoxon signed-rank test; $n = 10$).

In spontaneously breathing rats, the median discharge rate of PGNs was 1.15 Hz in control conditions ($n = 12$; range, 0.48–2.5 Hz) and 1.04 Hz in conditions of enhanced CRD ($n = 8$; range, 0.49–3.18 Hz). A statistical analysis between pairs recorded in control and conditions of enhanced CRD revealed that the discharge rates were not significantly different ($p = 0.14$; paired Wilcoxon signed-rank test; $n = 4$).

DISCUSSION

In this study we have demonstrated that the activities of PGNs making up the population innervating an artery, the CVA, are capable of dynamic synchronization. Our experimental evidence suggests that this is achieved by synchronization of multiple (T-rhythm) oscillators through entrainment by CRD. This conclusion is reached on the basis of a number of key observations. First, sympathetic activity supplying the tail, recorded from the VCN, showed a more prominent rhythmical component when CRD was enhanced than that seen when CRD was absent. Second, simultaneous recordings from pairs of CVA PGNs demonstrated that their T-rhythm frequencies could be different, and their activity was not necessarily synchronous. This indicates that the discharges of PGNs are driven by multiple T-rhythm oscillators. Although the primary source of this oscillatory activity has not yet been established, recent work from our laboratory has provided evidence to indicate that the T-rhythm may be gener-

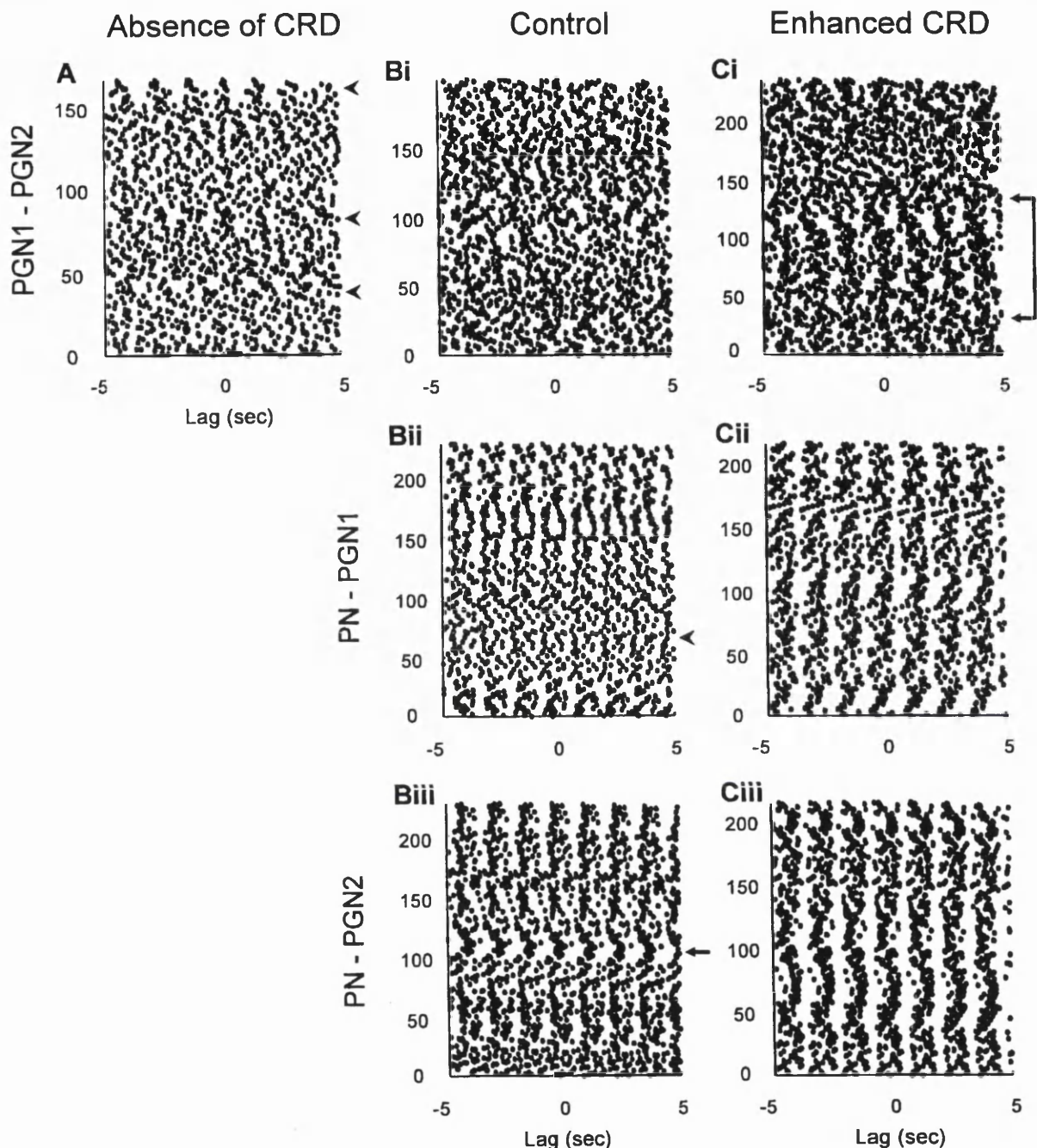


Figure 11. Dynamic change of rhythmic PGN→PGN and PN→PGN synchronization evaluated by the correlation raster plot under three conditions of CRD. The two PGNs and the period of analysis are the same as those in Figures 7 and 8. If the phase difference between two activities is relatively constant across time, a vertical striation will be observed in the raster plot. *A*, Absence of CRD: no definite pattern is present in the PGN1→PGN2 raster plot, although transient phase-locked periods can be observed (arrowheads). *B*, Control condition. *Bi*, PGN1→PGN2: the phase difference of the two units varies across time. *Bii*, PN→PGN1 and *Biii*, PN→PGN2, in some parts during data collection, the PGNs are synchronized with PN but periods of asynchrony (*Bii*, arrowhead) or changes of the phase difference (*Biii*, arrow) are also observed. *C*, Enhanced CRD. *Ci*, PGN1→PGN2: although phase drifting is still apparent (as in the absence of CRD and in control), there are also periods of rhythmic synchronization indicated by vertical striations (between arrows). *Cii*, PN→PGN1 and *Ciii*, PN→PGN2: rhythmic synchronization between the PN and PGNs is more apparent across time than previously.

ated in the CNS (Smith and Gilbey, 1998b). However, at present we do not rule out the possibility that the sympathetic ganglia could play an important role in both the generation and modulation of the rhythmic outflow. Third, studies of the degree of synchronization between two PGNs under the conditions of different CRD revealed that in the absence of CRD, PGN→PGN

rhythmic discharges were uncorrelated (i.e., asynchronous), whereas when CRD was enhanced there was a high probability of synchronization. This change in the level of synchronization was not accompanied by a significant change in the discharge rate of PGNs. We also demonstrated that the temporal interaction between these oscillators is not static at a particular level of CRD,

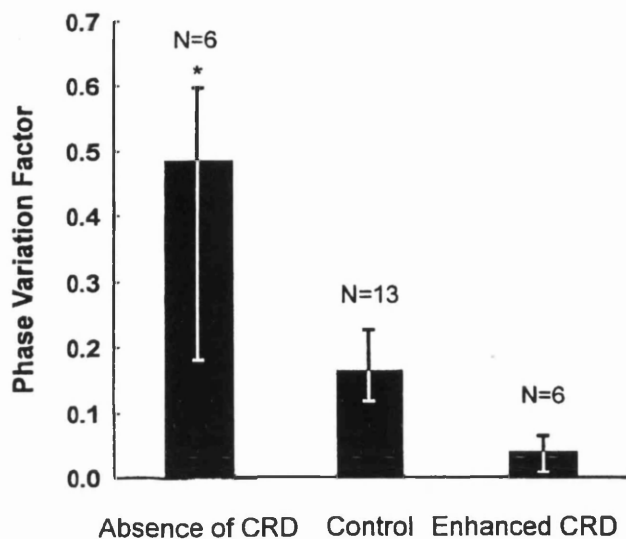


Figure 12. Dynamic stability of rhythmical synchronization between PGNs evaluated by the phase variation factor (see Materials and Methods) in artificially ventilated animals under three conditions of CRD. Data are presented as medians and first and third quartiles. The level of phase variation factor is inversely proportional to the level of stability. The asterisk indicates that the phase variation factor in the absence of CRD is significantly higher than in conditions of enhanced CRD (Wilcoxon rank-sum test; $p < 0.02$).

because PGN→PGN and PN→PGN synchronization was observed to undergo considerable dynamic variation. In the absence of CRD, although there was no PGN→PGN rhythmical correlation, there were transient phase-locked periods revealed by the raster plots. The high level of this dynamic variation was also reflected in the marked power density variation in the VCN autospectrum. By contrast, when CRD was enhanced, PGN→PGN rhythmical correlation was strong, as reflected in the rhythmicity of cross-correlograms and the frequently observable vertical striated patterns in the raster plots. This strong entrainment by CRD was also indicated by a reduced variation of power density across time in the VCN autospectrum. Thus, CRD appears to minimize the fluctuation of phase difference between PGN discharges and stabilize the frequencies of the T-rhythm oscillators.

We propose that the principle of dynamic synchronization revealed at the single neuron level in this study may also operate at the whole-nerve level of the sympathetic nervous system. In fact, this is indicated in a series of experiments by Gebber and colleagues (Gebber, 1980; Gebber et al., 1994a,b; Zhong et al., 1997) in which analysis of whole-nerve activity revealed that activity of different nerves may be driven by separate oscillators capable of coupling. They demonstrated that the coherence between the activities of different nerves was found to vary between experiments. This observation is consistent with the observed dynamic coupling seen in the results from the present study.

We hypothesize here that dynamic coupling may reveal one important mechanism whereby appropriate patterns of sympathetically mediated cardiovascular response are effected that support, for example, complex behaviors. Indeed dynamic coupling in sympathetic control may be regarded as an extension of the idea of “binding” (Farmer, 1998) into the dimension of autonomic control, and this is considered further below.

Differences between population and PGN→PGN activity profiles

The dual approach of examining correlations both in whole-nerve (VCN) activity and in PGN→PGN activity allowed us to explore the relationship between the activity profile of a neuronal population and its individual components. Importantly, our comparisons indicate that the emergent properties of multiunit activity can be different from those that would be predicted from PGN→PGN relationships.

One apparently paradoxical observation was that in the absence of CRD, although the autospectra of VCN activity revealed a rhythmical component suggesting that some of the rhythmical discharges of PGNs were synchronized (Fig. 4*Ai*), no significant PGN→PGN rhythmical synchronization was observed (Fig. 8*A*). This paradox can be explained, however, as the autospectrum of a population composed of many weakly coupled or uncoupled oscillators with similar frequencies can still have a peak in the frequency range of its constituents. The power density around the peak depends on the number of units in the population, the strength of correlation between units, and the distribution of phase difference (Christakos, 1986, 1994).

The findings of the present study showing that separate oscillators driving the discharges of PGNs innervating the same target organ can be asynchronized provide an explanation for the frequently observed broad, rather than sharp, configuration of whole sympathetic nerve activity autospectra (Kocsis et al., 1990; Gootman et al., 1991; Allen et al., 1993). Consequently, it is no longer necessary to question whether the rhythm seen in sympathetic nerves arises from a well defined biological oscillator in view of its seemingly aperiodic nature (Bachoo and Polosa, 1987). Based on the observations reported in this paper, we suggest that the aperiodic or quasiperiodic nature of whole-nerve activity may be explained through dynamic synchronization of multiple sympathetic oscillators with “free-run” frequencies that may not be exactly the same.

Functional significance of synchronization of sympathetic activity

Our observations on synchrony in conjunction with those of others (Vallbo et al., 1979; McAllen and Malpas, 1997) can be viewed from at least two perspectives when considering possible functional implications. First, the dynamic synchrony observed in a functionally defined population of PGNs may be a manifestation of neural processes that provide the necessary plasticity that enables the nervous system to generate appropriate patterns of sympathetic response to support various behaviors. Second, synchrony may have important consequences for neuroeffector transmission and the end organ response.

With regard to synchrony and central processing, previous work has indicated that synchronous (bursty) sympathetic activity may be related to, for example, cardiac and respiratory rhythms (Adrian et al., 1932), intermittent isometric exercise (Victor et al., 1995), and in pathological conditions, epileptiform discharges (Lathers et al., 1987). Such synchrony may be purely caused by imposition of other oscillating activities on the sympathetic nervous system, “irradiation” (Koeppen et al., 1981). However, the results of the present study support the view that synchrony of sympathetic discharge may sometimes indicate coupling of multiple oscillators. If this is the case, our observations are consistent with the idea that the nervous system may use oscillatory neural activity to bind together various pools of neurons to produce patterned sympathetic responses: different combinations of neu-

rons being bound according to the required autonomic response. Furthermore, our results suggest that under some conditions, for example when the CRD is enhanced, the sympathetic and respiratory networks may bind together through correlated firing to form a highly coordinated network. It has been proposed that such binding is particularly easily achieved in oscillating networks (Singer, 1993; Farmer, 1998). The concept of binding is not a novel one and has been promoted by sensory physiologists for a number of years and recently in relation to skeletal muscle motor control (Farmer, 1998). Although the synchronization of single PGNs controlling other cardiovascular targets has not been examined, the dynamic coupling of multiple oscillators reported in this study probably applies to other targets because robust rhythmicity and phenomena suggesting entrainment have been reported in a number of studies, in several different species, in which multiunit sympathetic activity has been recorded (e.g., cat, Taylor and Gebber, 1975; dog, Camerer et al., 1977; and goat, Toda et al., 1996). For example, Gebber and colleagues (Gebber, 1980; Zhong et al., 1997) have proposed, on the basis of correlation studies, that sympathetic oscillators driving sympathetic activity to a variety of sympathetic nerves may be entrained by phasic input from arterial baroreceptors and CRD.

Concerning the idea of synchrony and neuroeffector transmission, enhanced sympathetic synchrony (burst discharges) has been reported in humans under conditions of stress (Callister et al., 1992; Nordin and Fagius, 1995; Morgan et al., 1996; Katragadda et al., 1997), and it has been proposed that the bursts of sympathetic activity may have important consequences for neuroeffector transmission and therefore the end organ response (Sneddon and Burnstock, 1984; Sjöblom-Widfelt et al., 1990). We propose that synchrony may bring about widespread depolarization of electrotonically coupled smooth muscle in blood vessels via ATP released from sympathetic nerve endings (Morris and Gibbins, 1992). This will lead to fast depolarizations via ligand-gated ion channels (North and Barnard, 1997) and consequent vascular constriction. Thus, enhanced synchronization under conditions of stress will result in a relatively rapid increase of vascular resistance and redistribution of blood flow.

In conclusion, the concept of synchrony as an encoding mechanism in nervous control is an emerging principle from a variety of studies. Importantly, our work is the first to demonstrate dynamic synchrony at the single neuron level in the sympathetic (peripheral) nervous system. We suggest that in addition to discharge frequency, the dynamic synchrony observed in this study may indicate another important encoding parameter in the sympathetic nervous control of the cardiovascular system.

REFERENCES

- Adrian ED, Bonk DW, Phillips G (1932) Discharges in the mammalian sympathetic nerves. *J Physiol (Lond)* 74:115-133.
- Allen AM, Adams JM, Guyenet PG (1993) Role of the spinal cord in generating the 2- to 6-Hz rhythm in rat sympathetic outflow. *Am J Physiol* 264:R938-R945.
- Bachoo M, Polosa C (1987) Lack of evidence of coupled oscillator mechanisms in the generation of sympathetic rhythms. In: *Organization of the autonomic nervous system—central and peripheral mechanisms* (Ciriello J, Calaresu FR, Renaud LP, Polosa C eds), pp 189-202. New York: Alan R. Liss.
- Bendat JS, Piersol AG (1986) *Random data: analysis and measurement procedures*. New York: Wiley.
- Callister R, Suwarno NO, Seals DR (1992) Sympathetic activity is influenced by task difficulty and stress perception during mental challenge in humans. *J Physiol (Lond)* 454:373-387.
- Camerer H, Stroh WM, Krienke B, Langhorst P (1977) Postganglionic sympathetic activity with correlation to heart rhythm and central cortical rhythms. *Pflügers Arch* 370:221-225.
- Chang H-S, Gilbey MP (1998) Rhythmic sympathetic activity recorded from the ventral collector nerve (VCN) innervating the rat tail. *J Physiol (Lond)* 506P:134P.
- Chang H-S, Smith JE, Staras K, Cotsell B, Gilbey MP (1998a) Multiple "oscillators" and the discharges of sympathetic neurons innervating the rat caudal ventral artery. *FASEB J* 12:A985.
- Chang H-S, Smith JE, Staras K, Gilbey MP (1998b) Synchronous and asynchronous rhythmic discharges of postganglionic sympathetic neurons innervating an identified blood vessel in the rat. *J Physiol (Lond)* 509P:123P-124P.
- Christakos CN (1986) The mathematical basis of population rhythms in nervous and neuromuscular systems. *Int J Neurosci* 29:103-107.
- Christakos CN (1994) Analysis of synchrony (correlations) in neural populations by means of unit-to-aggregate coherence computations. *Neuroscience* 58:43-57.
- Czyzyk-Krzaska MF, Trzebski A (1990) Respiratory-related discharge pattern of sympathetic nerve activity in the spontaneously hypertensive rat. *J Physiol (Lond)* 426:355-368.
- Farmer SF (1998) Rhythmicity, synchronization and binding in human and primate motor systems. *J Physiol (Lond)* 509:3-14.
- Fetz EE (1997) Temporal coding in neural populations? *Science* 278:1901-1902.
- Gebber GL (1980) Central oscillators responsible for sympathetic nerve discharge. *Am J Physiol* 239:H143-H155.
- Gebber GL, Zhong S, Barman SM, Paitel Y, Orer HS (1994a) Differential relationships among the 10-Hz rhythmic discharges of sympathetic nerves with different targets. *Am J Physiol* 267:R387-R399.
- Gebber GL, Zhong S, Barman SM, Orer HS (1994b) Co-ordination of the cardiac-related discharges of sympathetic nerves with different targets. *Am J Physiol* 267:R400-R407.
- Gootman PM, Gandhi MR, Steele AM, Hundley BW, Cohen HL, Eberle LP, Sica AL (1991) Respiratory modulation of sympathetic activity in neonatal swine. *Am J Physiol* 261:R1147-R1154.
- Haselton JR, Guyenet PG (1989) Central respiratory modulation of medullary sympathoexcitatory neurons in rat. *J Am Physiol* 256:R739-R750.
- Johnson CD, Gilbey MP (1994) Sympathetic activity recorded from the rat caudal ventral artery *in vivo*. *J Physiol (Lond)* 476:437-442.
- Johnson CD, Gilbey MP (1996) On the dominant rhythm in the discharges of single postganglionic sympathetic neurons innervating the rat tail artery. *J Physiol (Lond)* 497:241-259.
- Katragadda S, Xie A, Puleo D, Skatrud JB, Morgan BJ (1997) Neural mechanism of the pressor response to obstructive and nonobstructive apnea. *J Appl Physiol* 83:2048-2054.
- Kenney MJ, Fedde MR (1994) Influence of different preamplifier band-pass cutoff frequencies on the basic pattern of sympathetic nerve discharge. *Biomed Sci Instrum* 30:111-116.
- Kocsis B, Gebber GL, Barman SM, Kenney MJ (1990) Relationships between activity of sympathetic nerve pairs: phase and coherence. *Am J Physiol* 259:R549-R560.
- Koepchen HP, Klüssendorf D, Sommer D (1981) Neurophysiological background of central neural cardiovascular-respiratory coordination: basic remarks and experimental approach. *J Auton Nerv Syst* 3:335-368.
- Koopmans LH (1995) *The spectral analysis of time series*. London: Academic.
- Lathers CM, Schraeder PL, Weiner FL (1987) Synchronization of cardiac autonomic neural discharge with epileptogenic activity: the lock-step phenomenon. *Electroencephalogr Clin Neurophysiol* 67:247-259.
- Marder E, Calabrese L (1996) Principles of rhythmic motor pattern generation. *Physiol Rev* 76:687-717.
- McAllen RM, Malpas SC (1997) Sympathetic burst activity: characteristics and significance. *Clin Exp Pharmacol Physiol* 24:791-799.
- Morgan BJ, Crabtree DC, Puleo DS, Badr MS, Toiber F, Skatrud JB (1996) Neurocirculatory consequences of abrupt change in sleep state in humans. *J Appl Physiol* 80:1627-1636.
- Morris JL, Gibbins IL (1992) Co-transmission and neuromodulation. In: *Autonomic neuroeffector mechanisms* (Burnstock G, Hoyle CHV eds), pp 33-119. Switzerland: Harwood Academic.
- Nordin M, Fagius J (1995) Effect of noxious stimulation on sympathetic

- vasoconstrictor outflow to human muscles. *J Physiol (Lond)* 489:885-894.
- North RA, Barnard EA (1997) Nucleotide receptors. *Curr Opin Neurobiol* 7:346-357.
- Perkel DH, Gerstein GL, Moore GP (1967a) Neuronal spike trains and stochastic point processes. I. The single spike train. *Biophys J* 7:391-418.
- Perkel DH, Gerstein GL, Moore GP (1967b) Neuronal spike trains and stochastic point processes. II. Simultaneous spike trains. *Biophys J* 7:419-440.
- Papoulis A (1991) Probability, random variables, and stochastic processes. Singapore: McGraw-Hill.
- Selverston AI, Moulins M (1985) Oscillatory neural networks. *Annu Rev Physiol* 47:29-48.
- Singer W (1993) Synchronization of cortical activity and its putative role in information processing and learning. *Annu Rev Physiol* 55:349-374.
- Sittiracha T, McLachlan EM, Bell C (1987) The innervation of the caudal artery of the rat. *Neuroscience* 21:647-659.
- Sjöblom-Widfelt N, Gustafsson H, Nilsson H (1990) Transmitter characteristics of small mesenteric arteries from the rat. *Acta Physiol Scand* 138:203-212.
- Smith JE, Jansen ASP, Gilbey MP, Loewy AD (1998) CNS cell groups projecting to sympathetic outflow of tail artery: neural circuits involved in heat loss in the rat. *Brain Res* 786:153-164.
- Smith JE, Gilbey MP (1998a) Segmental origin of sympathetic preganglionic neurones regulating the tail circulation in the rat. *J Auton Nerv Syst* 68:109-114.
- Smith JE, Gilbey MP (1998b) Rhythmical discharges in the sympathetic supply to the rat tail are of central origin. *J Physiol (Lond)* 513.P:81P.
- Sneddon P, Burnstock G (1984) ATP as a co-transmitter in rat tail artery. *Eur J Pharmacol* 106:149-152.
- St-John WM, Bianchi AL (1985) Responses of bulbospinal and laryngeal respiratory neurons to hypercapnia and hypoxia. *J Appl Physiol* 1201-1207.
- Taylor DG, Gebber GL (1975) Baroreceptor mechanisms controlling sympathetic nervous rhythms of central origin. *Am J Physiol* 228:1002-1003.
- Toda K, Tatsumi E, Taenaka Y, Masuzawa T, Takano H (1996) Sympathetic nerve activities in pulsatile and nonpulsatile systemic circulation in anaesthetized goats. *Am J Physiol* 271:H15-H22.
- Valbo AB, Hagbarth K-E, Torebjork HE, Wallin BG (1979) Somatosensory, proprioceptive, and sympathetic activity in human peripheral nerves. *Physiol Rev* 59:919-957.
- Victor RG, Secher NH, Lyson T, Mitchell JH (1995) Central command increases muscle sympathetic nerve activity during intense intermittent isometric exercise in humans. *Circ Res* 76:127-131.
- Winfrey AT (1980) The geometry of biological time. Berlin: Springer.
- Zhong S, Zhou S-Y, Gebber GL, Barman SM (1997) Coupled oscillators account for the slow rhythms in sympathetic nerve discharge and phrenic nerve activity. *Am J Physiol* 272:R1314-R1324.

Appendix XI

List of Abbreviations

BP: Blood pressure

CRD: Central respiratory drive

CVA: Caudal ventral artery

FFT: Fast Fourier transformation

f_{INT} : Intrinsic frequency

f_{LIC} : Frequency of lung inflation cycle-related activity

JPSP: Joint peri-stimulus scatter plot

LIC: Lung inflation cycle

MDR: Mean discharge rate

OCRP: Ordinary correlation raster plot

PGN: Postganglionic sympathetic neurone

PN: Phrenic nerve

RCRP: Reordered correlation raster plot

RPD: Relative power density

SNS: Sympathetic nervous system

TP: Tracheal pressure

TTL: Transistor to transistor logic

VCN: Ventral collector nerve

V_T : Tidal volume

REFERENCES

- ABELES, M. (1991). *Corticonics*. Cambridge, UK: Cambridge University Press.
- ADRIAN, E.D. & BRONK, D.W. (1932). Discharges in mammalian sympathetic nerves. *J. Physiol.* **74**, 115-133.
- AERTSEN, A.M. & GERSTEIN, G.L. (1985). Evaluation of neuronal connectivity: sensitivity of cross- correlation. *Brain Res.* **340**, 341-354.
- AERTSEN, A.M., GERSTEIN, G.L., HABIB, M.K. & PALM, G. (1989). Dynamics of neuronal firing correlation: modulation of "effective connectivity". *J. Neurophysiol.* **61**, 900-917.
- ALLEN, A.M., ADAMS, J.M. & GUYENET, P.G. (1993). Role of the spinal cord in generating the 2- to 6-Hz rhythm in rat sympathetic outflow. *Am. J. Physiol.* **264**, R938-45.
- ANDERSEN, P. (1960). Interhippocampal impulses II. Apical dendritic activation of CA1 neurons. *Acta Physiol. Scand.* **48**, 178-208.
- ANDERSSON, P.O. (1983). Comparative vascular effects of stimulation continuously and in bursts of the sympathetic nerves to cat skeletal muscle. *Acta Physiol. Scand.* **118**, 343-348.
- ASHTON, J.H. & CASSIDY, S.S. (1985). Reflex depression of cardiovascular function during lung inflation. *J. Appl. Physiol.* **58**, 137-145.
- AYERS, J.L. & SELVERSTON, A.I. (1979). Monosynaptic entrainment of an endogenous pacemaker network: a cellular mechanism for von Holst's magnet effect. *J. Comp. Physiol.* **129**, 5-17.
- BACHOO, M. & POLOSA, C. (1986). The pattern of sympathetic neurone activity during expiration in the cat. *J. Physiol.* **378**, 375-390.
- BACHOO, M. & POLOSA, C. (1987a). Lack of evidence of coupled oscillator mechanisms in the generation of sympathetic rhythms. In *Organization of the autonomic nervous system - Central and peripheral mechanisms* ,

eds. CIRIELLO, J., CALARESU, F.R., RENAUD, L.P. & POLOSA, C., pp. 189-202. New York: Alan R. Liss.

BACHOO, M. & POLOSA, C. (1987b). Properties of the inspiration-related activity of sympathetic preganglionic neurones of the cervical trunk in the cat. *J. Physiol.* **385**, 545-564.

BALKOWIEC, A., KUKULA, K. & SZULCZYK, P. (1995). Functional classification of afferent phrenic nerve fibres and diaphragmatic receptors in cats. *J. Physiol.* **483**, 759-768.

BARMAN, S.M. & GEBBER, G.L. (1976). Basis for synchronization of sympathetic and phrenic nerve discharges. *Am. J. Physiol.* **231**, 1601-1607.

BARMAN, S.M., GEBBER, G.L. & ZHONG, S. (1992). The 10-Hz rhythm in sympathetic nerve discharge. *Am. J. Physiol.* **262**, R1006-14.

BARMAN, S.M., ORER, H.S. & GEBBER, G.L. (1995). A 10-Hz rhythm reflects the organization of a brainstem network that specifically governs sympathetic nerve discharge. *Brain Res.* **671**, 345-350.

BENDAT, J.S. & PIERSOL, A.G. (1986). *Random data: analysis and measurement procedures*. New York: John Wiley & Son.

BLOOMFIELD, P. (1976). *Fourier analysis of time series: an introduction*. New York: John Wiley & Sons.

BOCZEK, F.A., HABLER, H.J., JÄNIG, W. & MICHAELIS, M. (1992). Respiratory modulation of the activity in sympathetic neurones supplying muscle, skin and pelvic organs in the cat. *J. Physiol.* **449**, 333-361.

BRAMBLE, D.M. & CARRIER, D.R. (1983). Running and breathing in mammals. *Science* **219**, 251-256.

BRILLINGER, D.R. (1976). Estimation of the second-order intensities of a bivariate stationary point process. *J. R. Stat. Soc.* **B38**, 60-66.

- BROCK, J.A. & CUNNANE, T.C. (1988). Electrical activity at the sympathetic neuroeffector junction in the guinea-pig vas deferens. *J. Physiol.* **399**, 607-632.
- BROCK, J.A. & CUNNANE, T.C. (1992). Electrophysiology of neuroeffector transmission in smooth muscle. In *Autonomic neuroeffector mechanisms*, eds. BURNSTOCK, G. & HOYLE, C.H.V., pp. 121-213. Switzerland: Harwood Academic.
- BRYANT, H.L., MARCOS, A.R. & SEGUNDO, J.P. (1973). Correlations of neuronal spike discharges produced by monosynaptic connections and by common inputs. *J. Neurophysiol.* **36**, 205-225.
- BULYGIN, I.A. (1983). A consideration of the general principles of organization of sympathetic ganglia. *J. Auton. Nerv. Syst.* **8**, 303-330.
- CALLISTER, R., SUWARNO, N.O. & SEALS, D.R. (1992). Sympathetic activity is influenced by task difficulty and stress perception during mental challenge in humans. *J. Physiol.* **454**, 373-387.
- CAMERER, H., STROH WERZ, M., KRIENKE, B. & LANGHORST, P. (1977). Postganglionic sympathetic activity with correlation to heart rhythm and central cortical rhythms. *Pflugers Arch.* **370**, 221-225.
- CHADWICK, D., HALLETT, M., JENNER, P. & MARSDEN, C.D. (1980). Observations on chloralose-induced myoclonus in guinea-pigs. *Br. J. Pharmacol.* **69**, 535-540.
- CHANG, H.-S., STARAS, K., SMITH, J.E. & GILBEY, M.P. (1999). Sympathetic neuronal oscillators are capable of dynamic synchronization. *J. Neurosci.* **19**, 3183-3197.
- CHENG, E.Y., KAY, J., HOKA, S., BOSNJAK, Z.J., COON, R.L., SEAGARD, J.L. & KAMPINE, J. (1989). Influence of lung inflation reflex on vascular capacitance in the systemic circulation. *Am. J. Physiol.* **257**, R1004-R1011
- CHEUNG, D.W. (1982). Spontaneous and evoked excitatory junction potentials in rat tail arteries. *J. Physiol.* **328**, 449-459.

- CHRIST, G.J., SPRAY, D.C., EL-SABBAN, M., MOORE, L.K. & BRINK, P.R. (1996). Gap junctions in vascular tissues: Evaluating the role of intercellular communication in the modulation of vasomotor tone. *Circ. Res.* **79**, 631-646.
- CHRISTAKOS, C.N. (1986). The mathematical basis of population rhythms in nervous and neuromuscular systems. *Int. J. Neurosci.* **29**, 103-107.
- CHRISTAKOS, C.N. (1994). Analysis of synchrony (correlations) in neural populations by means of unit-to-aggregate coherence computations. *Neuroscience* **58**, 43-57.
- CLARK, F.J. & VON-EULER, C. (1972). On the regulation of depth and rate of breathing. *J. Physiol.* **222**, 267-295.
- COHEN, M.I. & GOOTMAN, P.M. (1970). Periodicities in efferent discharge of splanchnic nerve of the cat. *Am. J. Physiol.* **218**, 1092-1101.
- COHEN, M.I., YU, Q. & HUANG, W.X. (1995). Preferential correlations of a medullary neuron's activity to different sympathetic outflows as revealed by partial coherence analysis. *J. Neurophysiol.* **74**, 474-478.
- CONNELLY, C.A. & WURSTER, R.D. (1985). Sympathetic rhythms during hyperventilation-induced apnea. *Am. J. Physiol.* **249**, R424-R431
- COOTE, J.H. (1988). The organisation of cardiovascular neurons in the spinal cord. *Rev. Physiol. Biochem. Pharmacol.* **110**, 147-285.
- CREAGER, R., DUNWIDDIE, T. & LYNCH, G. (1980). Paired-pulse and frequency facilitation in the CA1 region of the in vitro rat hippocampus. *J. Physiol.* **299**, 409-424.
- CRICK, F. (1994). *The astonishing hypothesis*. London: Simon & Schuster.
- CRITCHLOW, V. & VON EULER, C. (1963). Intercostal muscle spindle activity and its r-motor control. *J. Physiol.* **168**, 820-847.
- CZYZYK-KRZESKA, M.F. & TRZEBSKI, A. (1990). Respiratory-related discharge pattern of sympathetic nerve activity in the spontaneously hypertensive rat. *J. Physiol.* **426**, 355-368.

- DALY, M.D., HAZZLEDINE, J.L. & UNGAR, A. (1967). The reflex effects of alterations in lung volume on systemic vascular resistance in the dog. *J. Physiol.* **188**, 331-351.
- DALY, M.D. & ROBINSON, B.H. (1968). An analysis of the reflex systemic vasodilator response elicited by lung inflation in the dog. *J. Physiol.* **195**, 387-406.
- DALY, M.D.B. (1985). Interactions between respiration and circulation. In *Handbook of Physiology, Section 3, The respiratory system, Volume III, Part II.* eds. CHERNIACK, N.S. & WIDDICOMBE, J.G., pp. 529-594. Bethesda: American Physiological Society.
- DAMPNEY, R.A. (1994). Functional organization of central pathways regulating the cardiovascular system. *Physiol. Rev.* **74**, 323-364.
- DE TROYER, A. (1996). Rib motion modulates inspiratory intercostal activity in dogs. *J. Physiol.* **492**, 265-275.
- DECHARMS, R.C. & MERZENICH, M.M. (1996). Primary cortical representation of sounds by the coordination of action-potential timing. *Nature* **381**, 610-613.
- DEMBOWSKY, K., CZACHURSKI, J. & SELLER, H. (1985). An intracellular study of the synaptic input to sympathetic preganglionic neurones of the third thoracic segment of the cat. *J. Auton. Nerv. Syst.* **13**, 201-244.
- DODGE, J.T., BEVAN, R.D. & BEVAN, J.A. (1994). Comparison of density of sympathetic varicosities and their closeness to smooth muscle cells in rabbit middle cerebral and ear arteries and their branches. *Circ. Res.* **75**, 916-925.
- ENGEL, A.K., ROELFSEMA, P.R., FRIES, P., BRECHT, M. & SINGER, W. (1997). Role of the temporal domain for response selection and perceptual binding. *Cereb. Cortex* **7**, 571-582.
- ERMENTROUT, G.B. & RINZEL, J. (1984). Beyond a pacemaker's entrainment limit: Phase walk-through. *Am. J. Physiol.* **246**, R102-R106.

- FARMER, S.F. (1998). Rhythmicity, synchronization and binding in human and primate motor systems. *J. Physiol.* **509**, 3-14.
- FARMER, S.F., HALLIDAY, D.M., CONWAY, B.A., STEPHENS, J.A. & ROSENBERG, J.R. (1997). A review of recent applications of cross-correlation methodologies to human motor unit recording. *J. Neurosci. Methods* **74**, 175-187.
- FETZ, E.E. (1997). Temporal coding in neural populations? *Science* **278**, 1901-1902.
- FUKUDA, Y., SATO, A., SUZUKI, A. & TRZEBSKI, A. (1989). Autonomic nerve and cardiovascular responses to changing blood oxygen and carbon dioxide levels in the rat. *J. Auton. Nerv. Syst.* **28**, 61-74.
- GALPERIN, A. & TANK, D.W. (1990). Odour-modulated collective network oscillations of olfactory interneurons in a terrestrial mollusc. *Nature* **345**, 437-440.
- GATH, I. (1974). Analysis of point process signals applied to motor unit firing patterns. I. Superposition of independent spike trains. *Math. Biosci.* **22**, 211-222.
- GAULTIER, C. & MORTOLA, J.P. (1981). Hering-Breuer inflation reflex in young and adult mammals. *Can. J. Physiol. Pharmacol.* **59**, 1017-1021.
- GEBBER, G.L. (1980). Central oscillators responsible for sympathetic nerve discharge. *Am. J. Physiol.* **239**, H143-55.
- GEBBER, G.L. & BARMAN, S.M. (1980). Rhythmogenesis in the sympathetic nervous system. *Fed. Proc.* **39**, 2526-2530.
- GEBBER, G.L. & BARMAN, S.M. (1981). Sympathetic-related activity of brain stem neurons in baroreceptor-denervated cats. *Am. J. Physiol.* **240**, R348-R355
- GEBBER, G.L., BARMAN, S.M. & KOCSIS, B. (1990). Coherence of medullary unit activity and sympathetic nerve discharge. *Am. J. Physiol.* **259**, R561-71.

- GEBBER, G.L., ZHONG, S. & BARMAN, S.M. (1995a). Synchronization of cardiac-related discharges of sympathetic nerves with inputs from widely separated spinal segments. *Am. J. Physiol.* **268**, R1472-83.
- GEBBER, G.L., ZHONG, S. & BARMAN, S.M. (1995b). The functional significance of the 10-Hz sympathetic rhythm: a hypothesis. *Clin. Exp. Hypertens.* **17**, 181-195.
- GEBBER, G.L., ZHONG, S., BARMAN, S.M. & ORER, H.S. (1994a). Coordination of the cardiac-related discharges of sympathetic nerves with different targets. *Am. J. Physiol.* **267**, R400-R407
- GEBBER, G.L., ZHONG, S., BARMAN, S.M., PAITEL, Y. & ORER, H.S. (1994b). Differential relationships among the 10-Hz rhythmic discharges of sympathetic nerves with different targets. *Am. J. Physiol.* **267**, R387-99.
- GEBBER, G.L., ZHONG, S., ZHOU, S.Y. & BARMAN, S.M. (1997). Nonlinear dynamics of the frequency locking of baroreceptor and sympathetic rhythms. *Am. J. Physiol.* **273**, R1932-45.
- GERBER, U. & POLOSA, C. (1978). Effects of pulmonary stretch receptor afferent stimulation on sympathetic preganglionic neuron firing. *Can. J. Physiol. Pharmacol.* **56**, 191-198.
- GERSTEIN, G.L. & KIANG, N.Y.S. (1960). An approach to the quantitative analysis of electrophysiological data from single neurons. *Biophys. J.* **1**, 15-28.
- GERSTEIN, G.L. & PERKEL, D.H. (1969). Simultaneously recorded trains of action potentials: analysis and functional interpretation. *Science* **164**, 828-830.
- GILBEY, M.P. & SPYER, K.M. (1997). Cardiorespiratory regulation. In *Neural control of the respiratory muscles*, eds. MILLER, A.D., BIANCHI, A.L. & BISHOP, B.P., pp. 259-269. New York: CRC press.

- GLASS, L., GRAVES, C., PETRILLO, G.A. & MACKEY, M.C. (1980). Unstable dynamics of a periodically driven oscillator in the presence of noise. *J. Theor. Biol.* **86**, 455-475.
- GLASS, L. & GUEVARA, M.R. (1981). Phase locking, period-doubling bifurcations, and irregular dynamics in periodically stimulated cardiac cells. *Science* **214**, 1350-1353.
- GLASS, L., GUEVARA, M.R., BELAIR, J. & SHRIER, A. (1984). Global bifurcations of a periodically forced biological oscillator. *Phys. Rev. A* **29**, 1348-1357.
- GLASS, L. & MACKEY, M.C. (1988). *From clocks to chaos: the rhythms of life*. Princeton: Princeton University Press.
- GOOTMAN, P.M., HUNDLEY, B.W. & SICA, A.L. (1996). The presence of coherence in sympathetic and phrenic activities in a developing mammal. *Acta Neurobiol. Exp.* **56**, 137-145.
- GRANT, R.T. (1963). Vasodilatation and body warming in the rat. *J. Physiol.* **167**, 311-317.
- GRAY, C.M. & SINGER, W. (1989). Stimulus-specific neuronal oscillations in orientation columns of cat visual cortex. *Proc. Natl. Acad. Sci. U. S. A.* **86**, 1698-1702.
- GREEN, J.H. & HEFFRON, P.F. (1967). Observations on the origin and genesis of a rapid sympathetic rhythm. *Arch. Int. Pharmacodyn. Ther.* **260**, 403-411.
- GUEVARA, M.R., SHRIER, A. & GLASS, L. (1986). Phase resetting of spontaneously beating embryonic ventricular heart cell aggregates. *Am. J. Physiol.* **251**, H1298-H1305
- GUTTMAN, R., FELDMAN, L. & JAKOBSSON, E. (1980). Frequency entrainment of squid axon membrane. *J. Membr. Biol.* **56**, 9-18.
- GUYENET, P.G. (1990). Role of the ventral medulla oblongata in blood pressure regulation. In *Central regulation of autonomic functions*, eds.

- LOEWY, A.D. & SPYER, K.M., pp. 145-167. New York: Oxford University Press.
- HÄBLER, H.-J., BARTSCH, T. & JÄNIG, W. (1999). Rhythmicity in single fiber postganglionic activity supplying the rat tail. *J. Neurophysiol.* **81**, 2026-2036.
- HÄBLER, H.-J., JÄNIG, W., KRUMMEL, M. & PETERS, O.A. (1993). Respiratory modulation of the activity in postganglionic neurons supplying skeletal muscle and skin of the rat hindlimb. *J. Neurophysiol.* **70**, 920-930.
- HÄBLER, H.J., BARTSCH, T. & JÄNIG, W. (1996). Two distinct mechanisms generate the respiratory modulation in fibre activity of the rat cervical sympathetic trunk. *J. Auton. Nerv. Syst.* **61**, 116-122.
- HÄBLER, H.J., JÄNIG, W. & MICHAELIS, M. (1994). Respiratory modulation in the activity of sympathetic neurones. *Prog. Neurobiol.* **43**, 567-606.
- HAINSWORTH, R. (1991). Reflexes from the heart. *Physiol. Rev.* **71**, 617-658.
- HALLIDAY, D.M., ROSENBERG, J.R., AMJAD, A.M., BREEZE, P., CONWAY, B.A. & FARMER, S.F. (1995). A framework for the analysis of mixed time series/point process data-theory and application to the study of physiological tremor, single motor unit discharges and electromyograms. *Prog. Biophys. Molec. Biol.* **64**, 237-278.
- HARDER, D.R. (1982). Membrane electrical activation of arterial smooth muscle. In *Vascular smooth muscle: metabolic, ionic, and contractile mechanisms*, eds. CRASS, M.F. & BARNES, C.D., pp. 71-97. New York: Academic Press.
- HASELTON, J.R. & GUYENET, P.G. (1989). Central respiratory modulation of medullary sympathoexcitatory neurons in rat. *Am. J. Physiol.* **256**, R739-50.
- HEDMAN, A.E., MATSUKAWA, K. & NINOMIYA, I. (1994). Origin of cardiac-related synchronized cardiac sympathetic nerve activity in anaesthetized cats. *J. Auton. Nerv. Syst.* **47**, 131-140.

- HILBORN, R.C. (1994). *Chaos and nonlinear dynamics*. New York: Oxford University Press.
- HIRST, G.D. & EDWARDS, F.R. (1989). Sympathetic neuroeffector transmission in arteries and arterioles. *Physiol. Rev.* **69**, 546-604.
- HUANG, Z.S., GEBBER, G.L., ZHONG, S. & BARMAN, S.M. (1992). Forced oscillations in sympathetic nerve discharge. *Am. J. Physiol.* **263**, R564-71.
- JALIFE, J. (1984). Mutual entrainment and electrical coupling as mechanisms for synchronous firing of rabbit sino-atrial pace-maker cells. *J. Physiol.* **356**, 221-243.
- JÄNIG, W. (1988). Pre- and postganglionic vasoconstrictor neurons: differentiation, types, and discharge properties. *Annu. Rev. Physiol.* **50**, 525-539.
- JÄNIG, W. & MCLACHLAN, E.M. (1992). Characteristics of function-specific pathways in the sympathetic nervous system. *Trends Neurosci.* **15**, 475-481.
- JOHNSON, C.D. & GILBEY, M.P. (1993). Recordings of activity from sympathetic fibres innervating blood vessels in the tail of the anaesthetised rat. *J. Physiol.* **467**, 14P.
- JOHNSON, C.D. & GILBEY, M.P. (1994). Sympathetic activity recorded from the rat caudal ventral artery in vivo. *J. Physiol.* **476**, 437-442.
- JOHNSON, C.D. & GILBEY, M.P. (1996). On the dominant rhythm in the discharges of single postganglionic sympathetic neurones innervating the rat tail artery. *J. Physiol.* **497**, 241-259.
- JOHNSON, C.D. & GILBEY, M.P. (1998a). Effects of aortic nerve stimulation on discharges of sympathetic neurons innervating rat tail artery and vein. *Am. J. Physiol.* **275**, R942-R949

- JOHNSON, C.D. & GILBEY, M.P. (1998b). Focally recorded single sympathetic postganglionic neuronal activity supplying rat lateral tail vein. *J. Physiol.* **508**, 575-585.
- KATRAGADDA, S., XIE, A., PULEO, D., SKATRUD, J.B. & MORGAN, B.J. (1997). Neural mechanism of the pressor response to obstructive and nonobstructive apnea. *J. Appl. Physiol.* **83**, 2048-2054.
- KAUFMAN, M.P., IWAMOTO, G.A., ASHTON, J.H. & CASSIDY, S.S. (1982). Responses to inflation of vagal afferents with endings in the lung of dogs. *Circ. Res.* **51**, 525-531.
- KELSO, J.A.S. (1995). *Dynamic patterns: the self-organization of brain and behavior*. Cambridge, MA: MIT Press.
- KENNEY, M.J. (1994). Frequency characteristics of sympathetic nerve discharge in anesthetized rats. *Am. J. Physiol.* **267**, R830-R840.
- KENNEY, M.J. & FEDDE, M.R. (1994). Influence of different preamplifier bandpass cutoff frequencies on the basic pattern of sympathetic nerve discharge. *Biomed. Sci. Instrum.* **30**, 111-116.
- KEZDI, P. & GELLER, E. (1968). Baroreceptor control of postganglionic sympathetic nerve discharge. *Am. J. Physiol.* **214**, 427-435.
- KIRKWOOD, P.A. & SEARS, T.A. (1978). The synaptic connexions to intercostal motoneurons as revealed by the average common excitation potential. *J. Physiol.* **275**, 103-134.
- KNOX, C.K. (1974). Cross-correlation functions for a neuronal model. *Biophys. J.* **14**, 567-582.
- KOCSIS, B. (1994). Basis for differential coupling between rhythmic discharges of sympathetic efferent nerves. *Am. J. Physiol.* **267**, R1008-1019.
- KOCSIS, B. (1995). Baroreceptor influence on the relationships between discharges of different sympathetic nerves of the cat. *J. Physiol.* **482**, 687-696.

- KOCSIS, B., GEBBER, G.L., BARMAN, S.M. & KENNEY, M.J. (1990). Relationships between activity of sympathetic nerve pairs: phase and coherence. *Am. J. Physiol.* **259**, R549-60.
- KUBOTA, A., OOTSUKA, Y., XU, T. & TERUI, N. (1995). The 10-Hz rhythm in the sympathetic nerve activity of cats, rats and rabbits. *Neurosci. Lett.* **196**, 173-176.
- LATHERS, C.M., SCHRAEDER, P.L. & WEINER, F.L. (1987). Synchronization of cardiac autonomic neural discharge with epileptogenic activity: the lockstep phenomenon. *Electroencephalogr. Clin. Neurophysiol.* **67**, 247-259.
- LEVICK, J.R. (1995). *An introduction to cardiovascular physiology*. Oxford, UK: Butterworth-Heinemann.
- LIOY, F., BLINKHORN, M.T. & GARNEAU, C. (1984). Regional hemodynamic effects of changes in PaCO₂ in the vagotomized, sino-aortic deafferented rat. *J. Auton. Nerv. Syst.* **12**, 301-313.
- LIPSITZ, L.A. & GOLDBERGER, A.L. (1992). Loss of 'complexity' and aging: Potential applications of fractals and chaos theory to senescence. *JAMA* **267**, 1806-1809.
- LIPSKI, J., COOTE, J.H. & TRZEBSKI, A. (1977). Temporal patterns of antidromic invasion latencies of sympathetic preganglionic neurons related to central inspiratory activity and pulmonary stretch receptor reflex. *Brain Res.* **135**, 162-166.
- LIPSKI, J., KANJHAN, R., KRUSZEWSKA, B. & RONG, W. (1996). Properties of presympathetic neurones in the rostral ventrolateral medulla in the rat: an intracellular study 'in vivo'. *J. Physiol.* **490**, 729-744.
- LISMAN, J.E. (1997). Bursts as a unit of neural information: Making unreliable synapses reliable. *Trends Neurosci.* **20**, 38-43.
- LIU, C., WEAVER, D.R. & STROGATZ, S.H. (1997). Cellular construction of a circadian clock: period determination in the suprachiasmatic nuclei. *Cell* **91**, 855-860.

- LOGAN, S.D., PICKERING, A.E., GIBSON, I.C., NOLAN, M.F. & SPANSWICK, D. (1996). Electrotonic coupling between rat sympathetic preganglionic neurones in vitro. *J. Physiol.* **495**, 491-502.
- MACEFIELD, V.G. & WALLIN, B.G. (1999). Respiratory and cardiac modulation of single sympathetic vasoconstrictor and sudomotor neurones to human skin. *J. Physiol.* **561**, 303-314.
- MACKEY, M.C. & GLASS, L. (1977). Oscillation and chaos in physiological control systems. *Science* **197**, 287-289.
- MACKEY, M.C. & MILTON, J.G. (1987). Dynamical disease. *Ann. N. Y. Acad. Sci.* **504**, 16-32.
- MALPAS, S.C. (1995). A new model for the generation of sympathetic nerve activity. *Clin. Exp. Pharmacol. Physiol.* **22**, 11-15.
- MALPAS, S.C. (1998). The rhythmicity of sympathetic nerve activity. *Prog. Neurobiol.* **56**, 65-96.
- MALPAS, S.C. & NINOMIYA, I. (1992). A new approach to analysis of synchronized sympathetic nerve activity. *Am. J. Physiol.* **263**, H1311-7.
- MALPAS, S.C. & NINOMIYA, I. (1992). Fundamental rhythm of renal sympathetic nerve activity in anesthetized cats. *J. Auton. Nerv. Syst.* **37**, 11-18.
- MARSHALL, J.M. (1994). Peripheral chemoreceptors and cardiovascular regulation. *Physiol. Rev.* **74**, 543-594.
- MARSHALL, J.M. & METCALFE, J.D. (1988). Cardiovascular changes associated with augmented breaths in normoxia and hypoxia in the rat. *J. Physiol.* **400**, 15-27.
- MATSUGU, M., DUFFIN, J. & POON, C.-S. (1998). Entrainment, instability, quasi-periodicity, and chaos in a compound neural oscillator. *J. Comput. Neurosci.* **5**, 35-51.
- MCALLEN, R.M. (1987). Central respiratory modulation of subretrofacial bulbospinal neurones in the cat. *J. Physiol.* **388**, 533-545.

- MCALLEN, R.M. & MALPAS, S.C. (1997). Sympathetic burst activity: characteristics and significance. *Clin. Exp. Pharmacol. Physiol.* **24**, 791-799.
- MICHAELS, D.C., MATYAS, E.P. & JALIFE, J. (1986). Dynamic interactions and mutual synchronization of sinoatrial node pacemaker cells. *Circ. Res.* **58**, 706-720.
- MOORE, G.P., SEGUNDO, J.P., PERKEL, D.H. & LEVITAN, H. (1970). Statistical signs of synaptic interaction in the neurons. *Biophys. J.* **10**, 876-900.
- MORGAN, B.J., CRABTREE, D.C., PULEO, D.S., BADR, M.S., TOIBER, F. & SKATRUD, J.B. (1996). Neurocirculatory consequences of abrupt change in sleep state in humans. *J. Appl. Physiol.* **80**, 1627-1636.
- MORRIS, J.L. & GIBBINS, I.L. (1992). Co-transmission and neuromodulation. In *Autonomic neuroeffector mechanisms*, eds. BURNSTOCK, G. & HOYLE, C.H.V., pp. 33-119. Switzerland: Harwood Academic.
- MURTHY, V.N. & FETZ, E.E. (1992). Coherent 25- to 35-Hz oscillations in the sensorimotor cortex of awake behaving monkeys. *Proc. Natl. Acad. Sci. U. S. A.* **89**, 5670-5674.
- NAKAYAMA, K., NIWA, M., SASAKI, S.-I., ICHIKAWA, T. & HIRAI, N. (1998). Morphology of single primary spindle afferents of the intercostal muscles in the cat. *J. Comp. Neurol.* **398**, 459-472.
- NILSSON, H., LJUNG, B., SJÖBLOM, N. & WALLIN, B.G. (1985). The influence of the sympathetic impulse pattern on contractile responses of rat mesenteric arteries and veins. *Acta Physiol. Scand.* **123**, 303-309.
- NINOMIYA, I., AKIYAMA, T. & NISHIURA, N. (1990). Mechanism of cardiac-related synchronized cardiac sympathetic nerve activity in awake cats. *Am. J. Physiol.* **259**, R499-506.
- NORDIN, M. & FAGIUS, J. (1995). Effect of noxious stimulation on sympathetic vasoconstrictor outflow to human muscles. *J. Physiol.* **489**, 885-894.

- O'LEARY, D.S. & JOHNSON, J.M. (1989). Baroreflex control of the rat tail circulation in normothermia and hyperthermia. *J. Appl. Physiol.* **66**, 1234-1241.
- O'LEARY, D.S., JOHNSON, J.M. & TAYLOR, W.F. (1985). Mode of neural control mediating rat tail vasodilation during heating. *J. Appl. Physiol.* **59**, 1533-1538.
- OFFNER, B., DEMBOWSKY, K. & CZACHURSKI, J. (1992). Characteristics of sympathetic reflexes evoked by electrical stimulation of phrenic nerve afferents. *J. Auton. Nerv. Syst.* **41**, 103-111.
- PAPOULIS, A. (1991). *Probability, random variables, and stochastic processes*. Singapore: McGraw-Hill.
- PAVLIDIS, T. (1973). *Biological oscillators: their mathematical analysis*. New York: Academic Press.
- PEPER, C.E. & BEEK, P.J. (1998). Distinguishing between the effects of frequency and amplitude on interlimb coupling in tapping a 2:3 polyrhythm. *Exp. Brain Res.* **118**, 78-92.
- PERKEL, D.H., GERSTEIN, G.L. & MOORE, G.P. (1967a). Neuronal spike trains and stochastic point processes. I. The single spike train. *Biophys. J.* **7**, 391-418.
- PERKEL, D.H., GERSTEIN, G.L. & MOORE, G.P. (1967b). Neuronal spike trains and stochastic point processes. II. Simultaneous spike trains. *Biophys. J.* **7**, 419-440.
- PETRILLO, G.A. & GLASS, L. (1984). A theory for phase locking of respiration in cats to a mechanical ventilator. *Am. J. Physiol.* **246**, 311-320.
- PETRILLO, G.A., GLASS, L. & TRIPPENBACH, T. (1983). Phase locking of the respiratory rhythm in cats to a mechanical ventilator. *Can. J. Physiol. Pharmacol.* **61**, 599-607.

- PINSKER, H.M. (1977a). *Aplysia* bursting neurons as endogenous oscillators. I. Phase-response curves for pulsed inhibitory synaptic input. *J. Neurophysiol.* **40**, 527-543.
- PINSKER, H.M. (1977b). *Aplysia* bursting neurons as endogenous oscillators. II. Synchronization and entrainment by pulsed inhibitory synaptic input. *J. Neurophysiol.* **40**, 544-556.
- PORTA, A., BASELLI, G., MONTANO, N., GNECCHI-RUSCONE, T., LOMBARDI, F., MALLIANI, A. & CERUTTI, S. (1996). Classification of coupling patterns among spontaneous rhythms and ventilation in the sympathetic discharge of decerebrate cats. *Biol. Cybern.* **75**, 163-172.
- PRIESTLEY, M.B. (1981). *Spectral analysis and time series*. London: Academic Press.
- RATHNER, J.A. & MCALLEN, R.M. (1998). The lumbar preganglionic sympathetic supply to rat tail and hindpaw. *J. Auton. Nerv. Syst.* **69**, 127-131.
- REDMOND, D. (1996). *Number theory: an introduction*. New York: Marcel Dekker.
- REID, J.V.O. (1969). The cardiac pacemaker: effects of regularly spaced nervous input. *Am. Heart J.* **78**, 58-64.
- RICHTER, D.W. & SPYER, K.M. (1990). Cardiorespiratory control. In *Central regulation of autonomic functions*, eds. LOEWY, A.D. & SPYER, K.M., pp. 189-207. New York: Oxford University Press.
- RICHTER, D.W., SPYER, K.M., GILBEY, M.P., LAWSON, E.E., BAINTON, C.R. & WILHELM, Z. (1991). On the existence of a common cardiorespiratory network. In *Cardiorespiratory and motor co-ordination*, eds. KOEPCHEN, H.P. & HUOPANIEMI, T., pp. 118-139. Berlin: Springer-Verlag.
- ROSENBERG, J.R., AMJAD, A.M., BREEZE, P., BRILLINGER, D.R. & HALLIDAY, D.M. (1989). The Fourier approach to the identification of

functional coupling between neuronal spike trains. *Prog. Biophys. Molec. Biol.* **53**, 1-31.

- ROSENBERG, J.R., HALLIDAY, D.M., BREEZE, P. & CONWAY, B.A. (1998). Identification of patterns of neuronal connectivity-partial spectra, partial coherence, and neuronal interactions. *J. Neurosci. Methods* **83**, 57-72.
- ROSENBLUM, L.D. & TURVEY, M.T. (1988). Maintenance tendency in coordinated rhythmic movements: Relative fluctuations and phase. *Neuroscience* **27**, 289-300.
- SEALS, D.R., SUWARNO, N.O. & DEMPSEY, J.A. (1990). Influence of lung volume on sympathetic nerve discharge in normal humans. *Circ. Res.* **67**, 130-141.
- SHANNON, R., SAPORTA, S. & LINDSEY, B.G. (1982). Transmission of intercostal muscle proprioceptor afferent information to medullary respiratory areas. *Exp. Neurol.* **78**, 222-225.
- SICA, A.L., HUNDLEY, B.W., RUGGIERO, D.A. & GOOTMAN, P.M. (1997). Emergence of lung-inflation-related sympathetic nerve activity in spinal cord transected neonatal swine. *Brain Res.* **767**, 380-383.
- SINGER, W. (1993). Synchronization of cortical activity and its putative role in information processing and learning. *Annu. Rev. Physiol.* **55**, 349-374.
- SINGER, W. (1996). Putative functions of temporal correlations in neocortical processing. In *Large-scale neuronal theories of the brain*, eds. KOCH, C. & DAVIS, J.L., pp. 201-237. Cambridge, Massachusetts: The MIT Press.
- SINGER, W. & GRAY, C.M. (1995). Visual feature integration and the temporal correlation hypothesis. *Annu. Rev. Neurosci.* **18**, 555-586.
- SITTIRACHA, T., MCLACHLAN, E.M. & BELL, C. (1987). The innervation of the caudal artery of the rat. *Neuroscience* **21**, 647-659.
- SJÖBLOM-WIDFELDT, N., GUSTAFSSON, H. & NILSSON, H. (1990). Transmitter characteristics of small mesenteric arteries from the rat. *Acta Physiol. Scand.* **138**, 203-212.

- SMITH, J.E. & GILBEY, M.P. (1998a). Rhythmical discharges in the sympathetic supply to the rat tail are of central origin. *J. Physiol.* **513**, 81P-81P.
- SMITH, J.E. & GILBEY, M.P. (1998b). Segmental origin of sympathetic preganglionic neurones regulating the tail circulation in the rat. *J. Auton. Nerv. Syst.* **68**, 104-114.
- SMITH, J.E., JANSEN, A.S.P., GILBEY, M.P. & LOEWY, A.D. (1998). CNS cell groups projecting to sympathetic outflow of tail artery: Neural circuits involved in heat loss in the rat. *Brain Res.* **786**, 153-164.
- SNEDDON, P. & BURNSTOCK, G. (1985). ATP as a co-transmitter in rat tail artery. *Eur. J. Pharmacol.* **106**, 149-152.
- ST-JOHN, W.M. & BIANCHI, A.L. (1985). Responses of bulbospinal and laryngeal respiratory neurons to hypercapnia and hypoxia. *J. Appl. Physiol.* **59**, 1201-1207.
- STJÄRNE, L. & STJÄRNE, E. (1995). Geometry, kinetics and plasticity of release and clearance of ATP and noradrenaline as sympathetic cotransmitters: roles for the neurogenic contraction. *Prog. Neurobiol.* **477**, 45-94.
- SUZUKI, S., ANDO, S., IMAIZUMI, T. & TAKESHITA, A. (1993). Effects of anesthesia on sympathetic nerve rhythm: power spectral analysis. *J. Auton. Nerv. Syst.* **43**, 51-58.
- TAYLOR, D.G. & GEBBER, G.L. (1973). Sympathetic unit responses to stimulation of cat medulla. *Am. J. Physiol.* **225**, 1138-1146.
- TAYLOR, D.G. & GEBBER, G.L. (1975). Baroreceptor mechanisms controlling sympathetic nervous rhythms of central origin. *Am. J. Physiol.* **228**, 1002-1003.
- TODA, K., TATSUMI, E., TAENAKA, Y., MASUZAWA, T. & TAKANO, H. (1996). Sympathetic nerve activities in pulsatile and nonpulsatile systemic circulation in anesthetized goats. *Am. J. Physiol.* **271**, H15-H22

- TRZEBSKI, A. & BARADZIEJ, S. (1992). Role of the rostral ventrolateral medulla in the generation of synchronized sympathetic rhythmicities in the rat. *J. Auton. Nerv. Syst.* **41**, 129-139.
- TRZEBSKI, A. & KUBIN, L. (1981). Is the central inspiratory activity responsible for pCO₂- dependent drive of the sympathetic discharge? *J. Auton. Nerv. Syst.* **3**, 401-420.
- TRZEBSKI, A., SMITH, M.L., BEIGHTOL, L.A., FRITSCH-YELLE, J.M., REA, R.F., ECKBERG & DL. (1995). Modulation of human sympathetic periodicity by mild, brief hypoxia and hypercapnia. *J. Physiol. Pharmacol.* **46**, 17-35.
- USREY, W.M., REPPAS, J.B. & REID, R.C. (1998). Paired-spike interactions and synaptic efficacy of retinal inputs to the thalamus. *Nature* **395**, 384-387.
- VAADIA, E., HAALMAN, I., ABELES, M., BERGMAN, H., PRUT, Y., SLOVIN, H., AERTSEN & A. (1995). Dynamics of neuronal interactions in monkey cortex in relation to behavioural events. *Nature* **373**, 515-518.
- VICTOR, R.G., SECHER, N.H., LYSON, T. & MITCHELL, J.H. (1995). Central command increases muscle sympathetic nerve activity during intense intermittent isometric exercise in humans. *Circ. Res.* **76**, 127-131.
- VON DER MALSBURG, C. (1990). A neural architecture for the representation of scenes. In *Brain organization and memory: cells, systems and circuits*, eds. MCGAUGH, J.L., WEINBERGER, N.M. & LYNCH, G., pp. 356-372. New York: Oxford University Press.
- VON DER MALSBURG, C. (1995). Binding in models of perception and brain function. *Trends Neurosci.* **5**, 520-526.
- VON HOLST, E. (1939). Relative coordination as a phenomenon and as a method of analysis of central nervous functions. In *The behavioural physiology of animals and man: the selected papers of Erich von Holst*, ed. MARTIN, R., pp. 33-135. London: Methuen & Co. Ltd.

- WEAVER, L.C. (1985). Organization of sympathetic responses to distension of urinary bladder. *Am. J. Physiol.* **248**, R236-40.
- WINFREE, A.T. (1980). *The geometry of biological time*. New York: Springer-Verlag.
- WU, L.G. & SAGGAU, P. (1994). Presynaptic calcium is increased during normal synaptic transmission and paired-pulse facilitation, but not in long-term potentiation in area CA1 of hippocampus. *J. Neurosci.* **14**, 645-654.
- XIA, J. & DULING, B.R. (1995). Electromechanical coupling and the conducted vasomotor response. *Am. J. Physiol.* **269**, H2022-H2030
- ZANZINGER, J., CZACHURSKI, J., OFFNER, B. & SELLER, H. (1994). Somato-sympathetic reflex transmission in the ventrolateral medulla oblongata: spatial organization and receptor types. *Brain Res.* **656**, 353-358.
- ZHANG, T.X., ROHLICEK, C.V. & POLOSA, C. (1982). Responses of sympathetic preganglionic neurons to systemic hypercapnia in the acute spinal cat. *J. Auton. Nerv. Syst.* **6**, 381-389.
- ZHONG, S., BARMAN, S.M. & GEBBER, G.L. (1992). Effects of brain stem lesions on 10-Hz and 2- to 6-Hz rhythms in sympathetic nerve discharge. *Am. J. Physiol.* **262**, R1015-R1024
- ZHONG, S., GEBBER, G.L., LIU, Y., ZHOU, S.-Y. & BARMAN, S.M. (1996). Comparison of results obtained with time- and frequency-domain analysis when searching for the 10-Hz rhythm in sympathetic nerve discharge. *Neurosci. Lett.* **211**, 113-116.
- ZHONG, S., HUANG, Z.S., GEBBER, G.L. & BARMAN, S.M. (1993). Role of the brain stem in generating the 2- to 6-Hz oscillation in sympathetic nerve discharge. *Am. J. Physiol.* **265**, R1026-35.
- ZHONG, S., ZHOU, S.Y., GEBBER, G.L. & BARMAN, S.M. (1997). Coupled oscillators account for the slow rhythms in sympathetic nerve discharge and phrenic nerve activity. *Am. J. Physiol.* **272**, R1314-R1324

ZUCKER, R.S. (1989). Short-term synaptic plasticity. *Annu. Rev. Neurosci.* **12**, 13-31.

ZUCKER, R.S. (1994). Calcium and short-term synaptic plasticity. *Biomed. Res.* **15**, 1-5.

